Dissertation

submitted to the

Combined Faculty of Natural Sciences and Mathematics

of the Ruperto Carola University Heidelberg, Germany

for the degree of

Doctor of Natural Sciences

Presented by

M.Sc. Johannes Ridinger

born in: Heidelberg, Germany

Oral examination: 27th May, 2019

HDAC10 in neuroblastoma chemoresistance

Referees: apl. Prof. Dr. Matthias Mayer

Prof. Dr. Olaf Witt

For my family.

I can live with doubt, and uncertainty, and not knowing.

I think it's much more interesting to live not knowing

than to have answers which might be wrong.

Richard P. Feynman

DECLARATION

I hereby declare that I have written the submitted dissertation "HDAC 10 in neuroblastoma chemoresistance" myself and that I have used no other sources or materials than those expressly indicated. I further have not applied to be examined at any other institution, nor have I used the dissertation in this or any other form at any other institution as an examination paper, nor submitted it to any other faculty as a dissertation.

Parts of the thesis have been published in **Ridinger et al. 2018.** Therefore, this thesis can contain text passages and subparts of figures of the respective publication, which I have written myself.

Heidelberg, 7th February, 2019

.....

Johannes Ridinger

ACKNOWLEDGEMENTS

I would like to take the opportunity to express my gratitude to the people who have contributed to the success of this project.

Prof. Dr. Olaf Witt, for providing such a great and supportive scientific environment. It was a pleasure to work in the department of Pediatric Oncology. This project would have not been possible without your support, criticism and invaluable input.

Dr. Ina Oehme for your excellent supervision, your patience, motivation and unexhaustible input. You have been a tremendous mentor and helped me grow as a scientist and as a person. I will sincerely miss our scientific discussions.

Prof. Dr. Matthias Mayer for being an inspiring teacher at university, for the willingness to be first examiner of this project, as well as for the valuable scientific input to the project as a TAC member.

Prof. Dr. Viktor Umansky and **PD Dr. Odilia Popanda** for your willingness to act as examiners.

The current and former members of the Witt lab family. I have been tremendously lucky to be able to work with such a great group of people. You have made my stay in the lab a special and enjoyable one: **Till, Jagoda, Heike, Sina, Romain, Jonas, Johannes (the other Johannes), Flo, Emily, Fiona, Lisa, Katharina, Sara, Juliane, Ginny, Michael, Diren, Alexander, Annika, Ramona, Aileen, Alex, Carina, Isabel** and **Dani**: I will miss the scientific and especially the non-scientific conversations, as well as the fun times during lab retreats and dinners. I would especially like to thank: **Emily Koeneke** for your second to none peanut butter cookies and being open to my countless questions with regards to organisatorial stuff, drugs and inhibitors, and of course for your great help as a language teacher. To the "San Francisco Connection": **Katharina Koerholz**, whom I supervised during her master's and doctoral studies: It was a joy to supervise you, to work and chat with you. And thanks of course for the fun bike trip through San Francisco. **Jagoda Wrobel** for giving me the opportunity to join you on a road trip along the beautiful coast of California. All the best for you and your little family. **Fiona Kolbinger** who witnessed all the highs and lows of the project and who endured my antics throughout the years. You have been a great help both inside and outside of the lab. I cannot thank you enough for your sincere friendship.

The collaborators and helpers within the DKFZ, who have significantly contributed to the success of this study**: Dr. Aubry Miller, Dr. Nikolas (Niki) Gunkel, Dr. Peter Schmezer, Dr. Martina Schnölzer, Dr. Uwe Warnken, Dr. Felix Bestvater, Manuela Brom, Reinhard Gliniorz, Lars Hellweg, Claudia Tessmer, Ulrike Ackermann** and **Natalie Erbe-Hofmann**.

Co-scientists and collaborators outside of the DKFZ and worldwide: **Dr. Bernd Hessling, Dr. Thomas Ruppert, Prof. Dr. Siavosh Mahboobi, Prof. Dr. Michael Hust, Dr. Robert Casero** and **Dr. Tracy**

Murray-Stewart. Special thanks to **Dr. Anne Hamacher-Brady** for the invaluable scientific input as a TAC member. You have contributed greatly to this work.

People from the DKFZ fifth and sixth floor who have made life as a Ph.D. student easier in one way or the other: **Dr. Stefan Pusch** for your technical support and the scientific and non-scientific discussions, **Jessica Eisel, Eric Poisel, Moritz Gartlgruber** and **Julia (Lulia) Zaman** for your contagious sense of humor. **Julia**, I would especially like to thank you for your help with figures and of course your invaluable friendship. And sorry of course for all the jokes at your expense.

The people of the Utikal lab, particularly **Dr. Lionel (Lio) Larribère** for discussions, scientific and otherwise, **Dr. Laura Hüser** for helping me with the final stages of successfully finishing my Ph.D., and of course **Dr. Daniel ("Dr. No") Novak**: you have become a great friend over the years.

People from the DKFZ-Bayer Joint Immunotherapeutics lab, for allowing me to (mis)use your flow cytometer. A special thank you to **Dr. Rafael (Rafa) Carretero** for your help with flow cytometric analyses. **Xenia, Giovanni, Sabrina** and **Melanie** for showing me how to "flush a cytometer properly" and for sharing a common sense of black humor.

To my former supervisors **Prof. Dr. Peter Altevogt**, **Dr. Sascha Keller** and **Dr. Niko Bretz:** You have been the greatest mentors I could have ever imagined.

My band mates and fellow musicians, especially Danny Joe and Marco for your sincere friendship.

Finally, and most importantly, I would like to thank **my family**, who has offered me a tremendous amount of support in good and bad times. Thank you for believing in me and for your endless inspiration, support and love.

.

ABSTRACT

Neuroblastoma is the most common extracranial solid tumor in childhood, and characteristically displays a wide variety of clinical outcomes. While prognosis is generally favorable in low-risk and intermediate-risk tumors, outcome remains poor in high-risk neuroblastoma, and infaust in case of relapse. Multidrug resistance is frequent in high-risk neuroblastoma and remains to be one of the major factors limiting treatment success despite intensive multimodal therapy regimens, highlighting the need for novel treatment approaches capable of reducing neuroblastoma drug resistance. Histone deacetylases (HDACs) are involved in numerous cancer-relevant pathways and have become attractive anti-tumor targets due to their excellent druggability. Broadband inhibition of HDACs is, however, associated with dose-limiting side effects, which can be possibly circumvented by the inhibition of individual tumor-relevant isozymes. Previous work of our group has shown that high expression of class IIb histone deacetylase HDAC10 supports chemoresistance of neuroblastoma cells by promoting macroautophagy. Data suggested that HDAC10 was critical for lysosomal function, but the precise lysosomal role of HDAC10 and its cellular substrates remained unknown.

The data presented in this study indicate that HDAC10 is crucial for lysosomal homeostasis in a number of highly drug-resistant neuroblastoma cell lines (SK-N-BE(2)-C, IMR-32, SK-N-AS) while being dispensable in others (Kelly, NB-1) and in non-transformed fibroblasts. In HDAC10-dependent cells, interference with HDAC10 function causes accumulation of lysosomes, a phenotype that is not observed in case of functional interference with the highly homologous class IIb member HDAC6. Depletion or inhibition of HDAC10 further interferes with downstream lysosomal processes such as lysosomal exocytosis, indicating that accumulating lysosomes are dysfunctional. Lysosomal accumulation and the inhibition of lysosomal exocytosis in turn promote intracellular accumulation of weakly basic chemotherapeutics such as doxorubicin, which does not remain sequestered in lysosomes but is also highly enriched in nuclei. Consequently, co-treatment with doxorubicin and HDAC10 inhibitors efficiently promotes cell death in treatment resistant neuroblastoma cell lines while sparing non-malignant cells.

Lysosomal exocytosis is an important pro-survival mechanism under cytotoxic treatment. Inhibition of HDAC10, and thus lysosomal exocytosis, sensitizes cells not only by promoting doxorubicin accumulation, but also by inhibiting the process of lysosomal exocytosis itself. Moreover, interference with HDAC10 function promotes accumulation of DNA double-strand breaks (DSBs) both in absence and presence of doxorubicin, suggesting an additional role for HDAC10 in DSB repair.

Preliminary data of mass spectrometric analyses of protein lysine acetylation after HDAC10 inhibition suggest that HDAC10 modulates acetylation of the V-ATPase subunit A and the Ku70/Ku80 complex member Ku80. It is thus conceivable that HDAC10 modulates lysosomal function at the level of

lysosomal acidification, as well as DNA repair at the level of non-homologous end joining of DSBs. The recently published function of HDAC10 as N^8-acetylspermidine deacetylase remains to be confirmed. Follow-up studies on the mechanistic role of HDAC10 could be greatly facilitated by a highly specific HDAC10 antibody. In this context, several promising HDAC10-reactive mouse hybridoma clones were generated, but recurring instability of the promising hybridoma clones delayed stable production of the antibody.

In summary, in this thesis, a novel function of HDAC10 in regulation of lysosomal downstream mechanisms was identified and a previously published role of HDAC10 in DNA repair was confirmed. These mechanisms possess the translational potential to overcome drug resistance in combination with chemotherapies.

ZUSAMMENFASSUNG

Das Neuroblastom ist der häufigste solide extrakranielle Tumor im Kindesalter und zeichnet sich durch sein variables klinisches Erscheinungsbild aus. Während die Heilungschancen bei Patienten der niederen und mittleren Risikogruppen in der Regel günstig sind, weisen insbesondere sogenannte Hochrisiko-Neuroblastome und rezidivierende Tumore eine schlechte bzw. infauste Prognose auf. Hochrisiko-Neuroblastome sind dabei häufig durch eine gesteigerte Resistenz gegenüber einer Vielzahl von Zytostatika gekennzeichnet, was trotz intensiver multimodaler Therapien zu einem Therapieversagen führt und die Notwendigkeit neuer resistenzbrechender Behandlungsansätze im Neuroblastom unterstreicht. Histondeacetylasen (HDACs) sind entscheidend an der Steuerung vieler krebsrelevanter Prozesse beteilig, was sie, zusammen mit ihrer exzellenten Wirkstoff-Bindungsfähigkeit, interessant für die Tumortherapie macht. Dabei geht die Breitbandinhibition der HDACs jedoch mit dosislimitierenden Nebenwirkungen einher, was mit der gezielten Hemmung der tumorrelevanten Enzyme umgangen werden könnte. Eine vorangegangene Studie unserer Arbeitsgruppe hat gezeigt, dass eine hohe Expression der Klasse IIb Histondeacetylase HDAC10 die Chemoresistenz von Neuroblastomzellen durch Antreiben der Makroautophagie fördert. Auch wenn die Daten dieser Studie darauf hindeuteten, dass HDAC10 bedeutend für die Lysosomenfunktion ist, blieben die genaue lysosomal Rolle der HDAC10 und deren nachgeschaltete zelluläre Substrate unbekannt.

Die in dieser Arbeit präsentierten Daten zeigen, dass HDAC10 in einigen der untersuchten Neuroblastommodelle (SK-N-BE(2)-C, IMR-32, SK-N-AS) eine entscheidende Rolle in der Homöostase sogenannter Lysosomen zukommt, während die Lysosomen anderer Neuroblastomzelllinien (Kelly, NB-1) und proliferierender Fibroblasten nicht durch HDAC10 beeinflusst sind. Bei einer Beeinträchtigung der HDAC10 Funktion kommt es in HDAC10-abhängigen Zellen zu einer Ansammlung von Lysosomen, was bei Hemmung der nahe verwandten HDAC6 nicht der Fall ist. Depletion und Inhibition von HDAC10 führen dabei weiterhin zu einer Störung nachgeschalteter lysosomaler Prozesse wie der lysosomalen Exozytose, was auf eine Dysfunktion der akkumulierenden Lysosomen hindeutet. In Folge der Ansammlung von Lysosomen und der Hemmung der lysosomalen Exozytose kommt es in den betreffenden Zelllinien zu einer Ansammlung schwach basischer Chemotherapeutika wie Doxorubicin, welche sich sowohl in Lysosomen und Zellkernen anreichern. Folglich führt die Kombinationsbehandlung mit Doxorubicin und HDAC10 Inhibitoren in Neuroblastomzellen, nicht aber in nicht-malignen Zellen, zu einer erhöhten Zelltodrate.

Die lysosomale Exozytose selbst wird zu einem wichtigen Überlebensmechanismen unter Zytostatikabehandlung. Die Hemmung von HDAC10, und damit der lysosomalen Exozytose, sensitiviert Neuroblastomzellen dabei nicht nur durch vermehrte intrazelluläre

Doxorubicinansammlung, sondern auch durch die Inhibition der lysosomalen Exozytose selbst. Des Weiteren erhöht die Hemmung der HDAC10 Funktion die Anzahl sogenannter DNA Doppelstrangbrüche sowohl in An- als auch in Abwesenheit von Doxorubicin, was auf eine Funktion von HDAC10 in der Reparatur von DNA Doppelstrangbrüchen hindeutet.

Vorläufige massenspektrometrische Analysen der Lysin-Acetylierung in Proteinen nach HDAC10-Hemmung weisen darauf hin, dass HDAC10 die Acetylierung von Untereinheiten der V-ATPase bzw. des Ku70/Ku80-Komplexes beeinflusst. Es ist also denkbar, dass HDAC10 die Lysosomenfunktion auf Ebene der lysosomalen Ansäuerung, und DNA Reparatur auf Ebene der nicht-homologen Endverknüpfnung (non-homologous end joining) reguliert. Die kürzlich publizierte Funktion von HDAC10 als N^8-Acetylspermidindeacetylase konnte in dem hier verwendeten Zellmodell noch nicht bestätigt werden. Zukünftige mechanistischen Studien würden durch einen hochspezifischen, bisher jedoch nicht verfügbaren, HDAC10 Antikörper vereinfacht. Im Rahmen dieses Projekts wurden mehrere vielversprechende HDAC10-reaktive Hybridomklone generiert, eine zuverlässige Produktion des HDAC10 Antikörpers verzögert sich jedoch bisher auf Grund wiederkehrender Instabilität dieser Hybridome.

Zusammenfassend konnte in dieser Arbeit eine neue Funktion von HDAC10 in der Regulation der Lysosomenfunktion gezeigt und eine bereits publizierte Rolle von HDAC10 in der DNA Reparatur bestätigt werden. Diese können als Angriffspunkte zur Minderung von Chemoresistenzen dienen.

TABLE OF CONTENTS

LIST OF ABBREVIATIONS

1D	One-dimensional
2D	Two-dimensional
2nd ab	Secondary antibody control
3D	Three-dimensional
α	Alpha
AA	Amino acid
ABC	ATP-biding cassette
ac	Acetylated
acetyl-CoA	Acetyl coenzyme A
AdoMetDC	S-adenosylmethionine decarboxylase
AFC	Amino-4-trifluoromethyl coumarin
AHSCT	Autologous hematopoietic stem cell transplantation
AKAP12	A-kinase anchor protein 12
AKT	RAC-alpha serine/threonine-protein kinase
ALK	Anaplastic lympoma kinase
ALR	Autophagic lysosome regeneration
ALT	Alternative lengthening of telomeres
AMP	Adenosine monophosphate
AMPK	AMP-activated protein kinase
ampl.	Amplified
APAO	N^1-acetylpolyamine oxidase
APC	Allophycocyanin
ATCC	American Type Culture Collection
ATG	Autophagy-related gene
ATP	Adenosine triphosphate
ATRX	Transcriptional regulator ATRX/ATP-dependent helicase ATRX
Autofl.	Autofluorescence
β	Beta
Baf	Bafilomycin
BARD1	BRCA1-associated RING domain protein 1
BCA	Bicinchoninic acid assay
BCRP	Breast cancer resistance protein
BECN1	Beclin-1
bHLH	Basic helix-loop-helix
BiP	Endoplasmic reticulum chaperone BiP (binding immunoglobulin protein)
BLAST	Basic local alignment search tool
BMP	Bone morphogenetic protein
BRET	Bioluminescence resonance energy transfer
BSA	Bovine serum albumin
Ca^{2+}	Calcium ion
CAMTA	Calmodulin-binding transcription activator 1
CASZ1	Zinc finger protein castor homolog 1
CCT	Chaperonin containing TCP-1
CD	Catalytic domain
cDNA	Complementary DNA
CHIP	E3 ubiquitin-protein ligase CHIP (Carboxy terminus of HSP70-interacting protein)
CK2	Casein kinase II
CLEAR	Coordinated lysosomal expression and regulation

cm^2	Square centimeter
CMA	Chaperone mediated autophagy
CMV	Cytomegalovirus (promoter)
CO_2	Carbon dioxide
CoREST	REST corepressor
CQ	Chloroquine
CTCL	Cutaneous T-cell lymphoma
CTD	C-terminal domain
CTL	Cytotoxic T-lymphocyte
ctrl	Control
Cu	Copper
Cy3	Cyanine dye 3
d	Days
Da	Daltons
DAPI	4',6-diamidino-2-phenylindole
ddH_2O	Double distilled water
DKFZ	Deutsches Krebsforschungszentrum
DMEM	Dulbecco's modified Eagle's medium
DMFO	Difluoromethylornithine
DMP	Dimethyl pimelimidate
DNA	Deoxyribonucleic acid
DNAJB8	DnaJ homolog subfamily B member 8
dNTPs	Nucleoside triphosphates
DPBS	Dulbecco's phosphate-buffered saline
DSBs	DNA double-strand breaks
DSMZ	German Collection of Microorganisms and Cell Cultures
E. coli	*Escherichia coli*
e.v.	Empty vector
EC_{50}	Half maximal effective concentration
ECACC	European Collection of Authenticated Cell Cultures
ECL	Enhanced chemiluminescence substrate
ECM	Extracellular matrix
EE	Early endosome
EFS	Event-free survival
EGF(R)	Epidermal growth factor (receptor)
EGFP	Enhanced green fluorescent protein
ELISA	Enzyme-linked immunosorbent assay
EMT	Epithelial-mesenchymal transition
ER	Endoplasmatic reticulum
ERBB2	Receptor tyrosine-protein kinase erbB-2
ERK	Mitogen-activated protein kinase/extracellular signal-regulated kinase
ERRα	Estrogen related receptor alpha
ESCRT	Endosomal sorting complexes required for transport
f.b.s.	Final bleed serum
FACS	Fluorescence activated cell sorting/flow cytometry
Fc	Fragment crystallizable (region)
FDA	U.S. Food and Drug Administration
FGF(R)	Fibroblast growth factor (receptor)
FoxO	Forkhead box protein O
FRET	Fluorescence resonance engergy transfer

FSC	Forward scatter
γ	Gamma
Glu	Glutamine
GRP78	78 kDa glucose-regulated protein (=BiP)
GTP	Guanosine triphosphate
GWAS	Genome-wide association study
Gy	Gray
h	Hours
H2	Histone H2
H_2O	Water
H_2O_2	Hydrogen peroxide
H3	Histone H3
H4	Histone H4
HAT	Histone acetyl transferase
Hda1	Histone deacetylase Hda1
HDAC	Histone deacetylase
HDACi	Histone deacetylase inhibitor
HGPRT	Hypoxanthine-guanine phosphoribosyltransferase
HOPS complex	Homotypic fusion and protein sorting complex
HPLC	High-performance liquid chromatography
HPRT	see HPGRT
HSF1	Heat shock factor protein 1
HSP	Heat shock protein
hygro	Hygromycin
IC_{50}	Half maximal inhibitory concentration
IDRF	Image-defined risk factor
IF	Immunofluorescence
IgG	Immunoglobulin G
IHC	Immunohistochemistry
IL-1β	Interleukin-1 beta
ILVs	Intra-luminal vesicles
IMDM	Iscove's modified Dulbecco's medium
INPC	International Neuroblastoma Pathology Classification
INRG	International Neuroblastoma Risk Group
INRGSS	The International Neuroblastoma Risk Group Staging System
INSS	International Neuroblastoma Staging System
IP	Immunoprecipitation
κ	Kappa
KAT	Lysine acetyl transferase
kDa	Kilodaltons
KDAC	Lysine deacetylase
KIF1B	Kinesin family member 1B
KLH	Keyhole limpet hemocyanine
KO	Knockout
LAMP	Lysosome associated membrane protein
LCD	Lysosomal cell death
LC-MS/MS	Liquid chromatography tandem-mass spectrometry
LE	Late endosome
LGP	Lysosomal glycoprotein
LIMP	Lysosome associated integral membrane protein

LIN28B	Protein lin-28 homolog B
λ_{max}	Wavelength of maximum excitation/emission
LMO1	Rhombotin-1/LIM domain only protein 1
LMP	Lysosomal membrane permeabilization
log	Logarithmic scale
LSD	Lysosomal storage disease
Luc	Luciferase
m.b.s.	Medium bleed serum
mA	Milliampère
MAF	Monoclonal antibody facility of the DKFZ
MARB1	Marbostat-100
MAX	MYC-associated factor X
MCOLN1	Mucolipin-1
MDR	Multidrug resistance
MEF2	Myocyte enhancer factor 2
min	Minutes
mir-34a	microRNA 34a
MIZ1	MYC-interacting zinc finger protein 1
Mk	Midkine
mm2	Square millimeter
MPR	Mannose-6-phosphate receptor
MRP1	Multidrug resistance-associated protein 1
MSH2	MutS homolog 2
mt	Mitochondrial
MTOC	Microtubule-organizing center
mTOR	Mammalian/mechanistic target of rapamycin
mTORC1	mTOR complex 1
mut.	Mutated
MVBs	Multivesicular bodies
MYCN	V-myc avian myelocytomatosis viral oncogene neuroblastoma derived homolog
n.a.	Not available
n.i.	Not investigated
n.s.	Not statistically significant at an alpha level of 0.05
NAD^+	Nicotinamide adenine dinucleotide
NBD	Nucleotide binding domain
N-CoR	Nuclear receptor corepressor
NES	Nuclear export signal
NF-κB	Nuclear factor kappa-light-chain-enhancer of activated B cells
NHEJ	Non-homologous end joining
NLS	Nuclear localization signal
Nluc	NanoLuciferase (NanoLuc)
norm.	Normalized
NTD	N-terminal domain
NTRK	Neurotrophic tyrosine kinase receptor
NuRD	Nucleosome remodeling deacetylase complex
OD	Optical density
ODC-1	Ornithine decarboxylase 1
OS	Overall survival
p	Chromosome short arm
p.i.s.	Pre-immune serum

P/CAF	Histone acetyltransferase PCAF (KAT2B)
p21	Cyclin dependent kinase inhibitor 1A (CDKN1A)
p27	Cyclin-dependent kinase inhibitor p27
p53	Cellular tumor antigen p53
PAGE	Polyacrylamide gel electrophoresis
PAS	Phagophore assembly site
PAT	N^8-spermidine acetyltransferase
PCR	Polymerase chain reaction
PDAC	Polyamine deacetylase
PE	Phycoerythrin
P-gp	P-glycoprotein
PHOX2B	Paired-like mesoderm homeobox (protein) 2B
PI3K	Phosphatidylinositol 3-kinase
PI3P	Phosphatidylinositol-3-phosphate
PKA	cAMP-dependent protein kinase A
polyQ	Polyglutamine
ppm	Parts per million
PTM	Posttranslational modification
Ptn	Pleiotrophin
pur.	Purified
PVDF	Polyvinylidene difluoride
q	Chromosome long arm
Rab	Ras-related protein Rab
RE	Recycling endosome
rel.	Relative to
RelA	Transcription factor p65/nuclear factor NF-kappa-B p65 subunit
RIPA	Radioimmunoprecipitation assay buffer
RNA	Ribonucleic acid
RNAi	RNA interference
ROS	Reactive oxygen species
Rpd3	Histone deacetylase Rpd3
RPMI	Roswell Park Memorial Institute medium
RSLC	Rapid separation liquid chromatography
RTK	Receptor tyrosine kinase
RT-qPCR	Real-time quantitative PCR
SAHA	Suberoylanilide hydroxamic acid/Vorinostat
scFv	Single-chain variable fragment
SD	Standard deviation
SDHA	Succinate dehydrogenase [ubiquinone] flavoprotein subunit, mitochondrial
SEM	Standard error of the mean
Ser	Serine
si	Small interfering RNA against postpositioned target gene
SILAC	Stable isotope labeling with amino acids in cell culture
Sin3	Transcriptional regulatory protein Sin3
Sir2	NAD-dependent protein deacetylase sirtuin-2
siRNA	Small interfering RNA
SIRT/Sirt	Sirtuin
SMC3	Structural maintenance of chromosomes protein 3
SMO	Spermine oxidase
SNAP29	Synaptosomal-associated protein 29

SNARE	Soluble NSF attachment protein receptor
Sox9	Transcription factor SOX9
SQSTM1/p62	Sequestosome-1/ubiquitin-binding protein p62
SSAT	Spermidine/spermine N^1-acetyltransferase
SSC	Side scatter
STAT3	Signal transducer and activator of transcription 3
STX17	Syntaxin-17
TBS	Tris-buffered saline
TBS-T	Tris-buffered saline and Tween
TEMED	Tetramethylethylenediamine
TERT	Telomerase reverse transcriptase
TFEB	Transcrition factor EB
TGN	Trans-Golgi network
TH	Tyrosine 3-hydroxylase
TRiC	TCP-1 Ring Complex
TSA	Trichostatin A
TU	Technische Universität
U.S.	United States
UK	United Kingdom
ULK1	Unc-51-like kinase 1
UPLC	Ultra performace liquid chromatography
UPR	Unfolded protein response
USA	United States of America
UV	Ultraviolet
V	Volts
VAMP7	Vesicle-associated membrane protein 7
VAMP8	Vesicle-associated membrane protein 8
V-ATPase	Vacuolar-type H+-ATPase
VH	variable domain of the antibody heavy chain
VL	variable domain of the antibody light chain
VPA	Valproic acid
Vps	Vacuolar protein sorting
w/o	Without
Wnt	Wingless/Int-1
wt	Wild type
x g	Number of times gravitational force
XRCC5	X-ray repair cross-complementing protein 5
zHDAC	Zebrafish HDAC
ZMBH	Zentrum für Molekulare Biologie Heidelberg
Zn^{2+}	Zinc ion
ZnF	Zinc finger domain

LIST OF FIGURES

LIST OF TABLES

A INTRODUCTION

1 Neuroblastoma - a childhood tumor of the neural crest

Neuroblastoma is a solid embryonal neuroendocrine tumor and the most common extracranial solid tumor in childhood, accounting for approximately 7% of total cancer cases diagnosed in children (Ward et al. 2014). It is by far the most common cancer in infancy with a median onset age of 18 months, and over 90 % of cases are diagnosed before the age of 10 (Ward et al. 2014; Matthay et al. 2016). Neuroblastoma is about 1.3-fold more common in males, although the reasons for this preference remain unknown (Ward et al. 2014; Kaatsch et al. 2018). In total, it is the second most frequent malignant tumor in children below the age of 14, but with an incidence of one child in 100,000 per year in Germany, neuroblastoma is a rare disease (Kaatsch et al. 2018). Nonetheless, neuroblastoma alone is responsible for about 15% of cancer-related deaths in children in the United States and thus ranks among the most devastating childhood tumors (Mueller and Matthay 2009).

Neuroblastomas originate from migrating cells of the neural crest, a temporary embryonal tissue that arises between the neural tube and the non-neuronal ectoderm during neural tube closure and gives rise to various cells and tissues such as the cells of the peripheral nervous system, the adrenal medulla, glia, craniofacial bone and cartilage and melanocytes (Crane and Trainor 2006). Initiation of the neural crest takes place at the border of the neural plate and the adjacent ectoderm, and is coordinated by a gradient of signaling factors that are secreted from the non-neuronal ectoderm and the underlying mesoderm, such as BMPs, Wnt and FGFs, Notch and retinoic acid (Prasad et al. 2012; Mayor and Theveneau 2013). In order to migrate, neural crest cells must then undergo a process called epithelial to mesenchymal transition, during which epithelial cells adapt a mesenchymal phenotype, leading to a loss of cellular polarity and adhesion that allows them to delaminate from the closing neural tube (Duband 2010; Mayor and Theveneau 2013). Delamination from the neural tube is followed by migration of neural crest cells along dorso- or ventrolateral routes, which, along with their site of origin along the anterior-posterior axis, determines neural crest cell fate (Krispin et al. 2010; Nitzan and Kalcheim 2013). Functionally, the neural crest can be divided into four partly overlapping domains or regions: The cranial, the cardiac, the vagal/sacral, as well as the trunk neural crest, all giving rise to different tissues and structures (Mayor and Theveneau 2013; Matthay et al. 2016). The trunk neural crest itself harbors two cell populations, one of which travels along the dorsolateral route and differentiates into melanocytes. The other, migrating ventrolaterally, gives rise to the dorsal root ganglia, as well as to sympathoadrenal progenitor cells, which differentiate into cells of the sympathetic nervous system, including chromaffin cells of the adrenal medulla and

sympathetic ganglia (Anderson 1993; Jiang et al. 2011; Matthay et al. 2016). Neuroblastomas arise in structures derived from the sympathoadrenal lineage and are therefore thought to originate from incompletely differentiated sympathoadrenal progenitor cells. They are found in the neuronal ganglia along the entire sympathetic nervous system, with the most common sites being the adrenal medulla and lumbar sympathetic ganglia (65 %), and more rarely the sympathetic ganglia of the chest (20 %), neck and pelvis (5 %) (Cheung and Dyer 2013). Given their close connection to neural crest cell fate, it is hardly surprising that neuroblastoma cells harbor alterations in genes that are relevant for neuronal development, such as *MYCN* and *ALK*, as well as in genes that are important for the differentiation of sympathoadrenal progenitor cells such as *PHOX2B* (Dubreuil et al. 2000; Goridis and Rohrer 2002; Raabe et al. 2008).

1.1 Genetic and genomic alterations in neuroblastoma

Due to its rareness and the paucity of recurrent mutations at disease diagnosis, the understanding of neuroblastoma carcinogenesis remains incomplete (Pugh et al. 2013). Given its early onset, environmental factors seem unlikely, and to date no environmental factor has been identified that significantly increases the risk for neuroblastoma, although maternal exposure to drugs and chemicals during pregnancy cannot be fully ruled out (McCall et al. 2005; Bluhm et al. 2006; Matthay et al. 2016). In contrast, a number of genetic and structural chromosomal aberrations have been identified and linked to both neuroblastoma pathogenesis and prognosis, the most important of which will be discussed below.

1.1.1 Mutations in the *ALK* and *PHOX2B* genes predispose for familial neuroblastoma

Intriguingly, and despite its early onset, cases of familial neuroblastoma that originate from germline mutations are exceedingly rare and only account for only 1-2 % of total neuroblastoma cases (Ward et al. 2014; Matthay et al. 2016). To date, mutations in only two genes, namely *ALK* and *PHOX2B*, have been identified as high penetrance predisposing factors of hereditary neuroblastoma, even though recent genome wide association studies suggest that common polymorphisms in other genetic loci such as *BARD1*, *LMO1* or *LIN28B* may contribute to neuroblastoma susceptibility (Cheung and Dyer 2013; Pugh et al. 2013; Matthay et al. 2016).

In 2008, activating mutations in the *ALK* gene were identified as the most common cause for familial neuroblastoma (Janoueix-Lerosey et al. 2008; Mosse et al. 2008; Matthay et al. 2016). *ALK* mutations, which are present in almost all cases of familial neuroblastoma as well as in 6-10% of sporadic neuroblastomas, are found within the kinase domain of the *ALK* gene, mainly affecting the amino acids R1275, F1174 and F1245, thereby triggering constitutive activation of ALK kinase activity

independent of ligand binding (Janoueix-Lerosey et al. 2008; Ogawa et al. 2011). The *ALK* gene encodes for a receptor tyrosine kinase, which is highly expressed in the developing nervous system along with its ligands Midkine and pleiotrophin (Wellstein 2012). It is essential for sympathetic neuronal development, promoting proliferation of sympathetic neurons via interaction with its ligands (Reiff et al. 2011). Tightly controlled expression of *ALK* is essential for balancing neuronal progenitor proliferation, differentiation and survival during embryogenesis (Yao et al. 2013). Notably, *ALK* is amplified in 3-4 % of sporadic neuroblastoma cases (Mosse et al. 2008; Reiff et al. 2011; Cheung and Dyer 2013), in some instances co-amplified with the *MYCN* oncogene, likely due to the proximity of the two genes on the short arm of chromosome 2 (2p) (Mosse et al. 2008; Matthay et al. 2016). Both *ALK* overexpression and aberrant activity have been found to promote proliferation and suppress cell death in neuroblastoma cell lines (Chen et al. 2008; George et al. 2008; Janoueix-Lerosey et al. 2008). Elevated *ALK* expression is associated with poor outcome (Schulte et al. 2011), and *ALK* and *MYCN* cooperatively drive neuroblastoma tumorigenesis (Schulte et al. 2013).

Germline mutations in the gene encoding for the paired homeodomain transcription factor *PHOX2B* were the first predisposing genetic aberrations discovered in familial neuroblastoma, although they occur at much lower frequency than *ALK* mutations (Mosse et al. 2004; Trochet et al. 2004). Mutations in *PHOX2B* are found in roughly 6 % of familial, as well as 4 % of sporadic neuroblastoma cases (Mosse et al. 2004; Trochet et al. 2004; Raabe et al. 2008; Louis and Shohet 2015). *PHOX2B* is an important regulator of neural crest development and it is mainly thought to promote sympathetic neuronal differentiation, as well as cell cycle exit (Pattyn et al. 1999; Trochet et al. 2005; Raabe et al. 2008; Cheung and Dyer 2013; Pei et al. 2013; Wang et al. 2014). On the other hand, *PHOX2B* has also been shown to have oncogenic potential, since high *PHOX2B* expression was found to directly promote expression of *ALK* (Bachetti et al. 2010).

1.1.2 MYCN amplification

A frequent, albeit not the most common, genetic alteration found in roughly 20-25 % of sporadic neuroblastomas is the amplification of the *MYCN* oncogene on chromosome 2p24 (Schwab et al. 1983; Huang and Weiss 2013; Matthay et al. 2016). Of all genetic and chromosomal aberrations known to occur in neuroblastoma, *MYCN* amplification possesses the highest predictive value for disease outcome and defines an aggressive tumor subtype with poor overall prognosis (Brodeur et al. 1984; Louis and Shohet 2015). Amplification of the *MYCN* gene leads to overexpression of the transcription factor MYCN, a basic helix-loop-helix (bHLH) transcription factor of the MYC family of transcription factors (Kohl et al. 1984; Dang 2012). Like other members of the MYC family, MYCN is considered as a master regulator of transcription that can both activate and repress gene transcription, mainly via heterodimerization with its interaction partners MAX and MIZ1, respectively

(Blackwood and Eisenman 1991; Peukert et al. 1997; Huang and Weiss 2013). Evidence shows that the MYC family member C-Myc (hereafter referred to as MYC) alone may regulate up to 10-15 % of all genes in human cells (Fernandez et al. 2003). High expression of MYCN drives neuroblastoma tumorigenesis in multiple ways. MYCN has been shown to affect a grand number of cancer hallmarks, including the promotion of uncontrolled proliferation, enhanced cell survival and self-renewal, angiogenesis, migration and metastasis formation (Tweddle et al. 2001; Ribatti et al. 2002; van Golen et al. 2003; Kang et al. 2008; Izumi and Kaneko 2012; Huang and Weiss 2013; Matthay et al. 2016). At the same time MYCN is able to block cell cycle exit and repress differentiation (Lasorella et al. 1996; Lasorella et al. 2002).

Physiologically, *MYCN* is highly, but not exclusively, expressed in the developing neural tissues of embryonic and newborn mice (Zimmerman et al. 1986; Laurenti et al. 2008). *MycN* knockout is lethal in mouse embryos (E10.5-E11.5) and MycN and Myc functions have been shown to be highly overlapping, although studies clearly suggest a non-redundant function of MycN in neuronal development (Charron et al. 1992; Sawai et al. 1993; Kenney et al. 2003; Hatton et al. 2006; Huang and Weiss 2013). Notably, the Myc family member C-Myc is known to be required for the maintenance of multipotency in neural crest cells (Bellmeyer et al. 2003; Sauka-Spengler and Bronner-Fraser 2008). Given the partly redundant functions of Myc family members, a similar role of aberrantly expressed *MYCN* in developing neuroblastomas is conceivable, possibly reflected by the finding that *MYCN* amplified tumors commonly display a lower grade of differentiation (Malynn et al. 2000; Cotterman and Knoepfler 2009; Loven et al. 2010; Huang and Weiss 2013). At the same time, earlier studies suggest that *MYCN* expression is required for ventral migration and neuronal differentiation of neural crest cells (Wakamatsu et al. 1997). Yet, mouse models with ectopic expression of *MYCN* in sympathetic precursor cells under the control of the *tyrosine hydroxylase (TH)* promoter clearly underline the oncogenic potential of *MYCN*, as mice developed neuroblastoma with high penetrance, although tumors occurred with significant latency and commonly displayed additional chromosomal alterations (Weiss et al. 1997; Olsen et al. 2017). More recently, the oncogenic potential of ectopic *MYCN* expression was also directly shown in murine neural crest cells (Olsen et al. 2017).

1.1.3 The role of segmental chromosomal copy number alterations and chromosomal translocations

A large number of neuroblastomas are characterized by the occurrence of genomic, as well as recurring segmental chromosomal alterations (Matthay et al. 2016), some of which are strongly associated with disease outcome (see section ***A1.2***). Karyotype analyses, for instance, show that DNA content in aneuploid neuroblastoma tumors can range from near-diploidy to near-tetraploidy, with

near-triploidy and near-diploidy occurring most frequently (Bourhis et al. 1991; Cohn et al. 2009). The most common chromosomal alteration, however, is the gain of the long arm of chromosome 17 (17q) via unbalanced translocation to other chromosomes. Gain of 17q occurs in over 50 % of neuroblastoma cases (Bown et al. 1999; Schleiermacher et al. 2004; Matthay et al. 2016), making it the single most common genetic event in neuroblastoma. Sectional loss of chromosome 1p occurs in up to 35 % of neuroblastoma cases and strongly correlates with *MYCN* amplification in that a high number of *MYCN* amplified tumors also show loss of 1p (Caron et al. 1996; Maris et al. 2001; Brodeur 2003). Another common deletion, which is observed in 35-45 % of neuroblastoma cases, occurs at the long arm of chromosome 11 (11q) (Attiyeh et al. 2005; Mlakar et al. 2017). As with the above described segmental alterations, deletions on 11q correlate with unfavorable disease outcome. In contrast to 17q gain or 1p loss however, 11q deletion displays a strong negative correlation with *MYCN* amplification (Caren et al. 2010) and is considered as an important predictor of poor outcome in *MYCN* non-amplified tumors (Caren et al. 2010; Schleiermacher et al. 2012; Mlakar et al. 2017). Finally, other recurring segmental alterations include gain of 1q, 2p and 14q, as well as loss of 3p and 4p, but they are of lower prognostic impact than the above-described alterations at 17q, 11q or 1p (Schleiermacher et al. 2012; Matthay et al. 2016).

Recurring losses and gains of the above described chromosomal sections suggest the presence of tumor suppressor genes and oncogenes at the respective genetic loci, but as of yet solely responsible gene has been found in the respective chromosomal segments. In case of chromosome 1p, however, evidence suggests the presence of multiple genes with tumor suppressive function, such as *CDH5* (Bagchi et al. 2007), *KIF1B* (Munirajan et al. 2008), *CAMTA1* (Henrich et al. 2011), *CASZ1* (Liu et al. 2011), as well as the micro RNA *mir-34A* (Welch et al. 2007; Wei et al. 2008; Henrich et al. 2012; Matthay et al. 2016).

1.1.4 TERT rearrangements and maintenance of telomeres

Recent evidence suggests that telomere maintenance plays a crucial role in the aggressiveness of high-risk neuroblastomas. Two independent studies have demonstrated that the *TERT* gene locus, which encodes for the reverse transcriptase subunit of the telomerase complex, is frequently translocated to genomic regions that contain strong enhancer elements, causing strong transcriptional activation of the *TERT* gene (enhancer hijacking) (Peifer et al. 2015; Valentijn et al. 2015). *TERT* rearrangements, which were observed in 23 and 31% of high-risk neuroblastomas, respectively, occurred mutually exclusive of *MYCN* amplification and identified a subgroup of aggressive tumors (Valentijn et al. 2015). Notably, *TERT* expression was high in *MYCN* amplified tumors despite the absence of *TERT* translocations, suggesting that telomere maintenance was as well crucial in this subset of high-risk tumors (Peifer et al. 2015).

Intriguingly, a number of high-risk tumors with neither *MYCN* amplification nor TERT rearrangement display alterations in the *ATRX* gene. The RNA helicase ATRX is required for the incorporation of histone variant H3.3 at genomic repeat sequences such as telomeres, leading to their epigenetic silencing (Wong et al. 2010; Udugama et al. 2015), and *ATRX* mutations are known to occur especially in neuroblastoma patients above 18 months of age (Cheung et al. 2012; Cheung and Dyer 2013). ATRX represses a homologous-recombination mediated mode of telomere elongation, known as alternative lengthening of telomeres, in a variety of cancers (Napier et al. 2015). Accordingly, neuroblastomas with ATRX mutations display an abundant number of telomeric repeats (Cheung et al. 2012; Peifer et al. 2015; Valentijn et al. 2015). Taken together, the above described studies suggest that telomere lengthening and maintenance are important features of high-risk neuroblastoma (Nicolai et al. 2015).

1.2 Disease staging and classification

Neuroblastomas rank among the most heterogeneous tumors with regards to course of disease. Observed clinical outcomes range from spontaneous regression, to differentiation to more benign ganglioneuroblastoma or ganglioneuromas, as well as to highly aggressive and metastatic disease with often fatal progression. Despite the unusually high rate of spontaneous regression - up to half of all neuroblastomas arising in the first year of life regress spontaneously -, about 36 % of neuroblastomas present with high-risk features at diagnosis, and survival rates in high-risk patients remain below 50 % despite intensive multimodal therapy (Woods et al. 1996; Schilling et al. 2002; Hero et al. 2008).

The clinical course of neuroblastoma can be partly estimated from tumor size, the extent of surgical resection, as well as metastatic burden at disease diagnosis. This provides the basis for the International Neuroblastoma Staging System (INSS), one of the two most widely used neuroblastoma staging systems (Brodeur et al. 1993; Matthay et al. 2016). Briefly, tumors are categorized into six stages, whereat patients with localized disease (stages 1-3) usually have a better prognosis than dose with metastatic disease (stage 4), with the exception of patients categorized as 4s (Berthold and Hero 2000; Cohn et al. 2009) (***Figure 1***). The International Neuroblastoma Risk Group Staging System (INRGSS) differs from the INSS in that stage is determined from tumor imaging, allowing for staging prior to treatment or surgery, as well as in that anatomical risk factors (so called image-defined risk factors/IDRFs) are included into the staging process. Moreover, children up to 18 months of age are grouped into stage MS, corresponding to stage 4s in the INSS (Monclair et al. 2009) (***Figure 1***).

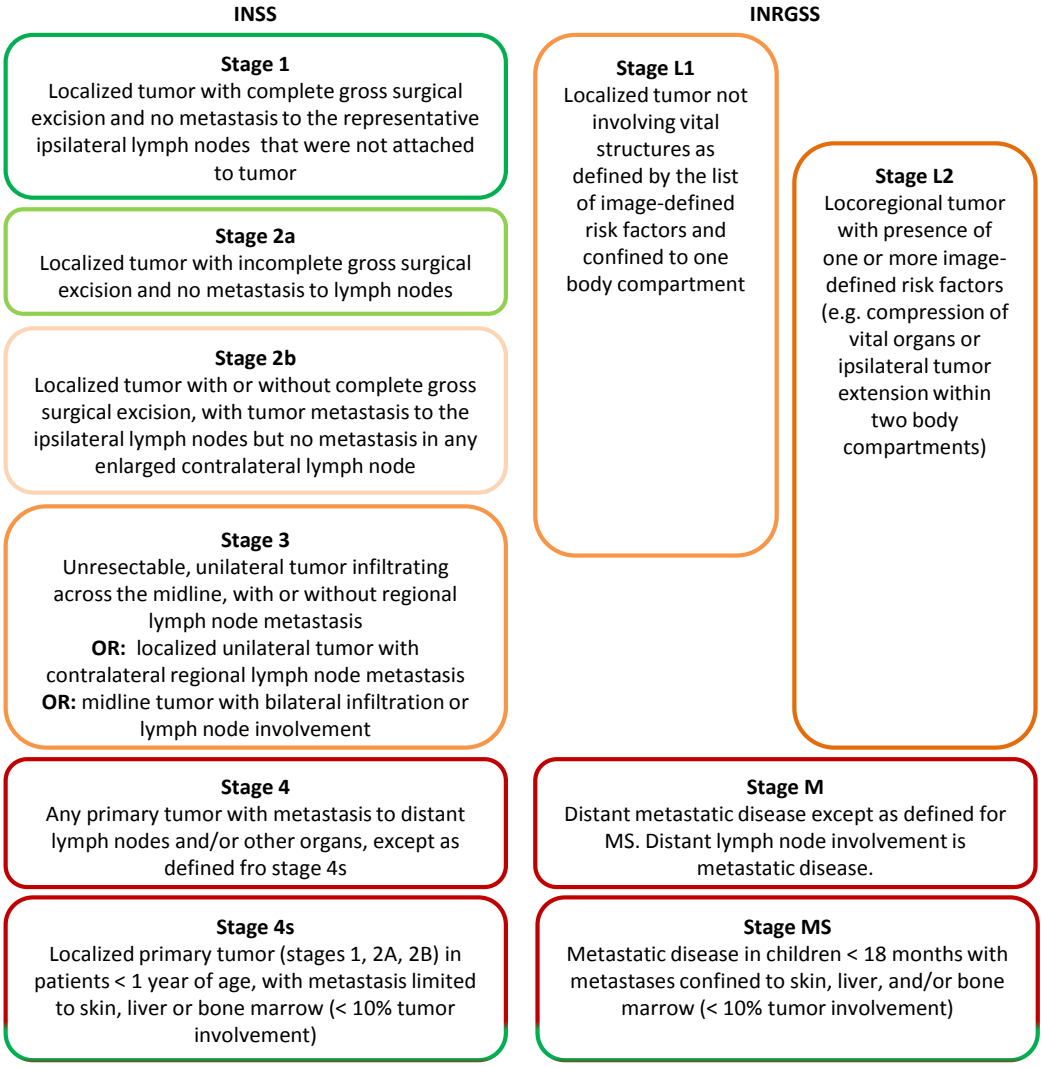

Figure 1: Staging of neuroblastoma according to the International Neuroblastoma Staging System (INSS) and the International Neuroblastoma Risk Group Staging System (INRGSS). *Figure adapted from (Matthay et al. 2016) and (Cohn et al. 2009).*

Finally, INRG classification describes the assignment of patients into pre-treatment risk groups (very low, low, intermediate and high risk) depending on INRGSS stage, as well as the presence or absence of risk factors with proven prognostic impact on clinical outcome, the most important of which will be summarized below (Cohn et al. 2009).

Age at diagnosis is of high prognostic impact in neuroblastoma, as overall survival rates decrease with increasing age of onset. Patients below 18 months of age display better 5-year event-free (82 %) and overall (88 %) survival rates than patients above that age (49 % EFS and 55 % OS) (Cohn et al. 2009; Matthay et al. 2016).

Neuroblastomas can have favorable or unfavorable histopathologic features, depending on the degree of neuroblast maturation, the amount of Schwannian stroma, as well as the mitosis-karyorrhexis index. These parameters, as well as patient age, are basis of the Shimada, or more recently, the International Neuroblastoma Pathology (INPC) classification system, in which stroma-

rich and more differentiated tumors are associated with favorable outcome (Shimada et al. 1984; Shimada et al. 1999; Cohn et al. 2009).

Furthermore, neuroblastomas can have favorable or unfavorable genetic and genomic features. Near-diploidy or tetraploidy, as well as structural chromosomal aberrations like deletions at 11q, 1p or gain of 17q and especially *MYCN* amplification, are associated with unfavorable prognosis (Cohn et al. 2009).

With the increasing availability of high-throughput profiling techniques in recent years, gene expression signatures have proven to be of significant prognostic value in neuroblastoma in various studies (De Preter et al. 2010; Oberthuer et al. 2010; Henrich et al. 2016; van Groningen et al. 2017). Thus, these methods, which enable tumor characterization with unprecedented precision, could become an important tool for neuroblastoma risk stratification in the near future.

1.3 Neuroblastoma prognosis and therapy

Neuroblastoma treatment regimens are dictated by the above described INRG pre-treatment risk stratification strategies and can include observation, surgery, radio- and chemotherapy, autologous hematopoietic stem cell transplantation, as well as immunotherapy and differentiation therapy (Matthay et al. 2016). In case of very low-risk tumors in infants, it is often sufficient to observe tumors without biopsy or surgery, unless tumors show signs of progression (Nuchtern et al. 2012; Matthay et al. 2016). Further standard treatment of low-risk tumors includes surgical removal of the bulk tumor mass, as well as limited chemotherapy in case of symptomatic tumors or tumors that have unfavorable features. Overall, survival rates in this group are excellent, with 99-100% overall survival and > 90 % event-free survival (Strother et al. 2012; Iehara et al. 2013; Matthay et al. 2016).

Intermediate risk tumors are standardly treated with limited cycles of chemotherapy and surgery if possible (Baker et al. 2010; Kohler et al. 2013; Defferrari et al. 2015; Matthay et al. 2016). Radiation therapy can be warranted in case of unresectable, progressing or refractory tumors (Matthay et al. 1998; Baker et al. 2010; Kohler et al. 2013; Defferrari et al. 2015). Overall five-year survival in the intermediate risk group is very good (> 90%), but can be as low as 70 % in children over 18 months of age with unresectable tumors (Matthay et al. 2016).

In contrast, prognosis in high-risk patients remains poor with five-year overall survival rates below 50 %, despite intensive multimodal treatment regimens that include myeloablative chemotherapy and autologous hematopoietic stem cell transplantation (AHSCT), external or ^{131}I-metaiodobenzylguanidine (MIBG)-based radiotherapy, as well as differentiating agents such as 13-cis retinoic acid (Pinto et al. 2015; Matthay et al. 2016). Treatment success of high-risk neuroblastomas is further limited by the occurrence of relapsed tumors in up to 50 % of high-risk patients (Pinto et al.

2015), and survival in relapsed high-risk patients remains exceedingly poor (London et al. 2011; Basta et al. 2016). These poor survival rates, along with the occurrence of often irreversible, therapy-induced, side effects such as hearing loss, impaired growth, infertility and secondary neoplasms clearly highlight the necessity of innovative and more targeted therapy approaches (Matthay et al. 2016).

2 Histone deacetylases (HDACs)

Histone deacetylases (HDACs) are a class of highly conserved enzymes that catalyze the removal of acetyl groups from lysine residues of proteins. Initially named after their first discovered substrate proteins, i.e. histones, it is now clear that histone deacetylases should be more precisely referred to as lysine deacetylases (KDACs), since they have a plethora of non-histone targets and thus affect a multitude of cellular processes apart from gene transcription and chromatin organization (Seto and Yoshida 2014; Scholz et al. 2015)(described in more detail in section ***A2.4***).

2.1 Molecular functions of lysine acetylation

Lysine acetylases and deacetylases are evolutionary highly conserved enzymes. They are found in both prokaryotes and eukaryotes (Kleff et al. 1995; Taunton et al. 1996; Starai et al. 2002; Gardner et al. 2006; Drazic et al. 2016), underlining the importance of lysine acetylation as an essential post-translational protein modification (Zhang et al. 2009a; Drazic et al. 2016). Lysine acetylation occurs on the ε-amino group of lysine residues of proteins and the transfer of the acetyl groups from acetyl-CoA to lysine residues is catalyzed by the family of lysine acetyl transferases (KATS, originally referred to as histone acetyl transferase (HATs)). It is thus a reversible and highly dynamic process, the equilibrium of which is tightly governed by two families of enzymes with opposing enzymatic activity (reviewed in (Yang and Seto 2008a; Witt et al. 2009)).

The best understood consequence of lysine acetylation both in yeast and higher eukaryotes is the modulation of higher genomic structure by reversible acetylation of histone proteins. The genome of eukaryotic cells is condensed into a highly dynamic polymeric structure called chromatin, the conformation and compactness of which depends on the organization of its fundamental repeating unit, the nucleosome (Jenuwein and Allis 2001). Nuleosomes themselves consist of roughly 150 base pairs of DNA that are wrapped around an octamer of four core histone proteins: two histone H2A/ H2B dimers, and a H3/H4 tetramer (Kornberg 1974; McGinty and Tan 2015). The flexible, N-terminal histone tails carry an extensive and reversible set of posttranslational modifications, including acetylation, methylation, ubiquitinylation and sumoylation, which together govern DNA accessibility and transcriptional activity and are often referred to as the "histone code" (Strahl and Allis 2000;

Jenuwein and Allis 2001; Kouzarides 2007). The acetylation state of histones strongly influences the compactness of the chromatin fiber and enables switching between a transcriptionally permissive or a repressive chromatin state, termed euchromatin and heterochromatin, respectively (Shogren-Knaak et al. 2006). Hyperacetylation of histones favors the formation of loosely packed, transcriptionally active euchromatin both by neutralizing positively charged lysine residues, thereby weakening histone interactions with the negatively charged DNA backbone, as well as by weakening intra- and inter-nucleosome interactions (Dorigo et al. 2003; Ye et al. 2005; Tessarz and Kouzarides 2014; Zhang et al. 2017a). Additionally, hyperacetylated histones are known to promote transcription by recruiting bromodomain-containing proteins and transcription factors (Dhalluin et al. 1999; Agalioti et al. 2002; Filippakopoulos and Knapp 2014). In contrast, hypoacetylation of histones is associated with tightly packed heterochromatin that is less accessible to transcription factors and transcriptionally silent.

Acetylation also occurs on proteins other than histones, but the function of non-histone protein acetylation is less well understood (Choudhary et al. 2014; Scholz et al. 2015). Various modes of action have been described, including the blockage of other lysine-specific modifications such as sumoylation or ubiquitinylation, which in turn can affect protein-protein interactions, protein localization or protein stability (Li et al. 2002; Zheng and Yang 2005; Yang and Seto 2008a). Moreover, it can directly alter the affinity of proteins to interacting molecules, including other proteins and DNA (Mujtaba et al. 2004; Friedler et al. 2005), or change the activity of enzymes in case of acetylation of an active site lysine residue (Starai et al. 2002), suggesting that acetylation is a way of fine-tuning the activity of the respective target protein.

2.2 Classification of the human HDAC family

The human HDAC family consists of 18 members. Depending on the co-factor required for their enzymatic function and the catalytic mechanism involved, they are divided into two families: The Zn^{2+}-dependent so called classical HDACs (***Figure 2***) and the NAD^{+}-dependent sirtuins (reviewed in (Seto and Yoshida 2014)). According to sequence homology to their yeast orthologues *Rpd3* and *Hda1,* classical HDACs can be further subdivided into HDAC classes I (HDACs 1, 2, 3 and 8), IIa (HDACs 4, 5, 7, 9), IIb (HDACs 6, 10) and class IV (HDAC11), while the Sir2-related sirtuins are also referred to as class III HDACs (reviewed in (Gregoretti et al. 2004; Yang and Seto 2008b)). In total, the human genome encodes for 11 classical HDACs and seven sirtuins.

Class I is comprised of HDACs 1, 2, 3 and 8, which share a high homology to the yeast histone deacetylase Rpd3 (***Figure 2***). Structurally, they are characterized by an N-terminal deacetylase domain and a C-terminal tail. The latter harbors one or more CK2 phosphorylation sites in case of HDACs 1-3, the phosphorylation of which promotes enzymatic activity and is further important for

complex formation (Pflum et al. 2001; Tsai and Seto 2002; Yang and Seto 2008b). HDACs 1-3 are found in nuclear multiprotein complexes, also termed corepressor complexes due to their repressive impact on transcription. While HDACs 1 and 2 associate with at least three such complexes (Sin3, NuRD and CoREST), HDAC3 seems to be more specifically located in a complex with N-CoR (Nagy et al. 1997; Ayer 1999; Wen et al. 2000; Hakimi et al. 2002; Denslow and Wade 2007; Seto and Yoshida 2014). Collective evidence shows that association with these complexes is required for full enzymatic activity of HDACs 1-3 (Wen et al. 2000; Alland et al. 2002; Boyer et al. 2004; Seto and Yoshida 2014). In contrast, HDAC8 has not been shown to be present in multiprotein complexes, suggesting that it can be enzymatically active in the absence of protein cofactors (Buggy et al. 2000; Wolfson et al. 2013). It lacks C-terminal CK2 phosphorylation sites and is instead negatively regulated by phosphorylation of a PKA phosphorylation site near its N-terminus (***Figure 2***) (Lee et al. 2004). HDAC8 is present in both nucleus and cytoplasm, but deacetylating activity on histones has only been shown in cell-free biochemical assays (Olson et al. 2014; Chakrabarti et al. 2015). Thus, in cells HDAC8 is thought to primarily deacetylate other substrates, such as the cohesin component SMC3 (Deardorff et al. 2012) and the estrogen receptor ERRα (Wilson et al. 2010).

Class II shares a catalytic domain homologous to the deacetylase domain of yeast Hda1, and is subdivided into two subclasses (***Figure 2***). Class IIa members are characterized by a C-terminal deacetylase domain and a long N-terminal section with further protein binding motifs that are not found in yeast Hda1 (Yang and Gregoire 2005; Yang and Seto 2008b). Class IIa members also harbor both nuclear localization (NLS) and export signals (NES) and are thus found both in the nucleus and cytoplasm. Their subcellular localization is governed by MEF2 and 14-3-3 protein binding sites in their N-terminal domain. Like HDACs 1-3, they are primarily thought to act as transcriptional repressors, although their expression seems to be tissue-specific (Parra and Verdin 2010). Moreover, it is still debated whether they require other HDAC members for substrate deacetylation as they have been repeatedly shown to possess low deacetylase activity (Lahm et al. 2007; Jones et al. 2008).

Class IIb members HDAC6 and HDAC10 do not possess an extended N-terminal domain, and are further unique within the HDAC family because they contain two putative enzymatic sites, the second of which is active only in case of HDAC6 (Guardiola and Yao 2002; Kao et al. 2002; Yang and Seto 2008b) (***Figure 2***). They are mainly localized in the cytoplasm and are thus thought to have largely cytoplasmic functions, although context-dependent nuclear localization has been shown for both proteins (Guardiola and Yao 2002; Seto and Yoshida 2014; Yang et al. 2015). While little is known about the function of HDAC10, HDAC6 is primarily known for its function as a deacetylase of α-tubulin (Hubbert et al. 2002). Moreover, HDAC6 is involved in cellular stress responses by modulating HSP90 chaperone function and by promoting aggresome formation and resistance to

proteotoxic stress via its C-terminal, ubiquitin-binding zinc finger domain (Hook et al. 2002; Kawaguchi et al. 2003; Bali et al. 2005).

The sole class IV HDAC member, HDAC11, is unique in that its catalytic domain is homologous to both class I and class II HDACs. Although it is highly conserved (Gao et al. 2002; Seto and Yoshida 2014), little is known about its physiological function apart from its role as a negative regulator of interleukin 10 expression in antigen-presenting cells, suggesting a role for HDAC11 in immune tolerance (Villagra et al. 2009).

Seven members - named SIRT1-7 according to their homology to the yeast deacetylase Sir2 - make up the HDAC class III. They are not classified as classical HDACs due to their dependency on NAD^+ rather than Zn^{2+} as co-factor. Furthermore, they show a diverse pattern of subcellular localization, with SIRT1 and SIRT2 shuttling between nucleus and cytoplasm, SIRT3 being present in nucleus and mitochondria, SIRT4 and SIRT5 being exclusively localized in mitochondria, and SIRT6 and 7 being localized to nucleus and nucleolus, respectively (Seto and Yoshida 2014).

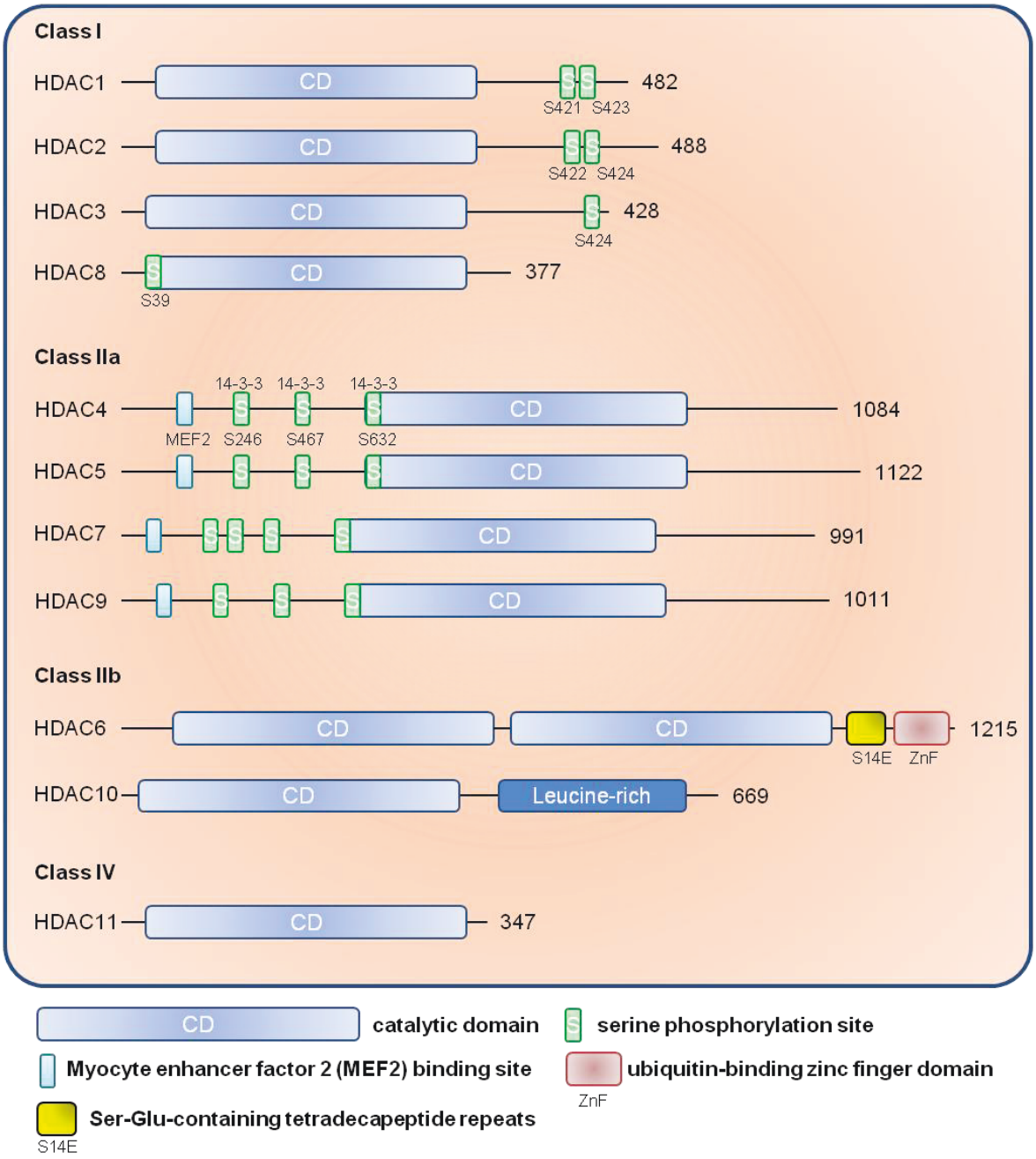

Figure 2: Classification and domain organization of the classical (Zn^{2+}-dependent) human HDACs. *HDACs are grouped into different classes according to their homology to yeast deacetylases Rpd3 (class I) and Hda1 (class II). Class IV member HDAC11 shares homology with both class I and II HDACs. HDACs can have various domains and sites of phosphorylation in their N- and C-terminal domains which regulate their function and localization, or can have additional functions (e.g. in case of the ubiquitin-binding domain of HDAC6). Numbers on the right indicate length in amino acids of the respective HDAC (full-length isoform). Figure was adapted and modified from (Yang and Seto 2008b) and (Seidel et al. 2015).*

2.3 Classical HDACs and their cancer relevant functions

It is becoming increasingly clear that cancer is not only a genetic, but to some degree also an epigenetic disease characterized by widespread epigenetic changes that cause large-scale changes in gene expression (Sharma et al. 2010; Sturm et al. 2014; Yu et al. 2014; Hashizume 2017). Given their

role as important epigenetic modifiers, it is hardly surprising that HDACs have been found to be critically involved in a number of cancer-relevant processes such as proliferation, apoptosis avoidance, angiogenesis, migration and metastasis formation (reviewed in (Witt et al. 2009; Hanahan and Weinberg 2011; Li and Seto 2016)). The activity of histone acetylating and deacetylating enzymes is tightly controlled in non-neoplastic cells, and often becomes deregulated upon malignant transformation. A shift towards aberrant activity of HDACs and the loss of certain histone acetylation marks has been observed in a number of cancers, often caused by deregulated HDAC expression, which is observed more frequently than mutations in HDACs (Yasui et al. 2003; Fraga et al. 2005; Ropero et al. 2006; Witt et al. 2009; Fullgrabe et al. 2011; Ceccacci and Minucci 2016). Increased HDAC activity is associated with increased heterochromatin formation and reduced gene expression. The latter often affects genes that govern cell cycle control, differentiation and apoptosis (Ropero and Esteller 2007; Witt et al. 2009). Nonetheless, the function of HDACs in cancer cannot be reduced to their role as epigenetic modifiers, as they are also known to target non-histone proteins with cancer-relevant functions (discussed below).

The class I HDAC members HDAC1, 2 or 3 have been observed to be overexpressed in a number of cancer entities, including gastric cancer (Choi et al. 2001; Weichert et al. 2008a), colorectal cancer (Weichert et al. 2008b) and prostate cancer (Halkidou et al. 2004). Overexpression in these tumors regularly correlated with poor prognosis, advanced disease stage, apoptosis resistance, increased proliferation, although elevated HDAC1 or HDAC3 expression also have been found to predict better disease-free survival in some tumor entities (Krusche et al. 2005; Zhang et al. 2005; Witt et al. 2009). HDAC2 specifically has been described to contribute to tumor cell survival in both medulloblastoma and neuroblastoma (Lodrini et al. 2013; Ecker et al. 2015). HDAC8, the class I member mainly targeting non-histone proteins, has been demonstrated to be upregulated in advanced stage (INSS stage 4) neuroblastomas, where it correlated with poor survival (Oehme et al. 2009a; Oehme et al. 2009b; Rettig et al. 2015). Mechanistically, class I have been repeatedly linked to cell cycle progression due to their ability to promote the expression of cyclins, while repressing expression of Cyclin-dependent kinase inhibitors such as p21 and p27 in various cancer cell lines (Wilson et al. 2006; Senese et al. 2007; Jung et al. 2012; Xie et al. 2012). HDAC1 has also been associated with increased chemoresistance in neuroblastoma, although a precise mechanism was not described (Buurman et al. 2012). To make matters more complex, tumorsuppressive functions have been reported for HDACs 1 and 2 in pre-tumor stages, which can switch to a tumor promoting function in the same model once tumors have established (Heideman et al. 2013; Santoro et al. 2013). Interference with HDAC8 function in particular has been reported to promote differentiation and cell cycle arrest in neuroblastoma cell lines by inducing p21 and NTRK expression suggesting that some HDACs are specifically involved in the regulation of genes that are required for neuronal or neural

crest cell differentiation (Oehme et al. 2009a; Oehme et al. 2009b; Rettig et al. 2015). This is possibly underlined by the fact that HDAC8 knockout mice show aberrant gene expression patterns in cranial neural crest cells, leading to perinatal mortality due to skull instability and frontocranial dysplasia (Haberland et al. 2009).

Class IIa HDACs 4, 5, 7 and 9 have been reported to be deregulated in a number of cancers, although the mode of action by which they exert their oncogenic function is often unknown. HDAC5 and HDAC9 levels have been shown to be elevated in medulloblastoma subgroups with poor prognosis and interference with HDAC5 or HDAC9 function impaired proliferation and viability of medulloblastoma cell lines (Milde et al. 2010). HDAC5 was also found in other studies to promote tumor cell proliferation and resistance to cell death (Fan et al. 2014; Feng et al. 2014). HDAC7, along with class I member HDAC1, has been reported to be necessary for the maintenance of cancer stem cells in breast cancer (Witt et al. 2017). Notably, HDAC7 was also reported have pro-angiogenic potential by blocking expression of the angiogenesis suppressor AKAP12 in endothelial cells, suggesting that HDAC7 might promote angiogenesis in a tumor setting (Mottet et al. 2007; Turtoi et al. 2012). Another recent study demonstrated that HDAC9 possesses pro-proliferative potential in breast cancer by positively regulating of Sox9 expression (Lapierre et al. 2016).

The role of class IIb HDACs in cancer is not well understood and high expression of these HDACs has been associated with both poor and good prognosis depending on study (Zhang et al. 2004; Sakuma et al. 2006; Oehme et al. 2013a; Jin et al. 2014; Tao et al. 2017; Zhang et al. 2017b). Whether these HDACs possess oncogenic or tumorsuppressive potential might therefore ultimately depend on tumor tissue and tumor environment. Mechanistically, HDAC6 has been described to promote cell motility and epithelial-mesenchymal transition, both of which have been linked to its ability to alter cytoskeletal dynamics via deacetylation of α-tubulin and the F-actin binding protein cortactin, the latter of which is also a direct target of class III HDAC Sirt1 (Hubbert et al. 2002; Shan et al. 2008; Zhang et al. 2009b). Moreover, HDAC6 is known to promote stress response in various disease models. It has been, for instance, described as a master regulator of protein aggregate formation and clearance under proteotoxic stress conditions (Kawaguchi et al. 2003; Boyault et al. 2007; Tran et al. 2007). Here, HDAC6 was shown to bind to unanchored ubiquitin C-termini within protein aggregates via its ubiquitin-binding zinc finger (ZnF) domain, and to promote their retrograde transport along microtubules to the microtubule-organizing center (MTOC), where they are incorporated into aggregate-containing compartments (aggresomes) (Kawaguchi et al. 2003; Ouyang et al. 2012). These aggresomes can then be degraded via autophagy (see section ***A3.2.2***). HDAC6 was also described as a promoter of productive autophagy by enabling autophagosome-lysosome fusion under basal and aggregation-induced autophagy (aggrephagy) conditions, while being dispensable for this process in case of starvation-induced autophagy (Lee et al. 2010b). To add to the complexity, HDAC6 has also

been proposed as a negative regulator of autophagy in one study (Yang et al. 2013). Finally, HDAC6 has emerged as a modulator of cell signaling and as a sensor of cell stress by deacetylating the cellular chaperone HSP90 (Bali et al. 2005; Kovacs et al. 2005). HSP90 chaperone function is known to be required for the function of various oncoproteins, including Bcr-Abl or ERBB2, that act as HSP90 client proteins (Bali et al. 2005; Neckers and Workman 2012). With regards to the fact that tumor cells often display proteotoxic stress due to their exposure to environmental or treatment stress, the above described studies suggest that HDAC6 could be involved in tumor stress resistance. However, a clear anti-tumor effect of HDAC6 inhibition remains to be shown.

The function of the other class IIb member, HDAC10, remains even more enigmatic, since no cellular bona-fide substrate has been described for this enzyme. Moreover, little is known about its interaction partners or the regulation of its function. A study in neuroblastoma suggests, however, that HDAC10 is critically involved in productive autophagy in neuroblastoma cells, where its absence leads to autophagosome accumulation and autophagic flux stop (Oehme et al. 2013a; Oehme et al. 2013b). This study also suggested that the inducible heat shock protein HSP70 could be a target of HDAC10 and that HDAC10 is a mediator of chemoresistance in neuroblastoma.

Only little is known about the cancer-related roles of the only class IV member HDAC11. A few studies, however, show that HDAC11 possesses tumor-promoting potential in neuroblastoma (Deubzer et al. 2013; Thole et al. 2017) and Hodgkin's lymphoma (Buglio et al. 2011).

2.4 Non-histone targets of HDACs

Histone deacetylases have a high number of non-histone targets and should be thus more precisely referred to as lysine deacetylases (KDACs). Examples of HDAC non-histone targets include α-tubulin at lysine 40, which is a target of HDAC6, as well p53, which has been shown to be a substrate of HDAC 1 and SIRT1 (Luo et al. 2000; Vaziri et al. 2001). Moreover, transcription factors like the NF-κB subunit RelA or STAT3 have been described as HDAC targets, suggesting that HDACs alter transcription not only on the level of histone acetylation (Greene and Chen 2004; Gupta et al. 2012). In fact, proteomics approaches suggest that lysine acetylation is abundant on non-histone proteins and that inhibition of classical HDACs increases acetylation at as many as 10 % of identified acetylation (Choudhary et al. 2009).

More recently, HDACs have also emerged as important regulators of cellular stress, which is partly mediated by their ability to reverse acetylation on heat shock proteins HSP70 and HSP90 (see following section).

2.4.1 Heat shock proteins (HSPs) as HDAC targets

A number of recent studies have identified heat shock proteins as potential HDAC targets. Heat shock proteins are highly conserved proteins that are found in all living organisms (Ashburner and Bonner 1979; Ingolia et al. 1982; Hunt and Morimoto 1985; Lindquist 1986; Li and Srivastava 2004). Their expression is induced by various stress stimuli including hypoxia, UV light, toxins, inflammation, and high temperature (reviewed in (Lindquist and Craig 1988; Ritossa 1996; Santoro 2000)). Heat shock proteins that help other proteins to achieve and stabilize their functional three-dimensional conformation are also called chaperones (Ellis 1987). Chaperones and their cofactors are organized in large cooperative networks and are essential in the processes of nascent protein folding, as well as in the refolding of denatured proteins, the prevention of protein aggregation, the maintenance of folded proteins in their functionally active conformation and the assembly of oligomeric complexes. Furthermore, they assist in protein trafficking and degradation (reviewed in (Hartl et al. 2011)). Chaperones are broadly grouped into six conserved families according to their molecular weight in kilodaltons: small HSPs (12-43 kDa), HSP40, HSP60 (chaperonins) HSP70, HSP90 and HSP110 (reviewed in (Schlesinger 1990; Hartl et al. 2011; Bakthisaran et al. 2015)). Of these, especially members of the HSP70, the HSP90 and the HSP60 family play a major role in protein folding (Langer et al. 1992; Frydman et al. 1994; Hartl et al. 2011). Although the mode of protein folding differs between these chaperones, they commonly recognize and bind to hydrophobic residues exposed to the surface of unfolded or misfolded proteins and promote protein folding by repeating substrate binding and release cycles that are driven by cycles of ATP binding and hydrolysis (Flynn et al. 1989; McCarty et al. 1995; Theyssen et al. 1996; Prodromou et al. 2000; Meyer et al. 2003a; Hartl et al. 2011; Mayer 2013). Given their central importance in numerous cellular stress responses, it is hardly surprising that aberrant chaperone expression and function have been associated with a variety of diseases, including cancer (reviewed in (Ciocca and Calderwood 2005; Rappa et al. 2012; Lindberg et al. 2015)). Apart from their transcriptional regulation, chaperone function is highly controlled at the posttranslational level, e.g. by binding of various cofactors and by posttranslational modifications such as phosphorylation, sumoylation, ubiquitination, glycosylation and acetylation (reviewed in (Scroggins and Neckers 2007; Cloutier and Coulombe 2013)). In this context, especially members of the chaperone classes HSP90 and HSP70 have been repeatedly reported to be modified by lysine acetylation and to be targeted by HDACs.

HSP90s are a very prominent example of regulation of chaperone activity by acetylation. They consist of three well-defined structural domains: a highly conserved N-terminal nucleotide binding domain responsible for ATP-binding and hydrolysis, a middle domain which binds client proteins and is also required for ATP hydrolysis, and a highly conserved C-terminal dimerization domain that also recruits cochaperones (Minami et al. 1994; Prodromou et al. 1997; Meyer et al. 2003b; Ali et al. 2006; Hartl

et al. 2011). HSP90s commonly work as dimers downstream of HSP70 and promote folding, refolding, as well as structural maturation and maintenance of client proteins, many of which are critically involved in cellular signal transduction (reviewed in (Taipale et al. 2010; Hartl et al. 2011)). Collective evidence suggests that HDAC6 acts as the main HSP90 deacetylating enzyme (Bali et al. 2005; Kovacs et al. 2005; Murphy et al. 2005; Scroggins et al. 2007; Yang et al. 2008; Kekatpure et al. 2009), although class I HDACs have been also proposed to deacetylate HSP90 (Nishioka et al. 2008; Zhou et al. 2008). Reversible acetylation of HSP90 modulates major HSP90 functions including its chaperone activity and binding to cochaperone p23 (Kovacs et al. 2005), activation of HSP90-dependent proteins (Bali et al. 2005; Scroggins et al. 2007; Yang et al. 2008; Kekatpure et al. 2009), as well as stability of such client proteins (Rao et al. 2008).

HSP70 possesses two major functional domains: an N-terminal ATPase domain and a C-terminal substrate binding domain, which can be sub-divided into a β-sandwich subdomain and an α-helical lid segment (Flaherty et al. 1990; Zhu et al. 1996; Hartl et al. 2011). In its ATP bound open conformation, HSP70, with the help of its cochaperone HSP40, binds to stretches of exposed hydrophobic amino acids of incorrectly folded proteins and helps to prevent their aggregation (Flynn et al. 1991; Cyr et al. 1992; Rudiger et al. 1997). ATP hydrolysis, which is assisted by HSP40, closes the α-helical lid of the substrate binding domain and stabilizes the substrate-chaperone interaction, while ADP dissociation and subsequent binding of a new ATP molecule result in substrate release and recycling (Ha and McKay 1995; McCarty et al. 1995; Theyssen et al. 1996; Mayer 2010; Hartl et al. 2011). Notably, HSP70 is known to work in a complex with or transfer partially folded substrates to other chaperones such as HSP90 for final maturation or to chaperonins (TRiC/CCT in eukaryotes) in case of unsuccessful folding (Langer et al. 1992).The human HSP70 family consists of thirteen members, which mainly differ in subcellular localization and stress inducibility. The constitutively expressed HSC70 (HSPA8) acts as housekeeping chaperone in the nucleus and cytoplasm (Ingolia and Craig 1982; Chappell et al. 1986; Beckmann et al. 1990; Daugaard et al. 2007b), while HSP70 family members HSPA1A and HSPA1B (below referred to as HSP70) are expressed when cells are exposed to stress stimuli such as hyperthermia or upon malignant transformation (Wu et al. 1985; Tavaria et al. 1996; Murphy 2013). HSPA5 (GRP78/BiP) is restricted to the ER lumen where it is responsible for protein translocation and quality control and acts as a critical sensor of ER stress and response regulator of the unfolded protein response (Haas and Wabl 1983; Munro and Pelham 1986; Ting and Lee 1988; Hamman et al. 1998; Bertolotti et al. 2000; Harding et al. 2002). Another member, called GRP75 or mtHSP70, is located in the mitochondrial matrix (Domanico et al. 1993; Bhattacharyya et al. 1995; Daugaard et al. 2007b). Expression of HSP70 is induced by application of HDAC inhibitors via epigenetic mechanisms, although the main heat shock response mediating transcription factor HSF1 requires deacetylation of lysine 80 by class III HDAC SIRT1 in order to promote expression of HSPs

(Zhao et al. 2006; Westerheide et al. 2009). At the same time, a small number of studies suggest that HSP70 function is also directly modulated by HDACs. HSP70 was hyperacetylated after treatment of human leukemia cells with pan-HDAC inhibitors (Rao et al. 2008). In a follow-up study, it was shown that six lysine residues (K88, K126, K159, K523, K558 and K560) were differentially acetylated after panobinostat treatment. Based on previous studies, the authors suggested HDAC6 as the major deacetylase of HSP70 (Rao et al. 2008; Yang et al. 2008; Yang et al. 2013). Functionally, acetylation of HSP70 lysine 159 was crucial for induction of autophagy (see section ***A3.2.2***) in breast cancer cells, where it facilitated formation of the autophagosome-inducing Beclin-1-Vps34 complex. The same group also proposed the ER-resident GRP78 as a target of HDAC6 (Rao et al. 2010). Here, the authors showed that acetylation of GRP78 on lysine 11 leads the dissociation partner of GRP78 from its ER interaction partner PERK, thereby triggering a lethal unfolded protein response (UPR) in human breast cancer cell lines. At the same time, another study suggests that HDAC10 potentially deacetylates HSP70 and that hyperacetylated HSP70 might impair lysosomal function (Oehme et al. 2013a). Acetylation of HSP70 at lysine 11 has also been reported and acetylation at this site switched HSP70 function from promoting protein folding to promoting their degradation. HSP70 was acetylated by the acetyl transferase ARD1 early during stress response, while being deacetylated by HDAC4 at later stages. Differential acetylation was associated with changes in cochaperone binding. The cochaperone HOP, which promotes the protein folding function of HSP70, was found to bind to acetylated HSP70, while deacetylated HSP70 bound to the co-chaperone CHIP that mediates ubiquitinylation and elimination of HSP70 targets (Seo et al. 2016).

Other HSP family members have been reported to be modulated by lysine acetylation including HSP10 (Lu et al. 2015) and HSP20 (Karolczak-Bayatti et al. 2011). Moreover, DNAJB8, a member of the HSP40 family that act as HSP70 cochaperones, interacts with HDACs 4, 6, and SIRT2, which deacetylate two C-terminal lysine residues. This was shown to be critical for the prevention of toxic polyglutamine protein aggregation and the accumulation of other misfolded proteins (Hageman et al. 2010).

2.4.2 Polyamines as potential targets of HDAC10

The recently published crystal structure of zebrafish HDAC10 suggests that HDAC10, due to its sterically constricted active site, is a polyamine rather than a lysine deacetylase (Hai et al. 2017). Polyamines are small, polycationic alkylamines, three of which - spermidine, spermine and putrescine - occur naturally in all living organisms with cellular concentrations in the millimolar range (Tabor and Tabor 1984; Casero and Marton 2007). Polyamines are essential in both prokaryotic and eukaryotic cells and their biosynthesis, transport and catabolism are tightly regulated (***Figure 3a***) (Casero and Marton 2007). Due to their cationic nature, they bind to anionic cellular macromolecules, and they

have been implicated in a number of physiological processes such as the structural maintenance of DNA and chromatin, protein synthesis, autophagy, the regulation of ion channels, as well as the scavenging of free radicals (Williams 1997; Das and Misra 2004; Casero and Marton 2007; Eisenberg et al. 2009; Park et al. 2010; Mandal et al. 2013; Baronas and Kurata 2014; Pasini et al. 2014). At the same time, their biosynthesis and metabolism have frequently been shown to be deregulated in a number of diseases including cancer (Casero and Marton 2007).

Polyamine synthesis critically depends on the activity of two rate-limiting enzymes, namely ornithine decarboxylase (ODC-1), which generates putrescine from ornithine, and S-adenosylmethionine decarboxylase (AdoMetDC), which converts S-adenosylmethionine to S-adenosylmethioninamine (Stanley et al. 1989; Pegg 2006). The latter intermediate provides the aminopropyl residue for the sequential synthesis of spermidine and spermine from putrescine by spermidine synthase and spermine synthase, respectively (Wahlfors et al. 1990; Korhonen et al. 1995). In the catabolic process, spermine and spermidine are degraded by the sequential action of two enzymes to spermidine and putrescine, respectively. First, they are acetylated at their respective N^1 position by spermidine/spermine N^1-acetyltransferase (SSAT) that transfers an acetyl group from acetyl-CoA to the respective polyamine (Casero and Pegg 1993). In a second step, N^1-acetylated spermine or spermidine are cleaved to spermidine and putrescine, respectively, by the peroxisomal enzyme N^1-acetylpolyamine oxidase (APAO) under the generation of 3-aceto-aminopropanal and H_2O_2 (Vujcic et al. 2003). Notably, spermine can also be directly cleaved to spermidine by the enzyme spermine oxidase (SMO) (Vujcic et al. 2002; Wang et al. 2003). Polyamines are both taken up and secreted by cells via a specific polyamine transport system, but this system remains incompletely characterized (Palmer and Wallace 2010; Uemura and Gerner 2011). However, one identified polyamine transporter, SLC3A2, was shown to specifically export N^1-acetylated polyamines (Uemura et al. 2008). In eukaryotic cells, spermidine can be also acetylated at its N^8 position by a nuclear enzyme, yielding N^8-acetyl spermidine (***Figure 3b***) (Libby 1980). N^8-acetyl spermidine can be processed back to spermidine by a cytoplasmic polyamine deacetylase (PDAC), and HDAC10 has been recently suggested as that PDAC (Blankenship 1978; Libby 1980; Hai et al. 2017). Based on the crystal structure from zebrafish HDAC10, the study demonstrated that HDAC10 harbors a conserved glutamate residue near its active site, which is not present in other HDACs and acts as a gatekeeper. Along with the sterically constricted active site of HDAC10, this gatekeeper was suspected to confer high specificity for positively charged acetylpolyamine substrates, or more specifically N^8-acetylspermidine. Subsequent biochemical analyses with recombinant human and zebrafish HDAC10 demonstrated that HDAC10 had high PDAC and low lysine deacetylase activity. However, the cellular function of N^8-acetylspermidine or the extent to which this spermidine derivative is present in cells remains unknown.

Importantly, the rate-limiting enzyme of polyamine synthesis, ODC-1, has been shown to be a direct transcriptional target of MYC transcription factors, including MYCN in neuroblastoma (Hogarty et al. 2008). Subsequent studies have shown that polyamine metabolism is often severely deregulated in high-risk neuroblastoma cases, and high ODC-1 expression was shown to be associated with poor outcome independently of *MYCN* amplification (Hogarty et al. 2008; Gamble et al. 2012). In various models, polyamines contribute to tumorigenicity by suppressing apoptosis (Singh et al. 2000; Babbar et al. 2003), increasing cell proliferation (Singh et al. 2000), as well as by promoting protein translation (Mandal et al. 2013), angiogenesis (Takigawa et al. 1990) and possibly autophagy (Eisenberg et al. 2009). Consequently, inhibitors that target polyamine metabolism and transport are attractive for anti-cancer therapy (Samal et al. 2013; Evageliou et al. 2016). Polyamine synthesis inhibitors, such as the ODC-1 inhibitor difluoromethylornithine (DMFO) have been repeatedly tested in clinical trials (NCT02139397; NCT03536728) in a variety of cancers including neuroblastoma, most recently also in combination with polyamine import inhibitors such as AMXT-1501 (Abeloff et al. 1984; Abeloff et al. 1986; Meyskens et al. 1986; Saulnier Sholler et al. 2015).

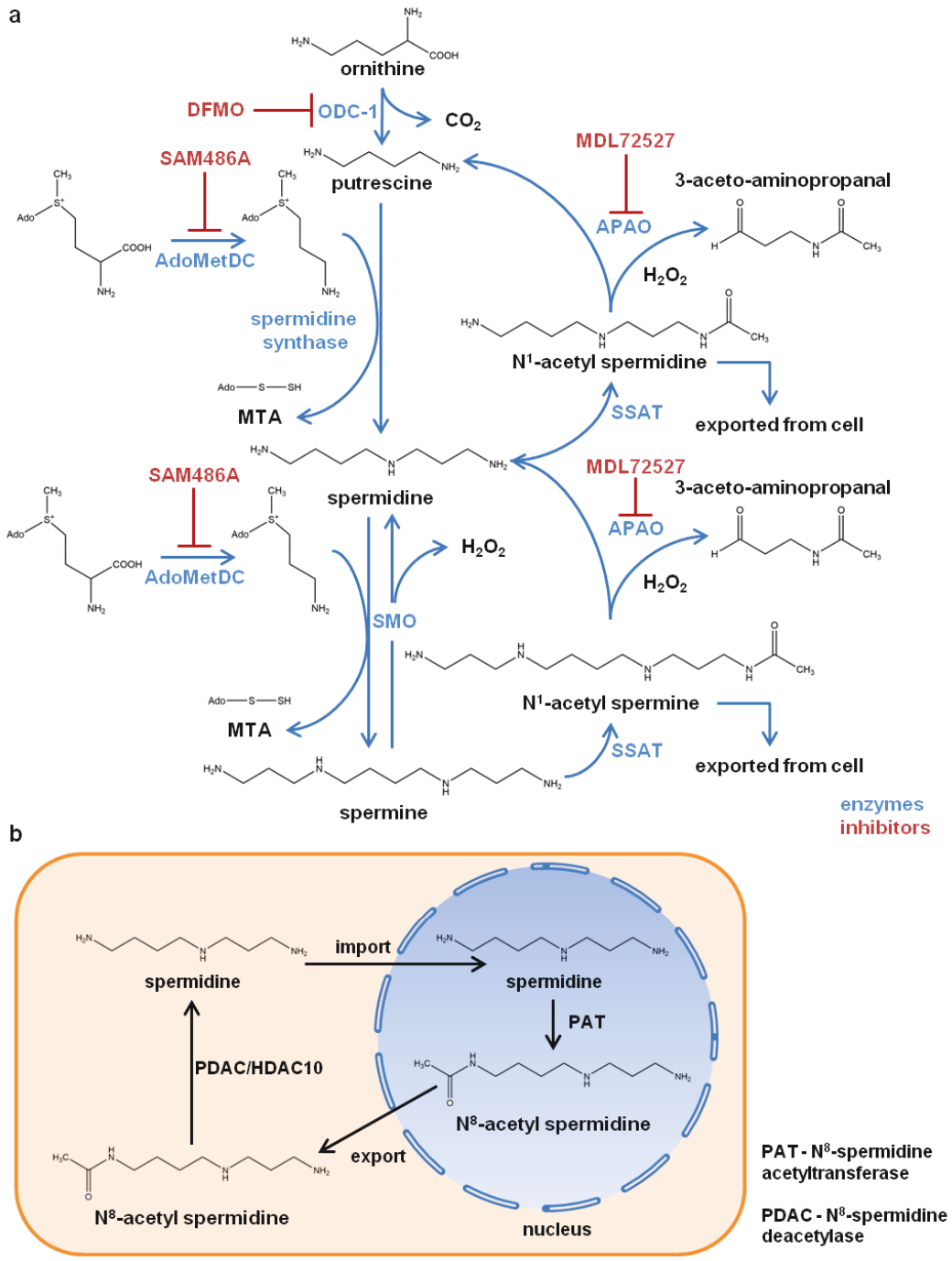

Figure 3: Synthesis and metabolism of polyamines. (a) *Ornithine decarboxylase (ODC-1) is the rate limiting enzyme of putrescine synthesis, while S-adenosylmethionine decarboxylase (AdoMetDC) provides the aminopropyl residue for the sequential synthesis of spermidine and spermine by converting the S-adenosylmethionine to S-adenosylmethioninamine. Spermidine/spermine N^1-acetyltransferase (SSAT) acetylates polyamines at their N^1 position and N^1-acetylated polyamines are then converted by the peroxisomal enzyme N1-acetylpolyamine oxidase (APAO) under the generation of 3-aceto-aminopropanal and H_2O_2). Spermine can also be directly cleaved to spermidine by the enzyme spermine oxidase (SMO).* ***(b)*** *In eukaryotic cells, spermidine can be also acetylated at its N^8 position by a nuclear acetyltransferase, yielding N^8-acetylspermidine. N^8-acetylspermidine can be processed back to spermidine by a cytoplasmic polyamine deacetylase (PDAC), and HDAC10 has been recently suggested as that PDAC. Figure (a) was adapted from (Casero and Marton 2007), figure (b) (Hai et al. 2017).*

2.5 HDAC inhibitors

Given their excellent druggability and critical importance in pathways that are relevant to the development of cancers and other diseases, HDACs have become an attractive target for clinical intervention and pre-clinical drug research (Witt et al. 2009). The initial discovery that trichostatin A (TSA) - a compound later found to be a broad-spectrum HDAC inhibitor - had anti-proliferative effects in transformed rat fibroblasts, triggered an enormous amount of follow-up research, ultimately leading to the discovery of numerous other substances with HDAC inhibitory capacity (Yoshida and Beppu 1988; Yoshida et al. 1990; Finnin et al. 1999; Sternson et al. 2001; Khan et al. 2008). Although these inhibitors share a common mode of action - namely the chelation of Zn^{2+} at the HDAC active site -, they are nevertheless chemically diverse and can be grouped into five classes according to the chemical structure of their zinc-binding group: Hydroxamic acids, cyclic tetrapeptides, ortho-aminoanilides (such as benzamides), aliphatic carboxylic acids and electrophilic ketones (***Figure 4***) (Wagner et al. 2013). Most HDAC inhibitors commonly have three structural features: The aforementioned zinc-binding group, a hydrophobic cap group which interacts with the surface of the target enzyme, and a non-mandatory hydrocarbon linker group (Wagner et al. 2013). Many of these substances inhibit HDACs rather unselectively and are therefore referred to as broad-spectrum (SAHA/vorinostat, trichostatin A) or pan-HDAC (panobinostat, abexinostat (PCI-24781)) inhibitors (Balasubramanian et al. 2008; Witt et al. 2009; Wagner et al. 2013). However, some inhibitors display a marked preference for a certain HDAC class, or even individual HDAC enzymes. These include for example class I HDAC inhibitors (e.g. entinostat (MS-275), valproic acid), as well as class IIb HDACs inhibitors, such as tubastatin A (Butler et al. 2010; Oehme et al. 2013a), bufexamac (Bantscheff et al. 2011) and tubacin (Haggarty et al. 2003; Bantscheff et al. 2011), the latter displaying a very high preference for HDAC6. Another example of a highly selective HDAC inhibitor is PCI-34051 which inhibits HDAC8 but not HDACs 1, 2, 3, 6 and 10 (Balasubramanian et al. 2008).

Five HDAC inhibitors have been approved to date for the treatment of hematological malignancies, four of which are FDA-approved (vorinostat, romidepsin, belinostat and panobinostat). Vorinostat and romidepsin are used for the treatment of cutaneous T-cell lymphoma, chidamide and belinostat for peripheral T-cell lymphoma and panobinostat for multiple myeloma (Mann et al. 2007; Piekarz et al. 2009; Whittaker et al. 2010; Poole 2014; Cheng et al. 2015; Laubach et al. 2015; Shi et al. 2015). Moreover, more than 20 HDAC inhibitors are currently tested in clinical trials, but all approved and most of the tested HDAC inhibitors are either broad-spectrum, pan- or class I selective HDAC inhibitors (Mottamal et al. 2015; Eckschlager et al. 2017). Clinical application of these inhibitors is commonly associated with severe dose-limiting side effects including gastrointestinal symptoms (anorexia, nausea, vomiting and diarrhea), myelosuppression (e.g. thrombocytopenia) and fatigue (Lane and Chabner 2009), possibly related to the fact that HDACs 1, 2, 3 epigenetically control the

expression of thousands of genes due to their presence in co-repressor complexes. This raises the question whether inhibition of individual HDACs by more selective compounds could be favorable in a clinical setting (Witt et al. 2009).

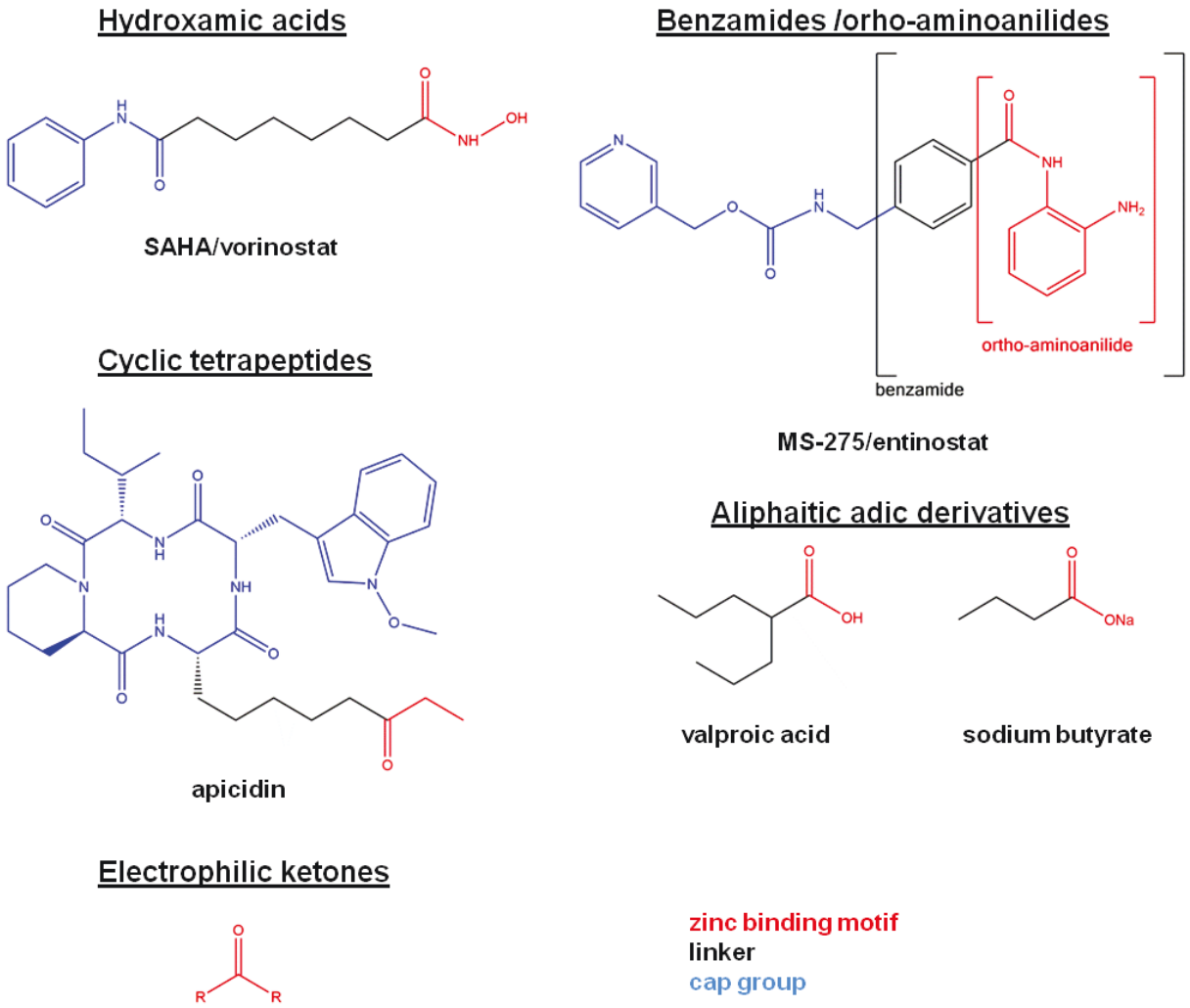

Figure 4: HDAC inhibitor classes and their molecular structure. *Figure adapted from (Wagner et al. 2013)*

3 Mechanisms of cancer drug resistance

Resistance to both cytotoxic and targeted treatment is still a major factor that limits therapy success in cancer. Many cancers are responsive to initial treatment but develop resistance through a variety of mechanisms. Such resistance mechanisms can be either intrinsic, i.e. resistance-mediating factors that are inherent to the bulk tumor cells before treatment, or acquired, meaning that resistance develops during treatment for instance by the acquisition of mutations or other adoptive responses (reviewed in (Longley and Johnston 2005; Holohan et al. 2013)). Moreover, resistance can be induced by the selection of therapy-resistant cell clones that pre-exist in the highly heterogeneous tumor microenvironment (Holohan et al. 2013). At the cellular level, such resistance mechanisms include the deregulation of apoptotic pathways (Miyashita and Reed 1992; Debatin and Krammer 2004;

Wilson et al. 2009; Ni Chonghaile et al. 2011), the presence of cancer stem cells (Singh and Settleman 2010), alterations in drug metabolism or mutations in drug targets (Kobayashi et al. 2005; Housman et al. 2014), increased DNA repair capacity (Bouwman and Jonkers 2012), activation of alternative or bypass signaling pathways (Engelman et al. 2007; Sergina et al. 2007), upregulation of resistance promoting stress responses such as autophagy (White 2012), as well as decreased drug uptake and increased drug efflux (Gottesman et al. 2002). Many of these resistance mechanisms have also been shown to be important in neuroblastoma treatment resistance (Keshelava et al. 2000; Michaelis et al. 2009; Khalil et al. 2012; Bresler et al. 2014; Murakami-Tonami et al. 2016; Bingel et al. 2017).

3.1 Drug efflux as a mechanism of cancer drug resistance

Cancer cells can reduce accumulation of cytotoxic drugs by increasing their efflux. Drug efflux is one of the most widely studied resistance mechanisms in cancer and has been largely attributed to the presence of ATP-dependent drug efflux pumps that belong to the ATP-binding cassette (ABC) transporter family (Gottesman et al. 2002). In humans, this family comprises 49 members, characterized by a highly conserved nucleotide binding domain and the presence of a more variable transmembrane domain in almost all of its members, which is also responsible for substrate recognition (reviewed in (Vasiliou et al. 2009; Housman et al. 2014)). Hydrolysis of ATP in the NBD induces a conformational change which allows for the transport of substrate across membranes against a concentration gradient (Sauna and Ambudkar 2001). ABC transporter substrates include a variety of different molecules including peptides, amino acids, sugars, as well as metal ions and a large number of hydrophobic compounds (Vasiliou et al. 2009). Apart from their physiological role, transporters, especially when present at high levels, have been associated with drug resistance in cancer, and three ABC transporters have been particularly well studied with respect to cancer drug resistance: multidrug resistance protein 1/ P-glycoprotein (MDR1/P-gp), multidrug resistance-associated protein (MRP1) and breast cancer resistance protein (BCRP/ABCG2) (reviewed in (Vasiliou et al. 2009; Robey et al. 2018)). These transporters recognize and drive efflux of a broad and partly overlapping set of substrates that include many first line cancer therapeutics including vinca alkaloids, anthracyclines, taxanes but also kinase inhibitors and thus promote to a plethora of anti-cancer drugs (Gros et al. 1986; Ueda et al. 1987; Szakacs et al. 2006; Dohse et al. 2010; Holohan et al. 2013; Housman et al. 2014). This phenomenon is also referred to as multidrug resistance (MDR). Not surprisingly, high expression of either of these transporters has been repeatedly linked to poor prognosis in various cancer entities including neuroblastoma (Filipits et al. 1999; Baekelandt et al. 2000; Steinbach et al. 2002; Haber et al. 2006; Vasiliou et al. 2009).

3.2 Lysosomes as mediators of drug resistance

Lysosomes are membrane-bound cytoplasmic organelles with an acidic lumen. Originally described by Belgian scientist Christian de Duve in 1955 (De Duve et al. 1955; De Duve and Beaufay 1959; de Duve 2005), they exist in all eukaryotic cells, although size and numbers vary between cell types (Perera and Zoncu 2016). Although lysosomes are the primary catabolic compartment in eukaryotic cells, an ever increasing body of evidence suggests that they are also critical regulators of cell homeostasis. They act as central cellular signaling hubs, controlling essential processes like cell proliferation(Stoscheck and Carpenter 1984), nutrient sensing, cell metabolism, stress response, organelle turnover and even cell death (Stoscheck and Carpenter 1984; Boya et al. 2003; Sancak et al. 2008; Zoncu et al. 2011; Kallunki et al. 2013). Not surprisingly, mutations in key lysosomal genes that impair lysosomal function are the cause of hereditary metabolic syndromes commonly referred to as lysosomal storage disorders (reviewed in (Platt et al. 2012)). In contrast to impaired lysosomal degradation capacity, efficient lysosomal function is reported to be important for the maintenance of multiple cancer hallmarks, such as evasion of cell death, deregulated cellular metabolism and even invasion and metastasis (Hanahan and Weinberg 2011; Appelqvist et al. 2013; Machado et al. 2015).

3.2.1 Lysosomal biogenesis and homeostasis

Lysosomes are highly dynamic organelles of heterogeneous size and cellular distribution, which can be identified by a set of hallmark features: They are electron-dense organelles surrounded by a single 7-10 nm phospholipid bilayer membrane that contains heavily glycosylated membrane proteins. Lysosomes are further characterized by their acidic luminal pH between 4.5 and 5.0 and their lack of mannose-6-phosphate receptors, the latter of which distinguishes them from the late endosomal compartment (reviewed in (Mullins and Bonifacino 2001; Mindell 2012)). In metazoan cells, the lysosomal diameter ranges from 0.1 µm to 1 µm under physiological conditions, but enlarged lysosomes are common under disease settings such as LSDs (Durchfort et al. 2012; Perera and Zoncu 2016). Lysosomes are usually found close to the nucleus in proximity to microtubule-organizing center (MTOC) (Matteoni and Kreis 1987) but changes in lysosomal position have been described upon cell stimulation, maturation, as well as malignant transformation (Nishimura et al. 2003; Stinchcombe et al. 2006; Korolchuk et al. 2011; Mrakovic et al. 2012; Willett et al. 2017).

The biogenesis of lysosomes is not fully understood, but it is commonly thought that lysosomes arise from fusion and maturation events of at least two pools of vesicles or vesicular compartments, namely *trans*-Golgi network derived vesicles and cargo-filled vesicular compartments such as late endosomes or autophagosomes (***Figure 5***) (Mullins and Bonifacino 2001; Luzio et al. 2003; Saftig and Klumperman 2009; Perera and Zoncu 2016). Thereby, at least three routes can be distinguished by which membranes and macromolecules are delivered to the lysosomal compartment, namely the

biosynthetic route, the endocytic route (including phagocytosis) and the auto-catabolic route of (macro-)autophagy, the latter of which will be discussed in more detail in section ***A3.2.2*** (Luzio et al. 2003). The biosynthetic route starts with the *de novo* synthesis of lysosomal proteins into the endoplasmic reticulum (ER), where they are processed and undergo N-glycosylation. After export to the Golgi apparatus and trimming of glycosylation, many but not all soluble lysosomal proteins, carry an exposed mannose-6-phosphate sugar which is recognized by so called Mannose-6-phosphate receptors (MPRs) at the *trans*-Golgi that promote packing of lysosomal enzymes into *trans*-Golgi network vesicles (Kaplan et al. 1977; Ullrich et al. 1978; Fedde and Sly 1985). Upon fusion of these vesicles with the slightly acidic late endosome, the enzymes dissociate from their receptors and the receptors are recycled to the Golgi, whereas the enzymes continue their way to the lysosome (Griffiths et al. 1988).

At the same time extracellular, as well as plasma membrane bound cargo, is delivered to lysosomes through various modes of endocytosis (Luzio et al. 2003). In the endocytic route, cargo passes through a continuum of intermediate organelles that undergo a maturation process associated with changes in morphology, lipid and protein composition, as well as gradual acidification of the involved organelles. Both early and late endosomes act as sorting stations that separate cargo receptors and cargo destined for recycling or degradation (Mayor et al. 1993; Jovic et al. 2010). While early endosomes are tubular in shape and located near the cell periphery, late endosomes are more spherical in shape and are located closer to the nucleus (reviewed in (Gruenberg and Stenmark 2004; Klumperman and Raposo 2014)). During the maturation to late endosomes, cargo destined for degradation is also, with the help of so called ESCRT complexes that recognize mono-ubiquitinated proteins, sorted into so called intra-luminal vesicles (ILVs), that give late endosomes their characteristic multivesicular appearance (Estable et al. 1957; Katzmann et al. 2001; Gruenberg and Stenmark 2004; Takahashi et al. 2015). The latter is the reason why late endosomes are often referred to as multivesicular bodies (MVBs) (Estable et al. 1957). While maturation of endosomes is the most likely mode of cargo trafficking through the endosomal system, exchange of cargo between endosomes and lysosomes is mainly achieved by transient fusion and fission processes, termed "kiss and run" (Storrie and Desjardins 1996), and, in some instances, complete fusion processes between endosomes and lysosomes (Mullock et al. 1998; Gan et al. 2009). Complete fusion events of lysosomes and late endosomes lead to the formation of hybrid organelles called endolysosomes, which likely are the primary compartment of macromolecule degradation (Mullock et al. 1998; Luzio et al. 2003; Luzio et al. 2014; Bright et al. 2016). Lysosomes are constantly regenerated from these hybrid organelles by tubulation, maturation and condensation processes in which endosomal membrane proteins are removed (Pryor et al. 2000; Yu et al. 2010; Bright et al. 2016). Lysosomes are thus considered as storage organelles for hydrolytic enzymes that can fuse with endosomes to

generate transient endolysosomal organelles (Bright et al. 2005; Luzio et al. 2007; Jahreiss et al. 2008; Bright et al. 2016). The biosynthetic intersects the endocytic route at various stages, highlighted by the delivery of membrane proteins, which can be trafficked to lysosomes directly and indirectly. On the indirect route, these proteins first enter the secretory route, leading to their presence at the plasma membrane, from where they are delivered to lysosomes via the endocytic route (Luzio et al. 2014).

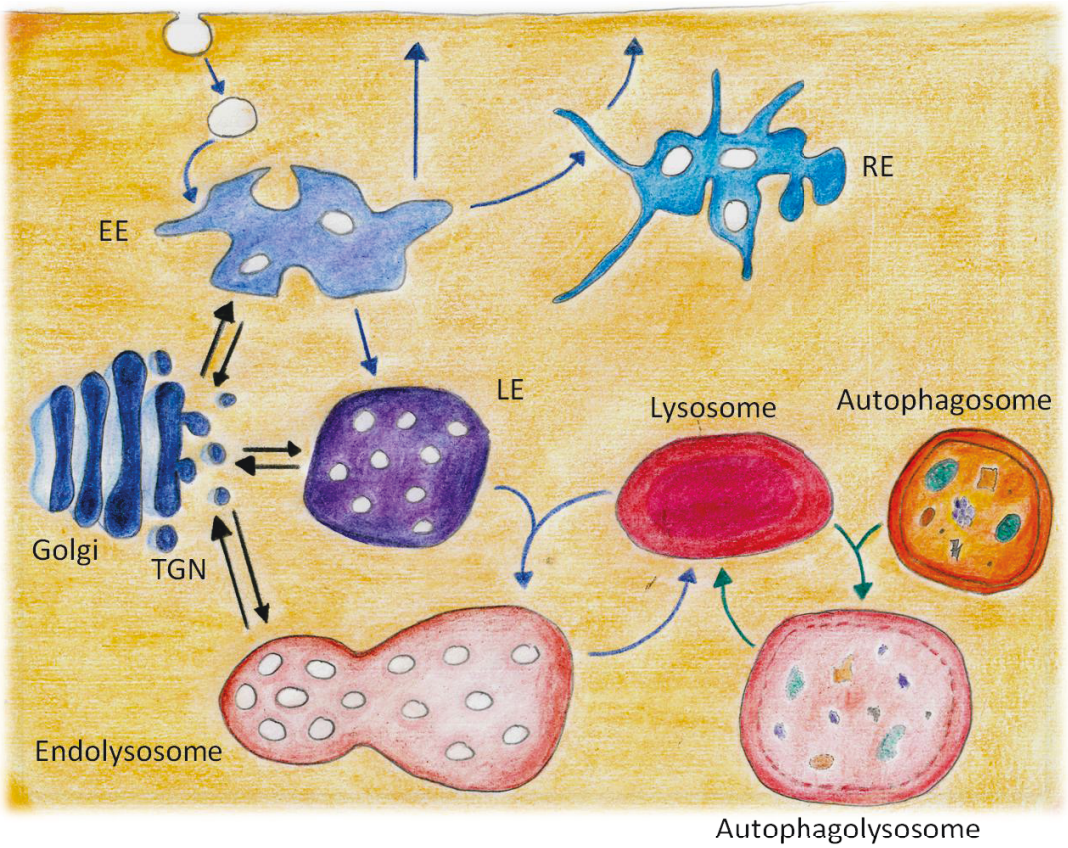

Figure 5: Lysosomal biogenesis and delivery of material to the lysosomal compartment involves biosynthetic, endocytic and autocatabolic routes. *On the biosynthetic route, lysosomal proteins (e.g. acid hydrolases) are synthesized into the ER where they are processed and undergo posttranslational modification. After export to the Golgi and trimming of N-glycosylation, they arrive at the trans-Golgi network, from where they are sorted to the endolysosomal compartment either directly (intracellular route, black arrows) or indirectly via the secretory pathway (secretion and re-internalization via endocytosis, not shown). Cargo and membrane material is deliverd to lysosomes either via the endocytic pathway (blue arrows) or macroautophagy (green arrows). On the endocytic route, endocytic vesicles deliver their material to early endosomes (EE), from where material can recycle to the plasma membrane either directly or via recycling endosomes (RE). EEs gradually convert to late endosomes (LE) in complex maturation process, during which they move centripetally to perinuclear areas while gradually becoming more acidic and accumulating intraluminal vesicles, that contain cargo destined for degradation. Both transient ("kiss and run") and complete fusion processes with lysosomes form a transient organelle, the endolysosome, where cargo is degraded, and from which lysosomes are constantly regenerated by fission processes. Additionally, intracellular materials including membranes, aged organelles and aggregates can be delivered to the lysosomal compartment via macroautophagy (see section* ***A3.2.2****). Here, intracellular cargo is first sequestered in a double membrane organelle termed the autophagosome. Fusion with lysosomes generates transient autophagolysosomes, from which lysosomes are constantly regenerated in a process called autophagic lysosome reformation. Figure modified from (Saftig and Klumperman 2009; Huotari and Helenius 2011; Luzio et al. 2014) and created in collaboration with Julia Zaman (Clinical Cooperation Unit Neuropathology, DKFZ). Organelle sizes are schematic and not representative of cellular organelle sizes.*

Lysosomal proteins and their functions

The proteins that govern lysosomal function can be coarsely divided into two categories: soluble hydrolases that are located within the lysosomal lumen, and integral lysosomal membrane proteins. Lysosomes are equipped with over 50 hydrolytic enzymes including proteases, peptidases, phosphatases, sulfatases, nucleases and glycosidases, which are referred to as acid hydrolases due to their functional optimum at low pH (Czupalla et al. 2006; Schroder et al. 2010; Sleat et al. 2013; Perera and Zoncu 2016). These enzymes are capable of degrading a large set of macromolecules, including proteins, lipids, nucleic acids and carbohydrates, the catabolic products of which can be transported across the lysosomal membrane into the cytosol where they are re-used for the synthesis of new macromolecules. One class of well-characterized lysosomal peptidases is the family of cathepsins, which are synthesized as inactive pro-enzymes and only become active after cleavage upon their packaging into lysosomes (reviewed in (Turk et al. 2012)). These small proteases are heavily involved in lysosomal bulk protein degradation as well as in the induction of cell death after lysosomal membrane permeabilization (LMP), also referred to as lysosomal cell death. LMP leads to the release of cathepsins to the cytosol and this release has been shown to trigger both apoptotic and necrotic modes of cell death depending on the extent of lysosomal permeabilization (Boya et al. 2003; Repnik et al. 2012; Aits and Jaattela 2013).

The limiting lysosomal membrane contains a high number of often heavily glycosylated proteins, also referred to as lysosome associated membrane proteins (LAMPs), lysosome associated integral membrane proteins (LIMPs) or lysosome glycoproteins (LGPs) (Luzio et al. 2003; Schroder et al. 2010). The high degree of glycosylation on their luminal domain allows them to form a glycoprotein layer called the glycocalyx, that prevents autodigestion of the lysosomal membrane by lysosomal hydrolases (Kornfeld and Mellman 1989; Peters and von Figura 1994; Perera and Zoncu 2016). Lysosomal membrane proteins like LAMP-1 and LAMP-2, which alone constitute up to 50 % of total lysosomal membrane protein, are therefore regarded as safeguards of lysosomal membrane integrity (Schwake et al. 2013). LAMP-1 and LAMP-2 are also involved in lysosomal positioning and fusion processes (Huynh et al. 2007), as well as in the import of cytosolic proteins during chaperone mediated autophagy, which is mediated by the LAMP-2 splice variant LAMP-2A (Bandyopadhyay et al. 2008). In addition, the lysosomal membrane contains various transporters, carriers, ion channels and pumps, as well as SNARE proteins such as VAMP7, which mediate fusion of lysosomes with other organelles or the plasma membrane (Pryor et al. 2004; Rao et al. 2004; Schwake et al. 2013). Via their cytosolic domain, lysosomal membrane proteins also recruit protein complexes involved in cell signaling and nutrient sensing (Sancak et al. 2008; Yonehara et al. 2017). Lysosomal membrane proteins thus govern all lysosome-related functions and are essential for lysosomal motility,

positioning, acidification, import of proteins, lipid homeostasis and export of degradation products (reviewed in (Saftig and Klumperman 2009)).

Among lysosomal membrane proteins are also members of the V_0/V_1-ATPase complex. This multi-subunit ATP-dependent proton pump uses energy from ATP hydrolysis to pump protons against their electrochemical gradient into the lysosome and is thus responsible for the acidification of the lysosomal lumen (Ohkuma et al. 1982; Forgac 1999). The V_0/V_1-ATPase complex consists of a cytoplasmic V_1 domain, which consists of subunits A-H and drives ATP hydrolysis, and the membrane-embedded V_0 domain made from six subunits (a, d, e, c, c'/Ac45, c''), which uses energy generated from ATP for proton translocation (Forgac 1999; Forgac 2007). The two subcomplexes are connected by central and peripheral stalks made from subunit D, F and subunits E and G respectively. This allows coupling of ATP hydrolysis to a rotary movement in V_0 subunit that is thought to mechanistically drive proton pumping (Mindell 2012). The activity of V-ATPases is tightly controlled and various mechanisms have been proposed how regulation is accomplished. One of those mechanisms is the reversible assembly and disassembly of the V-ATPase complex into the V_1 and V_0 subunits (Sautin et al. 2005). At least in yeast, disassembly *in vivo* seems to be at least partly controlled by a non-homologous region of the catalytic subunit A in the V_1 subcomplex (Shao et al. 2003). Evidence further suggests that V-ATPase activity can be controlled at the level of coupling efficiency, i.e. the amount of protons pumped per hydrolyzed ATP molecule. Mutations in various V-ATPase subunits have been shown to affect coupling efficiency. Interestingly, a subset of mutations in subunits A and d can increase the coupling efficiency of the V-ATPase complex, suggesting that the native or wild type ATPase is not optimally coupled (Shao et al. 2003; Owegi et al. 2006; Forgac 2007).

Functions and regulation of the lysosomal compartment

The best characterized function of the lysosome is the degradation and recycling of aged macromolecules and organelles, as well as the degradation of extracellular or cell-foreign materials including pathogens (Wei et al. 2005; Pryor and Raines 2010; Platt et al. 2012). Extracellular material is transported to the lysosome by various modes of endocytosis or phagocytosis while aged organelles, macromolecules or non-degradable aggregates typically reach the lysosome by various modes of autophagy (see section ***A3.2.2***). These molecules are then degraded with the help of lysosomal hydrolases and their monomers cross the lysosomal membrane either passively or by means of various lysosomal transporters. However, the function of the lysosome cannot be simply reduced that of a cellular waste bag. In fact, lysosomes have pivotal roles in other cell physiological processes such as lipid metabolism, cholesterol homeostasis, plasma membrane repair, cell signaling and control of cell metabolism (reviewed in (Settembre et al. 2013)). Lysosomes and so called lysosome-related organelles additionally have cell-specific functions unrelated to degradation. These

include pigment-carrying melanosomes in melanocytes or lytic granules in cytotoxic T-lymhpocytes (Mullins and Bonifacino 2001; Marks et al. 2013). In a process that is not fully understood, lysosomes fuse with the plasma membrane and release their content to the extracellular space. This process, which will be discussed in more detail in section ***A3.2.3***, is called lysosomal exocytosis and has been shown to be important for several physiological processes such as osteoclast differentiation, bone resorption or plasma membrane repair (Andrews 2000; Reddy et al. 2001; Zhao et al. 2008; Yang et al. 2012; Ferron et al. 2013). It is also becoming increasingly clear that lysosomes act as a central control hub of cellular signaling pathways, with a special role in cellular nutrient sensing and thus metabolic control (Sancak et al. 2008; Zoncu et al. 2011; Perera and Zoncu 2016). One of the first insights into how lysosomes control cellular signaling came from the observation that the EGF receptor, upon ligand binding, is internalized into endosomes and later degraded in the lysosome (Gorden et al. 1978; Stoscheck and Carpenter 1984; Felder et al. 1990). This ligand induced degradation is required for negative feedback regulation and has been also described for other cell surface receptors (Sorkin and von Zastrow 2009). More recently, the lysosome has emerged as a central nutrient sensor that regulates the mammalian target of rapamycin (mTOR) signaling pathway, which is essential for cell growth and metabolic homeostasis (Laplante and Sabatini 2012). One of the two mTOR signaling complexes, mTORC1, is recruited to lysosomes via Rag GTPases, which become activated upon accumulation of amino acids in the lysosome (Sancak et al. 2008; Sancak et al. 2010; Zoncu et al. 2011). Recruitment to lysosomes is required for mTORC1 kinase activity and thus activation of downstream pro-growth signaling pathways (Sancak et al. 2008; Groenewoud and Zwartkruis 2013). In contrast, amino acid starvation leads to the dissociation of mTORC1 from the lysosomal membrane, its inactivation, and therefore the activation of the self-degradative program of autophagy, underlining the importance of the lysosome in balancing biosynthetic and catabolic programs (Settembre et al. 2013; Demetriades et al. 2014).

Intriguingly, lysosomes are also involved in regulating their own biogenesis by modulating the activity of the transcription factor TFEB, the master regulator of a lysosomal gene network called the coordinated lysosomal expression and regulation (CLEAR) network (Sardiello et al. 2009).

Analogous to mTORC1, TFEB is recruited to the lysosomal membrane by Rag GTPases under nutrient supplied conditions and becomes phosphorylated by mTORC1 and/or ERK2 (Pena-Llopis et al. 2011; Settembre et al. 2011; Martina et al. 2012; Roczniak-Ferguson et al. 2012; Settembre et al. 2012; Martina and Puertollano 2013). Phosphorylation of TFEB at Ser142 and Ser211 leads to its retention in the cytoplasm by binding of 14-3-3 proteins, thereby inhibiting its transcriptional activity (Settembre et al. 2011; Roczniak-Ferguson et al. 2012). Under starvation, TFEB becomes dephosphorylated and translocates to the nucleus where it promotes the expression of genes with key roles in lysosomal biogenesis and lysosome related pathways including autophagy, endocytosis,

exocytosis and lipid catabolism (Medina et al. 2015). This suggests that TFEB is involved in the global control of lysosomal biogenesis and lysosome-related catabolic processes (Palmieri et al. 2011; Settembre et al. 2013).

3.2.2 Autophagy - an auto-catabolic process involving lysosomes

The term autophagy describes a cellular "self-eating" process, in which cellular components such as aged or damaged organelles, as well as damaged or aggregated proteins, are degraded and recycled with the help of lysosomes in order to generate energy, nutrients and monomeric building blocks for macromolecules under stress conditions. Such stress conditions are for example starvation, hypoxia, oxidative stress, protein aggregation, ER stress and treatment with cytotoxic drugs (Katayama et al. 2007; Dikic and Elazar 2018).

Depending on how cytoplasmic material is delivered to lysosomes, at least three modes of autophagy can be distinguished: Chaperone-mediated autophagy, which involves direct delivery of cytosolic proteins that carry a KFERQ-like motif to lysosomes with the help of heat shock protein HSC70 and cochaperones. HSC70 binds, unfolds, and delivers target proteins to a complex of the lysosomal membrane protein LAMP-2A, which in turn translocates the unfolded protein directly into the lysosomal lumen (Cuervo and Dice 1996; Salvador et al. 2000; Kaushik and Cuervo 2018). Microautophagy describes the direct engulfment of cytoplasmic material by lysosomes via invagination of the lysosomal membrane itself (Arstila and Trump 1968; Li et al. 2012). In contrast, macroautophagy, by far the most common mode of autophagy and hereon referred to as autophagy, involves an extra organelle. Here, cytoplasmic material is sequestered within double-membrane organelles, termed autophagosomes, which deliver their material to lysosomes for degradation, either by complete fusion with lysosomes or by a kiss-and-run mechanism (see section ***A3.2.1***) (Arstila and Trump 1968; Ohsumi 2014; Dikic and Elazar 2018). Although especially macroautophagy was regarded as a bulk degradation process for a long time, evidence suggests that it can be a highly selective process, and organelle-specific modes of autophagy including mitophagy, lysophagy, pexophagy, nucleophagy have been described (reviewed in (Okamoto 2014)).

The process of autophagy involves a number of highly conserved proteins, termed autophagy-related, which are encoded by *ATG* genes (Tsukada and Ohsumi 1993; Mizushima et al. 1998; Nakatogawa et al. 2009). They mostly govern three very critical events in the early phase of autophagy, namely the nucleation, elongation and maturation of the autophagosome (Mizushima et al. 2010; Ohsumi 2014).

Formation of the autophagosome is commonly thought to occur at the ER, although membranes derived from other organelles including Golgi, mitochondria, endosomes and the plasma membrane have been shown to contribute to this process (reviewed in (Martens et al. 2016)), and at least four

major protein complexes control formation of the autophagosome. In its best characterized mode, autophagy initiation under starvation conditions is controlled positively by the AMP-activated protein kinase (AMPK) or negatively by the mTORC1 complex, which sense ATP:AMP ratio and lysosomal amino acids, respectively (Sancak et al. 2008; Oakhill et al. 2011). These modulate function of the Unc-51-like kinase 1 complex made of ULK1/ATG1, ATG13, FIP200 and ATG101, by activating (AMPK) or inactivating (mTORC1) phosphorylation of the ULK1 kinase (Kim et al. 2011; Dikic and Elazar 2018). The ULK1 complex is recruited to the phagophore assembly site (PAS) by a ternary complex of ATG17-ATG31-ATG29, where ULK1 activates the class III PI3K complex I, consisting of the class III PI3K VPS34, Beclin-1, ATG14, AMBRA1 and p15, by phosphorylating Beclin-1 (Suzuki et al. 2007; Russell et al. 2013; Dikic and Elazar 2018). The latter complex generates phosphatidylinositol-3-phosphate (PI3P) at the PAS, which recruits PI3P binding proteins like WIPI2. WIPI2, in turn, recruits the ATG12-ATG5-ATG16L1 complex (Dooley et al. 2014). This complex, together with ATG4B, ATG7 and ATG3 mediates the processing and conjugation of ATG8 family members (including LC3) to membrane-resident phosphatidylethanolamine, thereby generating the lipidated, membrane-bound form LC3-II, the main autophagosome marker (Mizushima et al. 1998; Ichimura et al. 2000; Kabeya et al. 2000; Hemelaar et al. 2003; Tanida et al. 2004; Fujita et al. 2008; Walczak and Martens 2013). Membrane-bound LC3-II then recruits factors required for cargo binding and elongation of the autophagosome membrane, thereby promoting the elongation process and autophagosome closure (Olsvik et al. 2015; Dikic and Elazar 2018). Autophagosome closure is then followed by a maturation process in which ATG proteins are cleared from the outer autophagosomal membrane, while proteins required for fusion with lysosomes are recruited (Dikic and Elazar 2018). The regulation of delivery of autophagosomal cargo to lysosomes is poorly characterized, but known to require the SNAREs syntaxin 17 (STX17) and SNAP29 on autophagosomes, as well as the lysosomal SNARE VAMP8 and the HOPS complex as tethering factor (Itakura et al. 2012; Jiang et al. 2014; Diao et al. 2015). Acidification of lysosomes is required for efficient turnover of autophagic substrates, but not necessary for autophagosome-lysosome fusion itself (Mauvezin et al. 2015; Mauvezin and Neufeld 2015).

Autophagy is transcriptionally regulated. One family of transcription factors with transcriptional activity on autophagy genes is the FoxO family, especially its members FoxO1 and FoxO3 (Zhao et al. 2007; Zhao et al. 2010; van der Vos et al. 2012). Similar to the lysosomal transcription factor TFEB, FoxO transcription factors are negatively regulated by phosphorylation, in this case mediated by AKT, which leads to their 14-3-3 protein dependent retention in the cytoplasm (Brunet et al. 1999). In addition, FoxO transcription factors are regulated via reversible acetylation mediated by the histone acetyltransferase CBP and the HDAC member SIRT1, respectively (Brunet et al. 2004; Daitoku et al. 2004; Zhao et al. 2010; Daitoku et al. 2011). Notably, lysosomal and autophagosome biogenesis are

also linked on a transcriptional levels via the lysosomal master regulator transcription factor TFEB that promotes the expression of both lysosomal and autophagy genes (see section ***A3.2.1***).

In the context of tumor formation, autophagy has been described to act as a "double-edged sword", meaning that it can have both tumor-promoting and tumor suppressive functions (White and DiPaola 2009). In early or even pre-malignant tumor stages, autophagy has tumor-suppressive capacity by clearing aged or damaged organelles such as mitochondria, which can produce reactive oxygen species (ROS) and thus promote tumor relevant processes such as the acquisition of mutations or inflammatory processes (Karantza-Wadsworth et al. 2007; Mathew et al. 2007). However, established tumors have been repeatedly shown to use or even depend on autophagy for the generation of amino acids and nucleotides, which in turn enables them to cope with a number of stress factors such as hypoxia, starvation, oxidative stress or cytotoxic treatment (Guo et al. 2013).

3.2.3 Lysosomal drug resistance mechanisms independent of autophagy

Lysosomes are involved in cancer drug resistance and progression independently of their role in autophagy. Cancer cells are known to be highly dependent on the efficient function of the lysosomal compartment. The lysosomal compartment undergoes striking changes during malignant transformation and cancer progression, including changes in volume of the lysosomal compartment, changes in lysosomal composition and positioning, as well as changes in enzymatic activity (Appelqvist et al. 2013; Piao and Amaravadi 2016). With regards to the latter, especially enhanced expression and secretion of lysosomal hydrolases has been repeatedly associated with cancer progression and metastasis formation (Gocheva et al. 2006; Vasiljeva and Turk 2008; Ramessur et al. 2010). Lysosomes have been also implicated in cancer multidrug resistance (MDR) and at least two distinct but partly interdependent mechanisms of lysosomal-mediated MDR have been described (***Figure 6***) (Zhitomirsky and Assaraf 2016).

Various substances are trapped in lysosomes by a mechanism called lysosomal sequestration or trapping (Zhitomirsky and Assaraf 2016) due to their hydrophobic and weakly-basic chemical properties. These include widely used first-line anti-cancer drugs such as daunorubicin, doxorubicin, vincristine, sunitinib and imatinib, which, after passively entering cells and lysosomes, become protonated in the lysosomal lumen, leading to the addition of extra charge that results in their trapping and accumulation within lysosomes (Hurwitz et al. 1997; Groth-Pedersen et al. 2007; Herlevsen et al. 2007; Chapuy et al. 2008; Zhitomirsky and Assaraf 2015; Zhitomirsky and Assaraf 2016). This compartmentalization phenomenon prevents them from reaching their cellular target and from exerting their cytotoxic activity (***Figure 6***). The ability of cells to trap chemotherapeutic drugs in lysosomes might be acquired during first-line treatment (Hurwitz et al. 1997; Altan et al. 1998), possibly as a consequence of drug-induced expansion of the lysosomal compartment (Gotink

et al. 2015; Zhitomirsky and Assaraf 2015). Lysosomal accumulation of weakly basic anti-cancer drugs critically depends on lysosomal acidification, which creates a pH gradient between lysosomes and cytoplasm (Zhitomirsky and Assaraf 2016). In this context, several studies have demonstrated that drug resistant cell lines adapt to cytotoxic treatment not only by promoting *de novo* biogenesis of lysosomes, but also by increasing the pH gradient between the cytoplasm and lysosomes, endosomes as well as *trans*-Golgi network vesicles, which is achieved by enhanced acidification of the aforementioned compartments (Schindler et al. 1996; Altan et al. 1998; Larsen et al. 2000; Gong et al. 2003; Hrabeta et al. 2015). As lysosomal trapping is not a single drug-specific mechanism, expansion of the lysosomal compartment also induces significant cross-resistance (Gotink et al. 2015). Intriguingly, drugs do not only passively enter lysosomes by diffusion, but are also actively pumped into lysosomes by various ABC transporters including P-glycoprotein, which can be present on intracellular membranes as well as vesicles (Molinari et al. 2002; Rajagopal and Simon 2003). This indicates that lysosomal sequestration is at least in parts an active process (Ferrao et al. 2001; Chapuy et al. 2008; Yamagishi et al. 2013).

Lysosomes do not only sequester weakly basic chemotherapeutic drugs but also cause their secretion in a process termed lysosomal exocytosis, i.e. the fusion of lysosomes with the plasma membrane whereby lysosomal cargo is released to the extracellular space (***Figure 6***) (Andrews 2000; Yanes et al. 2013; Machado et al. 2015; Zhitomirsky and Assaraf 2017). Even before the description of lysosomal exocytosis, it was known that lysosome related organelles of various cell types can act as secretory granules. It is now known that lysosomal exocytosis can occur in all cell types from the pool of conventional lysosomes (Rodriguez et al. 1997; Page et al. 1998; Blott and Griffiths 2002). Lysosomal secretion has been implicated in various important physiological mechanisms, including plasma membrane repair, bone resorption in osteoclasts, as well as various pathogen defense mechanisms. (Reddy et al. 2001; Zhao et al. 2008; Appelqvist et al. 2013; Luzio et al. 2014).

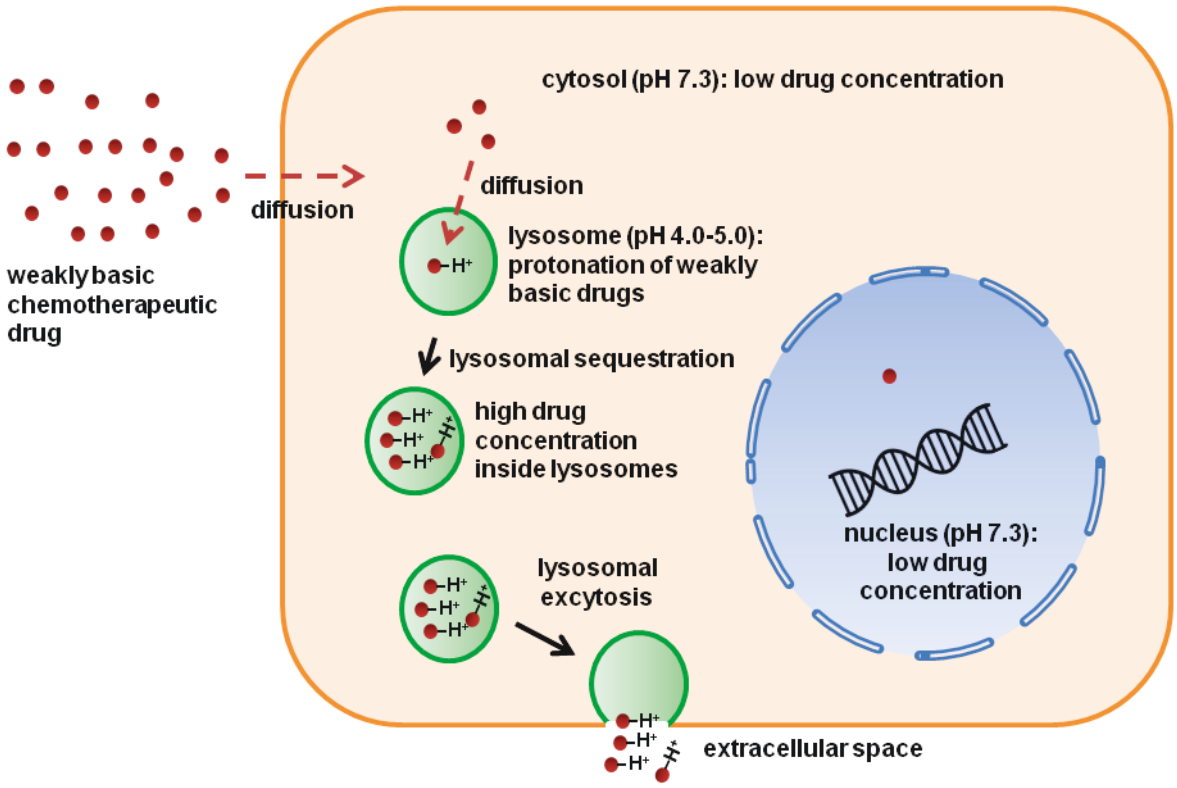

Figure 6: Lysosomal drug resistance mechanisms independent of autophagy. *Lysosomes promote resistance to weakly basic hydrophobic drugs independently of autophagy by at least two distinct mechanisms. Firstly, weakly basic drugs can become trapped in lysosomes in a process termed lysosomal sequestration, where the drug becomes protonated due to the low lysosomal pH, reducing its ability to diffuse out of the lysosome. Secondly, lysosomes can fuse with the plasma membrane in a process called lysosomal exocytosis, leading to the secretion of lysosomal content to the extracellular space.*

Despite its identification more than 20 years ago, the regulation of lysosomal exocytosis and its underlying molecular machinery are still poorly understood (Rodriguez et al. 1997). It is a two-step processes, where lysosomes are first recruited to the plasma membrane in a Ca^{2+}-independent fashion, while fusion with the plasma membrane occurs in a second step after elevation of cytoplasmic Ca^{2+} levels, leading to the presence of lysosomal transmembrane proteins like LAMP-1 at the plasma membrane (Jaiswal et al. 2002; Tucker et al. 2004). Key proteins involved in lysosomal exocytosis include the v-SNARE VAMP7 and the calcium sensor synaptotagmin VII on lysosomes, the t-SNAREs SNAP23 and syntaxin 4 on the plasma membrane, as well as Rab proteins (Rao et al. 2004; Laulagnier et al. 2011). After formation of the trans-SNARE complex, lysosomal exocytosis further requires an increase in intracellular Ca^{2+} levels to trigger membrane fusion, which is most likely released from lysosomes themselves via the lysosomal transporter MCOLN1 (LaPlante et al. 2006; Medina et al. 2011).

Lysosomal exocytosis is not only involved in the clearing of lysosome-sequestered drugs, but it might even be triggered by lysosomal drug accumulation. A recent report suggests that lysosomal accumulation of weakly basic chemotherapeutics induces nuclear translocation of the lysosomal master regulator TFEB, which in turn activates a transcriptional program that promotes lysosomal

exocytosis (Medina et al. 2011; Zhitomirsky and Assaraf 2017). Finally, lysosomal exocytosis also promotes cancer progression via the release of lysosomal hydrolases including cathepsins that degrade extracellular matrix proteins and enhance cancer cell invasiveness (Fonovic and Turk 2014; Machado et al. 2015).

B MATERIALS

1 Cell culture

1.1 Cell lines

Cell line	Tissue of origin	Tumor type	Genetic alterations/ Characteristics	Supplier
SK-N-BE(2)-C/ BE(2)-C (I-type)	Bone marrow (metastasis)	Neuroblastoma	*MYCN* ampl., *TP53* mut.	ECACC, Salisbury, UK
IMR-32 (N-type)	Abdominal primary tumor	Neuroblastoma	*MYCN* ampl.	DSMZ, Darmstadt, Germany
IMR-32 e.v.	see above	Neuroblastoma	*MYCN* ampl., stably transfected with pCMV / hygro-Negative Control Vector	see above
IMR-32 HDAC10	see above	Neuroblastoma	*MYCN* ampl., pCMV/hygro-FLAG HDAC10	see above
Kelly (N-type)	Primary tumor	Neuroblastoma	*MYCN* ampl., *TP53* mut. *ALK* mut. (F1174L)	DSMZ, Darmstadt, Germany
SK-N-AS (S-type)	Bone marrow (metastasis)	Neuroblastoma	*TP53* mut.	M. Schwab, DKFZ, Heidelberg, Germany
HAP1 wild type	Bone marrow (parental KBM-7 cell line)	Chronic Myelogenous Leukemia (CML)	Near haploid	Horizon Discovery, Cambridge, UK
HAP1 HDAC10 knockout	See above	See above	Near haploid, *HDAC10* knockout	Horizon Discovery, Cambridge, UK
HAP1 HDAC8 knockout	See above	See above	Near haploid, *HDAC8* knockout	Horizon Discovery, Cambridge, UK
Hybridoma cell lines	B-lymphocytes from popliteal lymph nodes (BALB/c mouse) fused with murine myeloma cell line Sp2/0-Ag-14	Murine myeloma/ hybridoma	Sp2/0-Ag-14: HGPRT deficient; eliminated endogenous antibody expression (Shulman et al. 1978), expresses aberrant non-productive κ light chain (abVκ) (Carroll et al. 1988)	ATCC, Manassas, Virginia, United States
VH7/ human fibroblasts	Skin	Non-transformed/ healthy donor	unknown	P. Boukamp, DKFZ, Heidelberg, Germany

Table 1: Cell lines.

1.2 Culture media

Medium	Additives	Cell lines
DMEM	10% FCS, 1% NEAA	SK-N-BE(2)-C, IMR-32, SK-N-AS, HEK293T, VH7 human fibroblasts
DMEM IMR-32 selection medium	10% FCS, 1% NEAA 170-225 µg/ml hygromycin B	IMR-32 e.v. and IMR-32 HDAC10 overexpressing cells
RPMI-1640	10% FCS	Kelly, NB-1
RPMI-1640 hybridoma medium	5% FCS, 2 mM Glutamine, 1 % Penicillin/Streptomycin, 1% NEAA, 0.5 mM sodium pyruvate	Hybridoma lines
IMDM	10% FCS	HAP1 wild type, HAP1 HDAC10 knockout, HAP1 HDAC8 knockout

Table 2: Cell culture media.

1.3 Solutions for cell culture

1.3.1 Versene (PBS/EDTA)

1 x PBS	495 ml
0.5 M EDTA pH 8.0 (filtered)	5 ml

Table 3: Versene (PBS/EDTA).

1.4 Inhibitors

1.4.1 Characterized histone deacetylase inhibitors

Compound	Supplier	Molecular weight	Stock concentration	Solvent	Storage
abexinostat (PCI-24781)	Selleckchem	397.42 g/mol	10 mM	DMSO	-20°C
bufexamac	Sigma	223.27 g/mol	100 mM	DMSO	-20°C
panobinostat	Cayman	349.43 g/mol	0.5 mM	DMSO	-20°C
PCI-34051	Selleckchem	296.32 g/mol	20 mM	DMSO	-80°C
entinostat (MS-275)	Biomol/USBio	376.416 g/mol	10 mM	DMSO	-80°C
tubacin	Santa Cruz	721.86 g/mol	1 mM	DMSO	-20°C
tubastatin A	BIOZOL	335.40 g/mol	10 mM	DMSO	-20°C
trichostatin A (TSA)	Calbiochem	302.374 g/mol	1 mM	DMSO	-20°C
valproic acid (VPA)	Sigma	144.211 g/mol	1 M	DMSO	-20°C
vorinostat	Selleckchem	264.30 g/mol	100 mM	DMSO	-20°C

Table 4: Characterized histone deacetylase inhibitors.

1.4.2 Investigational Compounds

Compound	Stock concentration	Solvent	Storage	Source
DKFZ-00477	10 mM	DMSO	-20°C	Dr. Aubry Miller, DKFZ
DKFZ-00494	10 mM	DMSO	-20°C	Dr. Aubry Miller, DKFZ
DKFZ-00495	50 mM	DMSO	-20 °C	Dr. Aubry Miller, DKFZ
DKFZ-00546	10 mM/50mM	DMSO	-20°C	Dr. Aubry Miller, DKFZ
DKFZ-00565	50 mM	DMSO	-20°C	Dr. Aubry Miller, DKFZ
DKFZ-00574	50 mM	DMSO	-20°C	Dr. Aubry Miller, DKFZ
DKFZ-00580	50 mM	DMSO	-20°C	Dr. Aubry Miller, DKFZ
Marbostat-100 (MARB1)	50 mM	DMSO	-20°C	Prof. Dr. Siavosh Mahboobi, Institute of Pharmacy, University of Regensburg, Germany

Table 5: Investigational compounds.

1.4.3 Other substances and inhibitors

Compound	Category	Supplier	Stock concentration	Solvent	Storage
bafilomycin A1	lysosomal V-ATPase inhibitor	Santa Cruz Biotechnology	10 µM	DMSO	-20°C
chloroquine	lysosomal inhibitor	Sigma-Aldrich	100 mM	water	-20°C
doxorubicin	chemotherapeutic agent	Calbiochem	10 mM (5.8 mg/ml)	water	-80°C
vacuolin-1	lysosomal exocytosis inhibitor	Calbiochem	10 mM	DMSO	-20°C
verapamil	P-glycoprotein inhibitor	Sigma	20 mM	DMSO	-20°C

Table 6: Other substances and inhibitors.

1.5 Nucleic acids

1.5.1 Small interfering RNAs (siRNAs)

Gene	siRNA ID/ product number	Catalog number	Company
Amb #1 (siCtrl #1)	n.a.	AM4611	Ambion, Huntingdon, UK
Amb #5 (siCtrl #5)	n.a.	AM4642	Ambion, Huntingdon, UK
ATG5 #6	SI02655310/ 1027415	GS9474	QIAGEN, Hilden, Germany
ATG5 #3	SI00069258/ 1027415	GS9474	QIAGEN, Hilden, Germany
BECN1 #5	SI05126534/ n.a.	SI05126534	QIAGEN, Hilden, Germany
FOXO3 #1	s5260	4392420	Ambion, Huntingdon, UK
FOXO3 #2	s5262	4392420	Ambion, Huntingdon, UK
FOXO3 #3	s5261	4392420	Ambion, Huntingdon, UK
HDAC1 #1	120418	AM51331	Ambion, Huntingdon, UK
HDAC1 #2	120419	AM16708	Ambion, Huntingdon, UK

HDAC1 #6	SI02663472/ 1027416	GS3065	QIAGEN, Hilden, Germany
HDAC2 #1	120208	AM51331	Ambion, Huntingdon, UK
HDAC2 #3	120210	AM51331	Ambion, Huntingdon, UK
HDAC3 #1	120349	AM51331	Ambion, Huntingdon, UK
HDAC3 #2	120350	AM16708	Ambion, Huntingdon, UK
HDAC6 #1	120451	AM16708	Ambion, Huntingdon, UK
HDAC6 #3	120450	AM51331	Ambion, Huntingdon, UK
HDAC10 #1	33581	AM16708	Ambion, Huntingdon, UK
HDAC10 #2	120681	AM16708	Ambion, Huntingdon, UK
HDAC11 #1	130749	AM16708	Ambion, Huntingdon, UK
HDAC11 #2	130750	AM16708	Ambion, Huntingdon, UK
siLAMP1 #1	s8080	4427037	Ambion, Huntingdon, UK
P-glycoprotein/ ABCB1 (pooled siRNA)	not available	L-003868-00-0005	GE Dharmacon, Lafayette, CO, USA

Table 7: Small interfering RNAs.

additional siRNAs (self-designed)

Gene	Sequence (sense)	Sequence (antisense)	Company
BECN1	5'-CAG UUU GGC ACA AUC AAU Att-3'	5'-UAU UGA UUG UGC CAA ACU Gtt-3'	Ambion, Huntingdon, UK

Table 8: additional siRNAs.

1.5.2 Primers for real-time RT-PCR

Gene	Sequence (forward)	Sequence (reverse)	Supplier
HDAC1	5'-TGA CGA GTC CTA TGA GGC CAT T-3'	5'-CCG CAC TAG GCT GGA ACA TC-3'	ThermoFisher Scientific, Braunschweig, Germany
HDAC2	5'-TGT GAG ATT CCC AAT GAG TTG C-3'	5'-GGT AAC ATG CGC AAA TTT TCA A-3'	ThermoFisher Scientific, Braunschweig, Germany
HDAC3	5'-CCT CAC TGA CCG GGT CAT G-3'	5'-ACC TGT GCC AGG GAA GAA GTA A-3'	ThermoFisher Scientific, Braunschweig, Germany
HDAC10	5'-CTC ACT GGA GCT GTG CAA AA-3'	5'-GAT CCT GTG TAG CCC GTG TT-3'	Sigma-Aldrich, Munich, Germany
HDAC10 alternative	5'-ATC TCT TTG AGG ATG ACC CCA-3'	5'-ACT GCG TCT GCA TCT GAC TCT C-3'	ThermoFisher Scientific, Braunschweig, Germany
HDAC11	5'-CAA TGG GCA TGA GCG AGA C-3'	5'-TGT GGC GGT TGT AGA CAT CC-3'	ThermoFisher Scientific, Braunschweig, Germany
HPRT	5'-TGA CAC TGG CAA AAC AAT GCA-3'	5'-GGT CCT TTT CAC CAG CAA GCT-3'	ThermoFisher Scientific, Braunschweig, Germany
LAMP2A	not provided by supplier	not provided by supplier	QIAGEN, Hilden, Germany assay #: QT00077063
P-gp/ ABCB1	5'-GGG ATG GTC AGT GTT GAT GGA-3'	5'-GCT ATC GTG GTG GCA AAC AAT A-3'	Sigma-Aldrich, Munich, Germany
SDHA	5'-TGG GAA CAA GAG GGC ATC TG-3	5'-CCA CCA CTG CAT CAA ATT CAT G-3'	ThermoFisher Scientific, Braunschweig, Germany

Table 9: Primers for real-time RT-PCR.

1.5.3 Primers for PCR amplification of HDAC10 fragments for antibody production

Name	Sequence (forward)	Sequence (reverse)	Supplier
HDAC10T1	5'- CGG GGA TCC ATG GAT GTG ACC GCT GTG CC -3'	5'- GCC AAG CTT GGA CAG GCC TCT CCG AA -3'	Sigma-Aldrich, Munich, Germany
HDAC10T2	5'- GCC GGA TCC ATG CAC GGA GCC CAG AGG C -3'	5'- GCC AAG CTT TAG CTG GGG TGT GGA GTT -3'	Sigma-Aldrich, Munich, Germany

Table 10: Primers for PCR amplification of HDAC10 fragments for antibody production. *BamHI and HindIII restriction sites are highlighted in green and orange, respectively.*

1.5.4 Plasmids

Plasmid name	Backbone	Insert	Resistance (bacteria/human)	Catalog number / reference
pCMV/hygro-FLAG HDAC10	pCMV/hygro -FLAG	human *HDAC10 (NM_032019.5)*	ampicillin/ hygromycin B	HG11507-M-F (Sino Biological)
pCMV / hygro-Negative Control Vector (FLAG-tagged)	pCMV/hygro -FLAG	none	ampicillin/ hygromycin B	CV005 (Sino Biological)
pEGFP-N1-TFEB	pEGFP-N1	human *TFEB (NM_001167827.2)*	kanamycin/ neomycin	#38119 (Addgene)

Table 11: Plasmids.

2 Buffers and solutions

2.1 Flow cytometry (FACS)

2.1.1 RPMI w/o Phenol Red

Medium	Additives
RPMI w/o Phenol Red	10 % FCS

Table 12: RPMI without Phenol Red.

2.1.2 FACS buffer (5 % FCS/PBS)

ingredient	volume
1x PBS	45 ml
FCS	2.5 ml

Table 13: FACS buffer.

2.1.3 Acridine orange staining solution

ingredient	concentration
Acridine orange solution (10 mg/ml)	0.01% (v/v) in RPMI w/o phenol red + 10 % FCS

Table 14: Acridine orange staining solution.

2.1.4 1x Fixation and permeabilization solutions for staining of nuclear antigens

Solution	Stock solution	Diluent
1x Fixation solution	4x Fixation/Permeabilization Concentrate (eBioscience)	Fixation/Permeabilization Diluent (eBioscience)
1x Permeabilization Solution	10x Permeabilization buffer (eBioscience)	De-ionized water

Table 15: Solutions for FACS staining of nuclear antigens.

2.2 Fluorescence microscopy and immunofluorescence

2.2.1 4% Paraformaldehyde (PFA) fixation solution

1x PBS	40 ml
16% PFA stock solution	10 ml

Table 16: 4% PFA fixation solution. *The solution was distributed to black 1.5 ml reaction tubes and stored at 20°C. Solution was thawed 1h before use.*

2.2.2 Blocking and permeabilization solutions for cytoplasmic and nuclear antigens

OT/microscopy slide blocking solution	10 % NGS, 0.25 % BSA, 0.1 % Triton-X 100 in PBS
Blocking solution (nuclear staining)	3 % BSA, 0.05% Triton-X 100 in 1x PBS
Permeabilization solution (cytoplasmic)	0.1 % Triton-X 100 in 1x PBS
Permeabilization solution (nuclear)	0.2 % Triton-X 100 in 1x PBS

Table 17: Blocking and permeabilization solutions for immunofluorescence

2.3 Immunoprecipitation

2.3.1 PBS-T (0.02 %)

ingredient	volume
1x PBS	200 ml
Tween 20	40 µl

Table 18: PBS-T for immunoprecipitation. *PBS-T was stored at 4°C.*

2.3.2 Triethanolamine buffer

ingredient	volume	final concentration
Triethanolamine	2.64 ml	0.2 M
PBS	100 ml	----
pH adjusted to 8.2 with concentrated HCl		

Table 19: Triethanolamine buffer. *Triethanolamine buffer was stored at 4°C.*

2.3.3 Dimethyl pimelimidate (DMP) solution for crosslinking

DMP stock solution

ingredient	amount/volume
DMP dihydro chloride	13 mg
Triethanolamine buffer	1 ml

Table 20: DMP stock solution. *DMP stock solution was freshly prepared directly before use.*

DMP working solution

ingredient	volume	final concentration
DMP stock solution	0.5 ml	20 mM
Triethanolamine buffer	0.7 ml	

Table 21: DMP working solution. *DMP working solution was freshly prepared directly before use.*

2.3.4 Quenching solution (50 mM Tris pH 7.5)

ingredient	amount/volume	final concentration
Trizma Base	1.22 g	50 mM
ddH_2O	200 ml	----
pH adjusted to 7.5 with concentrated HCl		

Table 22: Quenching solution. *Quenching solution was stored at 4°C.*

2.4 Colony formation assay

2.4.1 Crystal violet staining solution

Ingredient	Final concentration
Crystal violet	1 % (w/v)
ethanol	70 % (v/v)
de-ionized water	30 % (v/v)

Table 23: Crystal violet staining solution.

2.5 Quantification of polyamines

2.5.1 10x SSAT breaking buffer

ingredient	amount/volume	final concentration
HEPES	1.2 g	50 mM
LiChroSolv water	100 ml	----
pH adjusted to 7.2 with NaOH		

Table 24: 10x SSAT breaking buffer. *SSAT breaking buffer was stored at -20°C and diluted in LiChroSolv water to yield 1x SSAT breaking buffer.*

2.6 Cathepsin Release Assay

2.6.1 Extraction buffer

Ingredient	Final concentration
Sucrose	250 mM
HEPES	20 mM
KCl	10 mM
$MgCl_2$	1.5 mM
EGTA	1 mM
EDTA	1mM
pH adjusted to 7.5 with NaOH	

Table 25: Extraction buffer for cathepsin release assay. *Buffer was stored at 4°C. DTT (8 mM), PMSF (1 mM) and digitonin (15 or 200 µg/ml) were added directly prior to use.*

2.6.2 Reaction buffer (2x)

Ingredient	Final concentration
Sodium acetate	50 mM
EDTA	8 mM
pH adjusted to 5.0 with HCl	

Table 26: Reaction buffer (2x) for cathepsin release assay. *Buffer was stored at 4°C. DTT (8 mM), PMSF (1 mM) were added directly prior to use.*

3 Western Blot

3.1 Buffers and solutions

Buffers and solutions for Western Blot were stored at room temperature unless otherwise indicated below.

3.1.1 Running gel buffer for SDS PAGE (1.5 M Tris pH 8.8)

Ingredient	Final concentration
Trizma Base	1.5 M
HCl (12.1 M)	Added dropwise to set pH to 8.8

Table 27: Running gel buffer for SDS PAGE.

3.1.2 Stacking gel buffer for SDS PAGE (0.5M Tris pH 6.8)

Ingredient	Final concentration
Trizma Base	0.5 M
HCl (12.1 M)	Added dropwise to set pH to 6.8

Table 28: Stacking gel buffer for SDS PAGE.

3.1.3 10x Running buffer for SDS PAGE

Ingredient	Final concentration
Trizma Base	25 mM
Glycine	1,9 M
SDS	1 % (w/v)
HCl (12.1 M)	Added dropwise to set pH to 8.3

Table 29: 10x Running buffer for SDS PAGE. *10x Running buffer was diluted in de-ionized water before use. Transfer buffer.*

3.1.4 Transfer buffer for western blot

Ingredient	Final concentration
Trizma Base	480 mM
Glycine	390 mM

Table 30: 10x Transfer buffer for western blot.

1x Transfer buffer

Ingredient	Volume
10x Transfer buffer	100 ml
Methanol	200 ml
ddH_2O	ad 1000 ml

Table 31: 1x Transfer buffer for western blot.

3.1.5 TBS and TBS-Tween (TBS-T) for western blot

Ingredient	Final concentration
Trizma Base	200 mM
NaCl	1.37 M
HCl (12.1 M)	added to set pH to 7.6

Table 32: 10x TBS for western blot.

1x TBS

Ingredient	Volume
10x TBS	100 ml
ddH_2O	900 ml

Table 33: 1x TBS for western blot.

1x TBS-T

Ingredient	Volume (final concentration)
10x TBS	100 ml (1x)
ddH_2O	900 ml
Tween 20	2 ml (0.2 % v/v)

Table 34: 1x TBS-T for western blot.

3.1.6 Blocking buffers for western blot

All blot membranes were blocked standard blocking buffer for Western Blot unless otherwise specified below

Standard blocking buffer for western blot membranes

Ingredient	Final concentration
Nonfat dry milk	20 % (w/v)
FCS (non-inactivated)	20 % (v/v)
BSA	3 % (w/v)
NGS	1 % (v/v)
Tween 20	0.2 % (v/v)
1x TBS	ad 1l

Table 35: Standard blocking buffer for western blot. *Blocking solution was stored in 50 ml aliquots at -20°C.*

BSA blocking solution

Ingredient	Final concentration	Antibodies used for
BSA	3 % (w/v) in TBS-T	FOXO3a, ATG5, ATG7

Table 36: BSA blocking solution for western blot. *BSA blocking solution for Western Blot was stored at 4°C.*

3.1.7 Antibody dilution buffers for western blot

Primary and secondary antibodies for Western blot were diluted in 2 % (w/v) nonfat dry milk in 1x TBS-T with the exception of antibodies listed in ***Table 36***, where primary and secondary antibodies were diluted in BSA blocking solution.

3.1.8 Lysis buffers for protein biochemistry

SDS lysis buffer for whole cell lysates

Ingredient	Volume/amount (final concentration)
Stacking gel buffer	12.4 ml (62.5 mM TRIS pH 6.8)
SDS	2 g (2 % w/v)
Glycerol	10 ml (10 % v/v)
ddH_2O	ad 100 ml

Table 37: SDS lysis buffer for whole cell lysates. *1mM DTT was added directly before use.*

Triton-X based lysis buffer for postnuclear lysates

Ingredient	Final concentration
Trizma Base	20 mM
NaCl	137 mM
Glycerol	10 % (v/v)
0.5 M EDTA pH 8.0	2 mM
Triton-X 100	0.2 - 1 %
HCl (12.1 M)	added dropwise to adjust pH to 8.0
ddH_2O	ad 100 ml

Table 38: Lysis buffer for postnuclear lysates. *Buffer was stored at -20°C. One cOmplete™ Mini EDTA-free Protease Inhibitor Cocktail Tablet was added per 10 ml of lysis buffer directly prior to use.*

1x RIPA buffer

Ingredient	Volume
Cell Signaling Technology (CST) RIPA buffer (10x)	2 ml
ddH_2O	ad 20 ml

Table 39: 1x RIPA buffer. *RIPA buffer was stored at -20°C. One cOmplete™ Mini EDTA-free Protease Inhibitor Cocktail Tablet was added per 20 ml of lysis buffer directly prior to use.*

3.1.9 4x Laemmli sample buffer

Ingredient	Volume	Final concentration
Stacking gel buffer pH 6.8	10 ml	62.5 mM Tris
Glycerol	8 ml	20 % (v/v)
SDS	1.6 g	4 %
Bromophenol blue	2 mg	0.005%
ddH_2O	ad 40 ml	-----

Table 40: 4x Laemmli sample buffer. *In case of reducing sample buffer 5% (v/v) β-Mercaptoethanol (14.3 M) were added. 4x Laemmli buffer was diluted in equal volume of ddH_2O to yield 2x Laemmli buffer.*

3.1.10 Coomassie Brilliant Blue staining solution

Ingredient	Final concentration
Brilliant Blue G	0.05 % (w/v)
Isopropanol	25 % (v/v)
Acetic acid	10 % (v/v)

Table 41: Coomassie Brilliant Blue staining solution. *Coomassie Brilliant Blue solution was filtered before use and stored protected from light.*

3.1.11 Ponceau S staining solution

Ponceau S solution (AppliChem)	5 ml
ddH_2O	45 ml

Table 42: Ponceau S staining solution.

3.1.12 further solutions for SDS PAGE and western blot

EDTA pH 8.0 stock solution	0.5 M EDTA (conjugate base) in ddH_2O, pH adjusted to 8.0 with HCl
10 % Ammoniumpersulfate (APS)	10% (w/v) in ddH_2O
1M Dithiothreitol (DTT) (1000x) stock solution	1M in ddH_2O

Table 43: Further solutions for SDS PAGE and western blot. *10% APS and 1 mM DTT were stored as aliquots at -20°C.*

3.2 Gels for SDS-PAGE

3.2.1 Running gels

	8 % gel	10 % gel	15 % gel
H_2O	4.05 ml	3.67 ml	2.67 ml
Running gel buffer	1.88 ml	1.88 ml	1.88 ml
Acrylamide/Bis solution (40% w/v)	1.5 ml	1.88 ml	2.88 ml
20 % SDS in H_2O	37.5 µl	37.5 µl	37.5 µl
10% APS	37.5 µl	37.5 µl	37.5 µl
TEMED	5 µl	5 µl	5 µl
Total volume (1 gel)	7.5 ml	7.5 ml	7.5 ml

Table 44: Running gels.

3.2.2 Stacking gel

H_2O	3.15 ml
Stacking gel buffer	1.25 ml
Acrylamide/Bis solution (40% w/v)	0.5 ml
20 % SDS in H_2O	25 µl
10% APS	25 µl
TEMED	5 µl
Total volume (2 gels)	5 ml

Table 45: Stacking gels.

3.3 Protein size standards

BenchMark Pre-stained Protein Ladder	ThermoFisher Scientific
Precision Plus Protein™ Kaleidoscope™ Prestained Protein Standards	Bio-Rad

Table 46: Protein size standards.

4 Antibodies

4.1 Primary antibodies for western blot analysis

Target/name	Source species, type	Immunogenic peptide/epitope	supplier	Dilution for Western Blot
acetylated H3	rabbit, polyclonal	Histone H3 amino acids 7-17, K14-ac	EMD Millipore	1:1000
acetylated SMC3 (Nishiyama et al. 2010)	mouse, monoclonal	amino acids 97-115, K105-ac, K106-ac	K. Shirahige, Institute for Molecular and Cellular Biosciences, University of Tokyo, Japan	1:5000

acetylated tubulin	mouse, monoclonal (6-11B-1)	acetylated sea urchin tubulin/epitope located within four residues of α-tubulin K40-ac	Sigma-Aldrich	1:1000
ATG5	rabbit, polyclonal	near C-terminal peptide of ATG5	Cell Signaling Technology	1:500 - 1:1000
ATG7	Rabbit, polyclonal	N-terminal peptide of ATG7	Cell Signaling Technology	1:500
β-actin	mouse, monoclonal (AC-15)	β-actin N-terminal peptide coupled to KLH		1:20,000 - 1:40,000
Beclin-1	goat, polyclonal	near N-terminal peptide of Beclin-1	Santa Cruz Biotechnology	1:1000
FoxO3a	rabbit, monoclonal (75D8)	peptide surrounding D50 of human FOXO3a	Cell Signaling Technology	1:500 - 1:1000
HDAC6	rabbit, polyclonal	amino acids 916-1215 of human HDAC6	Santa Cruz Biotechnology	1:1000
HDAC8	rabbit, polyclonal	amino acids 1-145 against human HDAC8	Santa Cruz Biotechnology	1:2000
HDAC10	rabbit, polyclonal	amino acids 2-16 of human HDAC10	Sigma-Aldrich	1:500
HSC70	rat, monoclonal (1B5)	full length hamster HSC70	Abcam	1:10,000
HSP70	mouse, monoclonal (C92F3A-5)	amino acids 436-503 of human HSP70	Santa Cruz Technology	1:1000
LAMP-1	mouse, monoclonal (H3A4)	NIH/3T3 mouse embryo fibroblast tissue culture cell membranes/recognizes LAMP1 luminal region	Developmental Studies Hybridoma Bank	1:1000
LAMP-2	mouse, monoclonal (H4B4)	full-length LAMP2	Santa Cruz Technology	1:1000
LC3B	rabbit, polyclonal	LC3B amino acids 2-15	Sigma-Aldrich	1:5000
p62/SQTM1	mouse, monoclonal (5F2)	recombinant human p62 amino acids 120-440	Biozol	1:1000
p62/SQTM1	rabbit, polyclonal	amino acids 256-269 of human p62 coupled to KLH	Sigma-Aldrich	1:1000
P-Glycoprotein for western blot	rabbit, monoclonal (E1Y7S)	recombinant protein surrounding Alanin 650 of human P-gp	Cell Signaling Technology	1:1000
Tubulin (α/β)	rabbit, polyclonal	full-length α/β–tubulin	Cell Signaling Technology	1:1000

Table 47: Primary antibodies for western blot analysis.

4.2 Primary antibodies for flow cytometry and immunofluorescence

Target/name	Source species, type	Immunogenic peptide/epitope	supplier	Dilution/concentration
γH2A.X	rabbit, monoclonal (20E3)	synthetic peptide surrounding phosphorylated S139 of human H2A.X	Cell Signaling Technology	1:200
LAMP-1	mouse, monoclonal (H3A4)	NIH/3T3 mouse embryo fibroblast tissue culture cell membranes/recognizes LAMP1 luminal region	Developmental Studies Hybridoma Bank	1-2.5 µg/ml
P-glycoprotein	mouse, monoclonal (MRK16)	Adriamycin resistant human K-562 cells/discontinuous extracellular epitope	Biozol	1:100
mouse IgG1 isotype control	mouse IgG1, monoclonal (NCG01)	not available	Dianova	final concentration equal to target antibody

Table 48: Primary antibodies for flow cytometry and immunofluorescence.

4.3 Secondary antibodies for western blot analysis

Target species	Source species	Type	Conjugation	supplier	Dilution
mouse	goat	IgG	horseradish peroxidase	Dianova, Hamburg, Germany	1:70,000
rabbit	donkey	IgG	horseradish peroxidase	Dianova, Hamburg, Germany	1:60,000 (1:10,000 in case of ATG5, ATG7, FOXO3a)
rat	goat	IgG	horseradish peroxidase	Santa Cruz, Heidelberg, Germany	1:20,000

Table 49: Secondary antibodies for western blot analysis.

4.4 Secondary antibodies for flow cytometry and immunofluorescence

Name	Target species	Source species	Conjugation	supplier	Dilution	Application
anti-mouse-Alexa 488	mouse	goat	Alexa Fluor® 488	Cell Signaling Technology, Leiden, Netherlands	1:500	Fluorescence microscopy

anti-mouse-APC	mouse	goat	Allophycocyanin (APC)	Dianova, Hamburg, Germany	1:200	Flow cytometry
anti-mouse-Cy3	mouse	goat	Cy3	Cedarlane Laboratories, Burlington, Canada	1:200	Fluorescence microscopy
anti-rabbit-Alexa 488	rabbit	goat	Alexa Fluor® 488	Life Technologies/Thermo Fisher Scientific, Braunschweig, Germany	1:500/ 1:1000	Flow cytometry/ Fluorescence microscopy
anti-rabbit-Alexa 568	rabbit	donkey	Alexa Fluor® 568	Life Technologies/Thermo Fisher Scientific, Braunschweig, Germany	1:500/ 1:1000	Fluorescence microscopy
anti-rabbit-Cy3	rabbit	goat	Cy3	Cedarlane Laboratories, Burlington, Canada	1:200	Fluorescence microscopy

Table 50: Secondary antibodies for flow cytometry and immunofluorescence.

5 Peptides for monoclonal antibody production

Peptide name	Amino acid sequence
HDAC10T1	NH_2-MRGSHHHHHHGSMDVTAVPMSPSSHSPEGRPPPLLPGGPVCKAAASAPSSLLDQPCLCPAPSVRTAVALTTPDITLVLPPDVIQQEASALREETEAWARPHESLAREEALTALGKLLYLLDGMLDGQVNSGIAATPASAAAATLDVAVRRGLSKLN-COOH
HDAC10T2	NH_2-MRGSHHHHHHGSMHGAQRLLCVALGQLDRPPDLAHDGRSLWLNIRGKEAAALSMFHVSTPLPVMTGGFLSCILGLVLPLAYGFQPDLVLVALGPGHGLQGPHAALLAAMLRGLAGGRVLALLEENSTPQLKLN-COOH

Table 51: Peptides for the production of monoclonal HDAC10 antibodies. *Amino acid sequence of peptides HDAC10T1 and HDAC10T2. HDAC10 amino acids are highlighted in green, the 6x histidine tag in orange.*

6 Chemicals, consumables and kits

6.1 Chemicals

Substance	Supplier
Acetic acid	Carl Roth, Karlsruhe, Germany
Acridine orange solution (10 mg/ml)	Sigma-Aldrich, Munich, Germany
Acrylamide/Bis solution, 40 % (w/v)	Serva Electrophoresis, Heidelberg, Germany
APS (Ammonium persulfate)	Sigma-Aldrich, Munich, Germany
Bromophenol blue	AppliChem, Darmstadt, Germany
BSA Type H1	Sigma-Aldrich, Munich, Germany
Cell Dissociation Buffer, enzyme-free, PBS-based	Thermo Fisher Scientific, Braunschweig, Germany
Collagen Type I (#C3867)	Sigma-Aldrich, Munich, Germany
cOmplete Mini™	Sigma-Aldrich, Munich, Germany

Brilliant Blue G	Sigma-Aldrich, Munich, Germany
DAPI (4',6-Diamidino-2-phenylindol)	AppliChem, Darmstadt, Germany
Digitonin	Sigma-Aldrich, Munich, Germany
DMEM	Lonza Group, Basel, Switzerland
DMP (Dimethyl pimelimidate dihydro chloride)	Sigma-Aldrich, Munich, Germany
DMSO (Dimethyl sulfoxide)	Sigma-Aldrich, Munich, Germany
DPBS	Lonza Group, Basel, Switzerland
DTT (Dithiothreitol)	AppliChem, Darmstadt, Germany
ECL Prime	GE Healthcare, Munich, Germany
EDTA (ethylene diamine tetraacetate)	GERBU Biotechnik GmbH, Heidelberg, Germany
EGTA (ethylene glycol-bis(β-aminoethyl ether)-N,N,N',N'-tetraacetic acid/egtazic acid)	Sigma-Aldrich, Munich, Germany
Ethanol	Sigma-Aldrich, Munich, Germany
FCS (fetal calf serum)	Sigma-Aldrich, Munich, Germany
Glycine	Sigma-Aldrich, Munich, Germany
Glycerol for molecular biology	Honeywell Riedel-de-Haën, Seelze, Germany
HCl (hydrochlorid acid 12.1 M)	Sigma-Aldrich, Munich, Germany
HEPES	Carl Roth, Karlsruhe, Germany
Hygromycin B solution	Sigma-Aldrich, Munich, Germany
IMDM	ThermoFisher Scientific, Braunschweig, Germany
Isopropanol	Sigma-Aldrich, Munich, Germany
KCl (potassium chloride)	Carl Roth, Karlsruhe, Germany
LiChrosolv® water LC-MS Grade	Merck Millipore, Darmstadt, Germany
Low melting agarose	Biozym Scientific, Hessisch Oldendorf, Germany
LysoTracker™ Red DND-99	ThermoFisher Scientific, Braunschweig, Germany
Methanol	Sigma-Aldrich, Munich, Germany
$MgCl_2$(Magnesium chloride)	Merck, Darmstadt, Germany
Milk powder	Carl Roth, Karlsruhe, Germany
NaCl (sodium chloride)	Sigma-Aldrich, Munich, Germany
NaOH (sodium hydroxide) 1M solution	Sigma-Aldrich, Munich, Germany
NaOH pellets	Sigma-Aldrich, Munich, Germany
NEAA (non-essential amino acids) 100x	Lonza Group, Basel, Switzerland
NGS (normal goat serum)	Dianova, Hamburg, Germany
Opti-MEM I	ThermoFisher Scientific, Braunschweig, Germany
Paraformaldehyde (PFA) 16% MeOH free	Alfa Aesar, Karlsruhe, Germany
Ponceau S solution	AppliChem, Darmstadt, Germany
PMSF (phenylmethane sulfonyl fluoride)	Sigma-Aldrich, Munich, Germany
RIPA buffer (10x)	Cell Signaling Technology, Leiden, Netherlands
RPMI 1640	ThermoFisher Scientific, Braunschweig, Germany
RPMI 1640, no Phenol Red	ThermoFisher Scientific, Braunschweig, Germany
Sodium acetate	Sigma-Aldrich, Munich, Germany
SDS (Sodium dodecyl sulfate)	Carl Roth, Karlsruhe, Germany
sodium pyruvate 100x	ThermoFisher Scientific, Braunschweig, Germany
Sucrose	Carl Roth, Karlsruhe, Germany
SYTOX Green Nucleic Acid Stain	ThermoFisher Scientific, Braunschweig, Germany
TEMED (N, N, N, N-Tetramethyl-Ethylenediamine)	Carl Roth, Karlsruhe, Germany
Triethanolamine	Sigma-Aldrich, Munich, Germany
Tris/HCl	Sigma-Aldrich, Munich, Germany
Triton-X 100	AppliChem, Darmstadt, Germany
Trizma Base	Sigma-Aldrich, Munich, Germany
trypsin-EDTA, 0.05 % (w/v)	ThermoFisher Scientific, Braunschweig, Germany

Tween 20 (polyoxyethylene sorbitan monolaureate)	GERBU Biotechnik GmbH, Heidelberg, Germany
Vi-Cell XR Cell Viability Analyzer™ solutions	Beckmann Coulter, Krefeld, Germany
Z-FR-AFC cathepsin L substrate (ALX-260-129)	Enzo Life Sciences, Lörrach, Germany

Table 52: Chemicals.

6.2 Consumables

Name	Supplier
Cell scraper	Sarstedt, Nürnbrecht, Germany
Chromatography Paper "Whatman CHR 3mm"	GE Healthcare, Munich, Germany
CometSlide™ 2 Well	Trevigen, Gaithersburg, United States
Conical tubes, 15 ml	ThermoFisher Scientific, Braunschweig, Germany
Conical tubes, 50 ml	ThermoFisher Scientific, Braunschweig, Germany
Dynabeads™ Protein G for Immunoprecipitation	ThermoFisher Scientific, Braunschweig, Germany
Falcon® 5mL Round Bottom Polystyrene Test Tube (FACS Tubes)	ThermoFisher Scientific, Braunschweig, Germany
Glassware	SCHOTT AG, Mainz, Germany
Ibidi 8-well µ-Slides	Ibidi GmbH, Martinsried, Germany
Microplates, 96 well, clear	Greiner Bio-One, Frickenhausen, Germany
Microplates, 96 well, white	Greiner Bio-One, Frickenhausen, Germany
Parafilm® M	Benis, Braine-l'Alleud, Belgium
PCR tube strips and domed caps	Thermo Fisher Scientific, Braunschweig, Germany
Pipette filter tips, 10 µl	nerbe plus, Winsen/Luhe, Germany
Pipette filter tips, 20 µl	nerbe plus, Winsen/Luhe, Germany
Pipette filter tips, 100 µl	nerbe plus, Winsen/Luhe, Germany
Pipette filter tips, 200 µl	nerbe plus, Winsen/Luhe, Germany
Pipette filter tips, 1000 µl	nerbe plus, Winsen/Luhe, Germany
Pipette tips, 2-10 µl	Steinbrenner Laborsysteme, Wiesenbach, Germany
Pipette tips, 20-200 µl	Steinbrenner Laborsysteme, Wiesenbach, Germany
Pipette tips, 1000 µl	Steinbrenner Laborsysteme, Wiesenbach, Germany
Polystyrene Round-Bottom Tube with Cell-Strainer Cap	Corning, Kaiserslautern, Germany
PVDF membrane	Bio-Rad Laboratories, Munich, Germany
Reaction tubes "Safe-Lock Tubes", 0.5 ml	Eppendorf, Hamburg, Germany
Reaction tubes "Safe-Lock Tubes", 1.5 ml	Eppendorf, Hamburg, Germany
Reaction tubes "Safe-Lock Tubes", 2.0 ml	Eppendorf, Hamburg, Germany
Serological pipettes, 5 ml	Sigma-Aldrich, Munich, Germany
Serological pipettes, 10 ml	Sigma-Aldrich, Munich, Germany
Serological pipettes, 25 ml	Sigma-Aldrich, Munich, Germany
Tissue culture dishes, 100x20 mm	Thermo Fisher Scientific, Braunschweig, Germany
Tissue culture flasks "Cellstar" 25 cm^2, 75 cm^2, 175 cm^2	Greiner Bio-One, Frickenhausen, Germany
Tissue culture plates, 6 well, 12 well, 96 well	Corning, Kaiserslautern, Germany
Tissue culture plates 96 well round bottom (U-base) TPP®	Sigma-Aldrich, Munich, Germany

Table 53: Consumables.

6.3 Commercial kits

Kit	Supplier
Amersham ECL Prime Western Blotting Detection Reagent	GE Healthcare, Munich, Germany
Cyto-ID® Autophagy Detection Kit 2.0	Enzo Life Sciences, Lörrach, Germany
eBioscience™ Foxp3 / Transcription Factor Staining Buffer Set	ThermoFisher Scientific, Braunschweig, Germany
Venor® GenM Classic Mycoplasma Detection Kit	Minerva Biolabs, Berlin, Germany
Pierce BCA Protein Assay Kit	ThermoFisher Scientific, Braunschweig, Germany
Pierce NE-PER Nuclear and cytoplasmic extraction reagents	ThermoFisher Scientific, Braunschweig, Germany
PlasmoTest™ Mycoplasma Detection Kit	InvivoGen, San Diego, CA, United States
QIAGEN RNeasy Mini Kit	QIAGEN, Hilden, Germany
qPCR Mastermix for SYBR® Green I	Eurogentec, Liège, Belgium
RevertAid First Strand cDNA Synthesis Kit	ThermoFisher Scientific, Braunschweig, Germany

Table 54: Commercial kits.

7 Equipment and instruments

Instrument	Supplier
ABI 7500 Real-Time PCR System with Dell™ Notebook	Applied Biosystems, Foster City, United States
Analytical Balance "BP 121S"	Sartorius, Göttingen, Germany
Barnstead™ GenPure™ xCAD Plus Ultrapure Water Purification System	ThermoFisher Scientific, Braunschweig, Germany
Benchtop centrifuge "Allegra X-12R"	Beckmann Coulter, Krefeld, Germany
Biometra T3000 Thermocycler	LabRepCo, Horsham, PA, United States
Blotting chamber "TransBlot® SD Semi-Dry Transfer Cell"	Bio-Rad Laboratories, Munich, Germany
Butane/Propane cartridge	Campingaz/Newell Brands, Hoboken, United States
Canon EOS 500D SLR digital camera	Canon, Krefeld, Germany
"CellMate® II Serological Pipette"	Matrix Technologies Corporation/ThermoFisher Scientific
Chemiluminescence imaging system "Chemi-Smart 5000"	Vilber Lourmat, Eberhardzell, Germany
Cell culture incubator "C200"	Labotect, Rosdorf, Germany
Cell culture sterile bench "Safe 2020"	ThermoFisher Scientific, Braunschweig, Germany
Cell culture sterile bench "Gelaire BSB4A"	ICN/MP Biomedicals, Illkirch Cedex, France
Cell counter "Vi-Cell XR Cell Viability Analyzer"	Beckman Coulter, Krefeld, Germany
Dark hood DH-10	Biostep, Burkhardtsdorf, Germany
DynaMag™-2 Magnet	ThermoFisher Scientific, Braunschweig, Germany
Electrophoresis chamber "Mini-Protean® Tetra System"	Bio-Rad Laboratories, Munich, Germany
Flow cytometer "FACSCalibur"	Becton, Dickinson and Company, Heidelberg, Germany
Flow cytometer "FACS Canto II"	Becton, Dickinson and Company, Heidelberg, Germany

Heating block "Thermomixer® comfort"	Eppendorf, Hamburg, Germany
Heat sealer "Folio"	Severin Elektro, Sundern, Germany
Heraeus Minifuge 4400 GL	Heraeus, Leverkusen, Germany
Incubator Heraeus B6420	Heraeus, Leverkusen, Germany
Innova 4230 refrigerated benchtop incubator	New Brunswick Scientific, Nürtingen, Germany
Light microscope "CKX31"	Olympus, Hamburg, Germany
Light microscope "CKX41" with reflected fluorescence system	Olympus, Hamburg, Germany
Light microscope "Zeiss LSM710" confocal microscope for fluorescence imaging	Carl Zeiss, Oberkochen, Germany
Magnetic stirrer with heating "MR-3001"	Heidolph Instruments, Schwabach, Germany
MatriGrid ridged scaffolds for 3D culture	TU Ilmenau, Ilmenau, Germany
Metafer4 automated cell scanning system	MetaSystems Hard & Software, Altlußheim, Germany
Microcentrifuge "5417 R"; rotor: "F 45-24-11"	Eppendorf, Hamburg, Germany
Micropipette “PIPETMAN Neo® P2N”	Gilson, Limburg-Offheim, Germany
Micropipette “PIPETMAN Neo® P10N”	Gilson, Limburg-Offheim, Germany
Micropipette “PIPETMAN Neo® P20N”	Gilson, Limburg-Offheim, Germany
Micropipette “PIPETMAN Neo® P200N”	Gilson, Limburg-Offheim, Germany
Micropipette “PIPETMAN Neo® P1000N”	Gilson, Limburg-Offheim, Germany
Micropipette "Eppendorf Research® 10-100 µl"	Eppendorf, Hamburg, Germany
Micropipette "Eppendorf Research® 0.5-10 µl"	Eppendorf, Hamburg, Germany
Microplate fluorescence reader "FLUOstar OPTIMA"	BMG Labtech, Ortenberg, Germany
Microwave oven "Severin MW 7869"	Severin Elektro, Sundern, Germany
Multi-axle rotating mixer "TRM 56"	IDL GmbH, Nidderau, Germany
Multichannel pipette "Finnipipette® Digital 40-200 µl"	ThermoFisher Scientific, Braunschweig, Germany
Multi Gel Unit FU300	Biostep, Burkhardtsdorf, Germany
NanoAcquity UPLC system	Waters GmbH, Eschborn, Germany
Nano Drop ND-1000 Spectrophotometer	PEQLab, Erlangen, Germany
pH meter "SevenEasy"	Mettler-Toledo, Gießen, Germany
Pipette controller "accu-jet® pro"	BRAND, Wertheim, Germany
Power supply "EV231"	PEQLab, Erlangen, Germany
Power supply "PowerPac™ Basic Power Supply"	Bio-Rad, Munich, Germany
Precision balance "440-47N"	KERN & SOHN, Balingen, Germany
Q Exactive™ HF hybrid quadrupole-Orbitrap Mass Spectrometer	ThermoFisher Scientific, Braunschweig, Germany
Refrigerator with freezer	Liebherr, Biberach an der Riß, Germany
Rocking platform "WT 16"	Biometra, Göttingen, Germany
Scanner "Perfection V700 photo"	Epson, Meerbusch, Germany
Test tube shaker "Reax top"	Heidolph Instruments, Schwabach, Germany
TQ Orbitrap XL Mass Spectrometer	ThermoFisher Scientific, Braunschweig, Germany
UltiMate 3000 RSLCnano UPLC system	ThermoFisher Scientific, Braunschweig, Germany
Ultra-low temperature freezer	ThermoFisher Scientific, Braunschweig, Germany
Universal 320R tabletop centrifuge (for plates)	Hettich Lab Technology, Tuttlingen, Germany
UV transilluminator "UST-15M-8K"	Biostep, Burkhardtsdorf, Germany
Vortexer "IKA VF2"	IKA Janke & Kunkel, Staufen im Breisgau, Germany
Waterbath	Memmert, Schwabach, Germany

Table 55: Equipment and instruments.

8 Software

Software	Supplier
Adobe Illustrator CS3	Adobe
Adobe Photoshop CS3 and CS6	Adobe
Argus® X1 Version 7	Biostep
EndNote X5	Thomson Reuters/Clarivate Analytics
FlowJo v10	FlowJo, LLC
GraphPad Prism Version 5.0	GraphPad Software Inc.
ImageJ 1.48v	National Institutes of Health
Microsoft Office 2007/2010	Microsoft
OPTIMA Microplate Reader Software Version 2.20R2	BMG Labtech
Scaffold 4.03	Proteome Software
Zen 2012 lite	Carl Zeiss

Table 56: Software.

9 Databases

Database	Website
Ensembl Genome Browser	www.ensembl.org
NCBI	www.ncbi.nlm.nih.gov
UniProt	www.uniprot.org

Table 57: Databases.

C METHODS

1 Cell Biological Methods

1.1 Cell culture and propagation of cells

Unless otherwise specified, all cell culture media, DPBS and trypsin-EDTA were pre-warmed to room temperature before use. All cell lines and short-term cultures were kept under standard cell culture conditions (37°C, 5 % CO_2, 95 % relative humidity) Adherent commercial cell lines (SK-N-BE(2)-C / BE(2)-C, IMR-32, Kelly, SK-N-AS, HAP1) were subcultured every 3-4 days when reaching 70-80% confluency. To that end, cells were briefly washed in DPBS and incubated in trypsin-EDTA for 3-4 minutes at 37°C. After addition of 5 ml of the respective culture medium (***Table 2***), cells were resuspended and either transferred to a new culture flask in an appropriate split ratio or transferred to a 50 ml centrifuge tube for cell counting and seeding.

For subculturing of semi-adherent cell lines (e.g. hybridomas), supernatant was transferred to a 50 ml centrifuge tube. Cells were detached by thorough pipetting, transferred to the respective centrifuge tube and centrifuged for 5 minutes at 230 x g. Cells were resuspended in 5 ml culture medium and transferred to a new culture flask in an appropriate split ratio.

Cell lines were checked weekly for mycoplasm contamination with the PlasmoTest™ Mycoplasma Detection Kit (InvivoGen), and mothly via PCR using the Venor® GenM Classic Mycoplasma Detection Kit (Minerva Biolabs). Cell lines were further checked for viral contamination by Multiplexion (Heidelberg, Germany) and cell identity was verified via DNA fingerprinting authentication (DMSZ, Germany).

1.2 Cryoconservation and defrosting of cells

Adherent cells were detached at 70-80 % confluency as described above and centrifuged for 5 minutes at 230 x g. The supernatant was removed and cells were resuspended in cryoconservation medium (respective cell medium supplemented with 10 % DMSO). Typically, cells from one 75 cm^2 flask were resuspended in 3-5 ml cryoconservation medium and quickly distributed to sterile cryoconservation vials at 1 ml per vial. The sample vials were immediately frozen at -20°C over night and transferred to -80°C the following morning for long-term storage.

To defrost cells, cryoconservation vials were thawed rapidly at room temperature and the cell suspension was immediately transferred to a 15 ml tube containing 9 ml of the respective culture

medium. For the removal of DMSO remnants, the supernatant was aspirated after centrifugation for 5 minutes at 230 x g. Depending on pellet size, cells were resuspended in 2 ml or 5 ml cell culture media and transferred to a 6-well plate or a 25 cm² flask. The culture medium was replaced on the following day. In case of stably transfected or transduced cells, antibiotic selection was started as soon as cells had been transferred to 75 cm² flasks.

1.3 Cell counting and seeding

For seeding, cell concentration and viability were assessed using a Vi-Cell XR automatic cell counter (Beckmann Coulter). Cell suspensions were then diluted in order to achieve the required cell density and cells were distributed to the respective cell culture vessel (cell numbers given in the sections for individual assays).

Seeding of cells on MatriGrid ridged scaffolds for 3D culture

Threedimensional cultures of BE(2)-C cells were cultivated on microcavity-containing, ridged scaffolds (MatriGrid structures with a diameter of 300 µm, depth of 207 µm and a total active area of 5 x 5 mm^2). MatriGrid scaffolds were coated with substratum (10 µg/cm^2 collagen type I), which allowed cells to adhere to the scaffold and dried for 2h. Cell suspension was added ($2.5*10^5$ cells per chip in 6-well plate) and allowed to adhere for at least 24h under standard cell culture conditions before beginning of treatment. Cells were allowed to grow on scaffolds for 3-7 days depending on assay. For retrieval of cells from scaffolds, cells were incubated in trypsin-EDTA for 4 minutes at 37°C.

1.4 Treatment of cells

For treatment of cells with antibiotics, chemotherapeutics or inhibitors, substances were diluted in the respective culture medium. If necessary, substances were pre-diluted in order to avoid pipetting of substance volumes below 1 µl. In case of adherent cells, the cell medium was aspirated completely before addition of treatment solutions. In case of semi-adherent cells, substances were directly added to the cell culture supernatant in order to avoid loss of floating cells.

1.5 Transient and stable transfections

Cells were transfected with plasmids using the QIAGEN Effectene Transfection Reagent. For transient transfections with pEGFP-N1-TFEB (***Table 11***), $1*10^6$ BE(2)-C cells were seeded on sterile 10 cm dishes 24h before the transfection procedure. The following day, 1 µg of plasmid was added to 100 µl of EC buffer. Next, 2 µl of Enhancer were added, samples were briefly vortexed and incubated at room temperature for 5 minutes. After addition of 7.5 µl Effectene, the transfection mix was again vortexed and incubated at room temperature for 30 minutes. After addition of 1 ml medium, the

transfection mix was added dropwise to cells on 10 cm dishes containing 3 ml of cell culture supernatant and incubated over night under standard cell culture conditions. Medium was changed the following day (10 ml per plate), and cells were transferred to 6-well dishes for treatment with HDAC inhibitors. Microscopic images were taken 72h-96h after transfection.

For stable transfections of IMR-32 cells with pCMV/hygro-FLAG HDAC10 or pCMV / hygro-Negative Control Vector (***Table 11***), $2*10^5$ cells were seeded in 6-well plates and transfected the following day as described above with the following modifications: Transfection mixes were filled up with 500 µl of medium before dropwise addition of the transfection mix to 6-wells containing cells and 1.5 ml culture supernatant. Medium was replaced the following day (3 ml per well). Antibiotic selection with hygromycin B was started 24h after transfection and selection medium was replaced every 3 days. Cells were propagated to larger culture vessels when reaching a confluency of 70%.

1.6 Transfection of cells with siRNAs

Cells were transfected with siRNA using the QIAGEN HiPerFect transfection reagent. To that end, $4*10^5$ cells were seeded on 10 cm dishes. The next day, 50 µl of pre-diluted siRNAs (2 µM) (***Table 7*** and ***Table 8***) were added to sterile 1.5 ml reaction tubes containing 20 µl HiPerFect transfection reagent and diluted to a final concentration of 100 nM using 930 µl Opti-MEM medium. The transfection reaction was mixed by flicking and brief centrifugation, followed by incubation at room temperature for 10 minutes. The transfection mix was then added dropwise to the 10 cm dishes containing 3 ml of cell culture supernatant and incubated over night under standard cell culture conditions. The following morning, the supernatant was aspirated and replaced by 10 ml fresh culture medium per plate. Cells transfected with siRNA were typically analyzed three to six days after transfection.

1.7 Flow cytometry (Fluorescence activated cell sorting - FACS)

Flow cytometry allows for the counting and the analysis of the physical and biochemical properties of particles (cells or beads) in fluids. Cellular properties like size, shape and granularity can be determined by means of forward and sideward light scattering (FSC = forward scatter, SSC = side scatter) and reflection. Flow cytometry is furthermore used to characterize single cells in suspension by their specific cell surface proteins, receptors or antigens. The use of fluorescently-labeled antibodies allows for the quantification of these cell-surface proteins on a single-cell scale. Finally, flow cytometry also allows for the quantitative detection of the cellular uptake and/or the retention of fluorescent dyes.

1.7.1 Flow cytometric analysis of cell surface protein expression

For flow cytometric analysis of cell surface protein expression, adherent cells were dissociated from dishes or flasks using non-enzymatic cell dissociation reagent for 5 minutes at 37°C. Detaching cells were resuspended in Phenol red free RPMI medium supplemented with 10 % FCS and counted using a Vi-Cell XR automatic cell counter (Beckmann Coulter). After centrifugation at 230 x g for 5 minutes at 4°C, 2.5-3*10^5 cells were resuspended in FACS buffer (***Table 13***) and transferred into a pre-cooled 96-well round bottom plate, followed by centrifugation at 180 x g for 3 minutes at 4°C. After each centrifugation step, the supernatant was discarded by careful tapping of the 96-well plate on paper tissue. Cells were stained with primary antibodies against P-gp, LAMP-1 or control antibody of identical isotype (***Table 48***) diluted in FACS buffer for 1.5 - 2 hours on ice. Cells were washed three times in 200 µl/well FACS buffer, followed by centrifugation as described above and incubated with either Alexa 488 or APC-labeled secondary antibody (***Table 50***) for 1h on ice. After three final washing steps, cells were resuspended in 130 µl/well FACS buffer and transferred to pre-chilled FACS tubes. Cells were analyzed on a BD FACSCanto II platform. Data from 10,000 cells per sample were acquired and analyzed using FlowJo® analysis software (version 10).

1.7.2 Flow cytometric analysis of DNA double strand breaks

Flow cytometry is not only suitable for the analysis of cell surface markers, but also allows for the quantification of intracellular and even nuclear proteins after fixation and permeabilization of cells with suitable buffers. Serine 139 phosphorylation of histone variant H2A.X (γH2A.X) is known to occur after the formation of DNA double strand breaks and the occurrence of nuclear γH2A.X foci is used as a reliable and quantitative marker for DNA double strand breaks (Rogakou et al. 1998; Kuo and Yang 2008). In order to assess DNA double strand breaks after treatment of cells with chemotherapeutics and/or HDAC inhibitors, cells were detached from dishes using trypsin-EDTA for 3 minutes at 37°C. Detaching cells were resuspended, counted and transferred to 96-well round bottom plates at 4*10^5 cells per well as described in section ***C1.7.1*** Cell pellets were fixed and permeabilized using the eBioscience™ Foxp3/Transcription Factor Staining Buffer Set (Thermo Fisher Scientific, see ***Table 15***). For fixation, cells were resuspended in 200 µl per well fixation solution (***Table 15***), followed by incubation on ice for 30 minutes. Cells were centrifuged at 180 x g and 4°C for 3 minutes. For nuclear permeabilization, cells were first resuspended in 50 µl per well 1x permeabilization buffer (***Table 15***), centrifuged as described above, and again resuspended in 200 µl per well 1x permeabilization buffer. Following centrifugation, cells were incubated for 1.5h at 4°C with primary antibody (***Table 48***) diluted in 1x permeabilization buffer (100 µl per well), followed by two to three washing steps in 200 µl per well 1x permeabilization buffer. After staining with Alexa 488 labeled secondary antibody for 1h at 4°C (***Table 50***), cells were washed as described above and

transferred to pre-chilled FACS tubes for analysis. FACS analysis was performed as described in section ***C1.7.1***.

1.7.3 Flow cytometric analysis of intracellular doxorubicin accumulation

Doxorubicin, also known as adriamycin, is a widely used chemotherapeutic agent that belongs to the class of anthracyclines, and is a commonly used drug in neuroblastoma therapy. It possesses a marked autofluorescence (excitation λ_{max} 427/501 nm; emission λ_{max} 552/585 nm), which can be used for the quantification of cellular doxorubicin concentrations.

Doxorubicin accumulation in 2D-cultured cells

Flow cytometric quantification of intracellular doxorubicin was performed as described in (Ridinger et al. 2018). Briefly, cells were seeded in 6-well dishes at densities of $1.5*10^5$ cells/well (BE(2)-C and SK-N-AS, HAP1, human fibroblasts) and $3*10^5$ cells/well (IMR-32, Kelly, NB-1). Cells were treated with doxorubicin for 24 - 48h at the following concentrations: 25 ng/ml, 50 ng/ml, 100 ng/ml (indicated in figure legends). Where indicated, cells were co-treated with HDAC6/10 inhibitors or lysosomal inhibitors. Where indicated, vacuolin-1 was directly added to doxorubicin-treated cells 1h or 24h before flow cytometric analysis.

In case of knockdown of HDAC6, HDAC10, ATG5 or P-glycoprotein in BE(2)-C cells, measurement was performed three days (ATG5), five days (P-glycoprotein) or six days (HDAC6/10) after transfection with siRNA (indicated in the respective figure legend). Cells were transferred to 6-well dishes ($1.5*10^5$ cells per well) 1-4 days after transfection and treated with 100 ng/ml doxorubicin. Where indicated, HDAC6/10i and lysosomal inhibitors were added for the last 24h.

After doxorubicin treatment, cells were washed with 1 ml per well ice-cold Phenol red free RPMI containing 10% FCS and detached using 500 µl per well trypsin-EDTA for 3 minutes at 37°C. Cells were resuspended by the addition of 500 µl per well RPMI, transferred to 1.5 ml reaction tubes, centrifuged for 3 minutes at 8600 x g and 4°C, resuspended in Phenol red free RPMI and transferred to pre-chilled FACS tubes. Doxorubicin fluorescence of 10,000 cells was quantified on a BD FACSCanto II platform using the PE filter setting.

Doxorubicin accumulation in 3D-cultured neuroblastoma cells

BE(2)-C cells were seeded in MatriGrid scaffold as described in section ***C1.3***. 24h prior to beginning of treatment. 3D cultures were treated with 500 ng/ml doxorubicin and co-treated with HDAC6/10 or lysosomal inhibitors where indicated. In case of ATG5, FoxO3a or Beclin-1 knockdown, BE(2)-C cells were seeded in MatriGrid scaffold 72h after transfection with siRNAs, grown for an additional 48 h and treated for the last 24h with 500 ng/ml doxorubicin. Cells were detached from MatriGrid scaffolds after one washing step with Phenol red free medium by trypsinization for 4 minutes at

37 °C, centrifuged and washed again in Phenol red free medium. Doxorubicin fluorescence was analyzed via flow cytometry as described in the previous section.

Doxorubicin washout experiments

BE(2)-C cells were seeded in 6-well dishes (one 6-well plate per timepoint) at a density of $1.5*10^5$ cells/well. One day post seeding, cells were pre-treated with HDAC6/10 inhibitors over night (12h) and labeled with high doxorubicin concentrations (1 µg/ml) the next day for 3h under standard cell culture conditions. After labeling with doxorubicin, cells were washed twice with pre-warmed medium and either directly analyzed for doxorubicin fluorescence after detachment (t_0 timepoint plate) or re-incubated for 3-6h with medium containing HDAC6/10, lysosomal inhibitors or solvent. Detachment of cells and analysis of doxorubicin fluorescence was performed as described in the sections above. Doxorubicin fluorescence at 3h and 6h after washout was normalized to fluorescence at t_0.

1.7.4 Flow cytometric analysis of staining with LysoTracker® Red DND-99

The LysoTracker® dyes are weakly basic organic compounds suitable to track acidic organelles. At a neutral pH, they are only partially protonated and therefore able to freely permeate across membranes. At low pH however, the LysoTracker dye becomes protonated and will therefore accumulate preferably in acidic organelles such as lysosomes. LysoTracker staining was performed as described in (Ridinger et al. 2018). Six days after siRNA transfection or 24 h after treatment with inhibitors, cells were stained with LysoTracker for 1h under standard cell culture conditions by direct addition of the LysoTracker dye to the cell supernatant (final concentration 50 nM). Post incubation, cells were washed with ice-cold Phenol red free RPMI and detached using 500 µl per well trypsin-EDTA for 3 minutes at 37°C. Cells were resuspended by addition of 500 µl ice-cold RPMI and the cell suspension was transferred to a pre-chilled 1.5 ml reaction tube. Cells were centrifuged for 3 minutes at 8600 x g and 4°C. After aspiration of the supernatant, cell pellets were resuspended in ice-cold RPMI and LysoTracker® Red fluorescence of at least 10,000 cells was quantified on a BD FACSCanto II platform using the PE filter setting.

1.7.5 Flow cytometric quantification of Cyto-ID® staining

For Cyto-ID staining of 2D- grown BE(2)-C cells, cells were seeded at a density of $1.5*10^5$ cells/well in 6-well plates. Where indicated, cells were treated over night with lysosomal inhibitors before staining with 0.5 ml of Cyto-ID staining solution (1 × assay buffer, 5% FCS, 1 μl Cyto-ID) for 30 min under standard cell culture conditions. Cells were detached as described in the section above.

In case of 3D cultures, BE(2)-C cells were seeded in MatriGrid scaffolds 72h after siRNA transfection, followed by growth for three more days under standard cell culture conditions. Where indicated,

cells were treated for the last 24h with lysosomal inhibitors. For staining (6d after-siRNA transfection), MatriGrid scaffolds were washed in Phenol red free medium, transferred to a fresh 6-well plate and stained with 0.5 ml of Cyto-ID staining solution (see above) for 30 min at 37 °C. Cells were washed in Phenol red free medium, trypsinized for 4 minutes at 37 °C, centrifuged and washed again. Cyto-ID fluorescence of at least 10,000 cells was quantified on a BD FACSCanto II platform using the Alexa 488 filter setting.

1.7.6 Flow cytometric quantification of acridine orange staining

Acridine orange is a weak base fluorophor that freely diffuses across cellular membranes. Protonation at low pH leads to trapping of the dye in the respective compartments (e.g. acidic vesicles, lysosomes or autophagolysosomes). Trapping and accumulation in lysosomes, in turn, causes the metachromatic shift from green to red fluorescence (Thome et al. 2016).

For staining of cells with acridine orange, BE(2)-C cells were seeded at $1.5*10^5$ cells/well into 6-well plate one or two days before staining. Cells were stained with acridine orange staining solution (1 µg/ml acridine orange in Phenol Red free RPMI (***Table 12*** and ***Table 14***) for 30 minutes at 37°C. Cells were detached for flow cytometric analysis as described in section ***C1.7.3***. Red acridine orange fluorescence of $2*10^4$ cells was quantified on a "FACSCalibur" flow cytometer.

1.8 Fluorescence microscopy

1.8.1 Fluorescence microscopic analysis of doxorubicin and LysoTracker® Red DND-99 and Cyto-ID® staining

For doxorubicin staining, BE(2)-C cells were seeded into ibidi 8-well µ-slides ($2*10^4$ cells per well) and allowed to attach to the slide surface for 24h. Cells were treated with 250 ng/ml doxorubicin in absence or presence of HDAC6/10i or lysosomal inhibitors for 24h. On the following day, cells were washed twice in PBS and fixed for 20 minutes using 4% PFA at room temperature. Fixed cells were again washed twice with PBS and counterstained with DAPI (0.25 µg/ml in PBS) or SYTOX Green (100 nM in PBS) for 10-15 minutes. For LysoTracker staining or Cyto-ID, cells were seeded into ibidi slides as described above, treated for 24h with HDAC6/10 inhibitors where indicated, and stained for 1h with 50 nM LysoTracker or for 30 minutes with 200 µl/well Cyto-ID staining solution (1 × assay buffer, 5% FCS, 1 µl Cyto-ID, 1 µg/ml Hoechst 33342) under standard cell culture conditions. Cells were washed as described above, fixed for 15 minutes (4% PFA at room temperature) and, in case of LysoTracker staining, counterstained as described above. Slides were imaged on a Zeiss LSM710 confocal microscope.

Cyto-ID imaging of 3D-grown BE(2)-C cells on 3D MatriGrid scaffolds

Cyto-ID imaging of 3D-grown BE(2)-C cells was performed as described according to (Bingel et al. 2017). Briefly, BE(2)-C cells were seeded at a density of $2.5*10^5$ cells per scaffold and grown for two days under standard cell culture conditions. One day prior to treatment, scaffolds were carefully transferred into 8-well μ-Slides (Ibidi) and treated in sterile Phenol Red free medium (***Table 12***) where indicated. For staining, slides were washed twice in 1x assay buffer supplemented with 5% FCS and stained with 200 µl/well CYTO-ID staining solution (1 × assay buffer, 5% FCS, 2 µl CYTO-ID, 1 µg/ml Hoechst 33342) for 30 min at 37 °C. Scaffolds were carefully washed with and finally completely submerged in Phenol Red free medium. Z-Stack imaging was performed on a Zeiss LSM710 confocal microscope.

1.8.2 Immunofluorescence

Staining of cytoplasmic antigens

BE(2)-C and IMR-32 cells were seeded into ibidi 8-well µ-slides at a density of $2\text{-}4*10^4$, and allowed to adhere to the slide surface for at least 24h (48h or longer in case of treatment). Cells were washed once in PBS, fixed in 4% PFA for 15 minutes (BE(2)-C) and 25 minutes (IMR-32), respectively, and washed again. Cells were permeabilized for 10 minutes with permeabilization solution for cytoplasmic antigens and blocked for 1h at room temperature with blocking solution for cytoplasmic antigens (***Table 17***). Cells were stained with respective antibodies at concentrations given in the respective figure legend in blocking solution over night (4°C) followed by 2x washing in PBS and incubation with the respective secondary antibody at room temperature for 2h on the following day. Slides were washed twice with PBS and nuclei were counterstained with DAPI (0.25 µg/ml in PBS) for 10 minutes at room temperature. Images were acquired on a Zeiss LSM710 confocal microscope.

Staining of chromatin-located antigens (γH2A.X staining)

BE(2)-C cells were seeded and fixed as described above. Cells were permeabilized for 30 minutes with permeabilization solution for nuclear antigens and blocked for 1h at room temperature with blocking solution for nuclear antigens (***Table 17***). Cells were stained with anti Phospho-Histone H2A.X (S139) primary antibody diluted in blocking solution over night (4°C), followed by 2x washing in PBS and incubation with Alexa-488-labeled secondary antibody at room temperature for 2h on the following day. Counterstaining of nuclei and imaging was performed as described above.

1.9 Trypan Blue Cell viability assay

The diazo dye Trypan Blue is routinely used to discriminate dead from viable cells, as it is effectively excluded from cells with an intact plasma membrane and therefore only stains dead cells with compromised membrane integrity. For 48 h and 96 h treatments, BE(2)-C cells and non-transformed

VH7 fibroblasts were seeded at a density of $1.5*10^5$ (24h, 48 h) and $7.5*10^4$ (96 h) cells per well, and treatment was started on the following day. After completion of treatment, cell supernatants were collected in 15 ml centrifuge tubes and cells were detached applying 500 µl per well trypsin-EDTA for 3 minutes at 37°C. Cells were resuspended by addition of 1 ml respective culture medium and the cell suspension was transferred to the 15 ml centrifuge tube containing the respective cell culture supernatant. Cells were centrifuged for 5 minutes at 335 x g and the supernatant was decanted. Cell pellets were resuspended in 800 µl culture medium and cell number, as well as cell viability were analyzed by automated trypan blue staining on a Vi-Cell XR Cell Viability Analyzer.

1.10 Colony formation assay

BE(2)-C cells were seeded into 6-well plates (800 cells per well) and treated the following day. After treatment for 24h, drugs were removed by washing with pre-warmed medium once and cells were allowed to grow for 11 more days. Colonies were stained with crystal violet staining solution (***Table 23***) for 10 minutes and carefully washed with ddH_2O. Plates were scanned (Perfection V700 photo, Epson), and colony growth was quantified on 16-bit binary pictures using the ITCN plugin in ImageJ (U. S. National Institutes of Health, Bethesda, MD, USA; http://imagej.nih.gov/ij/).

1.11 Cathepsin Release Assay

BE(2)-C cells were seeded at $1*10^6$ cells per dish on 10 cm plates and allowed to adhere overnight. Cells were treated for 24h with HDAC inhibitors as indicated in the respective figure legend. On the following day, cells were washed with PBS, harvested with enzyme-free cell dissociation buffer (5 minutes 37°C) and counted. For triplicate measurement, $1.875*10^4$ cells were transferred into a pre-chilled 1.5 ml reaction tube, pelleted for 4 minutes at 200 x g, washed once in ice-cold PBS and pelleted again for 3 minutes at 18,000 x g. Cell pellets were lysed in 75 µl ice-cold extraction buffer (containing either 15 µg/ml or 200 µg/ml digitonin) and incubated for 12 minutes on ice before addition of the same volume of freshly prepared 2 x cathepsin reaction buffer. After addition of 7.5 µl cathepsin substrate (Z-FR-AFC), each 50 µl of the reaction mix were distributed to three wells of a clear bottom 96-well plate. AFC fluorescence was quantified on a FLUOstar OPTIMA microplate reader (excitation 380 nm, emission 520 nm) every 10 minutes (1 kinetic cycle) for at least 17 cycles.

1.12 NanoBRET assay

NanoBRET is a BRET-based in-cell tracer displacement assay which measures the competitive displacement of a fluorescently labeled tracer (e.g. the pan HDAC inhibitor SAHA) from NanoLuc® luciferase coupled enzymes. Tracer displacement reduces the transfer of donor/NanoLuc® fluorescence to the acceptor fluorophor (Non-Chloro-TOM/NCT dye) on the tracer. Therefore, a high

ratio of acceptor to donor signal directly reflects high target engagement by the tracer, while a low ratio reflects displacement of the tracer and therefore binding of a competitive inhibitor (Marks et al. 2011; Robers et al. 2015).

NanoBRET assays were performed in the group of Cancer Drug Discovery (Dr. Aubry Miller, DKFZ) as described in (Kolbinger et al. 2018; Ridinger et al. 2018). Briefly, HeLa cells stably expressing NanoBRET plasmids NanoLuc®-HDAC6 FL Fusion Vector or NanoLuc®-HDAC10 FL Fusion Vector (Promega, Madison, WI, USA) were seeded at a density of 20.000 cells per well into white 96 well plates. Tracer (0.3µM) and respective inhibitors were added in separate pipetting steps, followed by incubation for 2h under standard cell culture conditions. For NanoBRET measurement, plates were equilibrated to room temperature for 10 minutes. Nanoglow substrate was diluted in Phenol Red free Opti-MEM and added to the cells. Measurement was performed within 10 minutes of substrate addition in a BMG Labtech CLARIOstar plate reader (donor emission: 460 nm, acceptor: 610 nm low pass filter). Data were normalized to negative controls (50 µM SAHA) and positive controls (no inhibitor), respectively, and BRET signal is given as ratio of acceptor to donor signal. IC_{50} values were calculated from normalized BRET ratios using nonlinear regression curve fit in GraphPad Prism version 5.0.

2 Biochemical Methods

2.1 Preparation of whole cell lysates and postnuclear supernatants

For whole cell lysates, cells were washed with DPBS and then collected in ice-cold DPBS using a cell scraper. Cell suspensions were transferred to pre-chilled 1.5 ml reaction tubes and centrifuged for 3 minutes at 8600 x g and 4°C. DPBS was aspirated and cell pellets were lysed in 100-300 µl SDS-lysis buffer + 1 µM DTT (***Table 37***) depending on pellet size. Whole cell lysates were immediately incubated at 95°C for 10 minutes and rigorously vortexed before centrifugation for 10 minutes at 11,000 x g and 15°C. The supernatant was then transferred to a fresh, pre-chilled 1.5 ml reaction tube and stored at -80°C.

For the generation of postnuclear lysates, cells were washed and collected as described above. Cell pellets were lysed in either Triton-X (1 % TX-100) or RIPA buffer (***Table 38*** and ***Table 39***) with freshly added cOmplete ™, Mini, EDTA-free Protease Inhibitor Cocktail (1 tablet per 10 ml lysis buffer). Lysates were vigorously vortexed and incubated for 20-30 minutes on ice, vortexing every 5-10 minutes to ensure efficient cell lysis. Cell debris and intact nuclei were precipitated by 15 minute centrifugation at 12,000 x g for 15 minutes. Supernatants were transferred to fresh, pre-chilled 1.5

ml reaction tubes and a 20 µl of each lysate was set aside for protein quantification. The remaining lysate was immediately mixed in a one in four ratio with 4 x SDS sample buffer + 5 % (v/v) β-mercaptoethanol and incubated for 10 minutes at 95°C. Boiled lysates were either directly used for SDS-PAGE or stored at -80°C.

2.2 Nuclear and cytoplasmic fractionation

The Pierce NE-PER Nuclear and cytoplasmic extraction reagents kit was used according to manufacturer's instructions for nuclear and cytoplasmic fractionation with slight modifications to cell number. Briefly, $7.5*10^6$ BE(2)-C cells were harvested by trypsinization and washed in ice-cold PBS. Cells were lysed in 200 µl CER I buffer, vigorously vortexed and incubated on ice for 10 minutes. Next, 11 µl of CER II buffer were added, followed by vortexing and incubation on ice for 1 minute. Lysates were centrifuged for 5 minutes at maximum speed and 4°C. The supernatant was transferred to a fresh, pre-chilled 1.5 ml reaction tube and the nuclear pellet was resuspended in 60 µl NER buffer, followed by rigorous vortexing for 15 seconds. The nuclear lysate was placed on ice for 40 minutes, with vigorous vortexing every 10 minutes. Finally, insoluble nuclear debris was removed by centrifugation at maximum speed and 4°C for 10 minutes and the nuclear lysate supernatant was transferred to a fresh, pre-chilled 1.5 ml reaction tube. Nuclear fractionation lysates were stored at -80°C.

2.3 Preparation of lysates for polyamine quantification

Whole cell lysates for Dansyl Chloride labeling of cellular polyamines (performed in the lab of Dr. Bob Casero, Baltimore, Maryland, United States) were prepared from $1.5*10^6$ BE(2)-C cells. Cells were detached from 10 cm dishes with trypsin-EDTA for 3 minutes at 37°C , counted and washed twice in ice-cold PBS. Cell pellets in 1.5 ml reaction tubes were resuspended in 75 µl ice-cold 1x SSAT breaking buffer (***Table 24***) and immediately quick frozen in a ethanol/dry-ice mixture. Polyamines lysates were stored at -80°C and shipped on dry ice. In case of nuclear polyamine lysates, nuclei were enriched and lysed as described in section ***C2.2***.

2.4 Immunoprecipitation

2.4.1 Covalent coupling of antibodies to Protein-G Dynabeads™

Protein G coupled Dynabeads™ were vortexed, transferred to a 2 ml microcentrifuge tube, washed once with 100 µl PBS-T (***Table 18***) and coupled to HSC70 and HSP70 antibody as indicated in ***Table 58*** by incubation for 1h at room temperature on an Eppendorf Thermomixer under agitation (700-750 rpm). Beads were washed once in 200 µl PBS-T and two times in 1ml triethanolamine buffer (***Table***

19). Crosslinking of antibodies to Protein G Dynabeads was performed by adding 1ml of 20 mM DMP working solution (***Table 21***) and 30 minute overhead rotation at room temperature. DMP was removed and remaining DMP was quenched by addition of 1ml quenching solution (***Table 22***) for 20 minutes at room temperature. Beads were washed two times in 1 ml PBS-T and directly used for IP or stored over night in 2x bead volume PBS-T at 4°C. Beads stored over night were re-equilibrated in 100 µl PBS-T directly prior to addition of lysates (see following section).

	coupling of HSC70 antibody (Abcam 1B5) 1x reaction	**coupling of HSP70 antibody (sc-66048) 1x reaction**
Dynabeads	22 µl	22 µl
Amount of antibody	3.3 µg	3.3 µg
Volume of antibody	3.3 µl	batch-dependent (roughly 65 µl)
Total coupling reaction volume	75 µl (72 µl PBS-T added)	75 µl (10 µl PBS-T added)

Table 58: Coupling of HSC70 and HSP70 antibodies to Dynabeads.

2.4.2 Cell lysis and immunoprecipitation

BE(2)-C cells were seeded at a density of $2*10^6$ cells per dish on multiple 10 cm dishes and grown for 24h before treatment with HDAC inhibitors for 24h. Plates were washed once with PBS and cells were detached using non-enzymatic cell dissociation reagent or versene for five minutes at 37°C. Detaching cells were resuspended in non-sterile cell culture medium and counted using a Vi-Cell XR automatic cell counter (Beckmann Coulter). Cell lysis was performed as indicated in ***Table 59*** and was allowed to continue for 20 minutes on ice with repeated vortexing before centrifugation for 10-15 minutes at 15,000 x g and 4°C. Five percent of postnuclear supernatant was drawn off as input control and the remaining supernatant was transferred to the respective antibody-coupled Dynabeads (see previous section), followed by careful resuspension and incubation on an Eppendorf Thermomixer for 5-6h under gentle agitation (700 rpm) in the cold room. After IP, 5% of supernatant was drawn off as flowthrough control. Beads were washed thrice in PBS-T (HSC70 IP) or RIPA buffer (HSP70 IP) and transferred into a fresh 2 ml microcentrifuge tube during each washing step. Bound proteins were eluted by 10 minute incubation in 30 µl (or 1.5 x original bead volume) 2x Laemmli buffer + 5 % β-mercaptoethanol at 95°C.

IP	**cell number (1x IP)**	**lysis buffer**	**lysis volume (1x IP)**
HSC70	$7.875*10^5$ ($7.5*10^5$ + 5 %)	Triton-X lysis buffer (0.2 % TX-100) (***Table 38***)	160 µl
HSP70	$5.25*10^6$ ($5*10^6$ + 5 %)	RIPA lysis buffer (***Table 39***)	160 µl

Table 59: Lysis conditions for HSC70 and HSP70 immunoprecipitation.

2.5 Protein quantification via the BCA assay

The Bicinchoninic acid (BCA) assay is a sensitive method to determine protein concentrations in solution. It is based on the Biuret reaction, i.e. the reduction of Cu^{2+} to Cu^{+} ions by proteins in alkaline solution. Under alkaline conditions, proteins - via peptide bonds, cysteine, tyrosine and tryptophan residues - reduce Cu^{2+} to Cu^{+}, which forms a purple complex with bicinchoninic acid (BCA) (Smith et al. 1985). Absorbance of this complex can be detected with a spectrophotometer at 562 nm. For the assay, BCA reagent A and B of the "Pierce BCA Protein Assay Kit" are mixed in a 50:1 ratio to obtain the BCA working solution. Protein lysates were typically diluted in a 1:5 or 1:10 ratio in their respective lysis buffer. Five µl of each dilution were added into a 96-well microplate as duplicates or triplicates and filled up with 200 µl BCA working solution. In order to determine protein concentration, 5 µl of albumin (BSA) standards of known concentrations ranging from 0-2 mg/ml, as well as a blank containing only the respective lysis buffer, were used to generate a blank corrected BSA standard curve. After 30-45 minutes of incubation at 37°C, absorbance at 570 nm was measured on a FLUOstar OPTIMA microplate reader.

2.6 SDS-polyacrylamide gel electrophoresis (SDS-PAGE)

SDS-PAGE describes a method in which proteins are separated via electrophoresis in a 2D gel-matrix. This method is useful for the analysis of protein mixtures, enabling for instance the crude determination of a protein's molecular weight or the subsequent transfer and immobilization of proteins on a synthetic membrane for further analysis. In order to ensure that the electrophoretic separation is independent of the protein's own net charge and thus almost exclusively dependent on the protein's molecular weight, protein lysates, gels and gel buffers are supplemented with the denaturing detergent sodium dodecyl sulphate (SDS). SDS interacts with proteins, forming negatively-charged SDS protein complexes that are characterized by a constant charge-to-mass ratio. SDS, along with heat denaturation at 95°C, further promotes the unfolding of proteins, rendering the separation also largely independent of the protein's secondary and tertiary structure. Reducing agents like DTT or β-Mercaptoethanol are commonly added to lysates in order to reduce inter- and intramolecular disulfide bonds and to destroy protein-protein interactions (quaternary structure).

Running and stacking gels were prepared according to ***Table 44*** and ***Table 45*** and whole cell- , as well as postnuclear protein lysates were denatured as described in section ***C2.1***. Between 20 and 60 µg of protein were loaded per lane depending on the detected antigen. In case of preparative gels for hybridoma supernatant testing, between 370 µg and 450 µg of postnuclear lysate were loaded per gel. The PAGE chamber was filled with 1x running buffer (***Table 29***) and gels were initially run at 80 V

until the bromophenol blue leading front entered the running gel, where voltage was increased to 120V until the desired separation was reached.

2.7 Western blotting

The term blotting describes a procedure during which nucleic acids or proteins are transferred from a gel onto a synthetic membrane. In case of western blotting, proteins are separated via SDS-PAGE according to their molecular weight and then transferred to a membrane via the application of an electric field. Proteins immobilized on the membrane can then be detected and identified with the help of specific antibodies.

2.7.1 Transfer of proteins onto a PVDF membrane (semi-dry blotting)

After completion of electrophoresis, running gels were carefully retrieved from the running chamber, briefly rinsed in de-ionized water and equilibrated in 1 x transfer buffer (***Table 31***). For the transfer of proteins to PVDF membranes, five Whatman chromatography papers (9 x 6.5 cm) were soaked in 1 x transfer buffer and placed on the anode (positive pole) of the blotting chamber. The PVDF membrane (8.5 x 6 cm) was activated in pure methanol, briefly washed in de-ionized water, equilibrated in 1 x transfer buffer for at least 1 minutes and placed on top of the lower Whatman stack. The gel was carefully placed on top of the membrane, followed by five more Whatman chromatography papers. Proteins were blotted at a constant current of 0.67 mA/cm^2 of membrane. Blotting times were adapted according to protein size and gel percentage (1h 30 minutes for small proteins < 25 kDa, 2h 30 minutes for proteins of 25 - 150 kDa and 2h 45 minutes up to 3h for proteins > 150 kDa). After transfer, membranes were put in pure methanol for 1 minute and stained for 2-3 minutes in Ponceau S staining solution in order to check for uniform protein transfer. Residual protein in gels was detected with Coomassie Brilliant Blue staining solution (30 minutes), followed by rinsing in de-ionized water until gels were sufficiently destained.

In case of preparative gels for hybridoma supernatant testing, membranes were carefully labeled with serial numbers at the top of the membrane when stained with Ponceau S solution. This later allowed for the identification of blot strips and corresponding hybridoma supernatants.

2.7.2 Immunodetection

In order to avoid non-specific binding of antibodies to the PVDF membrane, membranes were blocked in either blocking solution (***Table 35***) or in 3 % BSA/TBS-T (***Table 36***) for 1h, depending on antibody (***Table 36***). Before application of primary antibody, antibodies were washed for 10 minutes in TBS-T and for 10 minutes in TBS. When membranes were used for testing of hybridoma supernatants, membranes were cut into small strips after washing with TBS-T. Membranes were

incubated with primary antibody (diluted in 2.5 % milk/TBS-T or 3% BSA/TBS-T) or hybridoma supernatants over night at 4°C. Unbound primary antibody was removed by 2 x washing in TBS-T and 2 x washing in TBS (10 minutes each), followed by incubation in peroxidase-conjugated secondary antibody for 1 h at room temperature. Again, unbound antibody was removed by washing as described above. A chemoluminescence substrate (ECL Prime), which releases light upon oxidation of luminol by peroxidases, was used for the detection of bound antibodies. To that end, membranes or fixed membrane strips were incubated with 1 ml of a freshly prepared 1:1 mixture of detection reagents 1 and 2 for 2-5 minutes at room temperature. Emitted light was detected using a Vilber Chemi-Smart 5000 chemoluminescence imaging system.

2.8 Liquid chromatography tandem-mass spectrometry (LC-MS/MS)

LC-MS/MS analyses in section ***E2.2.2*** were performed by the Core Facility for Mass Spectrometry and Proteomics (ZMBH, Heidelberg, Germany). Briefly, immunoprecipitated HSP70/HSC70 proteins were separated by 1D SDS-PAGE (NuPAGE Novex 4-12% Bis-Tris, Invitrogen), and the gel area including the mass range of the target proteins, was excised and digested by trypsin. Peptides were separated on an UltiMate 3000 RSLCnano (Thermo Scientific) using an in-house (ZMBH) packed C18 reversed-phase column of 35 cm length (140 min gradient from 3% to 40% acetonitril). Peptides were then directly injected into a Q Exactive HF Orbitrap LC-MS/MS. Analysis of peptides was performed using an untargeted data-dependent approach, in which precursors had been selected according to their intensity for MS/MS analysis. In addition, a targeted approach was applied, which allows for the detection of specific peptides with higher sensitivity. An inclusion list of masses, calculated from theoretical ion masses of possible acetylated tryptic peptides of the target proteins (see above), has been added to the analysis to ensure MS/MS acquisition of these targets. MS/MS spectra from all samples were using Mascot search engine (version 2.1.0.81) against a manually compiled database that contained the sequence of the target proteins. Fragment ion tolerance was set to 20 ppm and parent ion tolerance to 10 ppm. Carbamidomethylation of cysteine residues was set as fixed modification. Variable modifications were: Deamidation of asparagine, oxidation of methionine and acetylation of lysine. MS/MS based peptide and protein identifications were evaluated using Scaffold, whereby peptide identifications were accepted if determined at greater than 95.0% probability by the Peptide Prophet algorithm with Scaffold delta-mass correction (Keller et al. 2002). Protein probabilities were assigned by the Protein Prophet algorithm (Nesvizhskii et al. 2003), and protein identifications were accepted if established at greater than 95.0% probability, containing at least one identified peptide. Proteins with similar peptides that could not be differentiated via MS/MS analysis alone were grouped to meet the principles of parsimony.

LC-MS/MS analysis in section ***E2.3*** were performed in the group of Dr. Martina Schnölzer (DKFZ, Heidelberg) as follows. 25 µg of protein lysates were separated by 1D SDS-PAGE (NuPAGE Novex 4-12% Bis-Tris, Invitrogen). Commassie staining was performed according to (Dyballa and Metzger 2009), and each lane was cut into 21 slices in the molecular weight region between 39 and 97 kDa. Tryptic digestion and extraction were performed as previously described (Shevchenko et al. 2006) with adaption to the volume of the gel slices. Peptide separation was performed on a nanoAcquity UPLC system (Waters GmbH) using a C18 trap column (180 µm ×20 mm, particle size 5 µm; Waters GmbH) (Aretz et al. 2013). Liquid chromatography separation was performed on a BEH130 C18 main-column (100 µ m × 100 mm, particle size 1.7 µm; Waters GmbH) at a flow rate of 0.4 µl/min. Peptides from each gel slice were separated by a 1 h gradient consisting of 95.9% water, 4% DMSO, 0.1% formic acid (**A**) and 0.1% formic acid, 99.9% acetonitrile (**B**) set as follows: from 0 to 4% **B** in 1 min, from 4 to 40% **B** in 39 min, from 40 to 60% **B** in 5 min, from 60 to 85% **B** in 0.1 min, 6 min at 85% **B**, from 85 to 0% **B** in 0.1 min, and 9 min at 0% **B**. Separated peptides were injected into a LTQ Orbitrap XL mass spectrometer.Data were acquired with XCalibur (version 2.0.7; Thermo Scientific), using scan cycles of one FTMS scan with a resolution of 60000 at m/z 400 and a range from 300 to 2000 m/z in parallel with six MS/MS scans in the ion trap of the most abundant precursor ions (Michalak et al. 2016). Peak lists were extracted from raw files using Mascot Daemon and subsequently searched against the SwissProt database (SwissProt 2017_04 (554241 sequences; 198410167 residues)) using Mascot (v2.4.0) with the following parameters: cysteine carbamidomethylation was used as fixed modification; methionine oxidation, deamidation of asparagine and glutamine and acetylation at lysine were set as variable modifications. Precursor tolerance was set to 7 ppm and 0.4 Da for fragment ions. Enzyme specificity was set to trypsin with an allowed maximum of five missed cleavages.

2.9 HDAC8 activity assay (HDAC-Glo assay)

All of the following steps were performed in the research group Cancer Drug Development (Dr. Aubry Miller, DKFZ Heidelberg). HDAC8 activity was measured in a 384-well format with the HDAC-Glo™ I/II Assay and Screening System, using recombinant HDAC8 enzyme (BPS Bioscience, 50008). Briefly, 250 ng/ml enzyme were used and inhibitors were used at concentrations ranging from 0.0188 nM to 10 µM. Enzyme and inhibitors were incubated for 30 minutes at room temperature, followed by addition of HDAC-Glo™ I/II reagent, shaking (800 rpm 30 s), centrifugation (300 x g for 1 min) and further incubation for 40 minutes at room temperature. Luminescence was quantified using a BMG Labtech CLARIOStar plate reader. Data were normalized to negative controls (30 µM PCI-34051) and positive controls (no inhibitor), respectively. IC_{50} values were calculated using nonlinear regression curve fit in GraphPad Prism version 7.04.

3 Molecular biological methods

3.1 RNA extraction from tumor cells

RNA from neuroblastoma cells was isolated with the QIAGEN RNeasy® Mini Kit according to the manufacturer's instructions. Briefly, cells grown 6-well plates (70 % confluency) were lysed in 350 µl RLT buffer supplemented with 1 % β-and mixed with an equal volume of 70 % ethanol before transfer to the RNeasy Mini Spin column and centrifugation at 10,000 x g for 1 minute. Columns were washed once in 350 µl RW1 buffer before on-column DNase digestion for 20 minutes at room temperature. Columns were washed again in RW1 buffer and twice in 500 µl RPE buffer, each step being followed by a centrifugation step (1-2 minutes 10,000 x g, according to manufacturer's instructions). Residual RPE buffer was removed by transfer to a fresh collection tube and high-speed centrifugation step at 13,000 x g for 1 minute. After transfer of the RNeasy column to a 1.5 ml microcentrifuge tube, RNA was eluted by addition of 40 µl of nuclease-free, followed by 1 minute incubation at room temperature and collection of the eluate by centrifugation (13,000 x g for 1 minute). RNA was stored at -80°C.

3.2 Determination of RNA concentration

RNA concentration was determined on a NanoDrop UV spectrophotometer, which measures absorbance of light by nucleic acids at 260 nm (OD_{260}/A_{260}) and calculates DNA or RNA concentrations via the Beer-Lambert law. An OD_{260} of 1.0 corresponds to 40 ng/µl RNA. Protein contaminations were controlled by measuring absorbance at 280 nm and an OD_{260}/OD_{280} ratio of 1.8 to 2.0 was considered as optimal. Degradation of nucleic acids and contaminations with aromatic solvents was checked for by measuring OD_{260}/OD_{230} ratio, where a ratio between 2.0 and 2.2 was considered as good.

3.3 Reverse transcription (cDNA synthesis)

Between 0.5 and 1 µg of RNA were reverse transcribed to cDNA using the ThermoFisher RevertAid First Strand cDNA Synthesis Kit. Briefly, the desired amount of RNA was transferred to a PCR tube and filled up to 12 µl with 1 µl of oligo (dT) primer and nuclease-free water. After 5 minute incubation at 65°C and cooling on ice, the reaction was filled up to 20 µl with reaction mastermix containing each 4 µl of 5 x Reaction Buffer, 1 µl RiboLock RNase Inhibitor, 2 µl of 10 mM dNTP Mix and 1 µl of M-MuLV reverse transcriptase. The reaction was incubated for 60 minutes at 42°C. For longterm storage, samples were kept at -80°C.

3.4 Real-time quantitative PCR (RT-qPCR)

Real-time quantitative PCR allows for both absolute and relative quantification of PCR-amplified DNA with the help of fluorescent reporter molecule (e.g. SYBR®-Green I), which upon binding of double-stranded DNA and excitation with blue light, emits green fluorescence light. Fluorescence of the dye increases proportionally with the amount of amplified DNA and the number of PCR cycles required until the fluorescence meets a pre-defined fluorescence threshold (Cycle of Threshold/CT value) can be used for relative or, with the help of a standard, absolute quantification of the original amount of template in the PCR mix.

Real-time quantitative PCR was performed using the qPCR Mastermix for SYBR® Green I from Eurogentec. For each gene of interest, a mastermix was prepared according to ***Table 60***or ***Table 61***, 25 µl of which were transferred into a 96-well plate per reaction. Each reaction was filled up with 5 µl of the respective pre-diluted cDNA (5 ng/µl). The PCR was run on an ABI 7500 Real-Time PCR System using the PCR program given in ***Table 62***. Expression of genes was normalized to the averaged expression of *SDHA* and *HPRT1*, which are constitutively expressed in stage 4 and 4S neuroblastoma (Fischer et al. 2005). Relative quantification of gene expression was performed using the $2^{-\Delta\Delta CT}$ method (Winer et al. 1999; Livak and Schmittgen 2001).

Reagent	Volume [µl]
2x Reaction Buffer	12.5
Diluted SYBR®	0.75
Forward Primer (100 µM)	0.08
Reverse Primer (100 µM)	0.08
nuclease-free water	6.59
cDNA (added in well)	5
total volume in well	25

Table 60: 1x RT-qPCR reaction for ThermoFisher primers. *Mastermixes for multiple reactions were prepared accordingly without addition of cDNA.*

Reagent	Volume [µl]
2x Reaction Buffer	12.5
Diluted SYBR®	0.75
QIAGEN QuantiTect Primers (10x)	2.5
nuclease-free water	4.25
cDNA (added in well)	5
total volume in well	25

Table 61: 1x RT-qPCR reaction for QIAGEN QuantiTect primers. *Mastermixes for multiple reactions were prepared accordingly without addition of cDNA.*

Stage	Step name	temperature	time	number of cycles
Holding stage	Uracil N-Gycosylase activation	50°C	2 min	1
	HotGoldStar DNA polymerase activation	95°C	10 min	
Cycling stage	denaturation	95°C	15 sec	40
	annealing and elongation	60°C	1 min	
Dissociation stage	complete dissociation	95°C	15 sec	1
	complete annealing	60°C	1 min	
	gradual dissociation	95°C	30 sec	
	annealing	60°C	-----	

Table 62: RT-qPCR parameters and program.

3.5 Comet assay (alkaline single cell electrophoresis)

BE(2)-C cells were seeded at a density of $1.5*10^6$ cells per 10 cm dish and treated with tubastatin A +/- doxorubicin for 18h as indicated in the respective figure legend. Untreated and γ-irradiated cells (5 Gy from a ^{137}Cs radiation source, at a dose rate of 1 Gy/min) were used as negative and positive control, respectively. Cells were subjected to alkaline single cell electrophoresis as described in (Mayer et al. 2002; Greve et al. 2012) with the following modifications: Cells were mixed with 0.7% low-melting temperature agarose before plating on two-well CometSlides™ and overnight lysis. Single cell electrophoresis was performed on the following day at 4°C. DNA damage was analyzed via automated fluorescence microscopy using the Metafer4 cell scanning and imaging platform as described in (Schunck et al. 2004). ‘‘Tail DNA in %” was used as parameter to assess DNA damage. Statistical evaluation was performed using Mann Whitney test in GraphPad Prism version 5.04.

4 Generation of HDAC10 antibodies

4.1 Production of HDAC10 peptides

All of the following steps were performed in the monoclonal antibody facility (MAF) of the DKFZ. Briefly, two fragments corresponding to amino acids 361 to 500 (HDAC10T1) and 501 to 617 (HDAC10T2) of full-length HDAC10 were PCR amplified from cDNA generated from RNA of BE(2)-C cells using the primers indicated in ***Table 10***. The respective fragments were cloned into pQE-8 vector using BamHI and HindIII restriction sites for the expression of N-terminally 6x histidine-tagged HDAC10T1 and HDAC10T2 protein. Vectors were transformed into chemically competent M15 *E. coli* cells and protein expression was induced by addition of IPTG (60 µM for 3.5h). His-tagged proteins were purified using Ni-NTA agarose (QIAGEN) under denaturing conditions (8M Urea).

4.2 Immunization of mice and production of murine monoclonal HDAC10 antibodies

Unless otherwise indicated., all of the following steps for the production of HDAC10-reactive hybridoma clones were performed in the monoclonal antibody facility (MAF) of the DKFZ. BALB/c wild type mice were injected on day zero with 20 µg of Ni-NTA purified HDAC10T2 peptide including Freund's complete adjuvant. Immune reactions were boosted by re-injection of antigen on day three (including Freund's incomplete adjuvant) and day six (without adjuvant). Mice were sacrificed on day 8, followed by fusion of B-lymphocytes from popliteal lymph nodes with Sp2/0 myeloma cells using polytheylene glycol 1500. Hybridomas were raised as described by (Köhler and Milstein 1975), and supernatants were checked for the production of IgG via ELISA starting seven days after fusion. HDAC10 reactivity of hybridoma supernatants was analyzed via immunoblot (performed by me as described in section ***C2.7***). Antibodies were purified from hybridoma supernatants using Protein G sepharose (GE Healthcare). Antibodies were eluted using glycine buffer (pH 10) and dialyzed against PBS.

4.3 Generation of monoclonal HDAC10 antibodies by antibody phage display

Antibody phage display screening allows for the generation of monoclonal antibodies without the immunization of animals. To that end, the genetic information of the antigen-binding regions of antibodies (variable heavy (VH) and variable light (VL) chains) are PCR-amplified (e.g. from naive human B cells) to generate an antibody gene phage display library, and fused to the gene encoding for the pIII surface protein of the M13 bacteriophage. Depending on the mode of PCR amplification, antibodies are then presented on the surface of the M13 phage either as Fab or scFV fragments. Fusing the genetic information of antibody variable regions to the pIII surface protein gene enables the generation of a whole library of phage particles, in which the antigen-binding function is physically linked to the genetic information that encodes the respective antibody within. The phage library allows for biochemical high-throughput affinity screening of antibody binding to any epitope in a cell-free assay (so called panning) and, in succession, for the quick production of recombinant monoclonal antibodies (reviewed in (Frenzel et al. 2017)).

The following steps were performed by Saskia Helmsing in the lab of Prof. Dr. Michael Hust (Department of Biotechnology, TU Braunschweig, Germany). Antibodies were selected from the human naive antibody gene phage display libraries HAL9/10 (Kugler et al. 2015) using microtiter plate immobilized antigen (HDAC10T1 and HDAC10T2, see ***Table 51***) as described in (Russo et al. 2018). Monoclonal scFvs were produced in microtiter plates and binder antibodies were screened by ELISA

as described in (Russo et al. 2018). Subsequently, binding scFvs were recloned into the vector pCSE2.6-mIgG2a-Fc-XP, produced as scFv-Fc in Expi293F™ cells (ThermoFisher Scientific) and purified by protein A (Jager et al. 2013).

D AIMS OF THE STUDY

Members of the HDAC family are aberrantly expressed in various cancer entities where they support numerous cancer relevant cellular processes. Consequently, HDAC inhibitors are of great interest for novel anti-tumor treatment regimens. Pan- and broad-spectrum HDAC inhibitors have shown promise in the treatment of hematological malignancies such as CTCL and multiple myeloma, and are currently being tested in numerous other clinical trials. Their success, however, is ultimately restricted by dose-limiting side effects, which are thought to arise from unspecific simultaneous inhibition of class I HDACs 1, 2 and 3. Such unspecific side effects can likely be circumvented by the inhibition of single HDAC isozymes that have a critical function in the respective tumor entity or subtype. HDAC10 is of high relevance in advanced stage neuroblastoma (stage 4), where its inhibition promoted sensitization of high-risk neuroblastoma cell lines to chemotherapeutic treatment in a previous study. This suggested HDAC10 inhibition as a strategy to reduce chemoresistance, a common problem in advanced stages of neuroblastoma. HDAC10 inhibition blocked late autophagic flux, i.e. the turnover of autophagic material in lysosomes, and increased intracellular acidic vesicles, which led to the hypothesis that HDAC10 governs lysosomal function or biogenesis in neuroblastoma cells. As of yet, protein downstream targets of HDAC10 have not been conclusively identified, but several studies suggest that class IIb HDACs 6 and 10 bind to and modulate lysine acetylation of HSP70 family members. Conversely, a recent study demonstrating poylamine deacetylase activity of HDAC10 in biochemical assays raised the question whether polyamines are the primary cellular HDAC10 substrates. Finally, while HDAC10 showed promise as a drug target in advanced-stage neuroblastoma and as improved HDAC10 inhibitors are currently being developed, mechanistic studies and validation of HDAC10 expression on patient tissue are currently hampered by the lack of suitable HDAC10 antibodies. The key items of this study thus were to:

- dissect how class IIb HDAC members HDAC6 and HDAC10 affect lysosomal composition of neuroblastoma cells.
- investigate lysosomal downstream processes upon interference with HDAC6/10 function.
- analyze lysosomal effector mechanisms and their link to increased chemosensitivity of neuroblastoma cells.
- verify downstream protein or non-protein targets of HDAC10 with a special focus on HSP70 family members and polyamines in neuroblastoma.
- generate a novel highly specific HDAC10 antibody suitable for immunofluorescence and immunohistochemistry approaches.

E RESULTS

1 HDAC10 and its role in lysosomal homeostasis, exocytosis and drug resistance

Ongoing research focuses on specific functions of single HDAC family members, which can be very diverse and often in opposing directions. For example HDAC inhibitors have differential effects on autophagy, with some inducing and others blocking autophagy (reviewed in (Koeneke et al. 2015)). In this context, a previous report of our research group suggests that HDAC10 is important for lysosomal homeostasis and trafficking to lysosomes (Oehme et al. 2013a; Oehme et al. 2013b). The latter function has also been associated with the other class IIb HDAC member HDAC6 (Gao et al. 2010; Lee et al. 2010b). Thus, given the high sequence homology of class IIb HDACs, a function of both HDAC6 and HDAC10 in lysosomal homeostasis is conceivable. Nevertheless, non-overlapping functions of the two HDACs exist, highlighted by their differential ability to deacetylate tubulin at lysine 40 (K40) (Hubbert et al. 2002). The role of class IIb HDACs HDAC6 and HDAC10 in lysosomal homeostasis in neuroblastoma was thus investigated in more detail in the following sections.

1.1 Depletion of HDAC10 but not HDAC6 causes the accumulation of lysosomes in neuroblastoma cells

1.1.1 Knockdown of class IIb HDACs 6 and 10 leads to the accumulation of the lysosomal membrane protein LAMP-2 in neuroblastoma cells

Changes in the lysosomal composition of cells, i.e. an expansion or a shrinkage of the lysosomal compartment, can be roughly estimated by analyzing levels of lysosomal markers, such as LAMP-2, on western blot. To investigate whether interference with class IIb HDAC function affected lysosomal numbers in neuroblastoma cells, HDAC6 and HDAC10 were individually depleted in SK-N-BE(2)-C cells, a highly chemoresistant neuroblastoma cell line (hereafter referred to as BE(2)-C) (Gogolin et al. 2013), using a pool of two siRNAs against either HDAC. Western blot analysis on whole cell lysates generated 72h (***Figure 7a***) and six days (***Figure 7b***) after siRNA transfection revealed elevated LAMP-2 levels in case of both HDAC6 and HDAC10 depletion at both time points. Densitometric quantification of n=4 experiments in case of six day knockdown revealed that the increase in LAMP-2 levels was statistically significant in case of either HDAC knockdown. LAMP-2 levels were significantly more elevated in case of HDAC10 knockdown compared to HDAC6 knockdown (***Figure 7c***). Substantial cross-reactivity of the used siRNA pools against the respective other HDAC transcript was

not observed, ruling out that increased LAMP-2 levels in case of HDAC6 knockdown were due to an off-target effect on HDAC10 and *vice versa* (***Figure 7a, b, d***). Rather, increased HDAC6 levels were repeatedly observed in case of HDAC10 depletion, suggesting that HDAC6 compensates for some of the HDAC10 functions. At the same, knockdown of HDAC6 but not HDAC10 increased tubulin acetylation, confirming that HDAC6 and HDAC10 have non-redundant functions in spite of their close structural relation (***Figure 7d***).

As increased LAMP-2 levels were especially striking in case of HDAC10 knockdown, it was investigated whether LAMP-2 was upregulated on a transcriptional level via real-time RT-PCR, using primers against the *LAMP2A* transcript (***Figure 7e***). *LAMP2A* transcript levels were not reproducibly elevated upon HDAC10 knockdown, suggesting that the robustly elevated levels of LAMP-2 protein were not caused by *de novo* expression of the *LAMP2* gene but rather by accumulation of lysosomes. Taken together, depletion of HDAC6 and especially HDAC10 increased the level of the lysosomal marker LAMP-2, pointing towards an enlargement of the lysosomal compartment in neuroblastoma cells.

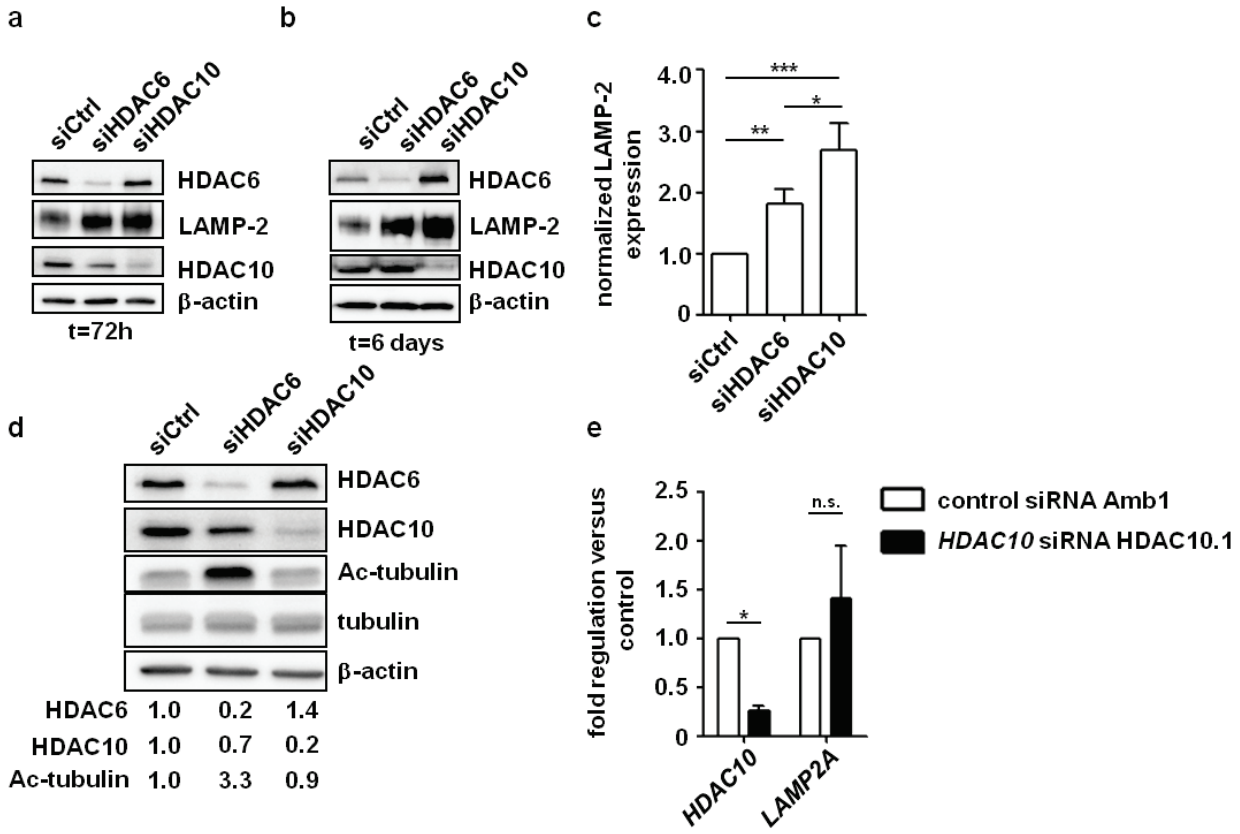

Figure 7: Knockdown of HDAC6 or HDAC10 promote accumulation of the lysosomal marker LAMP-2 in neuroblastoma cells.(a, b) *Western blot analysis of LAMP-2 expression72h* ***(a)*** *and 6d* ***(b)*** *after transfection with siRNAs against HDAC6 and HDAC10 or control siRNAs.* ***(c)*** *Densitometric quantification of LAMP-2 expression on western blot 6d after siRNA transfection (n=4 experiments) .****(d)*** *Western blot analysis of tubulin acetylation 72h after transfection with siRNAs against HDAC6 and HDAC10. Numbers below the blot indicate expression of the respective protein normalized to β-actin (HDAC6/10) and relative to siCtrl, or normalized to total tubulin (acetylated tubulin) and relative to siCtrl.* ***(e)*** *Real-time RT-PCR analysis of HDAC10 and LAMP2A transcript expression knockdown of HDAC10. Bar graph depicts fold regulation versus cells transfected with control siRNA of n=3 experiments. Statistical analyses were performed on non-normalized data using unpaired* ***(c)*** *or paired* ***(e)*** *two-tailed t-test (***p < 0.001; **0.001 ≤p <0.01; *0.01 ≤ p < 0.05). Error bars represent standard error of the mean (SEM). Parts of figure published in (Ridinger et al. 2018).*

1.1.2 Knockdown of HDAC10 but not HDAC6 results in the accumulation of acidic lysosomes

The analysis of LAMP-2 levels after knockdown of HDAC6 and HDAC10 suggested that both class IIb HDACs might cause lysosomal accumulation. However, expression of LAMP-2 alone is not sufficient for the identification of lysosomes, as it is also expressed on endosomes. Furthermore, lysosomes can be highly divergent with regards to their luminal pH (Johnson et al. 2016). Thus, the lysosomal phenotype after depletion of HDAC6 and HDAC10 was characterized more closely with the acidotropic LysoTracker DND-99 probe. This dye consists of a fluorophor coupled to a weak base, which can freely cross membranes at neutral pH but gets trapped when protonated and thus stains lysosomes and lysosome-related structures such as endolysosomes or autophagolysosomes (Pierzynska-Mach et al. 2014). To demonstrate lysosomal specificity of the dye in BE(2)-C cells, cells

were treated for 24h with lysosomal inhibitors. Confocal fluorescence microscopy analysis confirmed that LysoTracker was localized in perinuclear vesicles under basal conditions. These very likely represented lysosomes, which are preferentially located in perinuclear regions due to their association with microtubules and the retrograde transport towards the microtubule-organizing center (MTOC) (***Figure 8a***). Treatment for 24h with the lysosomal V-ATPase inhibitor bafilomycin A1, which hindered acidification, almost completely abrogated LysoTracker accumulation, while low concentrations of chloroquine, a lysosomotropic agent that sequesters lysosomal protons, increased vesicular LysoTracker staining. This effect is probably caused by an expansion of the lysosomal compartment (***Figure 8a***), which has been reported for lower doses or short exposures to chloroquine (Boya et al. 2003). In contrast, prolonged exposure to higher concentrations of chloroquine is known to cause both alkalinization of lysosomes as well as lysosomal membrane permeabilization (Boya et al. 2003; Enzenmuller et al. 2013). Accordingly, treatment with 25 µM chloroquine reduced lysosomal staining and caused a shift of LysoTracker fluorescence from vesicles to cytoplasm and nuclei due to strong alkalinization of lysosomes under this condition (***Figure 8a***).

To test if the LysoTracker probe was applicable for medium throughput methods such as flow cytometry, mean cellular LysoTracker fluorescence after treatment with lysosomal inhibitors was quantified via flow cytometry and compared to microscopy data (***Figure 8b-d***). Living cells were discriminated from cellular debris via forward and side scatter according to ***Figure 8b***. Analogous to the microscopic analysis, 24h application of bafilomycin A1 caused a strong reduction in cellular LysoTracker fluorescence, while low concentrations of chloroquine (5 µM) increased LysoTracker fluorescence (***Figure 8c, d***). Thus, although lacking the spatial information of fluorescence microscopy, flow cytometric quantification of LysoTracker staining served as an estimation of cellular lysosomal content.

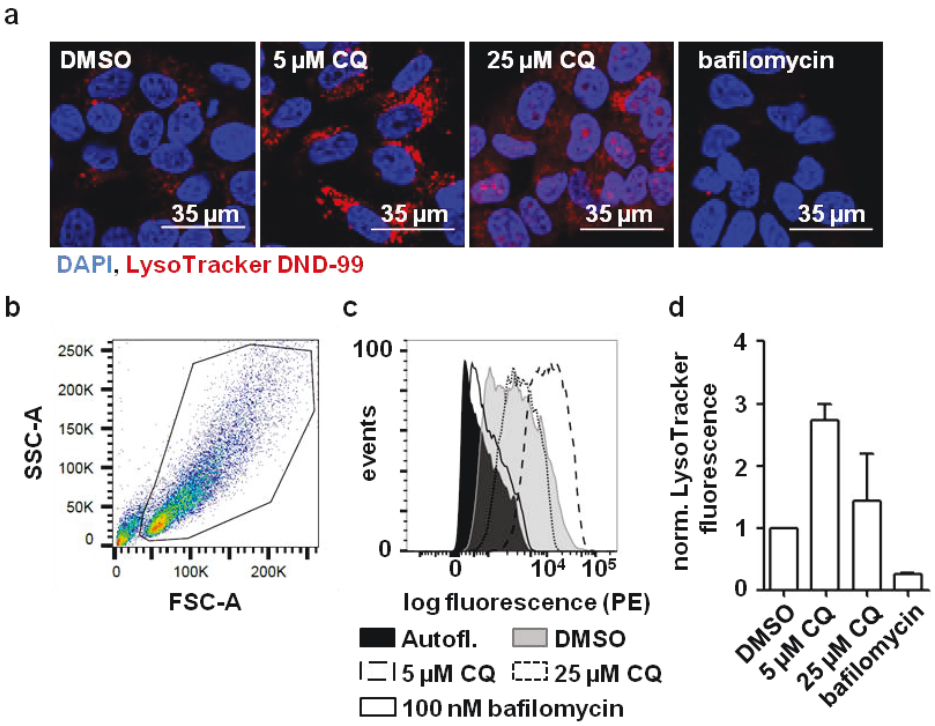

Figure 8: Characterization of LysoTracker staining in BE(2)-C cells. (a) *Fluorescence microscopic analysis LysoTracker DND-99 staining 24h after treatment with lysosomal inhibitor chloroquine (CQ) or vacuolar ATPase inhibitor bafilomycin (100 nM). Nuclei were counterstained with DAPI.* ***(b)*** *Flow cytometric gating of BE(2)-C neuroblastoma cells according to forward (FSC-A) and side (SSC-A) scatter.* ***(c)*** *Histogram showing flow cytometric analysis of LysoTracker staining 24h after treatment with indicated substances.* ***(d)*** *Normalized mean LysoTracker fluorescence from flow cytometric analysis (n=2 experiments) 24h after treatment with indicated substances. Error bars represent standard deviation (SD).*

BE(2)-C cells transfected with HDAC10 siRNA pools reproducibly and significantly displayed increased LysoTracker accumulation compared to cells transfected with control siRNA. This was not observed in case of HDAC6 knockdown. These results were confirmed by the use of another acidotropic dye, acridine orange. Similar to LysoTracker dyes, acridine orange is a weak base fluorophor that accumulates in acidic vesicles, where protonation leads to trapping of the dye. Trapping and accumulation in lysosomes, in turn, causes the metachromatic shift from green to red fluorescence (Moriyama et al. 1982; Thome et al. 2016). Analogous to the LysoTracker staining, acridine orange accumulated in BE(2)-C cells upon HDAC10 but not HDAC6 knockdown (***Figure 9c***). Taken together with the results described in section ***E1.1.1***, these data indicate that acidic lysosomal vesicles accumulate upon HDAC10 but not upon HDAC6 depletion. Thus, HDAC6 and HDAC10 have non-overlapping functions in lysosomal homeostasis in BE(2)-C neuroblastoma cells.

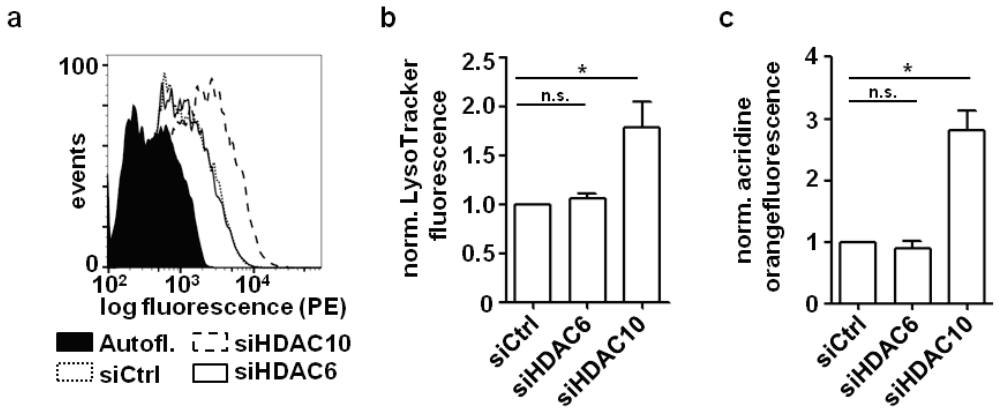

Figure 9: Knockdown of HDAC10 increases LysoTracker staining in BE(2)-C neuroblastoma cells. (a) *Histogram showing flow cytometric analysis of LysoTracker staining in BE(2)-C cells 6d after transfection with siRNAs against HDAC6 and HDAC10 or with control siRNAs.* ***(b)*** *Mean LysoTracker fluorescence of n=4 experiments quantified via flow cytometry. Fluorescence was normalized to fluorescence in siCtrl transfected cells.* ***(c)*** *Flow cytometric analysis of acridine orange staining 6d after transfection with siRNAs. Fluorescence of n=3 experiments was quantified and normalized to cells transfected with control siRNAs. Statistical analyses were performed on non-normalized data using paired two-tailed t-test (***p < 0.001; **0.001 ≤p <0.01; *0.01 ≤ p < 0.05). Error bars represent standard error of the mean (SEM). Parts of figure published in (Ridinger et al. 2018).*

1.1.3 HDAC10 knockdown causes accumulation of acidic lysosomes throughout the cytoplasm

Although LysoTracker dyes are known to accumulate in acidic cellular compartments, the flow cytometric data given in section ***E1.1.2*** did not provide spatial information on the subcellular LysoTracker distribution after HDAC6 and HDAC10 knockdown and thus could not fully rule out the possibility of unspecific LysoTracker accumulation in the cytoplasm under these conditions. Hence, HDAC6 and HDAC10 depleted, LysoTracker stained, BE(2)-C cells were also analyzed via confocal fluorescence microscopy. LysoTracker accumulated in perinuclear lysosomes in cells transfected with control or HDAC6 siRNAs (***Figure 10***). While no increase in lysosomal number was observed in case of HDAC6 knockdown, cells with HDAC10 knockdown contained higher amounts of lysosomal vesicles, confirming flow cytometric data from section ***E1.1.2***. In case of HDAC10 knockdown, an increased number of lysosomes appeared not only in the perinuclear cloud but also throughout the cytoplasm and close to the cell periphery. Taken together, the above described data indicate that depletion of class IIb HDAC10 but not HDAC6 causes a substantial enlargement of the lysosomal compartment in neuroblastoma cells.

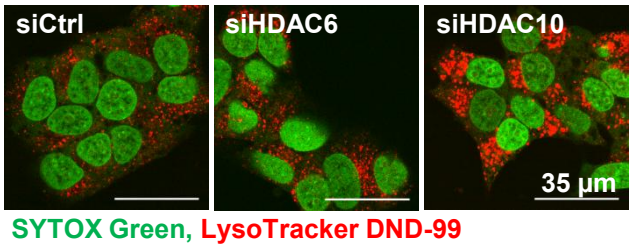

Figure 10: Knockdown of HDAC10 but not HDAC6 causes expansion of the lysosomal compartment in BE(2)-C neuroblastoma cells. *BE(2)-C cells were stained with LysoTracker DND-99 6d after transfection with siRNAs against HDAC6, HDAC10 or control siRNA and analyzed via confocal fluorescence microscopy. Nuclei were counterstained with SYTOX Green. Figure published in (Ridinger et al. 2018).*

1.2 Inhibition of class IIb member HDAC10 causes accumulation of acidic lysosomes in neuroblastoma cells

1.2.1 HDAC10 inhibition causes accumulation of acidic lysosomes throughout the cytoplasm

The experiments described in section ***E1.1*** show that depletion of HDAC10 but not HDAC6 increases the lysosomal compartment in BE(2)-C cells. This raised the question, if lysosomal accumulation after HDAC10 depletion was due to the reduction of enzymatic function of HDAC10. To date, no inhibitor is available that selectively blocks HDAC10 function, but various studies suggest that tubastatin A (Butler et al. 2010; Oehme et al. 2013a) and bufexamac (Bantscheff et al. 2011) are dual specific HDAC6/10 inhibitors while tubacin has a strong preference for HDAC6 (Butler et al. 2010). As no deacetylation substrate protein solely specific for HDAC10 has been described, activity of class IIb inhibitors tubastatin A and tubacin against HDAC10 could not be investigated on western blot level. The affinity of tubastatin A and tubacin towards HDAC10 was therefore assessed in NanoBRET assays (performed in the group of Cancer Drug Development (Dr. Aubry Miller) at the DKFZ) (***Figure 11a***). This BRET-based in-cell tracer displacement assay measures the competitive displacement of a fluorescently labeled tracer (in this case the pan HDAC inhibitor SAHA) from NanoLuc® luciferase coupled HDAC10 enzyme. Tracer displacement reduces the transfer of donor/NanoLuc® fluorescence to the acceptor fluorophor (Non-Chloro-TOM/NCT dye) on the tracer. Therefore, a high ratio of acceptor to donor signal directly reflects high target engagement by the tracer, while a low ratio reflects displacement of the tracer and therefore binding of a competitive inhibitor (Marks et al. 2011; Robers et al. 2015). NanoBRET analysis of tubastatin A and tubacin binding to HDAC10 in HeLa cells confirmed that the suspected dual HDAC6/10 inhibitor tubastatin A had a high affinity towards HDAC10 in the low nanomolar range (IC_{50} approx. 8 nM). In contrast, the suspected HDAC6 specific but HDAC10 non-reactive inhibitor tubacin displayed a roughly 200 fold lower affinity towards HDAC10 than tubastatin A (IC_{50} approx. 1600 nM) (***Figure 11b***).

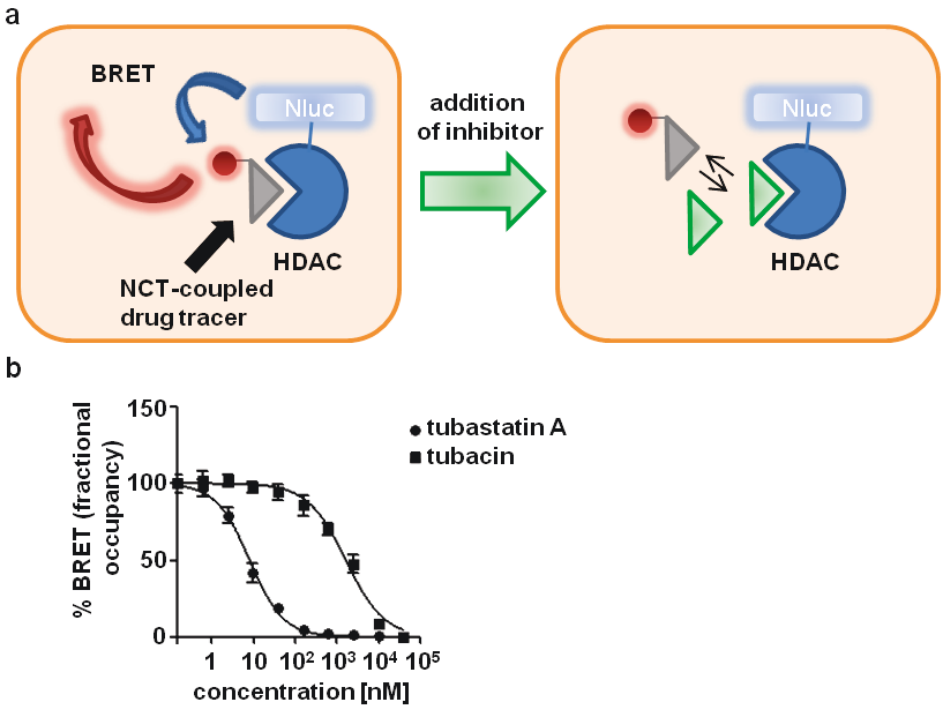

Figure 11: In cell target engagement (NanoBRET) assay reveals differential HDAC10 binding capability of HDAC6/10 inhibitor tubastatin A and HDAC6 inhibitor tubacin. (a) *Principle of the NanoBRET assay. The assay measures displacement of a fluorescently (Non-Chloro-TOM/NCT dye) labeled tracer (SAHA) from NanoLuc® luciferase coupled HDAC10 enzyme. Tracer displacement reduces the transfer of donor/NanoLuc® fluorescence to the acceptor fluorophor on the tracer.* ***(b)*** *Tracer displacement from HDAC10 by tubastatin A and tubacin in HeLa cells. Graph depicts tracer signal relative to total NanoLuc signal (% fractional occupancy, y-axis) versus logarithmic drug concentration in nM (x-axis). Curves were generated via non-linear curve fitting (variable slope) using GraphPad Prism version 5.0. NanoBRET assays were performed by Lars Hellweg in the group of Cancer Drug Development (Dr. Aubry Miller) at the DKFZ. Parts of figure published in (Ridinger et al. 2018).*

In flow cytometric LysoTracker assays performed after 24h treatment of BE(2)-C cells with HDAC6 or HDAC6/10 inhibitors, cells treated with dual specific inhibitor tubastatin A displayed significantly higher levels of LysoTracker fluorescence than vehicle-treated cells, while 24h application of HDAC6 inhibitor tubacin had no effect (***Figure 12a, b***). Treatment with the previously published HDAC6/10 inhibitor bufexamac (Bantscheff et al. 2011) also substantially increased lysosomal staining in BE(2)-C cells. Inhibition of HDAC6 as the cause for lysosomal accumulation under the experimental conditions above was further excluded by western blot analysis of tubulin K40 acetylation. Here, 24h treatment of BE(2)-C cells with bufexamac, tubastatin A and tubacin collectively induced strong acetylation of tubulin, confirming that all three class IIb inhibitors were excellent HDAC6 inhibitors at the concentrations used in the LysoTracker experiments (***Figure 12c***). The HDAC6 inhibitor tubacin even induced stronger tubulin acetylation than the HDAC6/10 inhibitor bufexamac while not inducing lysosomal accumulation. Thus, lysosomal accumulation was not caused by HDAC6 inhibition.

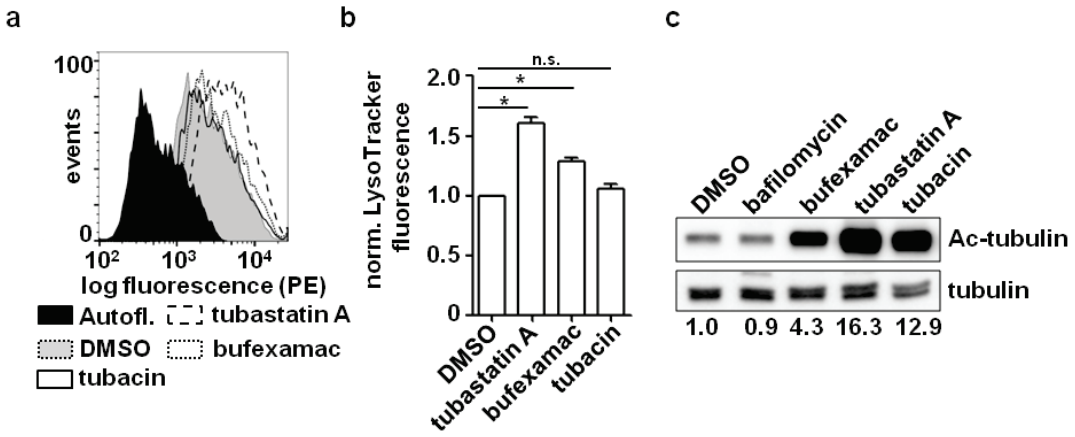

Figure 12: Inhibition of HDAC10 but not HDAC6 promotes lysosomal accumulation in BE(2)-C neuroblastoma cells. (a) *Analysis of LysoTracker staining via flow cytometry 24h after treatment with HDAC6/10 inhibitors tubastatin A (7.5 µM), bufexamac (30 µM) or HDAC6 inhibitor tubacin (7.5 µM). Fluorescence histogram shows percentage of cells (y-axis) versus fluorescence (x-axis).* ***(b)*** *Quantification of mean LysoTracker fluorescence via flow cytometry of n=4 experiments. LysoTracker fluorescence was normalized to mean fluorescence in DMSO treated cells.* ***(c)*** *Western blot analysis of tubulin K40 acetylation 24h after treatment with HDAC6/10 inhibitors (concentrations as described in* ***(a)****).Numbers below blot indicate densitometric quantification of acetylated tubulin signal versus total tubulin normalized to the DMSO control. Statistical analyses were performed on non-normalized data using paired two-tailed t-test (***p < 0.001; **0.001 ≤p <0.01; *0.01 ≤ p < 0.05). Error bars represent standard error of the mean (SEM). Figure published in (Ridinger et al. 2018).*

Fluorescence microscopic analysis of LysoTracker staining after 24h inhibition of HDAC6 and HDAC10 further revealed that treatment with HDAC6/10 inhibitors tubastatin A and bufexamac increased the number of LysoTracker positive vesicles compared to solvent-treated cells (***Figure 13***). Analogous to the data obtained after HDAC10 knockdown (***Figure 10***), lysosomal vesicles after HDAC6/10 inhibition were not restricted to the perinuclear cloud or preferentially localized at the cell periphery, but rather spread throughout the cytoplasm. In contrast, specific HDAC6 inhibition caused neither accumulation nor re-localization of lysosomes (***Figure 13a***).

In line with real-time RT-PCR data, which indicate that interference with HDAC10 function did not cause *de novo* transcription of lysosomal genes, HDAC10 inhibition did not cause translocation of the lysosomal master regulator TFEB (see section ***A3.2.1***) to the nucleus (***Figure 13b***), suggesting that HDAC10 inhibition did not cause *de novo* lysosomal biogenesis via the CLEAR network.

Taken together with knockdown data described in section ***E1.1***, these data suggest that inhibition of HDAC10 but not HDAC6 enzymatic function causes expansion of the lysosomal compartment in neuroblastoma cells, likely via the accumulation of lysosomes.

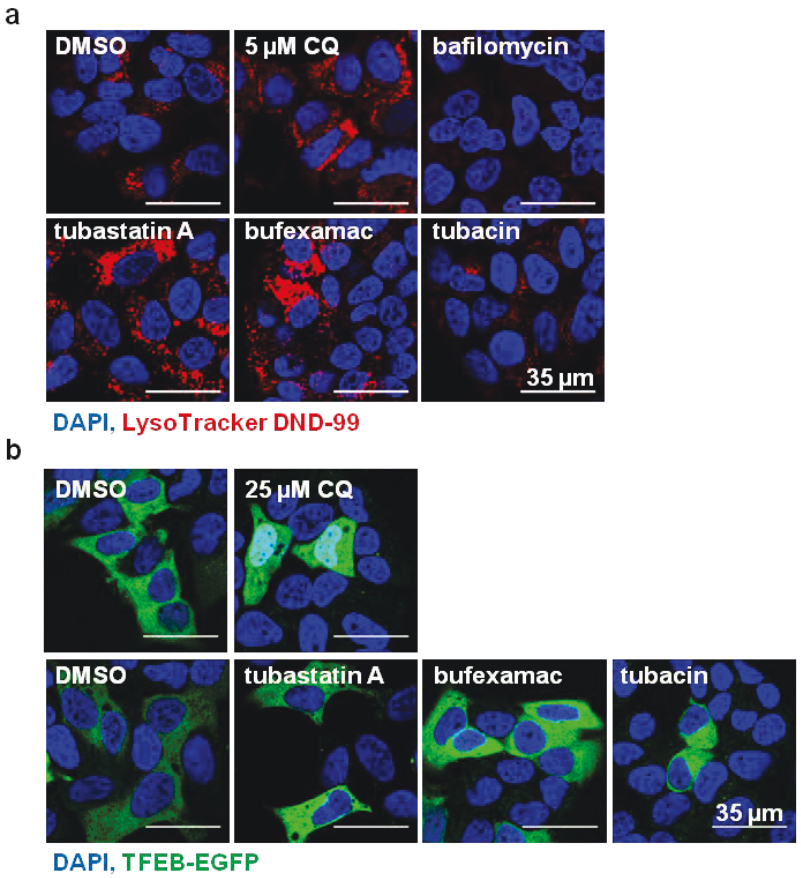

Figure 13: Inhibition of HDAC10 but not HDAC6 is followed by an expansion of the lysosomal compartment in BE(2)-C neuroblastoma cells. (a) *BE(2)-C cells were stained with LysoTracker DND-99 24h after treatment with HDAC6/10 inhibitors tubastatin A (7.5 µM), bufexamac (30 µM), HDAC6 inhibitor tubacin (7.5 µM) or lysosomal inhibitors chloroquine (5 µM) and bafilomycin (100 nM).* ***(b)*** *BE(2)-C cells were transfected with TFEB-EGFP and treated 48h post plasmid transfection with HDAC6/10 inhibitors tubastatin A (7.5 µM), bufexamac (30 µM), HDAC6 inhibitor tubacin (7.5 µM) or lysosomal inhibitor chloroquine (25 µM) for 24h. Cells in* ***(a, b)*** *were analyzed via confocal fluorescence microscopy. Nuclei were counterstained with DAPI. Representative images for each treatment are shown. Parts of figure published in (Ridinger et al. 2018).*

1.2.2 HDAC10 binding and inhibitory capability of tubastatin A derivatives are determined by the presence of a nitrogen atom in the inhibitor's cap group

The results described in the previous sections show that HDAC10 but not HDAC6 inhibition causes the accumulation of lysosomes in neuroblastoma cells. Previous studies from our lab have further identified HDAC10 inhibition as a potential strategy to sensitize neuroblastoma cells to chemotherapy, making HDAC10 an attractive target for neuroblastoma therapy. In this context, inhibitors with high specificity for HDAC10 over HDAC6 are of great interest, as they allow for the precise disentanglement of HDAC6 and HDAC10 specific effects in preclinical studies. As such inhibitors are currently not available (see section ***E1.2.1 Figure 12c*** and (Bantscheff et al. 2011)), the collaborating group of Drug Development (Dr. Aubry Miller) at the DKFZ synthesized a number of tubastatin A derivatives with a modified cap group structure in order to perform structure-activity

relationship studies (shown in ***Figure 14a***). NanoBRET testing of HDAC6 and HDAC10 binding capacity in HeLa cells (assays performed in the group of Aubry Miller) yielded tubastatin A related compounds with significantly altered HDAC10 activity (summarized in ***Figure 14b***). A subset of these derivatives was tested for lysosomal accumulation via the LysoTracker assay, as data in section ***E1.2.1*** suggested lysosomal accumulation regarded as a functional readout for HDAC10 inhibition in BE(2)-C cells. Their ability to induce lysosomal accumulation after overnight treatment was compared to tubastatin A using a concentration series that ranged from 0.1 µM to 10 µM. Of note, tubastatin A concentrations above 10 µM were highly cytotoxic and reduced lysosomal staining likely due to induction of cell death and were thus excluded from further analysis, as they occasionally caused a paradoxical decrease in LysoTracker staining (***Figure 14c***).

Compounds where a basic nitrogen atom within the tricyclic tetrahydro-γ-carboline cap structure of tubastatin A was replaced or removed showed markedly decreased HDAC10 binding capacity in NanoBRET assays (***Figure 14b***). Accordingly, the respective compounds did not induce lysosomal accumulation in BE(2)-C cells (***Figure 14d***). Of these compounds, DKFZ-00494 had reduced HDAC10 activity but retained full HDAC6 inhibitory capacity, while DKFZ-00495 additionally displayed reduced affinity towards HDAC6 in both NanoBRET assays and accordingly on the level of tubulin acetylation (***Figure 14b, e***). The absence of lysosomal accumulation in case of treatment with the DKFZ-00494 compound despite its full HDAC6 inhibitory capacity again confirmed that lysosomal accumulation phenotype described in section ***E1.2.1*** occurred independently of HDAC6 inhibition and was thus a good readout for HDAC10 inhibition. Structurally, the DKFZ-00494 compound was characterized by the replacement of the basic nitrogen in the tetrahydro-γ-carboline cap structure by a sulphur atom. The reduced HDAC10 affinity of the DKFZ-00494 compound suggested that HDAC10 binding capacity was likely not due to the nucleophilic nature of the basic nitrogen atom, as replacement with a highly nucleophilic sulphur atom strongly reduced HDAC10 binding capacity. Instead, it is possible that the nitrogen atom mediates interaction with HDAC10 by other mechanisms, e.g. by forming hydrogen bonds with amino acid residues near the HDAC10 catalytic site (discussed in section ***F1.5*** and ***F2***).

Notably, HDAC10 binding capability did not strictly require the localization of the basic nitrogen atom within a tetrahydro-γ-carboline structure, as for example modification of the nitrogen-containing heterocyclic structure (DKFZ-00546) did not reduce but rather slightly increased HDAC10 binding capability in NanoBRET assays while leaving HDAC6 activity unchanged (***Figure 14b***). In fact, NanoBRET data for DKFZ-00574, a ring-opened tubastatin A analog containing an indazole structure in the cap group, also displayed slightly increased HDAC10 activity over tubastatin A. Thus, the tetrahydro-γ-carboline itself was not required for HDAC10 activity. Rather, the data suggest that the basic amine nitrogen mediates tight binding to HDAC10 via its chemical properties (discussed in section ***F1.5***). (***Figure 14b***). Enhanced HDAC10 and unchanged HDAC6 inhibitory capacity of the

DKFZ-00546 and DKFZ-00574 compounds were confirmed in BE(2)-C cells, where both compounds induced lysosomal accumulation at lower concentrations than tubastatin A and also caused a higher maximal LysoTracker staining, while not displaying substantially changed ability to induce tubulin acetylation (***Figure 14d, e***).

In summary, these data indicate that the HDAC10 binding capability of tubastatin A and its derivatives critically depends on the presence of a basic nitrogen atom within the inhibitor's cap group.

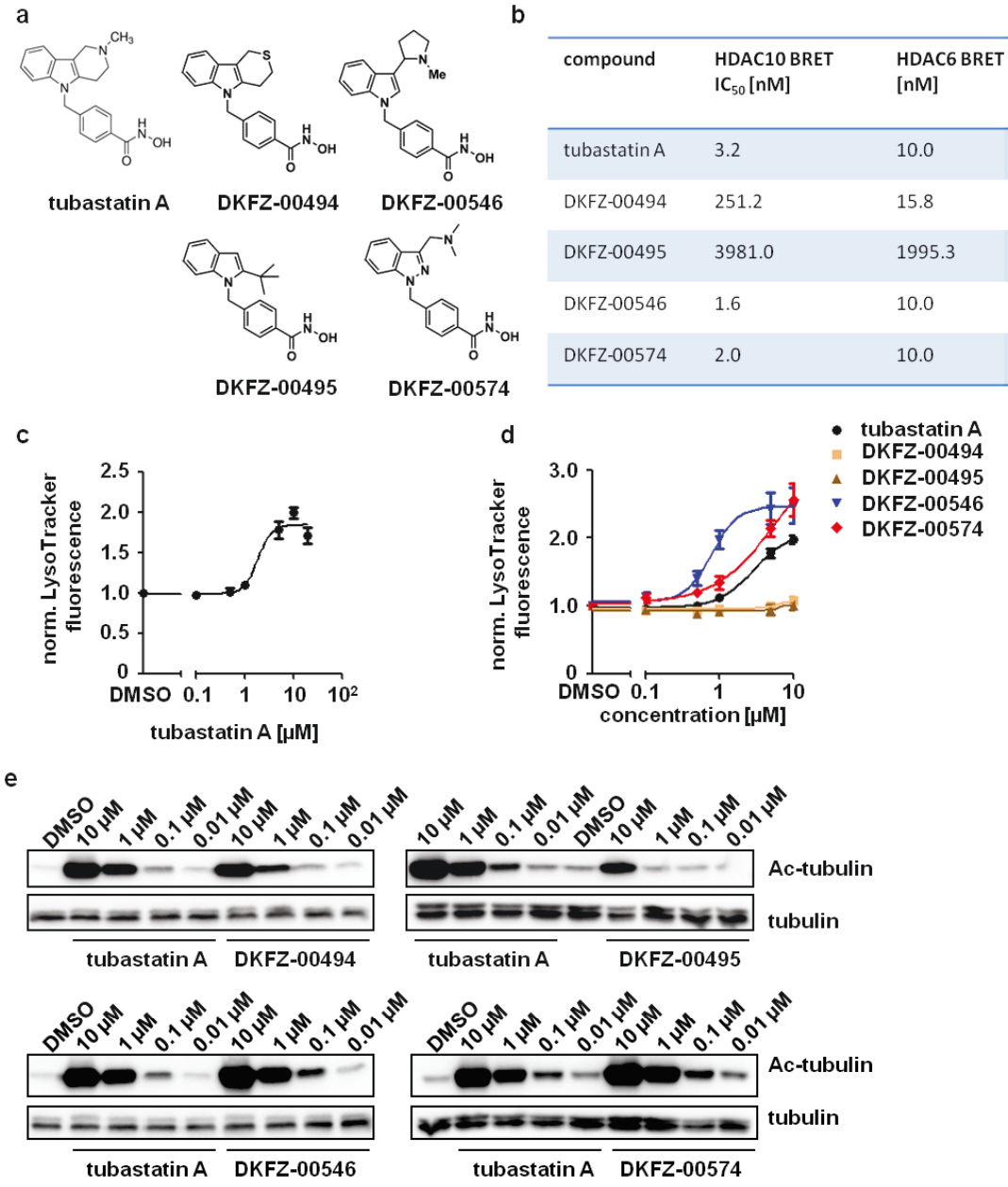

compound	HDAC10 BRET IC_{50} [nM]	HDAC6 BRET IC_{50} [nM]
tubastatin A	3.2	10.0
DKFZ-00494	251.2	15.8
DKFZ-00495	3981.0	1995.3
DKFZ-00546	1.6	10.0
DKFZ-00574	2.0	10.0

Figure 14: HDAC10 binding capacity of HDAC6/10 inhibitors is determined by the presence of a basic nitrogen atom in the inhibitor's cap group. (a) *Structural formula of tubastatin A derivatives, where the basic nitrogen in the cap group was ablated (central panel) or modified (right panel).* ***(b)*** *HDAC10 and HDAC6 binding activities determined by NanoBRET assays. Tubastatin A derivatives were synthesized and NanoBRET assays were performed in HeLa cells in the group of Cancer Drug Development (Dr. Aubry Miller) at the DKFZ.* ***(c, d)*** *Flow cytometric analysis of LysoTracker staining in BE(2)-C neuroblastoma cells 24h after treatment with tubastatin A* ***(c)*** *and tubastatin A derivatives* ***(d)****. Graphs depict mean LysoTracker fluorescence normalized to DMSO control (y-axis) versus logarithmic concentration (x-axis). Curves were generated using non-linear curve fitting(variable slope) in GraphPad Prism version 5.0.* ***(e)*** *Western blot of tubulin acetylation in BE(2)-C cells 24h after treatment with tubastatin A and tubastatin A derivatives. Error bars in this figure represent standard error of the mean (SEM).*

1.2.3 Triple HDAC6/8/10 inhibiting tubastatin A derivatives lose their inhibitory activity on HDAC6/8/10 in BE(2)-C cells

Both HDAC8 and HDAC10 have been described as potential drug targets in neuroblastoma and their inhibition can promote neuroblastoma cell differentiation and sensitization to chemotherapy, respectively (Oehme et al. 2009b; Oehme et al. 2013a; Rettig et al. 2015). Unpublished data show that co-inhibition of HDAC8 and 10 in combination with chemotherapy is very efficient in inducing cell death in neuroblastoma cell lines (Koeneke, unpublished data), making dual HDAC8/10 inhibition an interesting option for neuroblastoma treatment. However, simultaneous application of multiple small molecule inhibitors in patients is challenging due to drug interactions and differential drug metabolism. The close structural relation of the HDAC6/10 inhibitor tubastatin A and the HDAC8 specific inhibitor PCI-34051 (Balasubramanian et al. 2008), which mainly differ in the position of the Zn^{2+} binding hydroxamic acid residue (***Figure 15a***), prompted the idea that synthesis of a chimeric molecule carrying two hydroxamic acid moieties and thus resembling both PCI-34051 and tubastatin A could circumvent this problem by creating a combined HDAC8/10 inhibitor. Due to its structural resemblance to tubastatin A, such an inhibitor would also inhibit HDAC6, thus creating a triple HDAC6/8/10 inhibitor. As HDAC6 inhibitors were well tolerated in multiple preclinical and clinical studies (Santo et al. 2012; Yee et al. 2016; Vogl et al. 2017), this was not regarded as an exclusion criterion for the synthesis of tubastatin A related HDAC8/10 inhibitors (below referred to as triple HDAC6/8/10 inhibitors).

The prototype compound, DKFZ-00477, carried an extra hydroxamic acid at its cap group and thus resembled the structure of both tubastatin A and PCI-34051 (***Figure 15a***). Surprisingly however, DKFZ-00477 displayed a 50-fold reduction in HDAC10 binding capacity compared to tubastatin A in HeLa cells (NanoBRET assay), as well as a slightly decreased HDAC8 binding capacity (8-fold) compared to PCI-34051 in biochemical assays (HDAC-Glo I/II assay) (***Figure 15b***). Accordingly, no lysosomal accumulation was observed when BE(2)-C cells were treated with DKFZ-00477 up to a concentration of 30 µM, confirming that it was an ineffective HDAC10 inhibitor in neuroblastoma cells (***Figure 15c***).

Addition of an extra hydroxamic acid to the cap group of the above described tubastatin A derivative DKFZ-00574 (section ***E1.2.2***) yielded the chimeric compound DKFZ-00580, another potential triple HDAC6/8/10 inhibitor, while shift of the DKFZ-00574 hydroxamic acid to the cap group yielded the PCI-34051 analogous, and thus expectedly HDAC8 specific, DKFZ-00565 (***Figure 15a***). HDAC-Glo I/II (HDAC8) and NanoBRET (HDAC10) data confirmed that the DKFZ-00574 derivative DKFZ-00565 was a potent HDAC8 selective inhibitor with low HDAC10 activity (***Figure 15b***). This was confirmed by analysis of the acetylation status of the SMC3 protein in BE(2)-C cells on western blot, a known HDAC8 downstream target (Deardorff et al. 2012), where the DKFZ-00565 compound was even

slightly more potent than the HDAC8 inhibitor PCI-34051 at concentrations lower than 8 µM (***Figure 15e***). As for the DKFZ-00477 compound, biochemical HDAC-Glo assays (HDAC8), as well as NanoBRET assays in HeLa cells (HDAC10) again revealed that the chimeric inhibitor had reduced potency on HDAC8 (4-fold) and HDAC10 (6.3 fold), respectively, although the loss of potency was not as drastic as for the DKFZ-00477 compound (***Figure 15b***). In marked contrast to NanoBRET data in HeLa cells, however, the DKFZ-00580 compound possessed no substantial HDAC10 activity in the LysoTracker assay in BE(2)-C cells, where no lysosomal accumulation was observed even at increased concentrations up to 30 µM (***Figure 15d***). Furthermore, DKFZ-00580 did not induce substantial SMC3 acetylation when used at concentrations up to 64 µM, suggesting that it further did not possess HDAC8 activity in BE(2)-C cells (***Figure 15e***). Analysis of tubulin acetylation revealed a significant drop in HDAC6 inhibitory capacity of DKFZ-00580 compared to the DKFZ-00574 compound (***Figure 15e***). Lacking or weak activity against either of the tested HDACs in BE(2)-C cells suggested that addition of a second hydroxamic acid residue possibly not only interfered with binding to the respective enzyme but also with efficient drug uptake, potentially by increasing polarity and thus reducing diffusion of the compound across the plasma membrane. It also appears that the above described chemical modifications differentially affected drug uptake between different cell lines, which would explain the discrepancies between NanoBRET assays (HeLa cells) and functional HDAC assays (BE(2)-C cells) (discussed in section ***F1.5***).

a

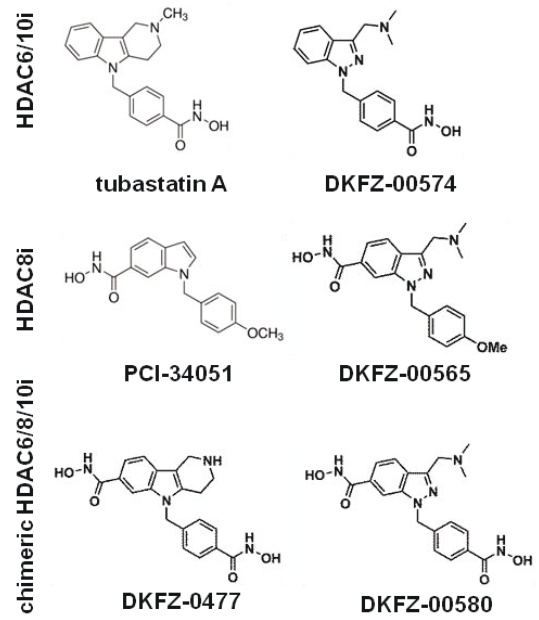

b

compound	HDAC10 BRET IC_{50} [nM]	HDAC8 enzyme IC_{50} [nM]
tubastatin A	3.2	1995.3
PCI-34051	> 10,000	63.1
DKFZ-0477	158.5	501.2
DKFZ-00565	1258.9	31.6
DKFZ-00574	2.0	794.3
DKFZ-00580	12.6	125.9

c

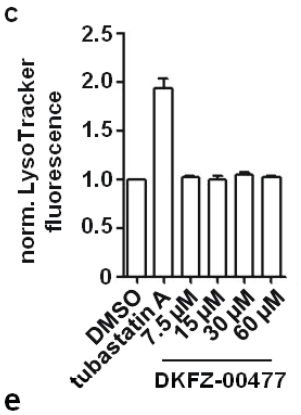

d

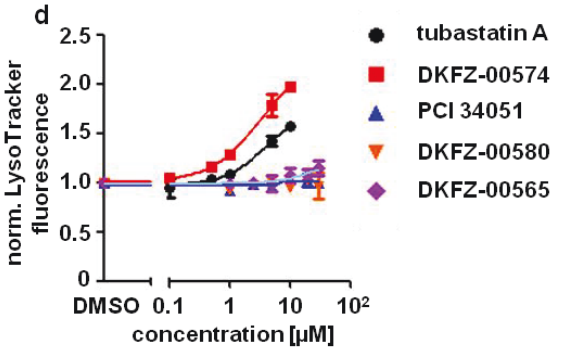

e

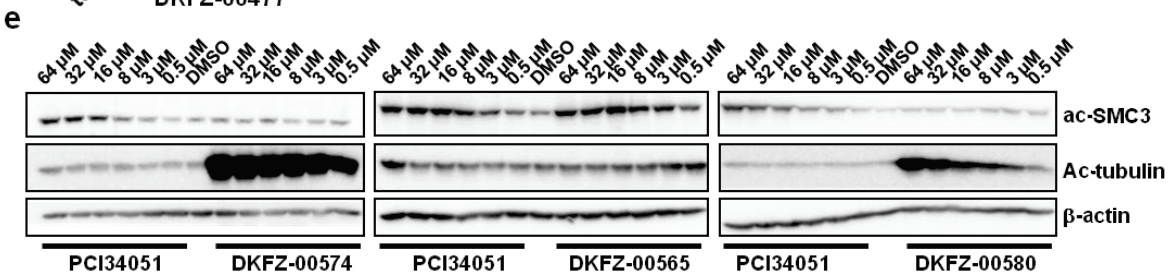

Figure 15: Triple HDAC6/8/10 inhibiting tubastatin A derivatives lose their HDAC6/8/10 inhibitory activity. (a) *Structural formulas showing tubastatin A derivatives with differential placement of the Zn^{2+} binding hydroxamic acid moiety, as well as chimeric, supposed HDAC6/8/10-active inhibitors with two hydroxamic acid groups (lower panel).* ***(b)*** *Summary of HDAC10 and HDAC8 binding activities determined by NanoBRET assays (HDAC10) and in vitro enzymatic assays (HDAC8). Compounds were synthesized and enzymatic assays were performed in the group of Cancer Drug Development (Dr. Aubry Miller) at the DKFZ.* ***(c)*** *Flow cytometric analysis of LysoTracker staining after 24h treatment of BE(2)-C cells with tubastatin A or the derivative DKFZ-00477 (n=2 experiments). Data were normalized to DMSO control.* ***(d)*** *Flow cytometric analysis of LysoTracker staining after 24h treatment of BE(2)-C cells with indicated compounds (n=2 experiments). Data were normalized to DMSO control. Graph depicts normalized mean LysoTracker fluorescence (y-axis) versus concentration (x-axis) Curves were generated using non-linear curve fitting (variable slope) in GraphPad Prism version 5.0.* ***(e)*** *Western blot analysis SMC3 (HDAC8 target) and tubulin acetylation in BE(2)-C cells after 24h treatment with indicated compounds. PCI-34051 treatment was used as positive control for HDAC8 inhibition. Error bars in this figure represent standard error of the mean (SEM).*

1.2.4 The HDAC6 specific inhibitor MARBOSTAT 100 (MARB1) inhibits HDAC10 at higher concentrations

MARBOSTAT 100 (hereafter referred to as MARB1) is a novel HDAC6 specific inhibitor that is structurally closely related to tubastatin A (***Figure 16a***), but has stronger selectivity for HDAC6 than previous HDAC6 inhibitors, as suggested in a recent report (Sellmer et al. 2018). NanoBRET assays in HeLa cells confirmed that MARB1 displays high affinity towards HDAC6 (IC_{50} 2.2 nM), with reduced affinity towards HDAC10 (IC_{50} 564 nM) compared to tubastatin A (IC_{50} 8 nM) (***Figure 16b***). Analysis of tubulin K40 acetylation via western blot further demonstrated strong HDAC6 inhibitory capacity of MARB1 in BE(2)-C cells, inducing robust tubulin acetylation above concentrations of 10 nM after overnight treatment (***Figure 16c***). The results in the previous sections (***E1.2.1*** and ***E1.2.2***) have shown that HDAC10 but not HDAC6 inhibition in BE(2)-C cells causes accumulation of lysosomes. Thus, the HDAC10 inhibitory capacity of MARB1 in BE(2)-C cells was analyzed by flow cytometric quantification of LysoTracker staining. MARB1 caused lysosomal accumulation at concentrations above 1 µM (EC_{50} 6.6 µM), suggesting that MARB1 also had HDAC10 inhibitory capacity at high concentrations in BE(2)-C cells (***Figure 16d***). Notably, while NanoBRET assays in HeLa cells showed a roughly 70-fold reduced affinity of MARB1 to HDAC10 over tubastatin A, LysoTracker analysis revealed a mere 2.3 fold shift in EC_{50}, possibly reflecting differential uptake of the two drugs in different cell systems. In this context, the data in the previous section (***E1.2.3***) suggest that even small modifications like the addition of a second hydroxamic acid moiety can cause significant discrepancies in drug uptake between different cell models. In this case, the chemical modification introduced in MARB1 might have affected drug uptake more drastically in HeLa than in BE(2)-C cells.

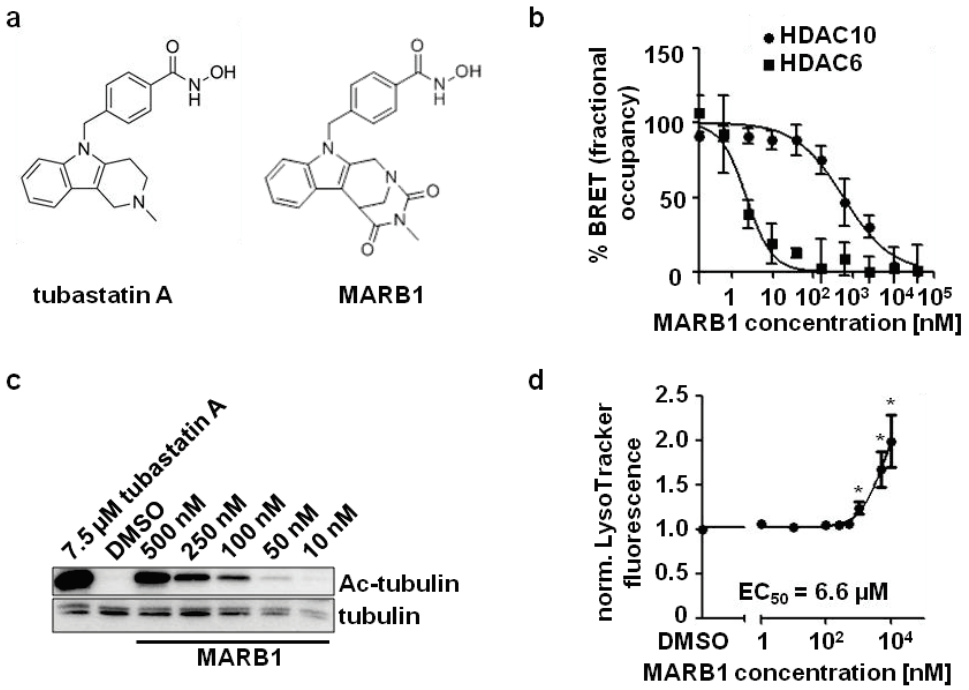

Figure 16: The tubastatin A derivative MARB1 binds HDAC10 at high concentrations and causes lysosomal expansion in BE(2)-C cells. (a) *Structural formula of HDAC6/10 inhibitor tubastatin A and supposed HDAC6-specific inhibitor MARBOSTAT 100 (MARB1). MARB1 was synthesized in the lab of Siavosh Mahboobi (Institute of Pharmacy, University of Regensburg).* ***(b)*** *NanoBRET analysis of MARB1 binding activity against HDAC6 and HDAC10 in HeLa cells. Graph depicts tracer signal relative to total NanoLuc signal (% fractional occupancy, y-axis) versus logarithmic drug concentration in nM (x-axis). NanoBRET assays were performed in the group of Cancer Drug Development (Dr. Aubry Miller) at the DKFZ.* ***(c)*** *Western blot analysis of tubulin acetylation after 24h treatment of BE(2)-C cells with tubastatin A and MARB1, respectively. Experiment was performed in collaboration with Fiona Kolbinger (Clinical Cooperation Unit, DKFZ).* ***(d)*** *Analysis of LysoTracker fluorescence via flow cytometry 24h after treatment with MARB1. Graph depicts mean LysoTracker fluorescence normalized to DMSO treated cells (y-axis) versus logarithmic drug concentration (x-axis). Curves in figures* ***(b)*** *and* ***(d)*** *were fitted via non-linear curve fitting (variable slope) using GraphPad Prism version 5.0. Statistical analysis in* ***(d)*** *was performed on non-normalized data using paired two-tailed t-test (***p < 0.001; **0.001 ≤p <0.01; *0.01 ≤ p < 0.05). Error bars represent standard error of the mean (SEM). Parts of figure published in (Ridinger et al. 2018).*

1.2.5 The pan HDACi abexinostat has a high affinity towards HDAC10 and causes lysosomal accumulation at clinically relevant concentrations

Collective evidence suggests that lysosomes are important mediators of chemoresistance in cancer making lysosomes an attractive target for clinical intervention (Kirkegaard and Jaattela 2009; Zhitomirsky and Assaraf 2016). The data described in section ***E1.1*** and ***E1.2*** show that interference with HDAC10 function alters lysosomal composition of neuroblastoma cells. Moreover, a previous publication from our lab shows that interference with HDAC10 function can reduce chemoresistance of neuroblastoma cells, making HDAC10 an interesting target for neuroblastoma therapy (Oehme et al. 2013a). However, none of the above tested HDAC10 inhibitors is currently used in clinical trials, and future clinical trials are for example hampered by their unfavorable pharmacokinetic profile (discussed in section ***F1.5***.). Thus, either FDA approved or Phase I/II tested pan and broad-spectrum

HDAC inhibitors were tested for their activity on HDAC10 in NanoBRET assays. Here, the pan inhibitor abexinostat (PCI-24781) (***Figure 17a***) displayed high HDAC10 activity in the nanomolar range (IC_{50} 0.74 nM) (***Figure 17b***). Analogous to other compounds with HDAC10 inhibiting activity (sections ***E1.2.1*** and ***E1.2.4***), abexinostat induced expansion of the lysosomal compartment in BE(2)-C cells (***Figure 17d***). Here, abexinostat was especially efficient, inducing lysosomal expansion at nanomolar concentrations with an EC_{50} of 183 nM. Importantly, the concentration at which abexinostat interfered with lysosomal homeostasis was well within the range of clinically achievable concentrations in patients, which can reach up to 500 nM (Morschhauser et al. 2015). Thus, the pan HDAC inhibitor abexinostat is capable of inhibiting HDAC10 and causing lysosomal accumulation at concentrations that are achievable in patient plasma, making it a promising compound for HDAC10 inhibition in future pre-clinical and clinical trials.

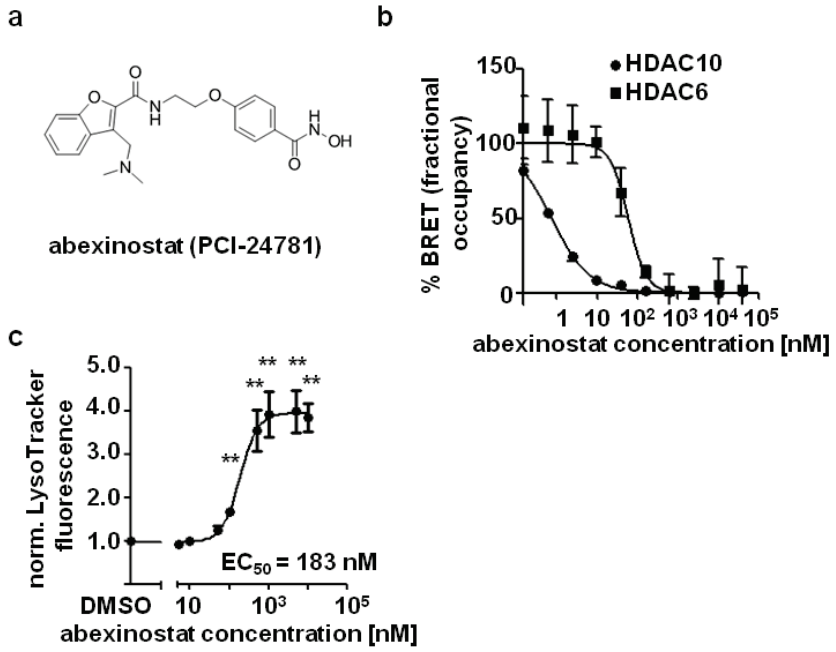

Figure 17: The pan HDAC inhibitor abexinostat (PCI-24781) shows strong activity on HDAC10 in NanoBRET and LysoTracker assays. (a) *Structural formula of abexinostat.* ***(b)*** *NanoBRET analysis of abexinostat binding activity against HDAC6 and HDAC10 in HeLa cells. Graph depicts tracer signal relative to total NanoLuc signal (% fractional occupancy, y-axis) versus logarithmic drug concentration in nM (x-axis). NanoBRET assays were performed in the group of Cancer Drug Development (Dr. Aubry Miller) at the DKFZ.* ***(c)*** *Analysis of LysoTracker fluorescence via flow cytometry after 24h treatment of BE(2)-C neuroblastoma cells with abexinostat. Graph depicts mean LysoTracker fluorescence normalized to DMSO treated cells (y-axis) versus logarithmic drug concentration (x-axis). Curves in figures* ***(b)*** *and* ***(c)*** *were generated via non-linear curve fitting (variable slope) using GraphPad Prism version 5.0. Statistical analysis in* ***(c)*** *was performed on non-normalized data using paired two-tailed t-test (***p < 0.001; **0.001 ≤p <0.01; *0.01 ≤ p < 0.05). Error bars represent standard error of the mean (SEM). Parts of figure published in (Ridinger et al. 2018).*

1.3 Non class IIb HDACs and their role in lysosomal homeostasis

1.3.1 Knockdown of class I, class IIb and class IV HDACs reveal that HDACs 10 and 11 most strongly influence lysosomal composition in BE(2)-C cells

Data in section ***E1.2.2*** have shown that treatment of BE(2)-C neuroblastoma cells with tubastatin A causes lysosomal accumulation at concentrations above 1 µM and that the lysosome-expanding property of tubastatin A could be attributed to its HDAC10 rather than HDAC6 inhibitory activity. Although tubastatin A is considered as a specific class IIb inhibitor in the literature, a binding to class I HDACS (especially HDAC1 (reported IC_{50} 16.4 µM)) at high concentrations cannot be fully ruled out (Butler et al. 2010). In fact, western blot analysis confirmed that 24h treatment of BE(2)-C cells with high concentrations of tubastatin A (10 µM) increased histone H3 acetylation, a target of HDACS 1, 2 and 3, suggesting that it interfered with functions class I HDACs at high concentrations (***Figure 18a***). Thus, in order to investigate how interference with the function of individual class I HDACs affected the lysosomal compartment, HDACs 1, 2, 3 were knocked down in BE(2)-C cells using pooled siRNAs against the respective HDAC. Knockdown of class IV member HDAC11 was included due to the relationship of its catalytic domain to both class I and class II HDACS (Gao et al. 2002; Seto and Yoshida 2014). Lysosomal content was analyzed via flow cytometric quantification of LysoTracker staining six days after siRNA transfection. Here, knockdown of all individual HDACs slightly induced lysosomal accumulation in BE(2)-C cells (***Figure 18b***). However, when averaged over three experimental replicates, only HDAC10 knockdown increased lysosomal numbers on a statistically significant level. Apart from HDAC10, knockdown HDACs 1 and 11 caused the most substantial increase in lysosomal staining, almost reaching statistical significance ($p = 0.09$ and $p = 0.07$, respectively). This suggested that, apart from HDAC10, HDACs 1 and 11 potentially contributed to lysosomal homeostasis in BE(2)-C cells. Nevertheless, interference with HDAC10 function most clearly caused lysosomal accumulation.

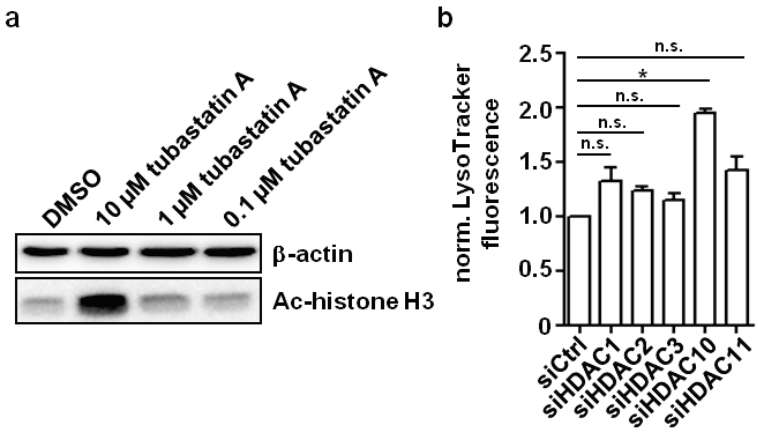

Figure 18: Analysis of lysosomal accumulation after RNAi-mediated knockdown of class I HDACs, as well as HDAC10 and HDAC11. (a) *Western blot analysis of tubulin acetylation after 24h treatment of BE(2)-C cells with various tubastatin A doses.* ***(b)*** *Flow cytometric analysis of LysoTracker staining 6d after knockdown of indicated HDACs. Bar graph depicts mean LysoTracker fluorescence normalized to siCtrl transfected cells of n=3 experimental replicates. Statistical analysis in* ***(b)*** *was performed on non-normalized data using paired two-tailed t-test (***p < 0.001; **0.001 ≤p <0.01; *0.01 ≤ p < 0.05). Error bars represent standard error of the mean (SEM). Parts of figure published in (Ridinger et al. 2018).*

1.3.2 The class I inhibitor MS-275 causes lysosomal accumulation while valproic acid does not

The data provided in section ***E1.3.1*** show that HDAC6/10 inhibitor tubastatin A induces histone H3 acetylation and thus likely inhibited class I HDACs at high concentrations. Moreover, knockdown of individual class I HDACs slightly, but not statistically significantly, induces lysosomal accumulation. This raised the question whether simultaneous inhibition of class I HDACs 1, 2, 3 could cause significant expansion of the lysosomal compartment in neuroblastoma cells. In order to investigate this, BE(2)-C cells were treated with valproic acid, a class I HDAC inhibitor (Wagner et al. 2013), or HDAC6/10 inhibitor tubastatin A for 24h and analyzed for lysosomal content via the LysoTracker assay. Here, valproic acid did not induce substantial lysosomal accumulation, while treatment with the HDAC6/10 inhibitor tubastatin A did (***Figure 19a***). At the same time, western blot analysis revealed that VPA treatment induced a much stronger increase in histone H3 acetylation (5.3 fold) than treatment with tubastatin A (1.3 fold) (***Figure 19b***). This again confirmed that lysosomal accumulation in case of tubastatin A treatment was most likely due to its HDAC10 inhibitory activity and not because of off-target activity on class I HDACs. Surprisingly, 24h treatment with MS-275, another class I HDAC inhibitor (Wagner et al. 2013), caused strong accumulation of lysosomes in preliminary experiments and it was thus suspected that MS-275 could have HDAC10 inhibitory activity (***Figure 19c***). NanoBRET analyses, however, did not show any binding activity of MS-275 against class IIb HDAC members HDAC6 or HDAC10 even at micromolar concentrations, excluding that its effects on the lysosomal compartment were due to an HDAC10 inhibitory activity (***Figure 19d***). Although expansion of the lysosomal compartment after MS-275 treatment cannot be fully

explained, knockdown data in section ***E1.3.1*** and data from class I inhibitor valproic acid (***Figure 19a***) make it unlikely that lysosomal accumulation after MS-275 treatment was due to its inhibitory effect on class I HDACs. Notably, MS-275 treatment was highly cytotoxic even at low concentrations, suggesting that an off-target effect could be responsible for lysosomal accumulation. In addition, the inhibitory activity of MS-275 on HDAC11 has not been characterized, and data in section ***E1.3.1*** suggest that interference with HDAC11 function can also cause lysosomal accumulation (discussed in section ***F1.1***).

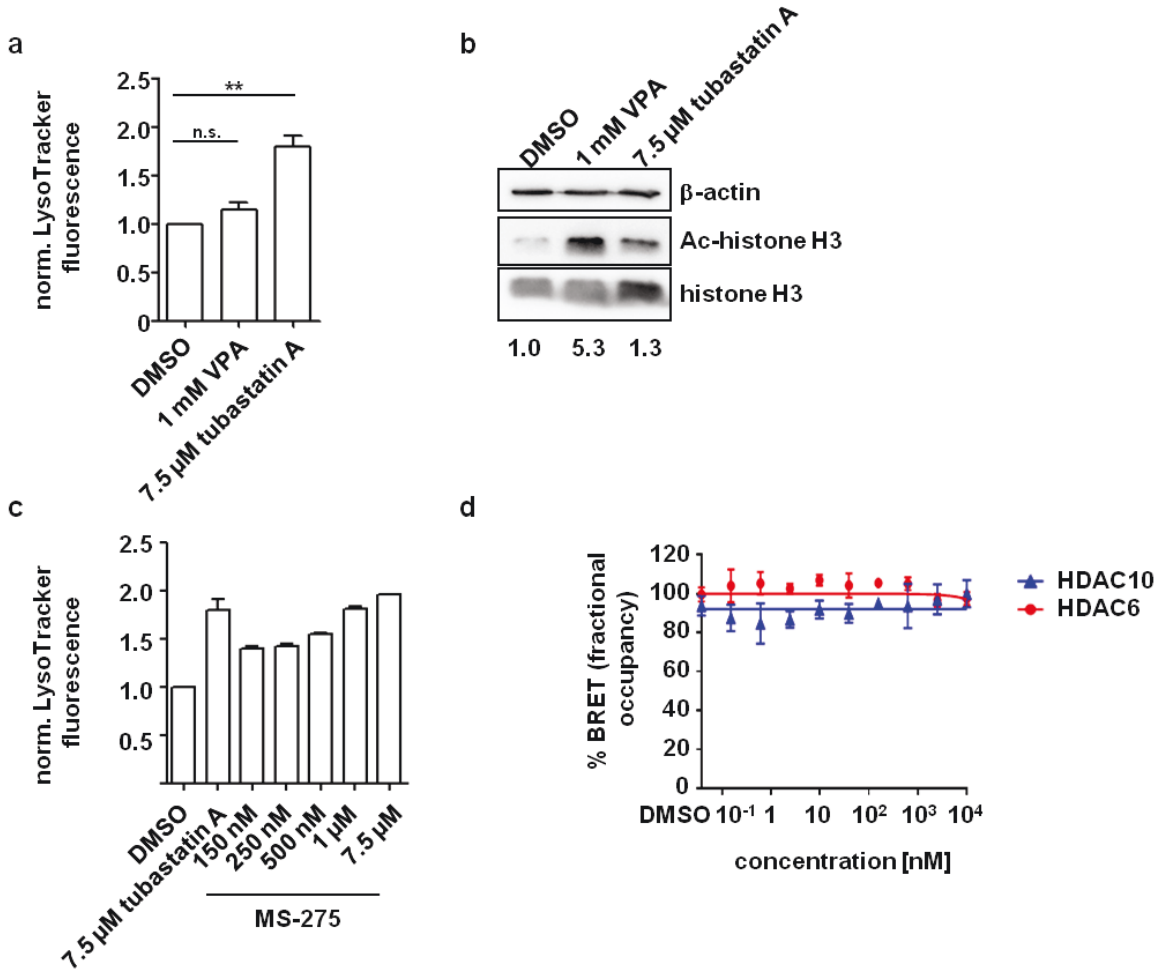

Figure 19: Analysis of lysosomal accumulation after treatment of BE(2)-C neuroblastoma cells with class I HDAC inhibitors valproic acid (VPA) and MS-275. (a) *Normalized fluorescence of LysoTracker staining 24h after treatment of BE(2)-C cells with VPA and tubastatin A (n=4 flow cytometry experiments).* ***(b)*** *Western blot analysis of histone H3 acetylation after 24h treatment of BE(2)-C cells with VPA and tubastatin A. Numbers below the blot indicate densitometric analysis of acetylated histone H3 signal normalized to total histone H3.* ***(c)*** *Flow cytometric analysis of LysoTracker staining 24h after treatment of BE(2)-C cells with MS-275 and tubastatin A (n=2 experiments).* ***(d)*** *NanoBRET analysis of MS-275 binding activity against HDAC6 and HDAC10 in HeLa cells. Graph depicts tracer signal relative to total NanoLuc signal (% fractional occupancy, y-axis) versus logarithmic drug concentration in nM (x-axis). NanoBRET assays were performed in the group of Cancer Drug Development (Dr. Aubry Miller) at the DKFZ. Statistical analysis in* ***(a)*** *was performed on non-normalized data using paired two-tailed t-test (***p < 0.001; **0.001 ≤p <0.01; *0.01 ≤ p < 0.05). Error bars represent standard error of the mean (SEM). Parts of figure published in (Ridinger et al. 2018).*

1.4 Interference with HDAC10 function causes doxorubicin accumulation in neuroblastoma cells

Altered lysosomal function has been repeatedly associated with cancer progression and therapy resistance. With regards to the latter, collective evidence suggests that enlargement of the lysosomal compartment can reduce the efficacy of many clinically chemotherapeutic drugs, including doxorubicin. Drugs with weakly basic chemical properties can, after passively entering lysosomes, become protonated and sequestered within lysosomes, preventing them from reaching their cellular drug target (see section ***A3.2.3***). Moreover, lysosomes can promote the secretion of sequestered drugs when they undergo lysosomal exocytosis (Machado et al. 2015). Given the observation that interference with HDAC10 function caused an enlargement of the lysosomal compartment (see section ***E1***), it was hypothesized that enlargement of the lysosomal compartment could be accompanied by increased intracellular accumulation or lysosomal sequestration of doxorubicin, one of the most important chemotherapeutic agents used in high-risk neuroblastoma therapy.

1.4.1 HDAC10 but not HDAC6 depletion causes intracellular doxorubicin accumulation

To investigate if lysosomal accumulation after interference with HDAC10 function altered cellular doxorubicin levels, BE(2)-C neuroblastoma cells were transfected with siRNAs against HDAC10, HDAC6 and control siRNAs, respectively. Cells were treated with doxorubicin for the last 24h and cellular doxorubicin fluorescence was quantified via flow cytometry. Knockdown of HDAC10 increased cellular doxorubicin fluorescence roughly 1.5-fold when compared to cells transfected with control siRNAs (***Figure 20a, b***). In contrast, depletion of HDAC6 caused a significant, albeit, small reduction of intracellular doxorubicin levels (***Figure 20a, b***). Thus, expansion of the lysosomal compartment after HDAC10 depletion in BE(2)-C cells described in section ***E1.1.2*** correlated with increased intracellular accumulation of doxorubicin.

The effects of HDAC10 depletion on doxorubicin accumulation was confirmed in a commercially generated near-haploid chronic myeloid leukemia (CML) cell line with an HDAC10 knockout (HAP1 HDAC10 KO). HDAC10 knockout cells accumulated slightly, but significantly, higher levels of doxorubicin than HAP1 wild type cells (HAP1 wt) (***Figure 20c-e***).

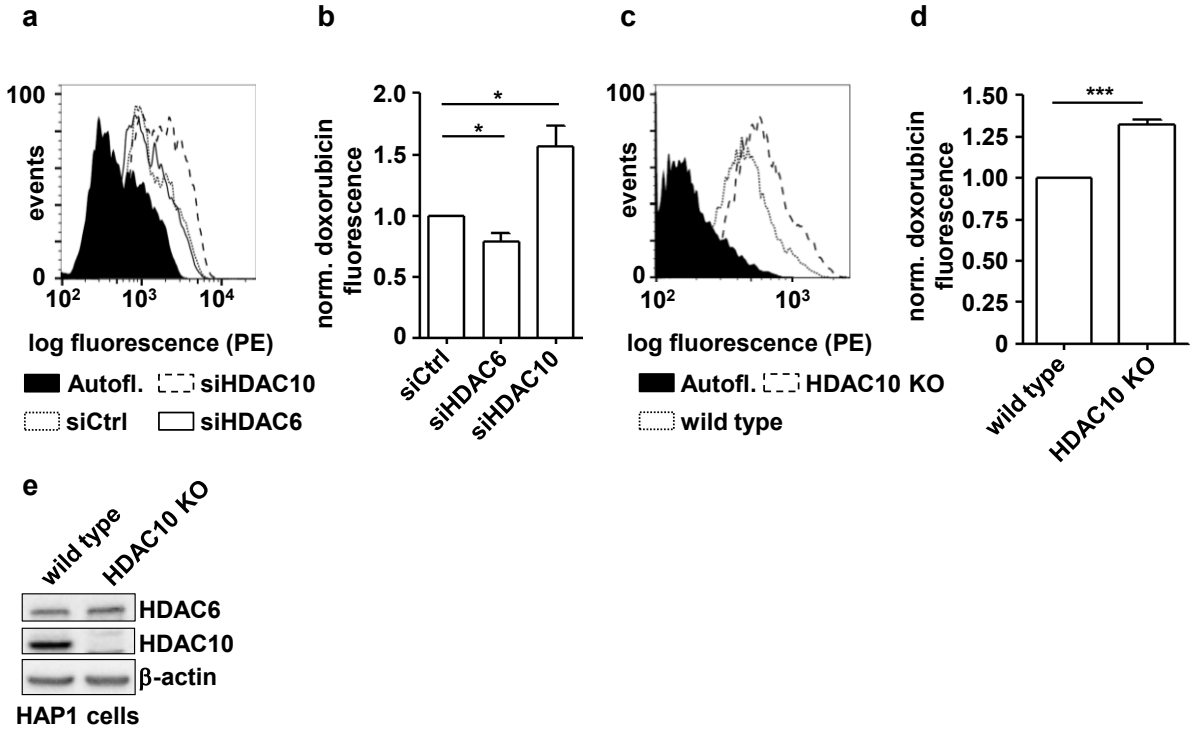

Figure 20: Depletion of HDAC10 but not HDAC6 causes intracellular accumulation of doxorubicin. (a, b) *Flow cytometric analysis of cellular doxorubicin fluorescence in BE(2)-C cells 6d after siRNA transfection. Cells were treated with doxorubicin for the last 24h. Histogram* ***(a)*** *depicts percentage of cells (y-axis) versus logarithmic fluorescence (x-axis). Mean doxorubicin fluorescence normalized to siCtrl transfected cells of n=5 experiments was quantified* ***(b)****.* ***(c, d)*** *Flow cytometric analysis of cellular doxorubicin fluorescence in HAP1 wild type versus HDAC10 knockout cells. Figures show representative histogram* ***(c)*** *and mean doxorubicin fluorescence normalized to wild type cells of n=6 experiments* ***(d)****.* ***(e)*** *Western blot analysis of HDAC10 expression in HAP1 cells. Statistical analyses were performed on non-normalized data using paired two-tailed t-test (***p < 0.001; **0.001 ≤p <0.01; *0.01 ≤ p < 0.05). Error bars represent standard error of the mean (SEM). Figure published in (Ridinger et al. 2018).*

1.4.2 HDAC10 but not HDAC6 inhibition causes accumulation of doxorubicin in a panel of highly aggressive neuroblastoma cell lines

The results described in section ***E1.1*** show that enlargement of the lysosomal compartment was not only observed in case of HDAC10 depletion but also when HDAC10 enzymatic function was inhibited. Given that lysosomal accumulation correlated with increased intracellular doxorubicin levels upon HDAC10 depletion, it was hypothesized that HDAC10 inhibition should cause a similar intracellular doxorubicin accumulation. The influence of HDAC6 and HDAC6/10 inhibitors on cellular doxorubicin accumulation was investigated by 48h co-treatment of BE(2)-C cells with doxorubicin and HDAC6 or HDAC6/10 inhibitors. Both HDAC6/10 inhibitors bufexamac and tubastatin A increased intracellular doxorubicin levels significantly compared to cells treated with doxorubicin and solvent only (***Figure 21a, b***). In contrast, specific inhibition of HDAC6 with tubacin did not alter intracellular doxorubicin levels, suggesting that increased doxorubicin accumulation after co-treatment with HDAC6/10 inhibitors was due to HDAC10 rather than HDAC6 inhibition (***Figure 21a, b***). In line with this, co-treatment with doxorubicin and MARB1 elevated doxorubicin levels only at concentrations, at which

MARB1 had strong inhibitory activity on HDAC10 and at which robust lysosomal induction was observed (***Figure 21c***) (5 µM and higher, also see ***Figure 16***). MARB1 had no effect on doxorubicin accumulation at lower concentrations which still clearly inhibited HDAC6 (***Figure 21c*** and ***Figure 16c***). Thus, in line with the effects described for HDAC10 knockdown in section ***E1.4.1***, doxorubicin accumulation after HDAC10 inhibition correlated with the before observed enlargement of the lysosomal compartment (also see section ***E1.2.1***). Elevated doxorubicin levels were also observed when BE(2)-C cells were co-treated with the pan-HDAC inhibitor abexinostat (Yang et al. 2011; Choy et al. 2015; Morschhauser et al. 2015). Data in section ***E1.2.5*** show that abexinostat had strong HDAC10 inhibitory activity and caused lysosomal accumulation at concentrations greater than or equal to 100 nM (***Figure 17c***). Increased doxorubicin accumulation was observed, when abexinostat was used at concentrations that caused strong lysosomal accumulation (equal to or greater than 500 nM).

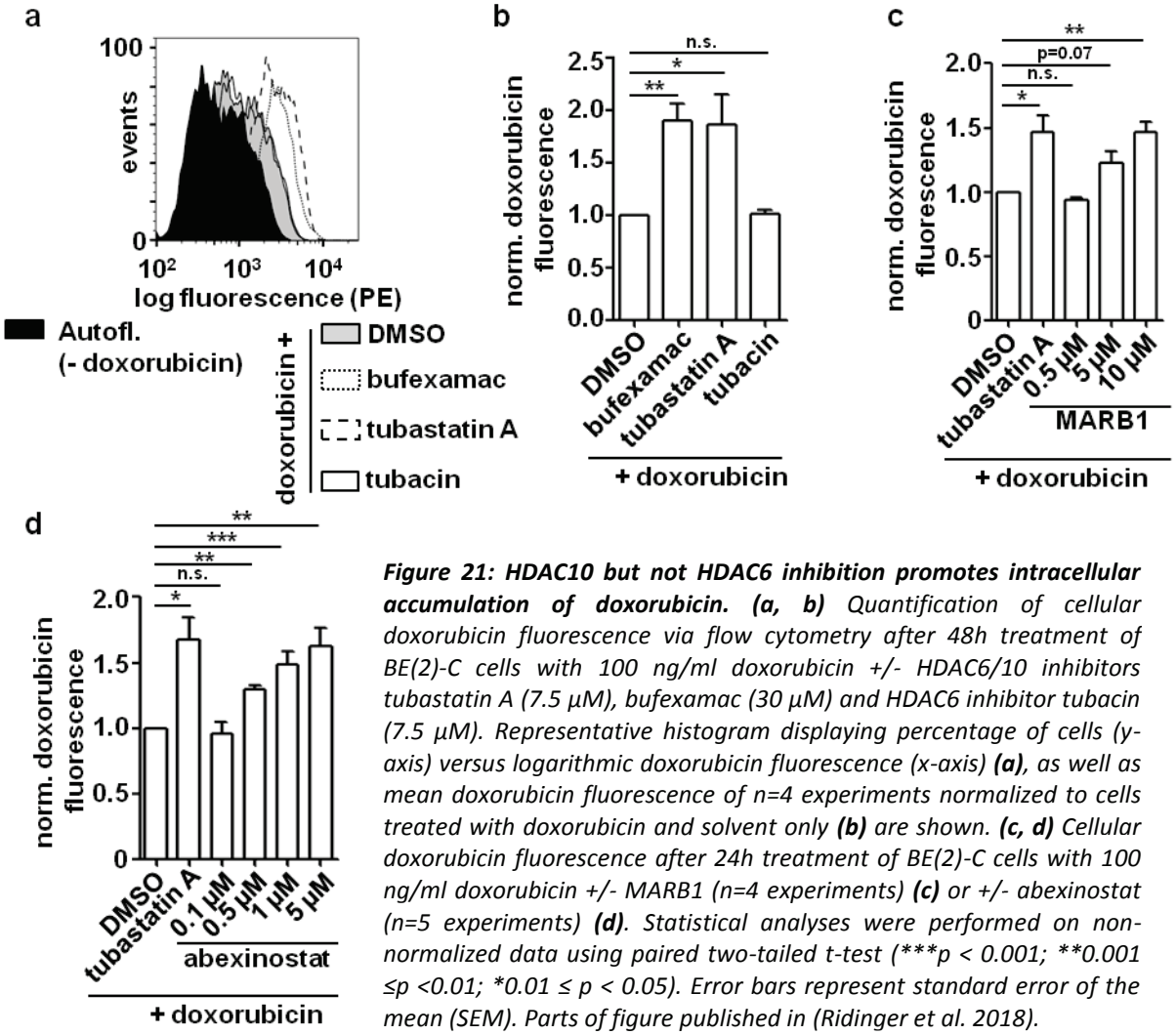

Figure 21: HDAC10 but not HDAC6 inhibition promotes intracellular accumulation of doxorubicin. (a, b) *Quantification of cellular doxorubicin fluorescence via flow cytometry after 48h treatment of BE(2)-C cells with 100 ng/ml doxorubicin +/- HDAC6/10 inhibitors tubastatin A (7.5 µM), bufexamac (30 µM) and HDAC6 inhibitor tubacin (7.5 µM). Representative histogram displaying percentage of cells (y-axis) versus logarithmic doxorubicin fluorescence (x-axis)* ***(a)****, as well as mean doxorubicin fluorescence of n=4 experiments normalized to cells treated with doxorubicin and solvent only* ***(b)*** *are shown.* ***(c, d)*** *Cellular doxorubicin fluorescence after 24h treatment of BE(2)-C cells with 100 ng/ml doxorubicin +/- MARB1 (n=4 experiments)* ***(c)*** *or +/- abexinostat (n=5 experiments)* ***(d)****. Statistical analyses were performed on non-normalized data using paired two-tailed t-test (***p < 0.001; **0.001 ≤p <0.01; *0.01 ≤ p < 0.05). Error bars represent standard error of the mean (SEM). Parts of figure published in (Ridinger et al. 2018).*

Co-treatment with tubastatin A also increased doxorubicin levels in other high-risk neuroblastoma cell lines, including IMR-32 and SK-N-AS cells (***Figure 22a, b***), albeit the effect in IMR-32 cells was small (1.2-fold increase), possibly due to low endogenous HDAC10 expression in this cell line (investigated in section ***E1.4.3***).

Taken together, these data show that interference with HDAC10 function, either by depletion or inhibition, increases intracellular accumulation of doxorubicin, which is likely connected to the before observed enlargement of the lysosomal compartment after interference with HDAC10 function.

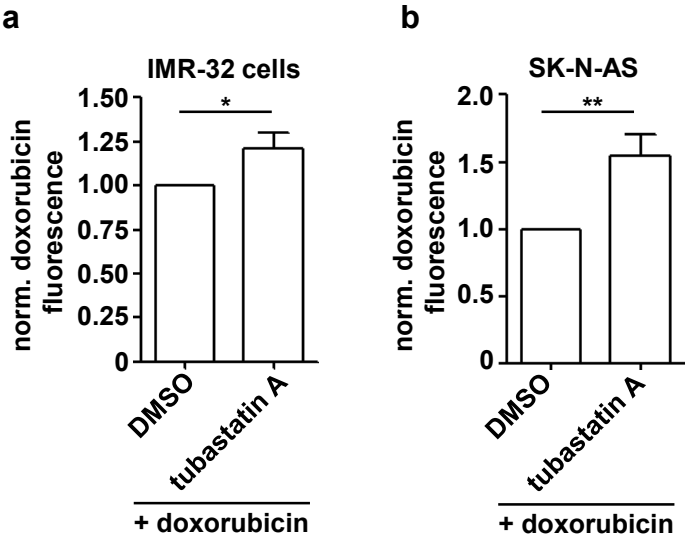

Figure 22: HDAC6/10 inhibitor tubastatin A also promotes doxorubicin accumulation in high-risk neuroblastoma cell lines other than BE(2)-C. (a) *Quantification of cellular doxorubicin fluorescence in IMR-32 cells via flow cytometry after co-treatment with 50 ng/ml doxorubicin +/- HDAC6/10 inhibitor tubastatin A (7.5 µM) for 18h (n=5 experiments).* ***(b)*** *Quantification of cellular doxorubicin fluorescence in SK-N-AS cells after via flow cytometry after co-treatment with 100 ng/ml doxorubicin +/- tubastatin A (7.5 µM) for 48h (n=4 experiments). Bar graphs depict doxorubicin fluorescence normalized. Statistical analyses were performed on non-normalized data using paired two-tailed t-test (***p < 0.001; **0.001 ≤p <0.01; *0.01 ≤ p < 0.05). Error bars represent standard error of the mean (SEM). Figure published in (Ridinger et al. 2018).*

1.4.3 HDAC10 protein levels in neuroblastoma cell lines are not predictive of doxorubicin accumulation

HDAC10 inhibition in the IMR-32 neuroblastoma cell line only caused a comparably small increase in intracellular doxorubicin when compared to BE(2)-C or SK-N-AS cells (section ***E1.4.2***). As IMR-32 cells are known to express low endogenous levels of HDAC10, it was hypothesized that HDAC10 protein levels might serve as a predictive marker of doxorubicin accumulation after HDAC10 inhibition.

The analysis of HDAC10 expression in a panel of neuroblastoma cell lines showed that BE(2)-C and SK-N-AS cells expressed relatively high amounts of HDAC10 protein, while expression in IMR-32 was low (***Figure 23a***). Notably, the two *MYCN* amplified high-risk neuroblastoma cell lines (Kelly, NB-1) showed intermediate levels of HDAC10 protein expression and it was hypothesized that co-treatment

of these cell lines with doxorubicin and tubastatin A should cause an intermediate increase in intracellular doxorubicin levels. However, co-treatment of neither Kelly nor NB-1 cells with tubastatin A reproducibly increased intracellular doxorubicin levels compared to cells treated with doxorubicin and solvent only (***Figure 23b***). Thus, HDAC10 protein levels did not predict doxorubicin accumulation after HDAC10 inhibition.

Intriguingly, HDAC10 inhibition with tubastatin A and bufexamac did not induce lysosomal accumulation in NB-1 and Kelly cells, the latter being known to react only to high concentrations of bufexamac (Oehme et al. 2013a) (***Figure 23c***). Accordingly, lysosomal accumulation in Kelly and NB-1 was also absent upon treatment with the pan HDAC inhibitor abexinostat (***Figure 23d***) The lack of lysosomal compartment expansion after HDAC10 inhibition possibly explains the lack of doxorubicin accumulation under these conditions, as above described data suggest that expansion of the lysosomal compartment was a prerequisite to doxorubicin accumulation. Although it remained unclear why interference with HDAC10 function caused lysosomal accumulation in some but not other neuroblastoma cell lines, it is conceivable that HDAC10 is not equally required for lysosomal homeostasis in all of the used cell lines (discussed in sections ***F1.1***, ***F1.2*** and ***F1.3***). Furthermore, the question remains whether such a bottleneck behavior can be predicted by the activation of certain pathways or by gene expression patterns (prospective biomarker, discussed in section ***F1.3*** and ***F1.5***).

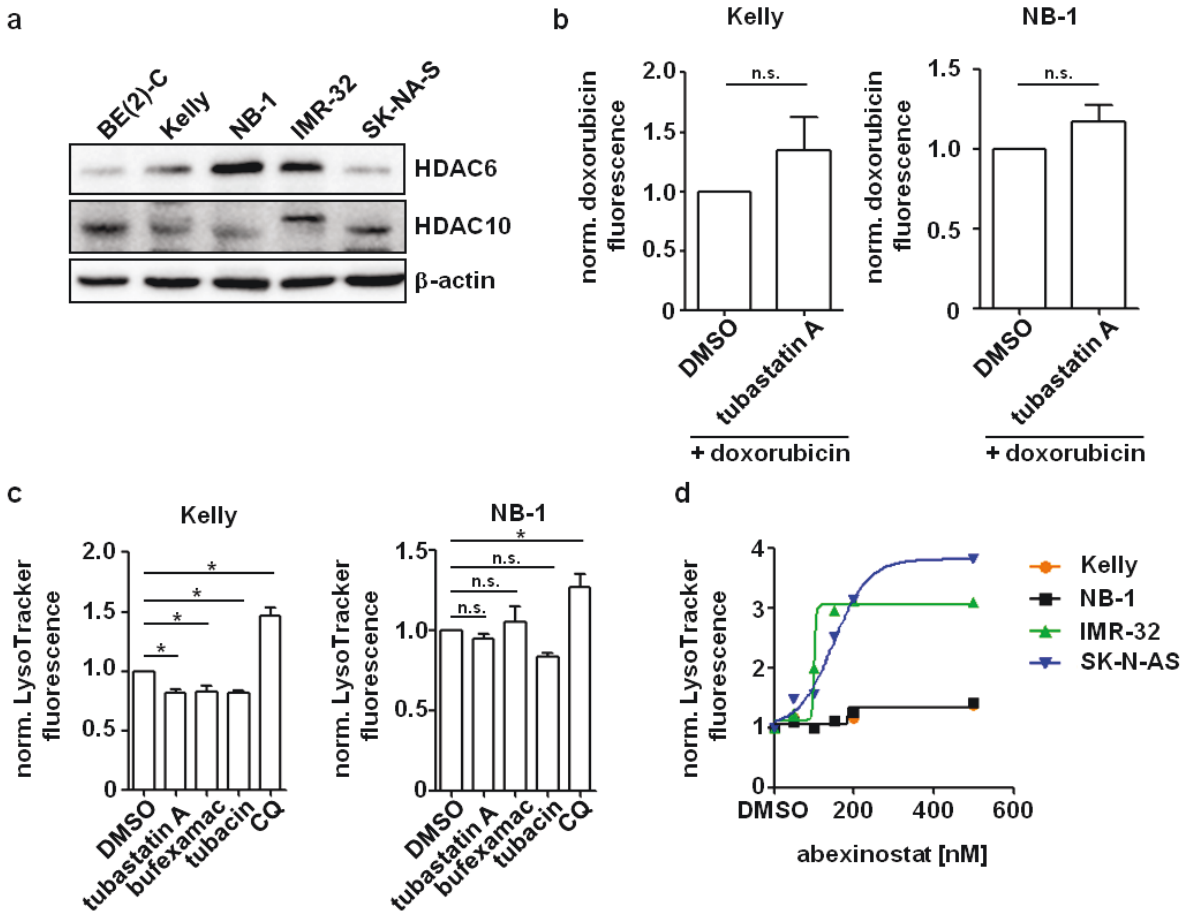

Figure 23: HDAC10 protein expression does not predict increased doxorubicin accumulation after addition of HDAC6/10 inhibitor tubastatin A. (a) *Western blot analysis of HDAC6 and HDAC10 expression in various high-risk neuroblastoma cell lines.* ***(b)*** *Flow cytometric analysis of doxorubicin accumulation in Kelly (n=6 experiments) and NB-1 (n=4 experiments) neuroblastoma cell lines after 48h co-treatment with 100 ng/ml doxorubicin and 7.5 µM tubastatin A. Mean doxorubicin fluorescence was normalized to cells treated with doxorubicin and solvent only.* ***(c)*** *Flow cytometric analysis of LysoTracker staining after 24h treatment with HDAC6/10 inhibitors tubastatin A (7.5 µM), bufexamac (30 µM), HDAC6 inhibitor tubacin (7.5 µM) and lysosomal inhibitor chloroquine (5 µM). Mean fluorescence of n=3 experiments was normalized to DMSO treated cells.* ***(d)*** *Flow cytometric analysis of LysoTracker staining in various neuroblastoma cell lines after 24h treatment with pan HDAC inhibitor abexinostat (n=1 experiment). Graph depicts mean Lysotracker fluorescence normalized to DMSO treated cells (y-axis) versus abexinostat concentration (x-axis). Curves were generated via non-linear curve fitting (variable slope) using GraphPad Prism version 5.0. Statistical analyses were performed on non-normalized data using paired two-tailed t-test (***p < 0.001; **0.001 ≤p <0.01; *0.01 ≤ p < 0.05). Error bars represent standard error of the mean (SEM).*

1.4.4 Both vesicular and nuclear levels of doxorubicin are increased after HDAC10 inhibition in BE(2)-C cells

Lysosomes can trap weakly basic chemotherapeutics such as doxorubicin and thereby reduce their efficacy (Zhitomirsky and Assaraf 2015; Zhitomirsky and Assaraf 2017). The data described in section ***E1.2.1*** show that HDAC10 inhibition increased lysosomal numbers in a set of neuroblastoma cells, which was accompanied by increased levels of intracellular doxorubicin. Therefore, HDAC10 inhibition might promote doxorubicin resistance by promoting its sequestration in lysosomes, which would stand in marked contrast to our previous study that demonstrated sensitization of

neuroblastoma cell lines to chemotherapy by HDAC10 inhibition (Oehme et al. 2013a). Subcellular doxorubicin localization in BE(2)-C cells was thus analyzed via confocal microscopy in presence or absence of tubastatin A. In cells treated with doxorubicin and solvent only, doxorubicin was mainly localized in the nucleus and, to a lesser extent, in perinuclear vesicles, which were presumably lysosomes (***Figure 24a***). Co-treatment with doxorubicin and HDAC6/10 inhibitor tubastatin A increased localization of doxorubicin in vesicles, and, as seen with lysosomal vesicles in section ***E1.2.1***, doxorubicin positive vesicles were not restricted to perinuclear areas. The acquisition of z-stack images, showed that cells co-treated with doxorubicin and tubastatin A also displayed a high number of strongly condensed and highly doxorubicin positive nuclei in a higher z-stage, likely representing nuclei of cells that are on the brink of cell death (***Figure 24b***). These highly doxorubicin positive nuclei were only rarely observed in case of treatment with doxorubicin and solvent only (***Figure 24c***). This suggested that HDAC10 inhibition blocked doxorubicin secretion rather than promoting its lysosomal sequestration, in turn increasing doxorubicin levels both in lysosomal vesicles and nuclei. Moreover, the data indicate that doxorubicin was leaking from lysosomes either by lysosomal permeabilization or passively by diffusion over time. Finally, the increased amounts of highly condensed nuclei after combination treatment reflected the onset of cell death, thereby confirming previously published data that combination of doxorubicin with HDAC6/10 inhibitors sensitizes neuroblastoma cells to doxorubicin treatment (also see section E***1.9***).

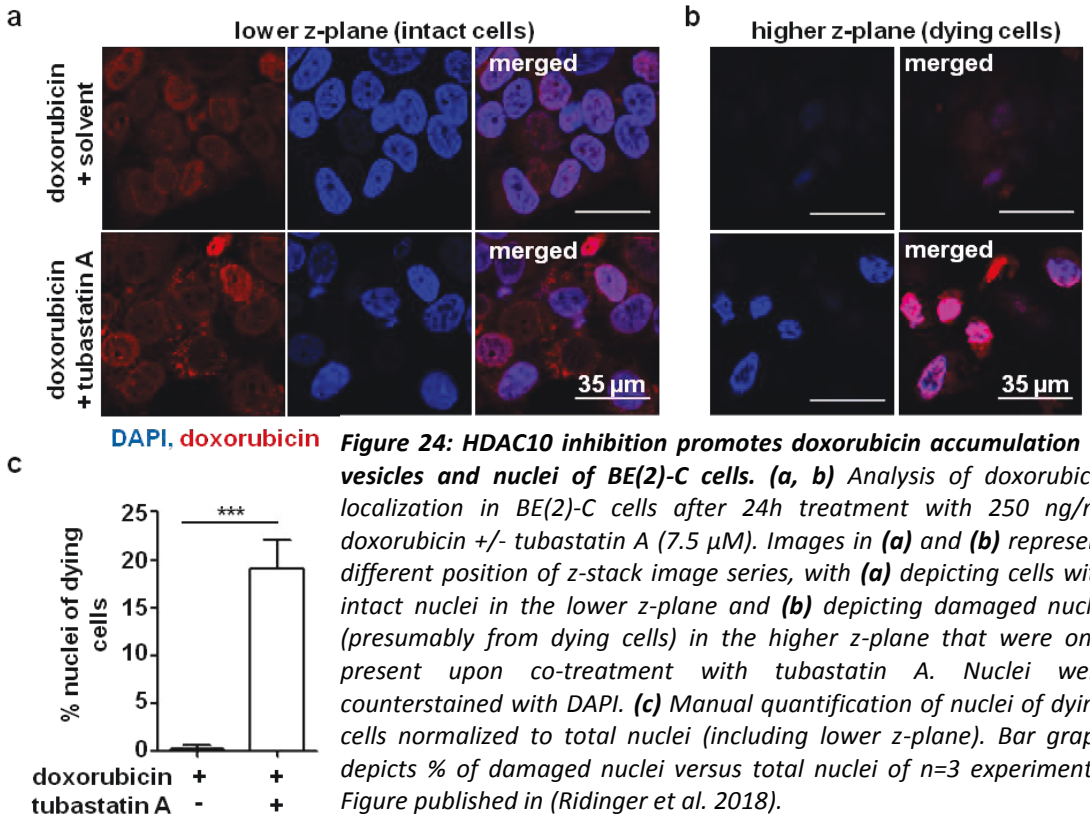

Figure 24: HDAC10 inhibition promotes doxorubicin accumulation in vesicles and nuclei of BE(2)-C cells. (a, b) *Analysis of doxorubicin localization in BE(2)-C cells after 24h treatment with 250 ng/ml doxorubicin +/- tubastatin A (7.5 µM). Images in* ***(a)*** *and* ***(b)*** *represent different position of z-stack image series, with* ***(a)*** *depicting cells with intact nuclei in the lower z-plane and* ***(b)*** *depicting damaged nuclei (presumably from dying cells) in the higher z-plane that were only present upon co-treatment with tubastatin A. Nuclei were counterstained with DAPI.* ***(c)*** *Manual quantification of nuclei of dying cells normalized to total nuclei (including lower z-plane). Bar graph depicts % of damaged nuclei versus total nuclei of n=3 experiments. Figure published in (Ridinger et al. 2018).*

1.4.5 HDAC10 inhibition does not promote lysosomal membrane permeabilization (LMP)

The finding that HDAC10 inhibition not only increased lysosomal but also nuclear doxorubicin levels (section ***E1.4.4***) raised the question whether HDAC10 inhibition caused the permeabilization of lysosomes, leading to the release of doxorubicin into the cytosol. To address this point, BE(2)-C cells were treated for 24h with HDAC6/10 inhibitors tubastatin A and bufexamac and release of cathepsin proteases from lysosomes into the cytosol was quantified in a cathepsin release assay. Here, the plasma membrane was permeabilized with low doses of digitonin (15 µg/ml), a concentration at which cytosolic extraction is achieved without permeabilization of lysosomes (Appelqvist et al. 2012); Koeneke unpublished). High doses of digitonin inducing permeabilization of both plasma- and lysosomal membranes (200 µg/ml) served as positive control. Cathepsin activity was then quantified by the turnover of a cathepsin substrate, which upon cleavage releases fluorescent AFC (amino-4-trifluoromethyl coumarin). HDAC6/10 inhibition occasionally caused cathepsin release into the cytosol in some but not all experiments. Thus, the increase of cathepsin release was not statistically significant (***Figure 25***). Although these results demonstrate that HDAC10 inhibition was unlikely to induce massive LMP, it cannot be excluded that incomplete LMP occurred (discussed in section ***F1.2***). In this context, recent studies show that, depending on the extent of LMP, cathepsins are not necessarily released from lysosomes, whereas other molecules, such as reactive oxygen species or smaller proteins, are (Ellegaard et al. 2015; Repnik et al. 2017). Further, a partial permeabilization of a small subset of lysosomes cannot be ruled out.

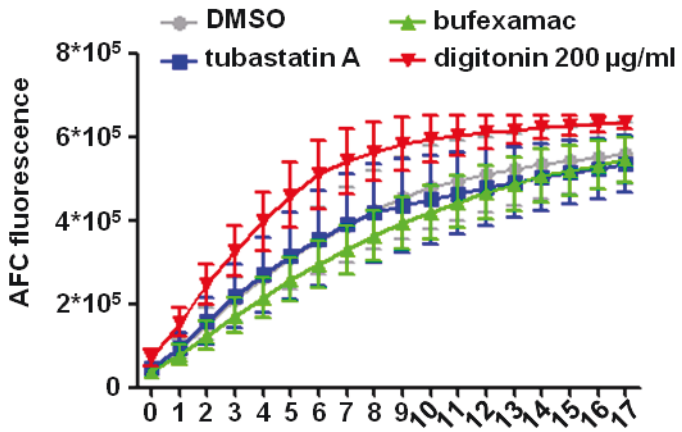

Figure 25: Inhibition of HDAC10 does not reproducibly induce cathepsin release from lysosomes. *Quantification of cathepsin substrate turnover (AFC release) over 17 kinetic cycles after 24h treatment of BE(2)-C cells with HDAC6/10 inhibitors tubastatin A (7.5 µM) and bufexamac (30 µM). Cathepsin release was quantified after addition of 15 µg/ml digitonin in order to selectively permeabilize the plasma membrane. Addition of 200 µg/ml digitonin was used as a positive control.*

1.5 HDAC10 inhibition does not promote cellular doxorubicin accumulation via P-glycoprotein inhibition

Cancer cells can acquire chemoresistance through the upregulation of various drug efflux pumps that are members of the ATP-binding cassette (ABC) transporter family (Gottesman et al. 2002). These ATP-driven pumps recognize and drive efflux of a broad and partly overlapping set of substrates that include many first line cancer therapeutics including vinca alkaloids, anthracyclines and taxanes, a phenomenon often referred to as multidrug resistance (MDR). Not surprisingly, high expression of either of these transporters has been repeatedly linked to poor prognosis in various cancer entities including neuroblastoma (Michaelis et al. 2009).

1.5.1 P-glycoprotein is expressed on the surface of neuroblastoma cells and promotes the secretion of doxorubicin

The finding that HDAC10 inhibition caused intracellular accumulation of doxorubicin in neuroblastoma cells raised the question whether HDAC6/10 inhibitors interfered with P-glycoprotein function/expression. BE(2)-C cells showed substantial expression of P-glycoprotein on their cell surface in flow cytometric measurements. (***Figure 26a***). In order to test if P-glycoprotein was involved in doxorubicin efflux from BE(2)-C cells, cells were transfected with pool of siRNAs against P-glycoprotein four days before addition of doxorubicin for the last 24h. P-glycoprotein knockdown efficiently reduced cell surface P-glycoprotein protein levels (***Figure 26b***), as well as total protein (***Figure 26c***) and transcript levels (***Figure 26d***) compared to cells transfected with control siRNAs. Flow cytometric quantification of cellular doxorubicin showed that BE(2)-C cells with P-glycoprotein knockdown accumulated roughly 1.3-fold higher levels of doxorubicin (***Figure 26e***). The effect of P-glycoprotein knockdown was confirmed by the P-glycoprotein inhibitor verapamil. Here, verapamil treated BE(2)-C cells displayed roughly 2.5-fold higher levels of doxorubicin when compared to DMSO treated cells (***Figure 26f***). These data indicate that P-glycoprotein participates in the disposal of doxorubicin from BE(2)-C cells.

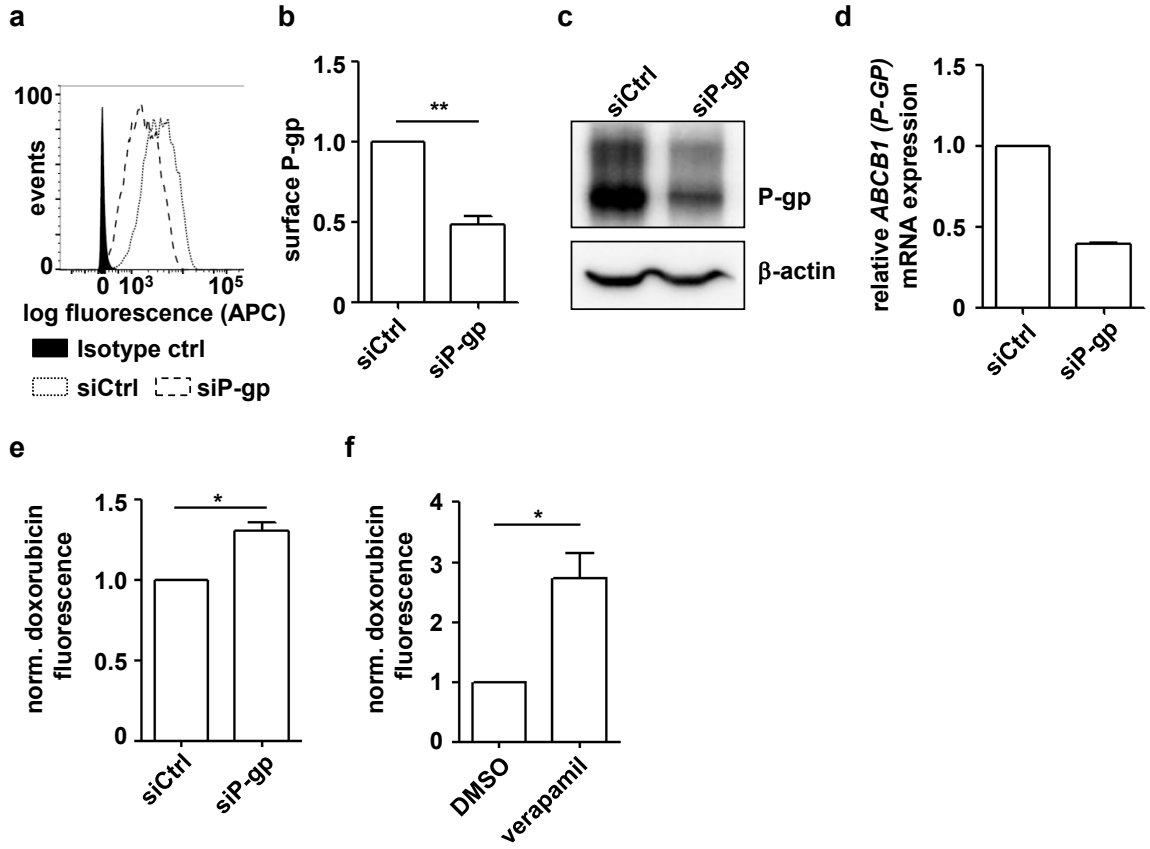

Figure 26: The ABC transporter P-glycoprotein promotes doxorubicin secretion from BE(2)-C neuroblastoma cells. ***(a, b)*** *Flow cytometric analysis of surface P-glycoprotein expression on BE(2)-cells 5d after siRNA transfection. Representative histogram depicting percentage of cells (y-axis) versus logarithmic antibody fluorescence (x-axis)* ***(a)*** *and surface P-glycoprotein expression normalized to siCtrl transfected cells of n=5 experiments* ***(b)*** *are shown.* ***(c)*** *Western blot analysis of total P-glycoprotein expression in BE(2)-C cells 5d after siRNA transfection.* ***(d)*** *Real-time RT-PCR analysis of P-glycoprotein transcript (ABCB1/P-GP) expression in BE(2)-C cells 5d after transfection of siRNA normalized to cells transfected with control siRNAs (n=1 experiment).* ***(e)*** *Flow cytometric analysis of intracellular doxorubicin in BE(2)-C cells transfected with P-glycoprotein and control siRNAs. Data were normalized to doxorubicin fluorescence in siCtrl cells.* ***(f)*** *Flow cytometric analysis of doxorubicin fluorescence in BE(2)-C cells after 24h treatment with 100 ng/ml doxorubicin +/- P-glycoprotein inhibitor (10 µM verapamil) normalized to cells treated with doxorubicin and solvent only. Statistical analysis was performed on non-normalized data using paired two-tailed t-test (***p < 0.001; **0.001 ≤p <0.01; *0.01 ≤ p < 0.05). Error bars represent standard error of the mean (SEM). Parts of figure published in (Ridinger et al. 2018).*

1.5.2 Increased doxorubicin accumulation in BE(2)-C cells after HDAC10 inhibition is not caused by interference with P-glycoprotein transport or function

To test whether HDAC10 inhibition interfered with P-glycoprotein transport to the plasma membrane, the effect of HDAC6/10 inhibitors tubastatin A and bufexamac on cell surface P-glycoprotein levels was analyzed via flow cytometry in BE(2)-C cells. Treatment of BE(2)-C cells with tubastatin A did not decrease surface levels of P-glycoprotein, nor did treatment with bufexamac (***Figure 27a***). Rather, a significant increase of surface P-glycoprotein levels was detected in case of treatment with tubastatin A, P-glycoprotein inhibitor verapamil or lysosomal exocytosis inhibitor

vacuolin-1, although the increase in surface expression was small and thus likely not substantial (***Figure 27a***). Thus, increased doxorubicin accumulation was not caused by impaired transport of P-glycoprotein to the plasma membrane.

Flow cytometric quantification of cellular doxorubicin levels in BE(2)-C cells transfected with P-glycoprotein and control siRNAs, respectively, showed that tubastatin A increased doxorubicin levels in both P-glycoprotein knockdown and control cells relative to treatment with doxorubicin and solvent only (***Figure 27b***). Notably, P-glycoprotein knockdown cells accumulated significantly higher levels of doxorubicin after HDAC10 inhibition than cells transfected with control siRNAs (***Figure 27b***). However, as shown in section ***E1.5.1***, P-glycoprotein knockdown cells accumulated higher doxorubicin levels already in their basal state. Thus, doxorubicin levels after HDAC10 inhibition were normalized to the respective basal doxorubicin levels of P-glycoprotein knockdown and control cells. Normalization revealed that tubastatin A equally promoted doxorubicin accumulation in P-glycoprotein knockdown and control cells (***Figure 27c***). In contrast, P-glycoprotein inhibitor verapamil displayed reduced efficacy on doxorubicin accumulation in cells with reduced levels of its substrate P-glycoprotein (***Figure 27a***). Taken together, these data indicate that intracellular doxorubicin accumulation after HDAC10 inhibition was not caused by interference with P-glycoprotein function.

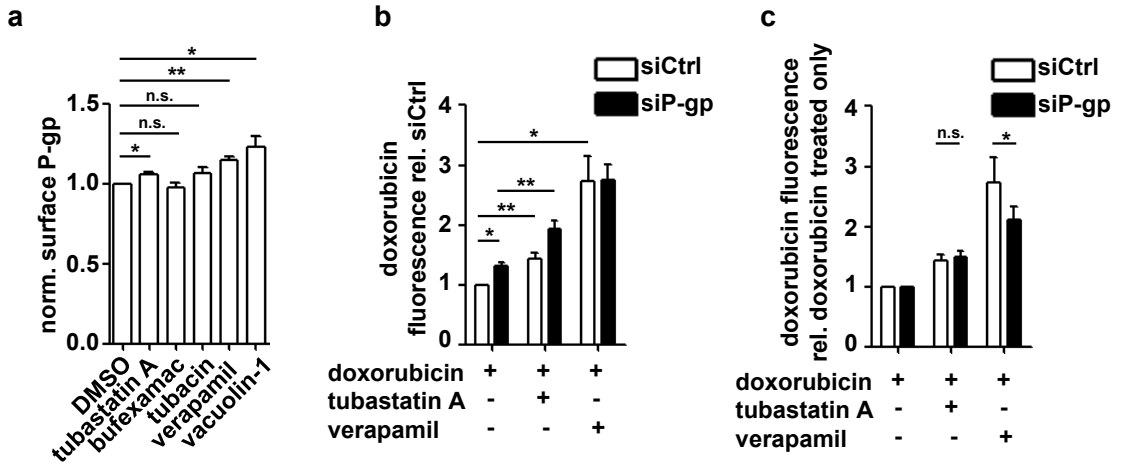

Figure 27: HDAC10 inhibition promotes doxorubicin accumulation in BE(2)-C cells independent of P-glycoprotein (P-gp). *Cell surface P-glycoprotein levels in BE(2)-C cells were analyzed via flow cytometry 24h after treatment with HDAC6/10 inhibitors tubastatin A (7.5 µM), bufexamac (30 µM), HDAC6 inhibitor tubacin (7.5 µM), P-glycoprotein inhibitor verapamil (10 µM) and lysosomal exocytosis inhibitor vacuolin-1 (10 µM). Mean fluorescence was normalized to cells treated with DMSO.* ***(b)*** *Flow cytometric analysis of intracellular doxorubicin accumulation 5d after siRNA transfection. Cells were treated for the last 24h with doxorubicin (100 ng/ml) +/- tubastatin A (7.5 µM) or verapamil (10 µM). Mean fluorescence normalized to doxorubicin fluorescence in DMSO treated siCtrl transfected cells is depicted (n=5 experiments).* ***(c)*** *Graph depicts data from graph* ***(b)*** *normalized to siCtrl transfected and siP-gp transfected cells, respectively. Statistical analysis was performed on non-normalized data using paired two-tailed t-test (***p < 0.001; **0.001 ≤p <0.01; *0.01 ≤ p < 0.05). Error bars represent standard error of the mean (SEM). Figure published in (Ridinger et al. 2018).*

1.6 HDAC10 promotes lysosomal exocytosis

1.6.1 Lysosomal exocytosis inhibition increases doxorubicin accumulation in neuroblastoma cells but not in fibroblasts

The results described in the previous section show that doxorubicin accumulation after HDAC10 inhibition is likely independent of P-glycoprotein function. Given the observation that interference with HDAC10 function leads to an expansion of the lysosomal compartment (section ***E1***) and in light of the fact that recent publications suggest lysosomal exocytosis as a mechanism of lysosome-mediated drug resistance, it was hypothesized that HDAC10 promoted doxorubicin secretion via this mechanism. Cells that undergo lysosomal exocytosis characteristically have high levels of the lysosomal marker LAMP-1 at their plasma membrane (Rodriguez et al. 1997), and flow cytometric quantification of plasma membrane LAMP-1 levels allows for the quantification of lysosomal exocytosis rates (Chakrabarti et al. 2003).

BE(2)-C cells had substantial amounts of LAMP-1 at their cell surface, suggesting that lysosomal exocytosis was occurring in this cell line (***Figure 28a***). Moreover, treatment of BE(2)-C cells with the lysosomal exocytosis inhibitor vacuolin-1 for 1h significantly reduced cell surface LAMP-1 levels, while total cellular LAMP-1 levels remained unchanged (***Figure 28a, b***). The specificity of the FACS staining for LAMP-1 was verified using siRNAs directed against LAMP-1, which was expectedly followed by a drop of plasma membrane and total LAMP-1 levels (***Figure 28c***, also see ***Figure 29b***). Addition of vacuolin-1 to doxorubicin treated cells for 1h or 24h caused a significant increase in cellular doxorubicin levels, indicating that BE(2)-C cells very likely used lysosomal exocytosis as a mechanism to dispose of doxorubicin (***Figure 28d***). In contrast, addition of vacuolin-1 did not raise intracellular doxorubicin levels in proliferating human fibroblasts from juvenile donors (***Figure 28e***), even though literature data show that lysosomal exocytosis occurs in fibroblasts (Rodriguez et al. 1997). Preliminary data from two experiments confirmed that the fibroblasts used in this study also exhibited basal levels of lysosomal exocytosis, as substantial cell surface LAMP-1 levels were detected and surface LAMP-1 levels were reduced by addition of vacuolin-1 for 1h (***Figure 28f***). However, the effect was smaller than in BE(2)-C cells (***Figure 28f***). Therefore, lacking doxorubicin accumulation in fibroblasts was not due to the absence of lysosomal exocytosis in these cells and the cause for this behavioral difference remained unknown (discussed in section ***F1.3***). Regardless, the differential behavior of fibroblasts and neuroblastoma cells with respect to doxorubicin accumulation after lysosomal exocytosis inhibition indicates that highly chemoresistant tumor cells might preferentially use and depend on lysosomal exocytosis as a way to dispose of chemotherapeutic drugs, allowing for a certain degree of tumor specificity when targeting this process.

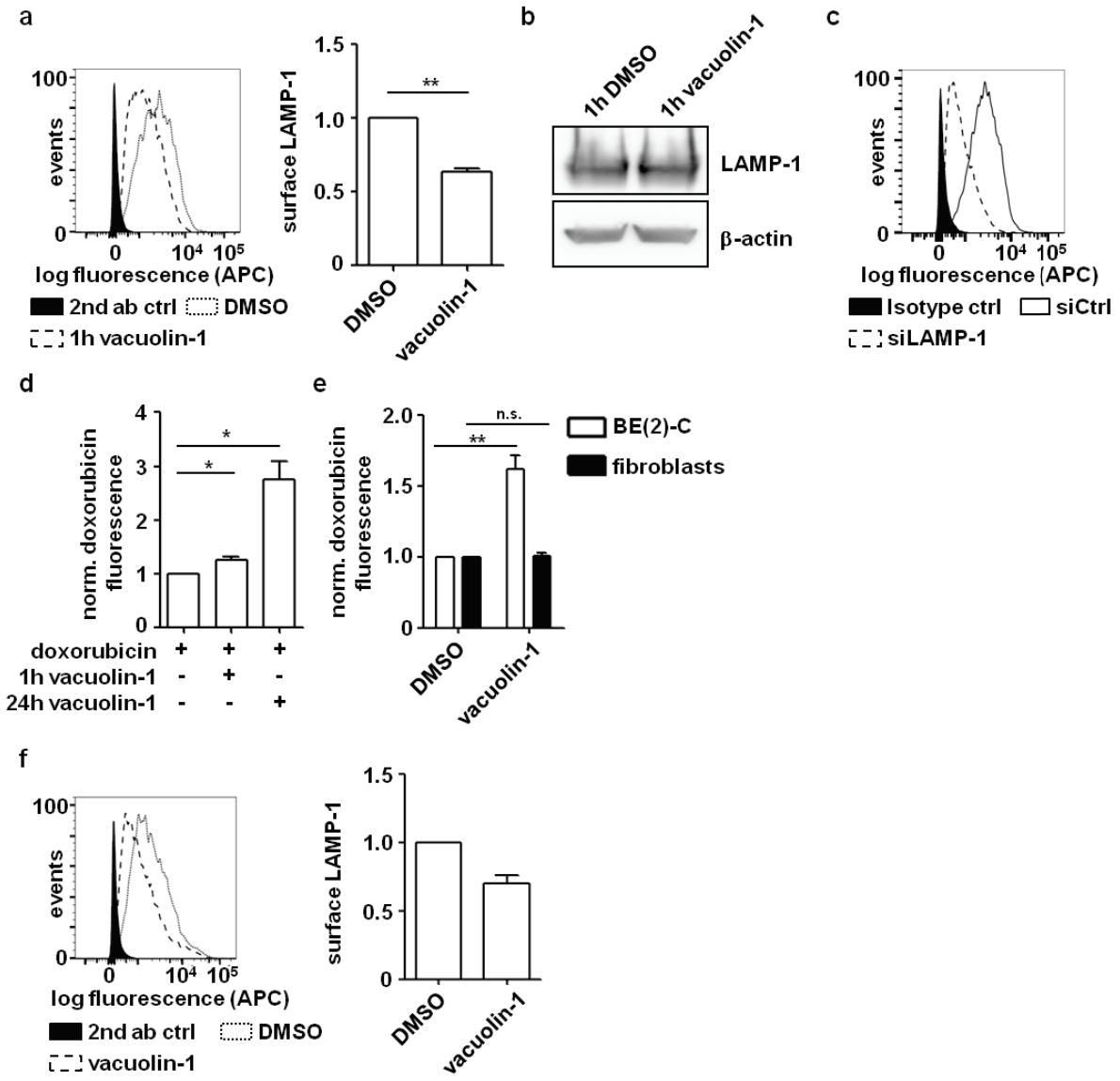

Figure 28: Inhibition of lysosomal exocytosis promotes doxorubicin accumulation in BE(2)-C neuroblastoma cells. ***(a)*** *Analysis of surface LAMP-1 staining in BE(2)-C cells via flow cytometry after 1h treatment with lysosomal exocytosis inhibitor vacuolin-1 (10 µM). Representative fluorescence histogram depicting percentage of cells (y-axis) versus fluorescence (x-axis) (left panel) and surface LAMP-1 levels normalized to DMSO treated cells of n=3 experiments (right panel).* ***(b)*** *Western blot analysis of total LAMP-1 expression in BE(2)-C cells after vacuolin-1 treatment.* ***(c)*** *LAMP-1 antibody specificity was tested on BE(2)-C cells transfected with LAMP-1 siRNAs six days after transfection. Histogram depicts percentage of cells (y-axis) versus logarithmic fluorescence (x-axis).* ***(d)*** *Flow cytometric analysis of doxorubicin fluorescence in BE(2)-C cells. Cells were treated with 100 ng/ml doxorubicin for 24h +/- 10 µM vacuolin-1 for 1h and 24h, respectively. Graph depicts doxorubicin fluorescence normalized to cells treated with doxorubicin and solvent only.* ***(e)*** *Cellular doxorubicin fluorescence in BE(2)-C cells versus fibroblasts was quantified via flow cytometry. Both cell types were treated for 24h with 100 ng/ml doxorubicin +/- 10 µM vacuolin-1. Fluorescence was normalized to the respective treatment condition with doxorubicin and solvent only.* ***(f)*** *Analysis of cell surface LAMP-1 expression in fibroblasts via flow cytometry after 1h treatment with 10 µM vacuolin-1. Representative fluorescence histogram depicting percentage of cells (y-axis) versus fluorescence (x-axis) (left panel) and surface LAMP-1 levels normalized to DMSO treated cells of n=2 experiments (right panel). Statistical analysis was performed on non-normalized data using paired two-tailed t-test (***p < 0.001; **0.001 ≤p <0.01; *0.01 ≤ p < 0.05). Error bars represent standard error of the mean (SEM). Parts of figure published in (Ridinger et al. 2018).*

1.6.2 Interference with HDAC10 function reduces lysosomal exocytosis rates

The data provided in the previous section show that interference with lysosomal exocytosis in BE(2)-C neuroblastoma cells promotes cellular doxorubicin accumulation similar to HDAC10 depletion or inhibition, prompting the idea that HDAC10 was involved in lysosomal exocytosis. In order to test this hypothesis, BE(2)-C cells were transfected with siRNAs against HDAC10 and HDAC6, respectively, as well as with control siRNAs. Six days after transfection, cells were analyzed for presence of LAMP-1 at the plasma membrane via flow cytometry. Here, cells with HDAC10 knockdown showed substantially decreased surface LAMP-1 levels, while the amount of surface LAMP-1 was slightly but not significantly increased upon HDAC6 knockdown (***Figure 29a***). This correlated with the finding that siRNA-mediated depletion of HDAC10 but not HDAC6 promoted doxorubicin accumulation in BE(2)-C cells (section ***E1.4.1***), suggesting a link between doxorubicin accumulation and reduced lysosomal exocytosis rates. Analysis of total LAMP-1 protein levels via western blot showed that knockdown of HDAC10 did not reduce, but rather slightly increased total cellular LAMP-1 levels (***Figure 29b***). This demonstrated that trafficking of LAMP-1 to the cell surface, and thus likely lysosomal exocytosis rates rather than LAMP-1 expression, was reduced upon depletion of HDAC10.

A similar phenotype was observed when HDAC10 enzymatic function was inhibited. Here, 6h treatment of BE(2)-C cells with HDAC6/10 inhibitors tubastatin A and bufexamac slightly but significantly reduced cell surface LAMP-1 levels, while treatment with HDAC6 specific inhibitor tubacin had no significant effect (***Figure 29c***). This indicated that HDAC10 but not HDAC6 enzymatic function promoted lysosomal exocytosis in BE(2)-C cells.

The data described in section ***E1.6.1*** show that lysosomal exocytosis inhibition did not promote doxorubicin accumulation in human fibroblasts. In line with this, fibroblasts did not display increased doxorubicin levels upon co-treatment with doxorubicin and HDAC6/10 inhibitors tubastatin A or bufexamac (***Figure 29d***). This, however, could not be attributed to failure of HDAC6/10 inhibitors to reduce lysosomal exocytosis in fibroblasts. Preliminary data of LAMP-1 surface staining in fibroblasts showed that HDAC6/10 inhibitors tubastatin A and bufexamac were capable of reducing LAMP-1 surface level and thus of inhibiting lysosomal exocytosis (***Figure 29e***), even though this effect was smaller than in BE(2)-C cells (***Figure 29e***). Therefore, the mechanistic reason for the discrepancy in doxorubicin accumulation between fibroblasts and BE(2)-C neuroblastoma cells after lysosomal exocytosis inhibition remained elusive (discussed in section ***F1.3***)

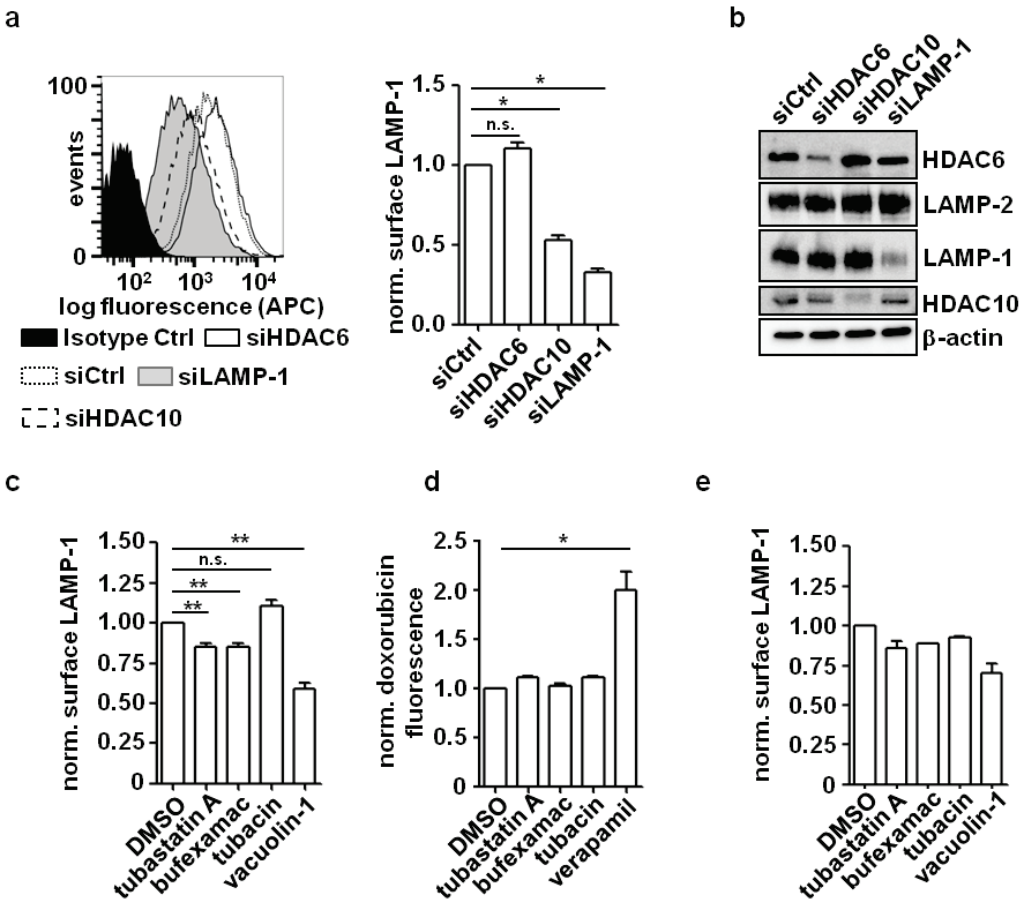

Figure 29: Interference with HDAC10 function inhibits lysosomal exocytosis. (a) *Quantification of surface LAMP-1 levels in BE(2)-C neuroblastoma cells via flow cytometry 6d after transfection with siRNAs. Histogram depicts percentage of cells (y-axis) versus logarithmic fluorescence (x-axis) of one representative experiment. Bar graph depicts mean surface LAMP-1 expression normalized to siCtrl transfected cells of n=3 experiments.* ***(b)*** *Western blot analysis of total LAMP-1 levels in BE(2)-C cells 6d after transfection with respective siRNAs.* ***(c)*** *Flow cytometric analysis of surface LAMP-1 levels after 6h treatment of BE(2)-C cells with HDAC6/10 inhibitors tubastatin A (7.5 µM), bufexamac (30 µM), HDAC6 inhibitor tubacin (7.5 µM). Lysosomal exocytosis inhibitor vacuolin-1 (10 µM) was added for 1h where indicated. Data of n=4 experiments are shown.* ***(d)*** *Flow cytometric analysis of doxorubicin accumulation in fibroblasts after 48h treatment with 100 ng/ml doxorubicin +/- HDAC6/10 inhibitors tubastatin A (7.5 µM), bufexamac (30 µM), tubacin (7.5 µM) or P-glycoprotein inhibitor verapamil (10 µM). Data of n=3 experiments were normalized to cells treated with doxorubicin and DMSO.* ***(e)*** *Flow cytometric analysis of surface LAMP-1 expression in fibroblasts treated for 6h with tubastatin A (7.5 µM), bufexamac (30 µM), tubacin (7.5 µM) and lysosomal exocytosis inhibitor vacuolin-1 (10 µM). Bar graph depicts mean fluorescence of n=2 experiments normalized to DMSO treated cells. Statistical analysis was performed on non-normalized data using paired two-tailed t-test (***p < 0.001; **0.001 ≤p <0.01; *0.01 ≤ p < 0.05). Error bars represent standard error of the mean (SEM). Parts of figure published in (Ridinger et al. 2018).*

1.6.3 Kinetic experiments show that HDAC10 inhibition decreases rates of doxorubicin secretion

Given that HDAC10 inhibition reduced lysosomal exocytosis rates in BE(2)-C cells, it was hypothesized that HDAC10 inhibition causes a delay in doxorubicin secretion and thus entails a longer retention of doxorubicin within cells. To test this hypothesis, a washout approach was performed, where BE(2)-C cells were pre-incubated for 12h with HDAC6/10 inhibitors and subsequently stained with high doxorubicin concentrations (1 µg/ml) for 3h. Doxorubicin was removed after 3h, cells were washed in

medium and HDAC6/10 inhibitors were re-added. Cellular doxorubicin levels were quantified via flow cytometry at the time of doxorubicin removal (t_0), as well as 3h (t_{3h}) and 6h (t_{6h}) after doxorubicin removal (***Figure 30a***). In case of HDAC10 inhibition with bufexamac or tubastatin A, cellular doxorubicin levels were already increased at t_0, which was not the case when HDAC6 was inhibited with tubacin (***Figure 30b***). These findings are in line with the observations described in section ***E1.4.2*** where doxorubicin accumulation after HDAC10 inhibition was observed at later timepoints.

Cells that had undergone pre-incubation with HDAC6/10 inhibitors tubastatin A and bufexamac indeed showed higher levels of cellular doxorubicin at t_{3h} and t_{6h}, and this was also observed when lysosomal exocytosis inhibitor vacuolin-1 was added after doxorubicin removal (***Figure 30c, d***). However, since doxorubicin levels were already considerably increased at t_0 in case of treatment with tubastatin A and bufexamac, data were normalized to the cellular doxorubicin fluorescence at t_0 of the given treatment condition. Thus ***Figure 30e, f*** shows the remaining doxorubicin fluorescence as a percentage of the fluorescence at t_0. Normalization clearly showed that treatment with HDAC6/10 inhibitors bufexamac and tubastatin A caused a significantly higher retention of doxorubicin at t_{3h} and t_{6h}, respectively. In marked contrast, HDAC6 specific inhibitor tubacin had no effect on doxorubicin retention.

Taken together, these data show that inhibition of HDAC10 but not HDAC6 slows down secretion of doxorubicin in BE(2)-C cells, most likely by reducing lysosomal exocytosis rates.

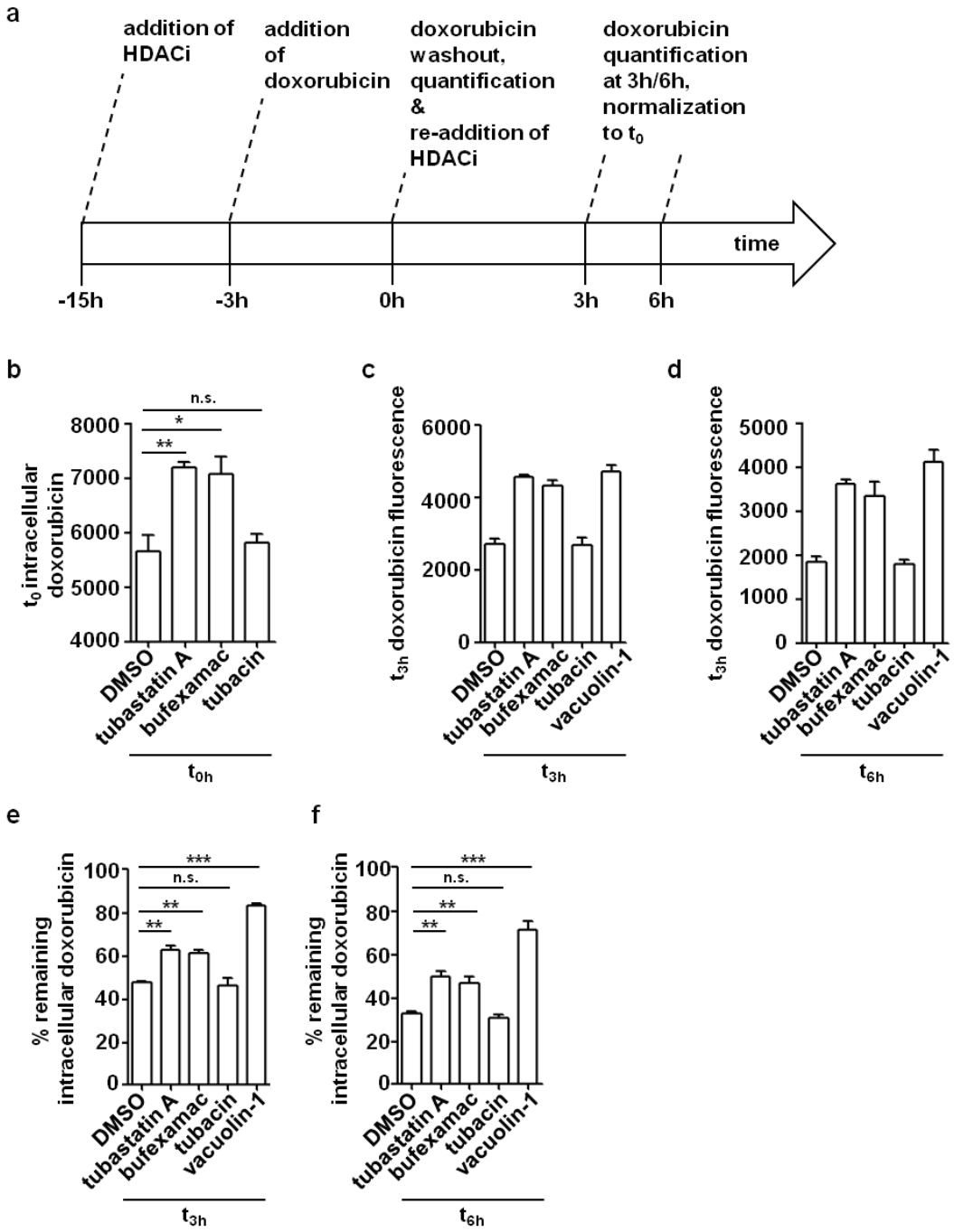

Figure 30: Doxorubicin secretion is slowed down after inhibition of HDAC10 but not HDAC6. (a) *Timeline of the washout experiment. BE(2)-C neuroblastoma cells were pre-incubated for 12h with HDAC6/10 inhibitors tubastatin A (7.5 µM), bufexamac (30 µM) and HDAC6 inhibitor tubacin (7.5 µM) before addition of high dose doxorubicin (1 µg/ml) for 3h. After doxorubicin washout, cellular fluorescence was quantified via flow cytometry at 0h (t_{0h}), 3h (t_{3h}) and 6h (t_{6h}) after doxorubicin removal.* ***(b)*** *Doxorubicin fluorescence at t_{0h}. Unnormalized data of n=3 experiments are shown.* ***(c, d)*** *Doxorubicin fluorescence at t_{3h}* ***(c)*** *and t_{6h}* ***(d)*** *of n=3 experiments without normalization to fluorescence at t_{0h}.* ***(e, f)*** *Doxorubicin fluorescence at t_{3h}* ***(e)*** *and t_{6h}* ***(f)*** *after normalization to the respective fluorescence at t_{0h}. Statistical analysis was performed on non-normalized data using unpaired two-tailed t-test (***p < 0.001; **0.001 ≤p <0.01; *0.01 ≤ p < 0.05). Error bars represent standard error of the mean (SEM). Parts of figure published in (Ridinger et al. 2018).*

1.7 Lysosomal accumulation after HDAC10 inhibition is possibly linked to inhibition of lysosomal exocytosis

The finding that HDAC10 promotes lysosomal exocytosis, led to the hypothesis that the before observed accumulation of lysosomes after HDAC10 inhibition is a consequence of lysosomal exocytosis inhibition. To test, whether reduced rates of lysosomal exocytosis caused the accumulation of lysosomes, BE(2)-C cells were treated with lysosomal exocytosis inhibitor vacuolin-1 for 1h and 24h, respectively, and analyzed for lysosomal content via flow cytometric evaluation of LysoTracker staining. Either treatment period significantly increased LysoTracker staining compared to cells treated with DMSO, indicating that lysosomal exocytosis inhibition caused accumulation of lysosomes (***Figure 31a***). To test if lysosomal exocytosis inhibition was upstream of lysosomal accumulation, a flux experiment was performed, where lysosomal exocytosis was inhibited via treatment with vacuolin-1 and combined with tubastatin A (***Figure 31b***). Under the assumption that lysosomal exocytosis was fully inhibited under the given conditions (10 µM vacuolin-1 for 24h), an increase in lysosomes in case of combination treatment versus vacuolin-1 treatment alone would speak in favor of *de novo* biogenesis of lysosomes upon HDAC10 inhibition. Addition of tubastatin A to vacuolin-1 did not significantly increase LysoTracker staining when compared to vacuolin-1 treatment alone (***Figure 31b***). These results indicated that lysosomal exocytosis inhibition, and not *de novo* biogenesis of lysosomes, is the cause of lysosomal accumulation upon HDAC10 inhibition.

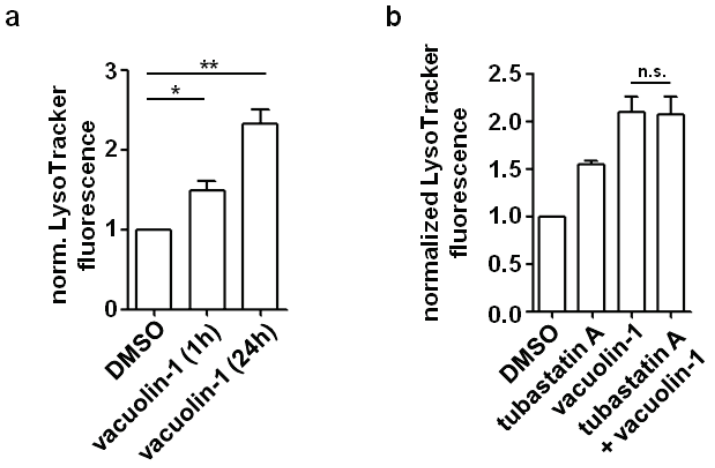

Figure 31: Lysosomal exocytosis inhibition causes the accumulation of lysosomes in BE(2)-C cells. (a) *Flow cytometric analysis of LysoTracker staining after 1h and 24h treatment with lysosomal exocytosis inhibitor vacuolin-1 (10 µM). Bar graph depicts normalized LysoTracker fluorescence normalized to DMSO treated cells.* ***(b)*** *Flow cytometric analysis of LysoTracker staining after 24h treatment with HDAC6/10 inhibitor tubastatin A (7.5 µM), vacuolin-1 (10 µM) and the respective combination. Statistical analysis was performed on non-normalized data using paired two-tailed t-test (***p < 0.001; **0.001 ≤p <0.01; *0.01 ≤ p < 0.05). Error bars represent standard error of the mean (SEM). Figure published in (Ridinger et al. 2018).*

1.8 Autophagy contributes to doxorubicin secretion in neuroblastoma, but only under three-dimensional culturing conditions

1.8.1 Autophagy does not contribute to doxorubicin secretion in 2D neuroblastoma monolayer cultures

Recent evidence suggests that lysosomal exocytosis is not a purely lysosomal event, but also includes other organelle or vesicle pools, such as autophagosomes and autophagolysosomes (Feeney et al. 2013). This raised the question whether autophagic vesicles contributed to the secretion of doxorubicin in neuroblastoma cells. Moreover, a study from our lab suggests a role for HDAC10 in late stage autophagic flux, where interference with HDAC10 function caused accumulation of autophagosomes (Oehme et al. 2013a). It was therefore conceivable that this pool of autophagosomes possibly contributed to doxorubicin secretion.

In order to test this hypothesis, BE(2)-C cells were transfected with siRNAs against ATG5, a key protein in autophagosome formation (see section ***A3.2.2***). Knockdown of ATG5 inhibits the autophagic pathway by interfering with autophagosome formation (Singh et al. 2009; Mizushima et al. 2010). In the case of autophagosomal contribution to doxorubicin secretion, cells should display increased doxorubicin levels in case of ATG5 depletion mediated autophagy disruption. Flow cytometric analysis of intracellular doxorubicin fluorescence showed that 2D grown BE(2)-C cells with ATG5 knockdown did not display increased doxorubicin levels when compared to cells transfected with control siRNAs (***Figure 32a, b***). Increased doxorubicin accumulation was also not observed in case of HDAC10 inhibition with tubastatin A (***Figure 32a***). Thus, autophagy or autophagosomes did not contribute to doxorubicin secretion in 2D cultured neuroblastoma cells, neither under basal nor under HDAC10-inhibited conditions.

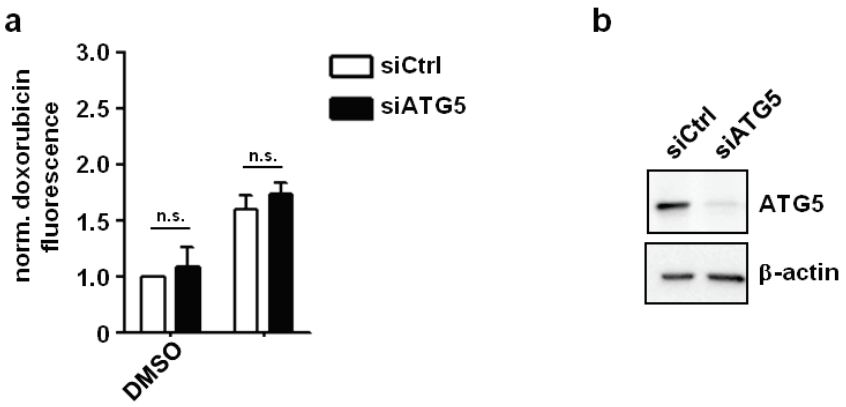

Figure 32: Knockdown of ATG5 does not cause doxorubicin accumulation in two-dimensionally cultured BE(2)-C cells. (a) *Flow cytometric analysis of cellular doxorubicin fluorescence 72h after transfection with siRNAs against ATG5 and control siRNAs, respectively. Cells were treated with doxorubicin (100 ng/ml) for the last 24h Bar graph shows mean doxorubicin fluorescence normalized to DMSO treated siCtrl transfected cells of n=3 experiments.* ***(b)*** *Western blot analysis of ATG5 knockdown. Statistical analysis was performed on non-normalized data using paired two-tailed t-test (***p < 0.001; **0.001 ≤p <0.01; *0.01 ≤ p < 0.05). Error bars represent standard error of the mean (SEM).*

1.8.2 Neuroblastoma cells grown in 3D show elevated levels of autophagy and partially depend on autophagy for the secretion of doxorubicin

Most cell culture tumor models are cultivated as flat 2D monolayers. These conditions are clearly different from the *in vivo* situation with regards to cell-cell contacts, cell signaling and cell morphology (Levinger et al. 2014). Moreover, blood, oxygen and nutrient supplies to certain tumor areas are restricted *in vivo* due to the three-dimensional growth of tumors. This, in turn, subjects a subset of bulk tumor cells to stress such as lack of oxygen or starvation. Activation of autophagy under stress conditions has been shown to protect tumor cells from cell death and promote tumor growth (Strohecker et al. 2013). In this context, a recent study from our group has demonstrated that neuroblastoma cells transcriptionally activate autophagy when grown in three-dimensional cultures and that autophagy protects neuroblastoma cells from chemotherapeutic treatment (Bingel et al. 2017). This raised the question whether autophagy could contribute to doxorubicin secretion under these, autophagy-activated, conditions. When cultivated under three-dimensional conditions in collagen type I coated ridged scaffolds (MatriGrid) (Weise et al. 2013), BE(2)-C cells form spheroid structures (see ***Figure 1b*** in Bingel et al., 2017). In the respective study, cells grown in 3D displayed slightly higher rates of conversion of the autophagosome marker LC3-I to the autophagosome-bound LC3-II under basal conditions, indicating that autophagy was increased under 3D conditions. LC3-II accumulation was strongly increased in 3D cells when the lysosomal V-ATPase inhibitor bafilomycin A1 was added, which blocks fusion of autophagosomes to lysosomes and stops turnover of autophagosomes. Stronger accumulation of autophagosomes in 3D versus 2D grown cells confirmed an increased basal autophagic flux in 3D grown BE(2)-C cells (see ***Figure 5h*** in Bingel et al., 2017).

To monitor autophagic flux in the spheroid itself, the green fluorescent cationic amphiphilic tracer (CAT) dye Cyto-ID was used, which, according to supplier information and literature data, stains autophagosomes while only negligibly staining lysosomes (Chan et al. 2012). To test if the Cyto-ID dye indeed stained autophagosomes rather than lysosomes, BE(2)-C cells were treated with low doses of lysosomal inhibitor chloroquine (CQ), a lysosomal inhibitor that interferes with the turnover of autophagic substrate in autolysosomes and at low concentrations leads to expansion of the lysosomal compartment, as well as with saturating concentrations of bafilomycin A1 which de-acidifies lysosomes (see section ***E1.1.2***). Under bafilomycin treated conditions, an autophagosome dye should display increased staining despite the disruption of lysosomal pH, as bafilomycin treatment causes the accumulation of autophagosomes, as shown by accumulation of the autophagosome marker LC-3II and the autophagosomal cargo receptor SQSTM1/p62 on western blot (***Figure 33a***). Flow cytometric and fluorescence microscopic analysis of Cyto-ID staining, however, revealed that, similar to LysoTracker staining described in section ***E1.1.2***, bafilomycin decreased Cyto-ID fluorescence, while low doses of CQ caused a fluorescence increase (***Figure 33b, c***). Thus, Cyto-ID was more likely an autophagolysosome or lysosome specific dye than a specific autophagosome dye.

Regardless, analysis of Cyto-ID staining via confocal immunofluorescence microscopy revealed that Cyto-ID positive cells were largely located in the inner zone of the tumor spheroid, suggesting that (autophago-)lysosomes and thus increased autophagic flux occurred in tumor cells within the spheroid (***Figure 33d***). This was even more apparent when CQ was added for the last 24h in order to block turnover of autophagolysosomes. Here, 3D grown BE(2)-C cells were highly positive for Cyto-ID in inner areas of the tumor spheroid. Taken together, these data show that BE(2)-C cells display elevated levels of autophagy when grown in 3D conditions.

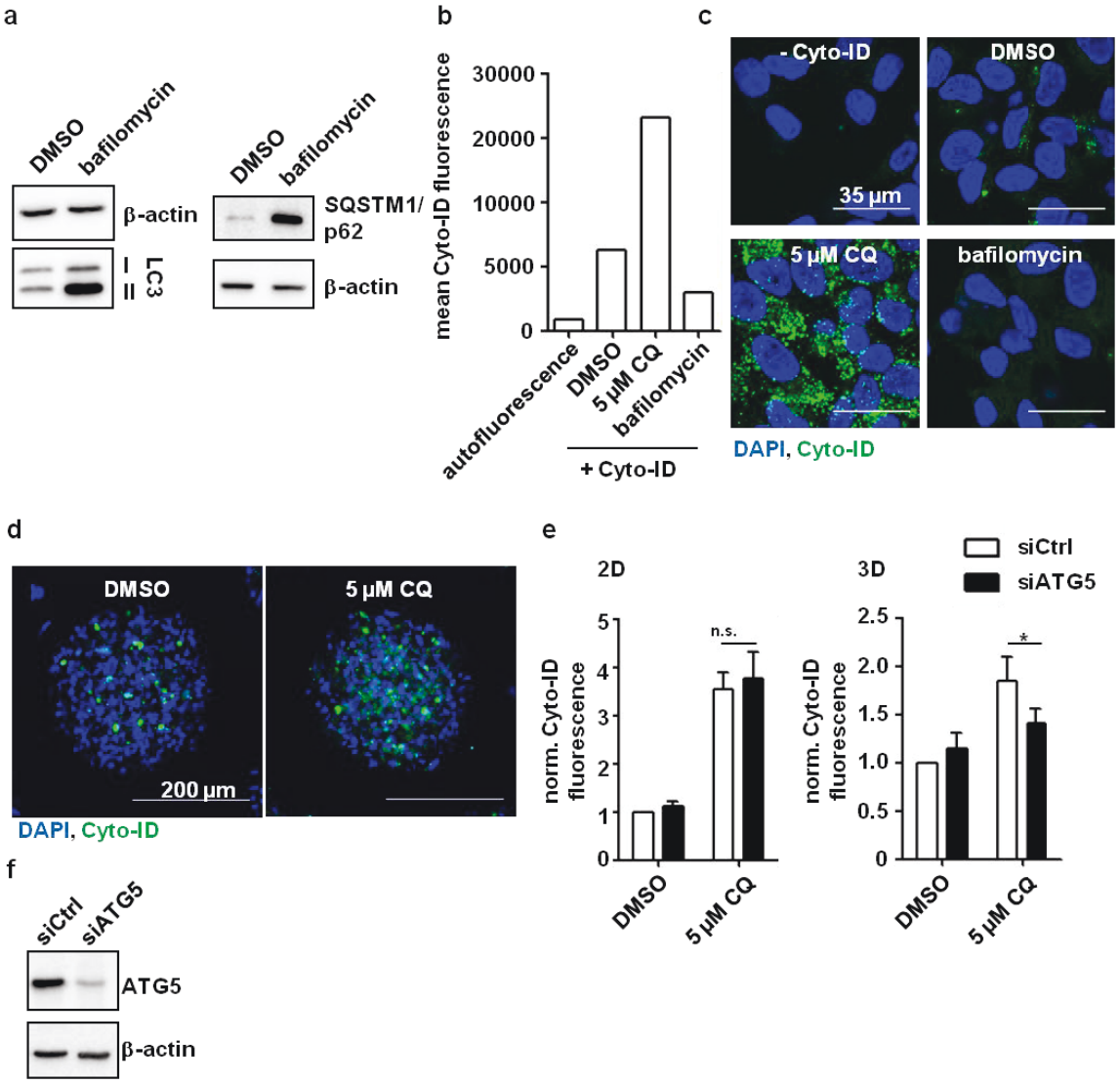

Figure 33: (Autophago-)lysosomal staining with the Cyto-ID dye shows that 3D-cultured BE(2)-C cells accumulate (autophago-)lysosomes in the inner section of the spheroid. ***(a)*** *Western blot analysis of LC3 conversion (left) and accumulation of the autophagosomal cargo receptor SQSTM1/p62 after 24h treatment with bafilomycin (100 nM).* ***(b, c)*** *Flow cytometric (n=1 experiment)* ***(b)*** *and immunofluorescence* ***(c)*** *analysis of Cyto-ID staining in BE(2)-C cells after 24h treatment with lysosomal inhibitor chloroquine and V-ATPase inhibitor bafilomycin (100 nM).* ***(d)*** *Confocal microscopy analysis of Cyto-ID staining in 3D-grown BE(2)-C cells. Images show maximum intensity projection of z-stack images covering the whole spheroid.* ***(e)*** *Flow cytometric analysis of Cyto-ID staining 72h after transfection with ATG5 and control siRNAs in two- and three-dimensionally cultured BE(2)-C cells. Where indicated, cells were treated with chloroquine for the last 24h. Bar graphs depict mean Cyto-ID fluorescence normalized to DMSO treated siCtrl cells of n=4 (2D) and n=5 experiments (3D).* ***(f)*** *Western blot analysis of ATG5 knockdown. Statistical analysis was performed on non-normalized data using paired two-tailed t-test (***p < 0.001; **0.001 ≤p <0.01; *0.01 ≤ p < 0.05). Error bars represent standard error of the mean (SEM).*

Two dimensional and 3D-grown BE(2)-C cells displayed a remarkable difference with regards to Cyto-ID staining under conditions where ATG5 was depleted and cells were additionally treated with CQ (***Figure 33e, f***). Under 2D conditions, cellular Cyto-ID fluorescence did not differ under CQ treatment between ATG5 knockdown and control cells, suggesting there was no difference in autophagolysosomal content. In contrast, siATG5 cells displayed lower Cyto-ID staining as control cells when they were grown under 3D conditions for the last 72h and CQ was added (***Figure 33e***). It is

conceivable that remaining levels of ATG5 after knockdown (***Figure 33f***) were sufficient to keep up basal autophagic flux required under 2D conditions, but insufficient under autophagy-dependent conditions in the 3D culture, leading to reduced lysosomal or autophagolysosomal content. This only became obvious under conditions where turnover of autophagosomes and autophagolysosomes was blocked (CQ treatment), suggesting a stronger contribution of the autophagic route to lysosomal and autophagolysosomal content under 3D conditions.

In contrast to 2D conditions (see section ***E1.8.1***), ATG5 knockdown under 3D conditions significantly increased doxorubicin accumulation in BE(2)-C cells compared to cells transfected with control siRNAs (***Figure 34a***). A similar increase in doxorubicin levels was observed when other important mediators of autophagy, such as Beclin-1 or the pro-autophagic transcription factor FoxO3a were depleted via RNAi (***Figure 34b***). It is thus conceivable that organelles from the autophagic route also contribute to lysosomal exocytosis under 3D conditions.

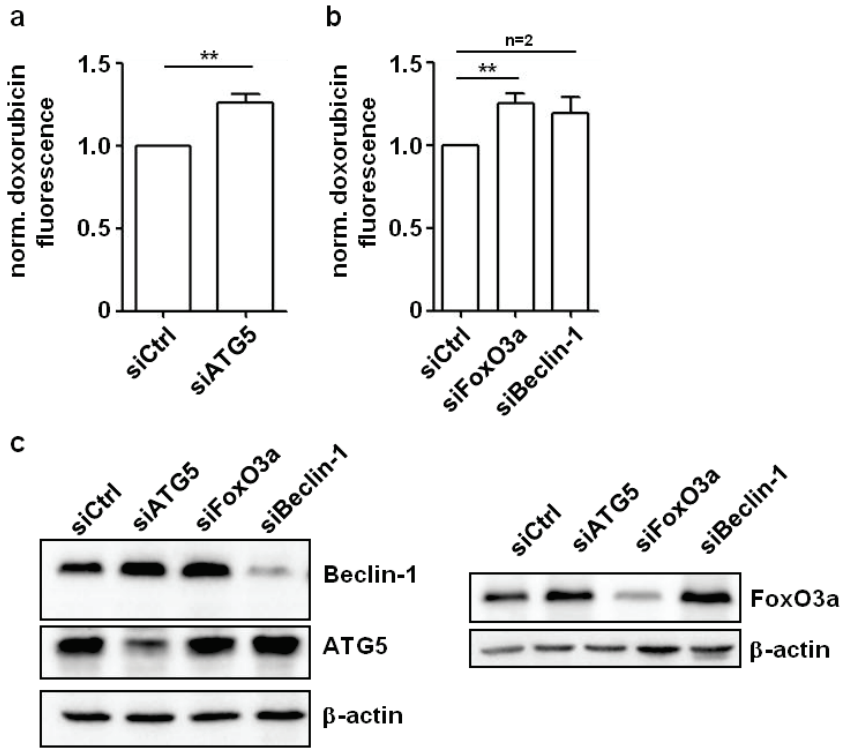

Figure 34: RNAi-mediated blocking of autophagy causes doxorubicin accumulation in three-dimensionally cultured BE(2)-C cells. (a, b) *Flow cytometric analysis of cellular doxorubicin fluorescence 5d after transfection with siRNAs against ATG5* ***(a)*** *FoxO3a and Beclin-1* ***(b)****. Cells were treated with doxorubicin (500 ng/ml) for the last 24h. Bar graphs show mean doxorubicin fluorescence normalized to siCtrl transfected cells of n=5 experiments (ATG5, FoxO3a) and n=2 experiments (Belcin-1), respectively.* ***(b)*** *Western blot analysis of ATG5, Beclin-1 and FoxO3a expression after knockdown. Statistical analysis was performed on non-normalized data using paired two-tailed t-test (***p < 0.001; **0.001 ≤p <0.01; *0.01 ≤ p < 0.05). Error bars represent standard error of the mean (SEM).*

1.8.3 HDAC10 is also involved in doxorubicin secretion in 3D cultured neuroblastoma cells

Recent data from our lab show that three-dimensionally cultured neuroblastoma cells are highly resistant to doxorubicin treatment and that resistance can be reverted by HDAC10 inhibition with bufexamac (Bingel et al. 2017). This raised the question whether HDAC10 also promoted doxorubicin secretion in 3D cultured neuroblastoma cells. To address this point, 3D grown BE(2)-C cells were treated with doxorubicin for 48h and co-treated with HDAC6/10 inhibitors tubastatin A and bufexamac, where indicated. Flow cytometric analysis of cellular doxorubicin fluorescence revealed that co-treatment with either HDAC6/10 inhibitor significantly increased doxorubicin accumulation in 3D grown BE(2)-C cells (***Figure 35a***). RNAi mediated knockdown of HDAC6 and HDAC10, respectively, revealed that HDAC10 but not HDAC6 depletion increased intracellular doxorubicin levels in 3D cultured cells (***Figure 35b, c***), analogous to the results obtained in 2D cultures (see section ***E1.4.1***). It is thus likely that HDAC6/10 inhibitors contribute to sensitization of 3D grown neuroblastoma cells to doxorubicin via inhibition of HDAC10-mediated lysosomal exocytosis.

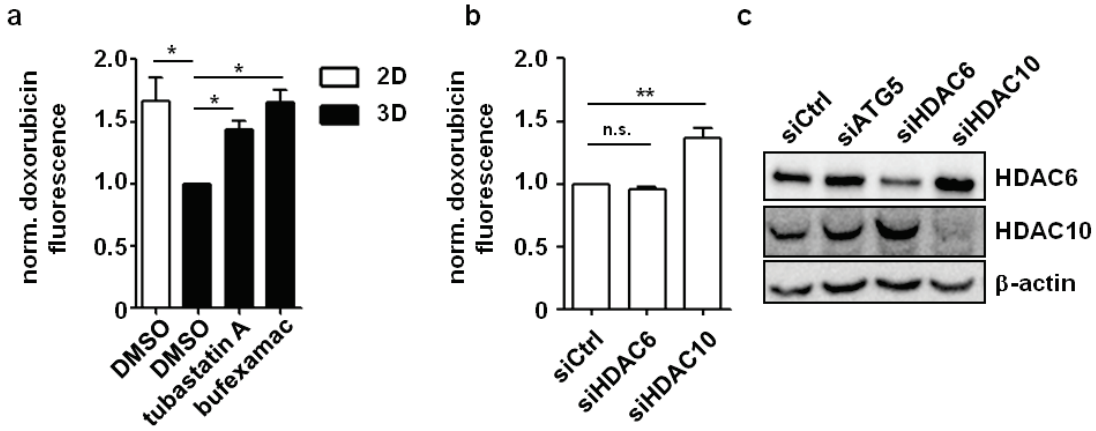

Figure 35: Inhibition and depletion of HDAC10 increase doxorubicin accumulation in three-dimensionally cultured BE(2)-C cells. (a) *Cellular doxorubicin fluorescence in 2D and 3D-cultured BE(2)-C cells was analyzed via flow cytometry. Cells were treated with 500 ng/ml doxorubicin for 24h and, where indicated, 3D-grown cells were treated with HDAC6/10 inhibitors tubastatin A (7.5 µM) and bufexamac (30 µM). Bar graph depicts mean doxorubicin fluorescence normalized to 3D-grown cells treated with doxorubicin and DMSO.* ***(b)*** *Flow cytometric analysis of cellular doxorubicin fluorescence in 3D-cultured BE(2)-C cells 5d after transfection with siRNAs. Cells were treated for the last 24h with 500 ng/ml doxorubicin. Bar graph depicts mean doxorubicin fluorescence normalized to siCtrl transfected cells.* ***(c)*** *Western blot analysis of HDAC6 and HDAC10 expression after RNAi-mediated knockdown. Statistical analysis was performed on non-normalized data using paired two-tailed t-test (***p < 0.001; **0.001 ≤p <0.01; *0.01 ≤ p < 0.05). Error bars represent standard error of the mean (SEM).*

1.9 HDAC10 inhibition increases doxorubicin sensitivity of neuroblastoma cells but not fibroblasts

The observation that lysosomal exocytosis inhibition by tubastatin A increased doxorubicin accumulation in neuroblastoma cells but not in non-transformed fibroblasts (see sections ***E1.4.2*** and

E1.6.1) raised the question whether tubastatin A could be used to selectively sensitize neuroblastoma cells to doxorubicin treatment, while sparing non-malignant cells such as fibroblasts. Such a selectivity towards malignant cells could, in turn, make HDAC10 an attractive target for clinical intervention.

1.9.1 Combination of doxorubicin with HDAC6/10 inhibitor tubastatin A induces cell death in neuroblastoma cells

To test whether HDAC6/10 inhibitor tubastatin A sensitizes neuroblastoma cells to doxorubicin treatment, BE(2)-C cells were treated with 100 ng/ml doxorubicin in the presence or absence of 7.5 µM tubastatin A. Cell viability and the number of viable cells were quantified via automated trypan blue staining, and compared to DMSO treated cells or to cells subjected to single treatment after 24h, 48h and 96h, respectively. Here, combination treatment with doxorubicin and tubastatin A substantially and significantly reduced cell viability at all investigated timepoints when compared to either solvent treated or single treated cells (***Figure 36a-c***). Treatment with tubastatin A alone slightly reduced cell viability after 48h and 96h, but this effect was not statistically significant at either timepoint (***Figure 36b, c***). Also, doxorubicin alone did not substantially affect cell viability within the first 48h of treatment, and only caused a prominent loss of cell viability after 96h (***Figure 36b, c***). The effect at 96h was not statistically significant, due to big variations in treatment efficiency with doxorubicin alone. This variation in doxorubicin efficiency at the 96h timepoint also caused the differences of doxorubicin treatment alone and the combination treatment with tubastatin A to be non-significant, even though cells that underwent combination treatment displayed substantially lower cell viability than cells treated with doxorubicin alone in each individual experiment (***Figure 36c***).

In addition to cell viability, the cell number after treatment was quantified to test for the cytostatic properties of the above described treatment combinations. Here, both single treatment with tubastatin A and especially doxorubicin were cytostatic after 48h and 96h (***Figure 36d-f)***. Combination of doxorubicin with tubastatin A further reduced the amount of viable cells compared to single treatment with doxorubicin, but this effect was not statistically significant as single treatment with doxorubicin alone also resulted in low cell numbers due to its highly cytostatic potential (***Figure 36d-f)***.

Taken together, combination treatment with tubastatin A and doxorubicin effectively induced cell death compared to single treatments, which were rather cytostatic than cytotoxic.

As the P-glycoprotein inhibitor verapamil was also capable of substantially increasing intracellular doxorubicin levels in BE(2)-C cells (see section ***E1.5.1***), it was hypothesized that combination treatment with doxorubicin and verapamil should reduce cell viability in a similar fashion as

combination of doxorubicin with tubastatin A. However, although combination treatment with verapamil was clearly cytostatic at early treatment timepoints (24h and 48h) (***Figure 36d, e***), effects on cell viability were delayed with the latter combination (***Figure 36a-c***). A substantial reduction in cell viability after combined treatment with doxorubicin and verapamil over doxorubicin treatment alone was only visible after 96h, although this effect was not statistically significant due to the high variance in doxorubicin efficiency (***Figure 36c***). It was thus hypothesized that sensitization of BE(2)-C cells to doxorubicin treatment by addition of HDAC6/10 inhibitor tubastatin A was not only caused by increased doxorubicin accumulation, but potentially by secondary and tertiary mechanisms (see sections ***E1.9.4*** and ***E1.10***).

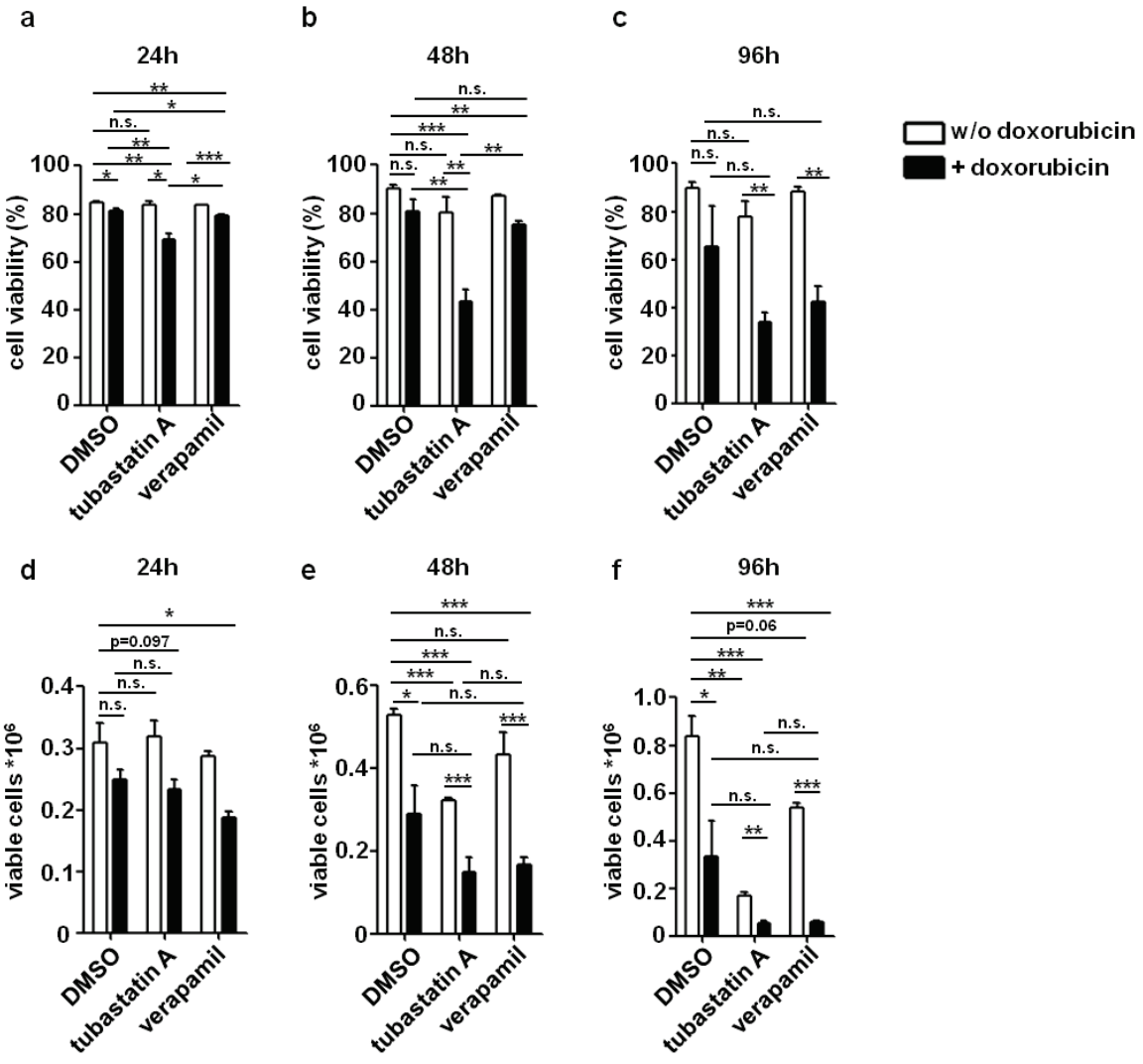

Figure 36: HDAC6/10 inhibition sensitizes BE(2)-C neuroblastoma cells to doxorubicin treatment. (a-c) *Viability of BE(2)-C cells after treatment with 100 ng/ml doxorubicin +/- tubastatin A (7.5 µM) and verapamil (10 µM) for 24h* ***(a)****, 48h* ***(b)*** *and 96h* ***(c)****, respectively.* ***(d-f)*** *Number of viable BE(2)-C cells after the above described treatments. Viability and cell number were analyzed via trypan blue exclusion on an automated cell counter. Statistical analysis was performed on non-normalized data using unpaired two-tailed t-test (***p < 0.001; **0.001 ≤p <0.01; *0.01 ≤ p < 0.05). Error bars represent standard error of the mean (SEM). Parts of figure published in (Ridinger et al. 2018).*

1.9.2 Combination of doxorubicin with HDAC6/10 inhibitor tubastatin A has cytostatic but not cytotoxic effects on fibroblasts

Treatment regimens that increase sensitivity of cancer cells should ideally target tumor cells while sparing non-malignant cells. Because of their ability to readily proliferate in culture, which makes them potentially sensitive to chemotherapeutic drugs, fibroblasts represent a suitable cell culture model to test combinatorial treatments that include cytostatic drugs. Human fibroblasts were treated with 100 ng/ml doxorubicin in the absence or presence of 7.5 µM HDAC6/10 inhibitor tubastatin A or 10 µM of the P-glycoprotein inhibitor verapamil. As for BE(2)-C cells in the section above, cell viability (***Figure 37a-c***) and the number of viable cells (***Figure 37d-f***) were measured by automated trypan blue staining after treatment for 24h, 48h and 96h, respectively. In marked contrast to BE(2)-C cells, double treatment with tubastatin A and doxorubicin did not substantially affect cell viability at 24h, 48 or 96h (***Figure 37a-c***). In fact, the only treatment regimen that slightly and significantly reduced cell viability in fibroblasts was the combination of doxorubicin with verapamil for 96h (***Figure 37c***).

Analogous to BE(2)-C cells, however, single treatment with doxorubicin or tubastatin A caused a substantial reduction in the number of viable cells, and viable cell numbers were further decreased by combination treatment with either HDAC6/10 inhibitor doxorubicin or P-glycoprotein inhibitor verapamil (***Figure 37d-f***).

Taken together, the data in sections ***E1.9.1*** and ***E1.9.2*** show that doxorubicin and tubastatin A, as well as their combination have cytostatic effects on both fibroblasts and neuroblastoma cells. However, in contrast to its mere cytostatic effect on fibroblasts, combination of doxorubicin and HDAC6/10 inhibitor tubastatin A clearly had cytotoxic potential in BE(2)-C neuroblastoma cells.

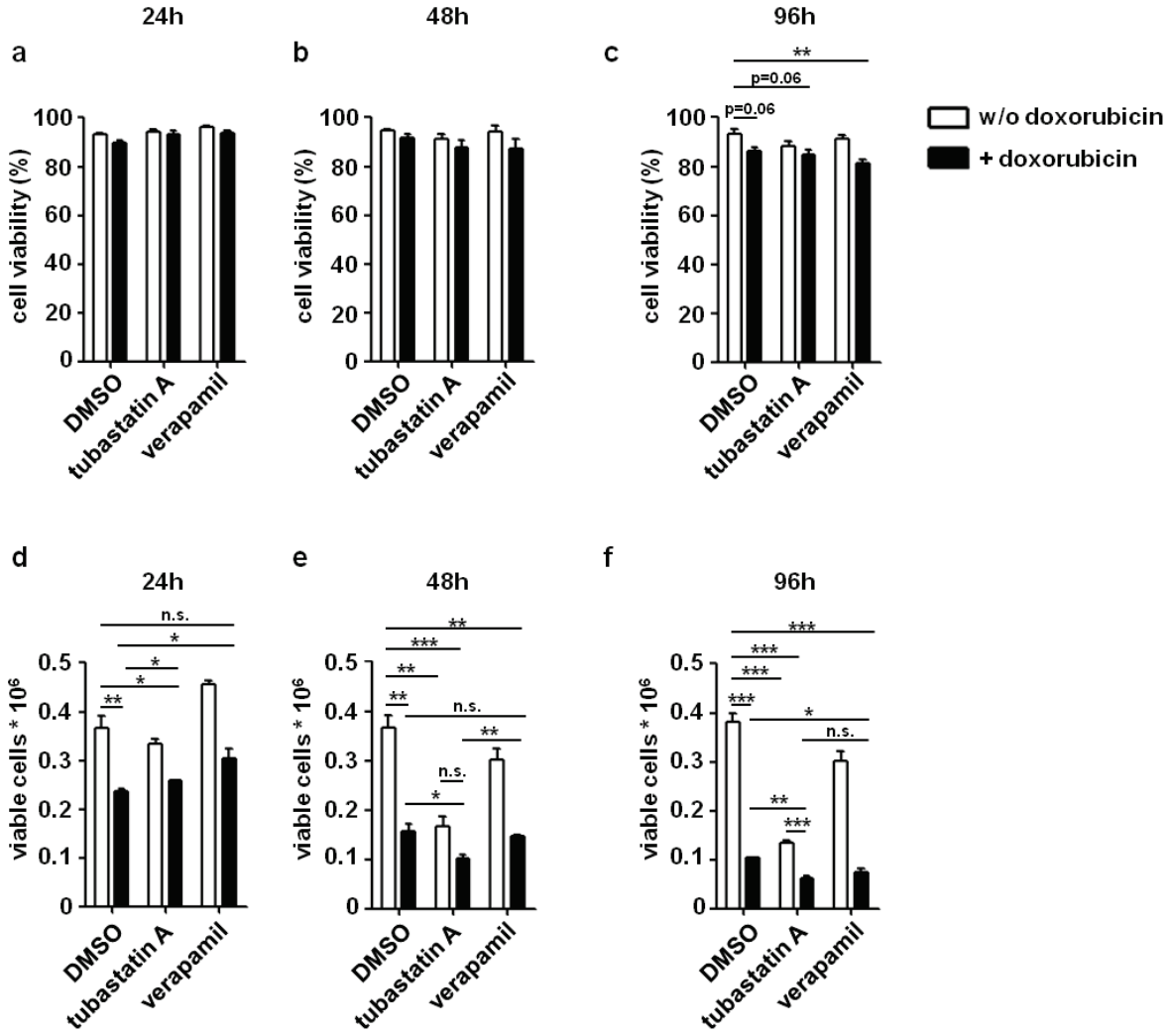

Figure 37: HDAC6/10 inhibition does not sensitize proliferating human fibroblasts cells to doxorubicin treatment. (a-c) *Viability of fibroblasts after treatment with 100 ng/ml doxorubicin +/- tubastatin A (7.5 µM) and verapamil (10 µM) for 24h* ***(a)****, 48h* ***(b)*** *and 96h* ***(c)****, respectively.* ***(d-f)*** *Number of viable fibroblasts after the above described treatments. Viability and cell number were analyzed via trypan blue exclusion on an automated cell counter. Statistical analysis was performed on non-normalized data using unpaired two-tailed t-test (***p < 0.001; **0.001 ≤p <0.01; *0.01 ≤ p < 0.05). Unless otherwise indicated by asterisks, differences were not statistically significant. Error bars represent standard error of the mean (SEM). Parts of figure published in (Ridinger et al. 2018).*

1.9.3 Combination of doxorubicin with HDAC6/10 inhibitor tubastatin A reduces colony formation of BE(2)-C neuroblastoma cells

The data presented in section ***E1.9.1*** demonstrate that combination treatment with doxorubicin and the HDAC6/10 inhibitor tubastatin A has cytotoxic effects on BE(2)-C neuroblastoma cells, while single treatment is rather cytostatic. Colony assays can reveal both cytostatic and cytotoxic drug characteristics in a single readout, i.e. the outgrowth of colonies in a recovery phase after a limited period of treatment.

Combination of tubastatin A with 100 ng/ml doxorubicin over a treatment period of 24h with eleven days of colony outgrowth substantially reduced colony formation compared to solvent control and

individual treatments, respectively (***Figure 38***). This was in line with the data from cell viability assays described in section ***E1.9.1***. Colony assays also reflected the cytostatic capacity of tubastatin A and doxorubicin, as both drugs were capable of reducing colony formation, although this effect was not significant in case of tubastatin A. The combination of doxorubicin and tubastatin A was also capable of reducing colony outgrowth at lower doxorubicin concentrations (50 ng/ml) that are potentially achievable in patient serum and which only slightly reduced colony formation on its own. Thus, tubastatin A sensitized highly chemoresistant BE(2)-C cells to clinically achievable concentrations of doxorubicin.

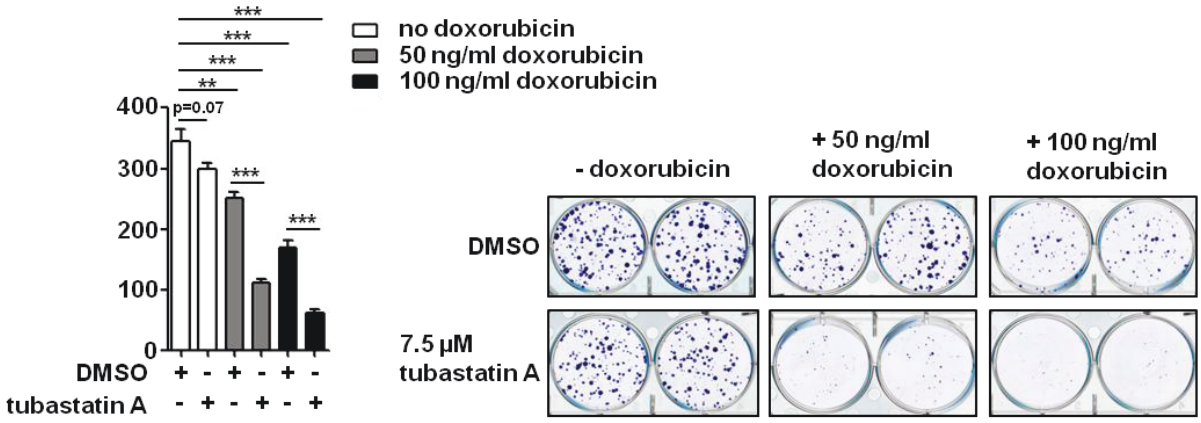

Figure 38: Colony formation of BE(2)-C cells is inhibited by combined treatment with doxorubicin and HDAC6/10 inhibitor tubastatin A. *BE(2)-C cells were treated for 24h with different doses of doxorubicin, 7.5 µM tubastatin A and the respective combination. Colonies were allowed to outgrow for eleven days after washout of drugs and colonies were stained with crystal violet. Bar graphs depict mean colony number. Statistical analysis was performed on non-normalized data using unpaired, two-tailed t-test (***p < 0.001; **0.001 ≤ p < 0.01; *0.01 ≤ p < 0.05). Error bars represent standard error of the mean (SEM). Figure published in (Ridinger et al. 2018).*

1.9.4 Lysosomal exocytosis inhibition itself contributes to sensitization of BE(2)-C cells to doxorubicin

The data presented in sections ***E1.6*** and ***E1.9*** show that HDAC6/10 inhibitors can promote doxorubicin accumulation in neuroblastoma cells by inhibition of HDAC10 mediated lysosomal exocytosis and that combination treatment of doxorubicin with HDAC6/10 tubastatin A sensitizes neuroblastoma cells to doxorubicin treatment. Surprisingly, however, sensitization to doxorubicin was less efficient with the P-glycoprotein inhibitor verapamil, even though the latter promoted stronger intracellular accumulation of doxorubicin than tubastatin A (***Figure 27b***). Thus, increased doxorubicin accumulation alone was not solely responsible for cell death induction after co-treatment with doxorubicin and tubastatin A.

Data in section ***E1.4.4*** show that HDAC6/10 inhibitor alters the subcellular localization of doxorubicin, raising the question whether doxorubicin was unable to reach the nucleus and in case of

combination with verapamil. Analysis of subcellular doxorubicin localization upon verapamil treatment via confocal immunofluorescence microscopy, however, showed that doxorubicin strongly accumulated in nuclei of BE(2)-C cells after verapamil treatment, thus ruling out that the lack of sensitization was due to altered subcellular localization of doxorubicin (***Figure 39a***). This led to the hypothesis that inhibition of lysosomal exocytosis itself could have contributed to sensitization of neuroblastoma cells to doxorubicin treatment. In order to investigate this, BE(2)-C cells were treated with doxorubicin and the lysosomal exocytosis inhibitor vacuolin-1 for 24h and cell viability was analyzed by automated trypan blue staining. Here, combination of doxorubicin with vacuolin-1 reduced cell viability in a similar fashion as combined treatment with doxorubicin and tubastatin A did (***Figure 39b***). Similar to tubastatin A treatment, vacuolin-1 alone did not substantially lower cell viability, indicating that inhibition of lysosomal exocytosis increased chemosensitivity of neuroblastoma cells only under stress conditions like doxorubicin treatment. Notably, no substantial cytotoxicity of the vacuolin-1 doxorubicin combination was observed in fibroblasts, again suggesting the inhibition of lysosomal exocytosis as a strategy to selectively target tumor cells (***Figure 39b***).

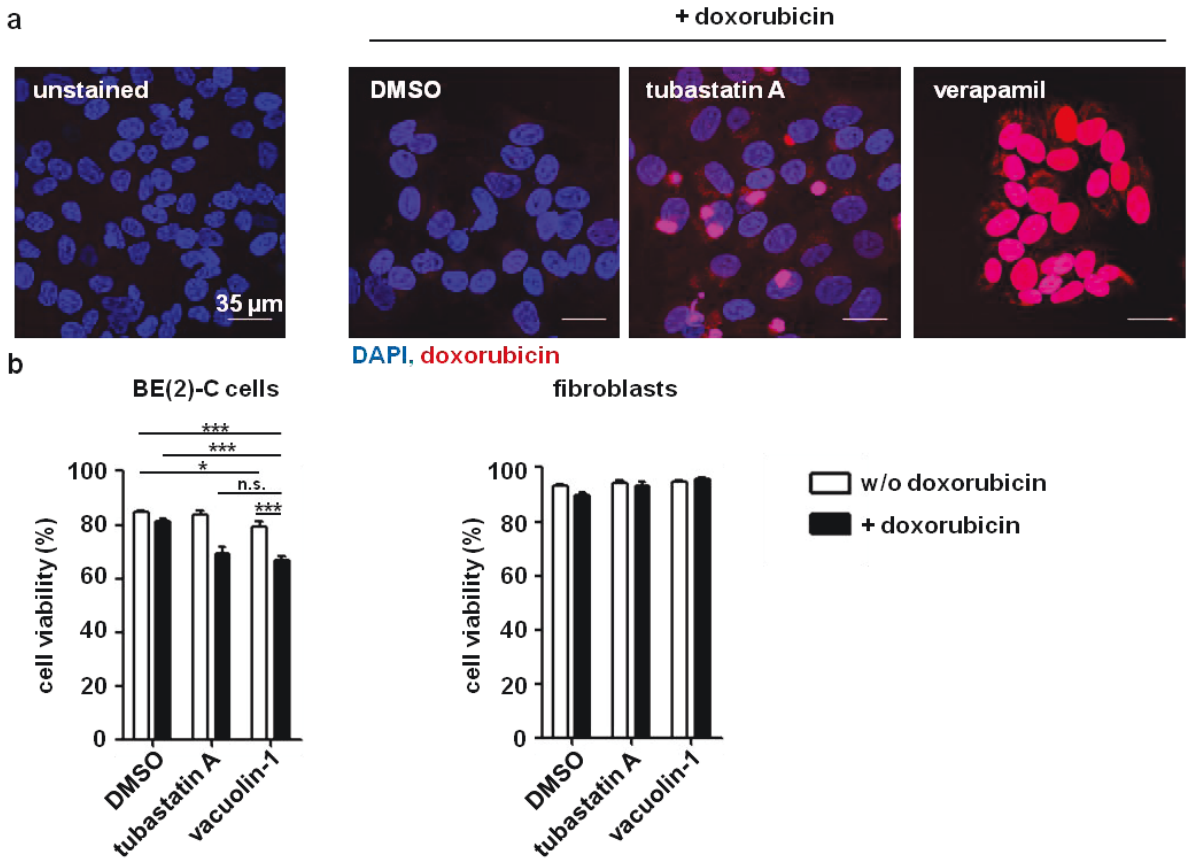

Figure 39: Lysosomal exocytosis inhibition itself contributes to sensitization of neuroblastoma cells to doxorubicin treatment. (a) *Confocal immunofluorescence analysis of cellular doxorubicin localization in BE(2)-C cells after 24h treatment with 250 ng/ml doxorubicin +/- HDAC6/10 inhibitor tubastatin A (7.5 µM) and P-glycoprotein inhibitor verapamil (10 µM). Images depict maximum intensity projection of z-stacks.* ***(b)*** *Viability of BE(2)-C cells and human fibroblasts after 24h treatment with 100 ng/ml doxorubicin +/- HDAC6/10 inhibitor tubastatin A (7.5 µM) or lysosomal exocytosis inhibitor vacuolin-1 (10 µM). Statistical analysis was performed on non-normalized data using unpaired two-tailed t-test (***p < 0.001; **0.001 ≤p <0.01; *0.01 ≤ p < 0.05). In case of fibroblasts, no statistically significant changes in viability were observed. Error bars represent standard error of the mean (SEM). Parts of figure published in (Ridinger et al. 2018).*

1.10 HDAC6/10 inhibition causes formation of DNA double-strand breaks (DSB) and increases doxorubicin induced DSBs

The results in section ***E1.9.1*** show that combination of the neuroblastoma chemotherapeutic doxorubicin with HDAC6/10 inhibitor tubastatin A induces cell death more rapidly than combination of doxorubicin with P-glycoprotein inhibitor verapamil, even though verapamil promoted stronger intracellular doxorubicin accumulation than tubastatin A (***Figure 27b***). Thus, enriched intracellular doxorubicin per se cannot be the only reason for sensitization of neuroblastoma cells to doxorubicin after HDAC10 inhibition, suggesting that additional mechanisms are involved in the induction of cell death. Doxorubicin is a DNA-intercalating agent which also induces DNA double strand breaks (DSBs) by a process called topoisomerase II poisoning (Nitiss 2009; Yang et al. 2014). In this context, recent studies have suggested a role of nuclear HDAC10 in DNA repair, with a special focus on DNA mismatch repair and the repair of DSBs (Kotian et al. 2011; Radhakrishnan et al. 2015; Islam et al.

2017). It was thus not only investigated if interference with HDAC10 function increased doxorubicin induced DSBs, but also if inhibition of HDAC10 itself enhanced the formation of DNA double strand breaks.

1.10.1 HDAC6/10 inhibition increases the formation of γH2A.X positive foci

Upon the formation of DSBs, cells quickly induce a DNA damage response and recruit DNA repair enzymes to DNA lesions. One of the earliest responses to DSBs includes the phosphorylation of histone variant H2A.X at serine 134 (so called γH2A.X), which is in turn incorporated into chromatin at the DSB site. This is followed by the formation of so called γH2A.X foci, which can be used as a readout for the amount of DSBs in a cell (Rogakou et al. 1998; Kuo and Yang 2008).

To investigate if HDAC6/10 inhibition enhanced the formation of DSBs, BE(2)-C neuroblastoma cells were, in an initial experiment, analyzed for the presence of chromatin foci that contained via confocal immunofluorescence microscopy (***Figure 40a***). Treatment with tubastatin A for 24h moderately increased DSBs while P-glycoprotein inhibitor verapamil did not. Moderate doses of doxorubicin (25 ng/ml) also induced low levels of DSBs, and these were substantially increased when combined with tubastatin A. This effect was not as pronounced when doxorubicin was combined with P-glycoprotein inhibitor verapamil at concentrations where verapamil induced stronger intracellular doxorubicin accumulation than tubastatin A (***Figure 40a, Figure 27b***). These data suggest that tubastatin A can increase DSB formation on its own and promote enhanced DSB formation under genotoxic treatment.

To establish an approach capable of quantifying DSBs, γH2A.X positive foci were measured by flow cytometric analysis on PFA fixed cells. Treatment of BE(2)-C cells with doxorubicin caused a dose-dependent increase in the percentage of γH2A.X highly positive cells, demonstrating that the fluorescent signal measured by flow cytometry correlated with the amount of γH2A.X positive lesions and thus likely DSBs (***Figure 40b***).

Confirming the results of immunofluorescence microscopy, addition of tubastatin A to doxorubicin significantly increased the amount of γH2A.X positive cells compared to doxorubicin treatment alone (***Figure 40c, d***). The increase in γH2A.X positive cells was significantly greater than when verapamil was combined with doxorubicin (***Figure 40d***). Single treatment of BE(2)-C cells confirmed a slight increase in γH2A.X positive cells in case of tubastatin A but not verapamil treatment and the DSB inducing capability of tubastatin A was also observed in IMR-32 cells (***Figure 40e***). Notably, single treatment with lysosomal exocytosis inhibitor vacuolin-1 did not cause elevated γH2A.X levels, and combination of vacuolin-1 with doxorubicin raised the percentage of γH2A.X highly positive cells in about the same magnitude as co-treatment with verapamil did, which was below the combination of

doxorubicin and tubastatin A (***Figure 40d, f***). Taken together with the data presented in sections ***E1.4.4***, ***E1.6.2***, ***E1.9.1*** and ***E1.9.4***, this indicate that HDAC6/10 inhibitor tubastatin A promoted sensitization of neuroblastoma cells to doxorubicin by at least three mechanisms: increased doxorubicin accumulation by lysosomal exocytosis inhibition, decreased stress resistance by lysosomal exocytosis inhibition, as well as induction of DNA double strand breaks.

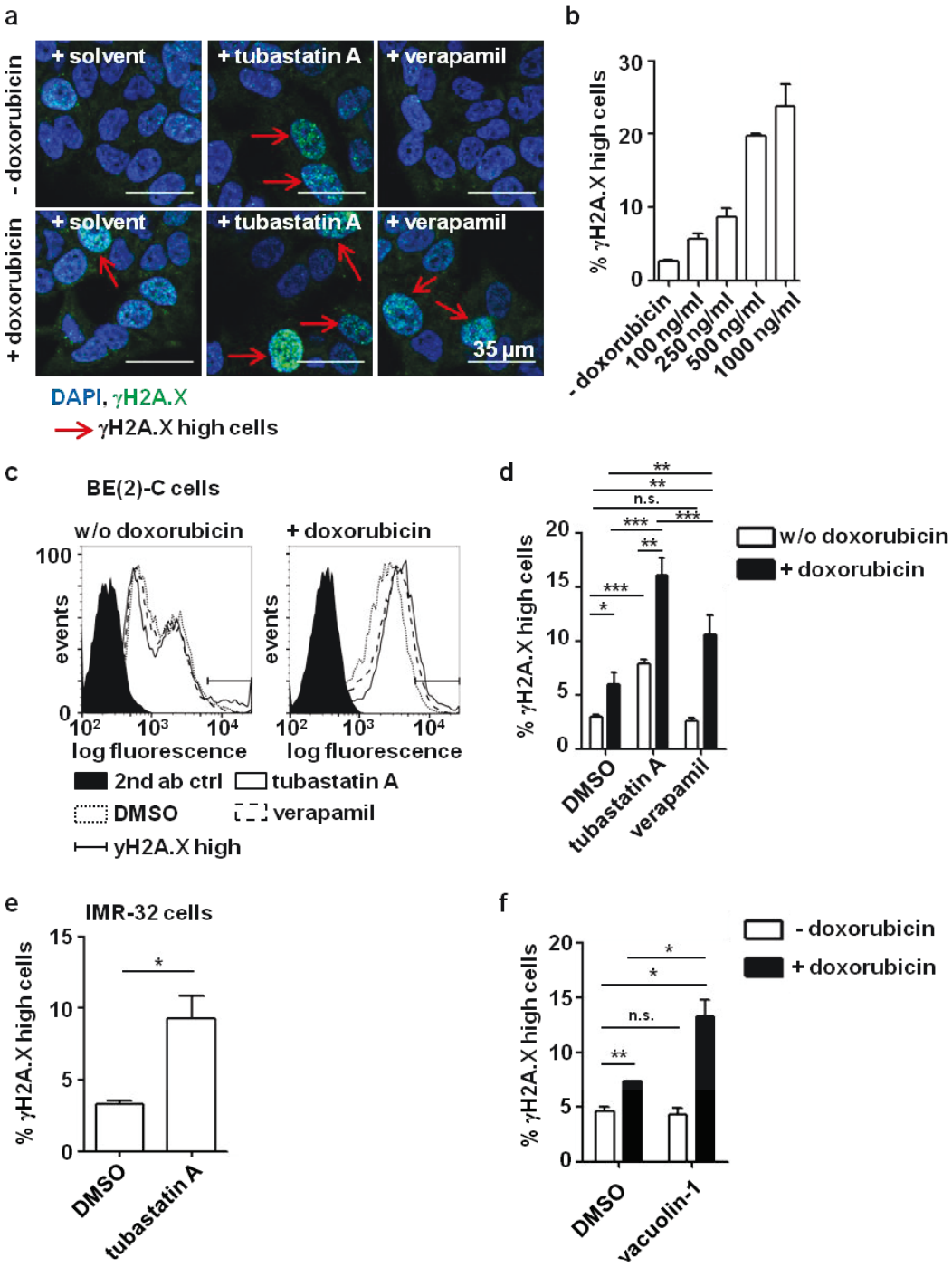

Figure 40: HDAC6/10 inhibition induces the formation of γH2A.X positive foci in neuroblastoma cells. (a) *immunofluorescence analysis of γH2A.X staining in BE(2)-C cells after 24h treatment with tubastatin A (7.5 µM), verapamil (10 µM) +/- 25 ng/ml doxorubicin. Red arrows indicated γH2A.X highly positive cells* ***(b)*** *Flow cytometric analysis of γH2A.X staining in BE(2)-C cells after 24h treatment with indicated doxorubicin concentrations. Number of highly γH2A.X positive cells was quantified in 2 experiments (2 technical replicates per experiment, one experiment shown).* ***(c)*** *Flow cytometric analysis of γH2A.X staining in BE(2)-C cells after 24h treatment with tubastatin A (7.5 µM), verapamil (10 µM) +/- 100 ng/ml doxorubicin. Fluorescence histograms depict percentage of cells (y-axis) and logarithmic γH2A.X fluorescence (x-axis). Ranged gates represent cells gated as highly γH2A.X positive.* ***(d)*** *Flow cytometric analysis γH2A.X positive BE(2)-C cells (n=6 experiments).* ***(e)*** *Flow cytometric quantification of γH2A.X positive cells in IMR-32 cells after 24h treatment with 7.5 µM tubastatin A.* ***(f)*** *Flow cytometric quantification of γH2A.X positive BE(2)-C cells after 24h treatment with 10 µM vacuolin-1 +/- 100 ng/ml doxorubicin (n= 4 experiments). Statistical analysis was performed on non-normalized data using paired two-tailed t-test (***p < 0.001; **0.001 ≤p <0.01; *0.01 ≤ p < 0.05). Parts of figure published in (Ridinger et al. 2018).*

1.10.2 HDAC6/10 inhibition increases the formation of doxorubicin induced DNA double strand breaks

γH2A.X positive foci are a very commonly used readout for the induction of DSBs. However, they can also occur upon replication fork stalling (Ewald et al. 2007). The physical presence of DNA damage can be quantified by a single cell electrophoresis approach called comet assay, in which agarose enclosed single cells are lysed under alkaline conditions and then subjected to an electric field. Here, damaged DNA leaves a tell-tale pattern of DNA migration that resembles a comet and quantification of percentage of tail DNA versus total DNA can be used as a readout to assess the amount of DNA damage.

Two independent comet assays (performed in the group of Dr. Peter Schmezer, Division of Epigenomics and Cancer Risk Factors, DKFZ, Germany) confirmed that addition of tubastatin A to doxorubicin treatment significantly increased the relative amount of tail DNA and thus DSBs compared to solvent treated cells or cells treated with 100 ng/ml doxorubicin only (***Figure 41***). As reported for γH2A.X positive foci, treatment with tubastatin A alone increased DSBs also in comet assays, although this effect was statistically significant in only one of the biological replicates. At the same time, however, treatment with 100 ng/ml doxorubicin alone did not significantly increase DNA damage in either replicate, suggesting that comet assays had a lower sensitivity for DSBs that the flow cytometric analysis of γH2A.X staining. Taken together with the previous section, these data indicate that HDAC6/10 inhibition with tubastatin A increases the formation DSBs in neuroblastoma cells, both as single treatment and much higher in combination with DNA-inducing agents such as doxorubicin.

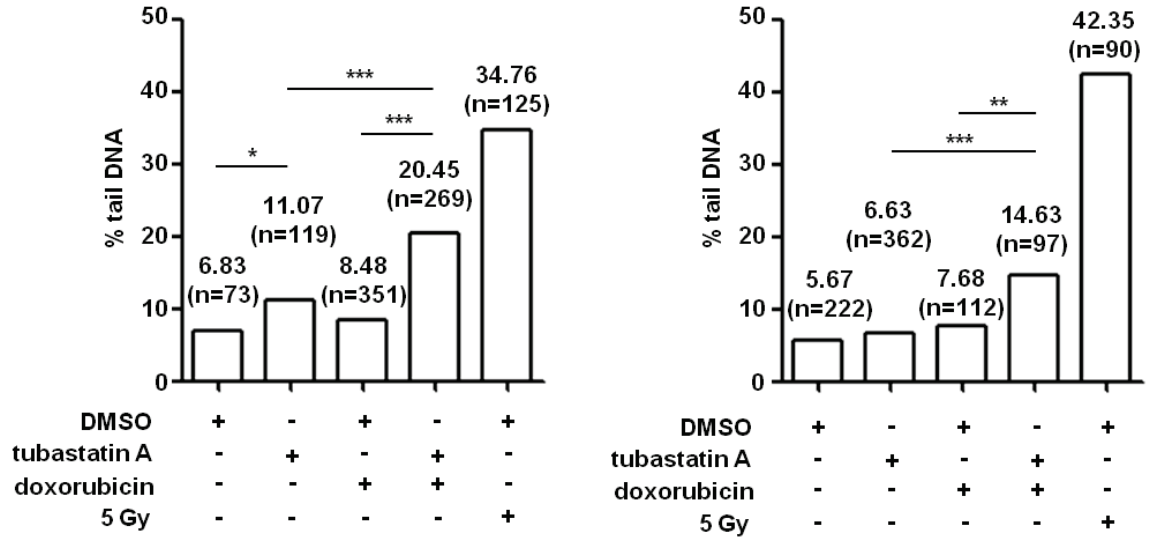

Figure 41: Analysis of DNA double strand breaks in BE(2)-C cells via comet assay (two biological replicates). *Cells were treated with HDAC6/10 inhibitor tubastatin A (7.5 µM) in absence or presence of 100ng/ml doxorubicin for 18h. Gamma ray irradiated cells (5 Gy, see methods section* ***C3.5****) served as positive control for DSBs. Bar graphs show median % tail DNA (y-axis) per treatment of each one biological replicate experiment. Numbers above bars give % tail DNA, as well as the number of analyzed nuclei in brackets. Statistical was performed using one-tailed Mann Whitney test. Parts of figure published in (Ridinger et al. 2018).*

2 Approaches to identify HDAC10 downstream targets

2.1 HDAC10 and its potential role as a polyamine deacetylase

The recently published crystal structure of zebrafish HDAC10 suggests that HDAC10 is a poor lysine deacetylase and rather acts as a polyamine deacetylase, specifically of N^8-acetylated spermidine (Hai et al. 2017). Polyamine metabolism is often severely deregulated in high-risk neuroblastoma cases, and high expression of the rate-limiting polyamine synthesizing enzyme ODC-1 is associated with poor outcome independently of *MYCN* amplification (Hogarty et al. 2008; Gamble et al. 2012). This raised the question whether HDAC10 also acts as a polyamine deacetylase in human neuroblastoma cells and whether HDAC10 function influences cellular polyamine levels. To investigate this, BE(2)-C cells were either treated with HDAC6/10 inhibitors for 24h or transfected with siRNAs against HDAC6 or HDAC10 for 3d and 6d, respectively. Cells were subjected to whole cell lysis using SSAT lysis buffer and then analyzed for the presence of polyamines and their acetylated derivatives via high performance liquid chromatography (HPLC) after dansyl chloride labeling in the collaborating group of Dr. Robert Casero (Johns Hopkins University, Baltimore, United States). Raw polyamine levels were normalized to protein concentration.

N^8-acetylspermidine was detected in none of the samples (data not presented as figure), possibly due to low abundance of that polyamine species in BE(2)-C cells. Since N^8-acetylatspermidine is generated in the nucleus and therefore potentially enriched in this compartment (Libby 1980),

nuclear fractions were enriched by nuclear-cytoplasmic fractionation prior to the generation of polyamine lysates. However, detection of N^8-acetylated polyamines also failed on nuclear lysates from both tubastatin A and DMSO treated cells (data not presented as figure). Furthermore, neither knockdown of HDAC6 or HDAC10 (***Figure 42a, b***), or inhibition of either enzyme (***Figure 42c***) consistently changed total levels of putrescine, spermidine and spermine.

Taken together these data suggest that class IIb HDACs do not control total polyamine levels in the above named cell model. Moreover, N^8-acetylation of spermidine should be investigated in other cell lines (currently ongoing), or in cellular supernatants, as preliminary data from our collaborators suggest that N^8-acetylspermidine is secreted (see discussion section ***F2***).

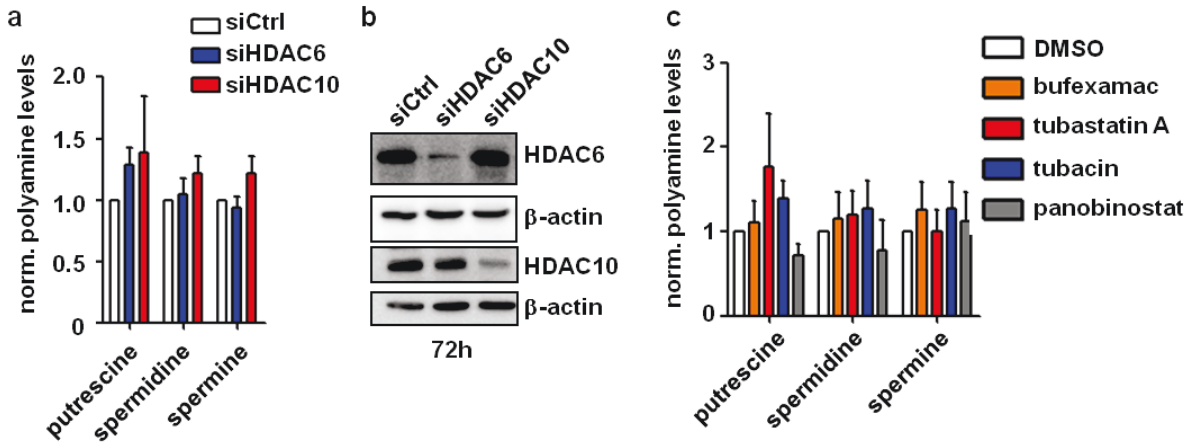

Figure 42: Interference with HDAC10 function does not alter polyamine levels in BE(2)-C neuroblastoma cells. ***(a)*** *HPLC quantification of polyamines per mg protein in BE(2)-C 72h after transfection with siRNAs against HDAC6 and HDAC10, respectively. Two replicate experiments were pooled.* ***(b)*** *Western blot analysis of knockdowns.* ***(c)*** *HPLC quantification of polyamines per mg protein in BE(2)-C whole cell lysates after 24h treatment with HDAC6/10 inhibitors tubastatin A (7.5 µM), bufexamac (30 µM), HDAC6 inhibitor tubacin (7.5 µM) and pan HDAC inhibitor panobinostat (10 nM). Levels of the respective polyamine were normalized to DMSO treated cells. All HPLC analyses were performed by Dr. Tracy Murray-Stewart in the lab of Dr. Bob Casero (Johns Hopkins University, Baltimore, United States).*

2.2 Analysis of lysine acetylation in HSP70 family members HSC70 and HSP70 after HDAC10 inhibition

Members of the HSP70 family of heat shock proteins have been repeatedly reported to be important for various modes of autophagy, as well as for lysosomal membrane integrity. Most famously, the constitutively expressed HSP70 family member HSC70 is a central mediator of chaperone-mediated autophagy, where it delivers cytosolic proteins destined for degradation to a lysosomal LAMP-2 complex, which in turn translocates the proteins into the lysosomes (Cuervo and Dice 1996; Salvador et al. 2000). In contrast, the stress-regulated HSP70 family members HSPA1A (HSP70-2, from here on referred to as HSP70) is known to act as a guardian of lysosomal membrane integrity in cancer (Daugaard et al. 2007a) and has been further shown to be required for the initiation of

autophagosome formation during macroautophagy (Yang et al. 2013). Several studies show that heat shock protein function can be heavily modified by lysine acetylation (Kovacs et al. 2005; Yang et al. 2013) and recent papers also hint at a potential interaction of HDAC10 with HSP70 family members HSC70 or HSP70 (Lai et al. 2010; Oehme et al. 2013a), making them a prime candidate downstream target of HDAC10.

2.2.1 Separate enrichment of heat shock proteins HSC70 and HSP70 via immunoprecipitation

Due to their high sequence homology, separate enrichment of HSC70 and HSP70 was prerequisite to identifying HDAC10 specific deacetylation sites in HSC70 and HSP70, respectively. To that end, two separate immunoprecipitation (IP) protocols were established using non-crossreactive HSC70 and HSP70 antibodies (***Figure 43a***) which allowed for the successful enrichment of HSC70 and HSP70 from BE(2)-C cells, respectively (***Figure 43b***). Specificity of the HSP70 and HSC70 pulldowns for either protein was confirmed both by using non-specific rat and mouse control IgG antibodies (***Figure 43c***) and by cross-incubating the blot of each pulldown with the antibody of the respective other HSP70 family member (***Figure 43d***). Here, no substantial cross contamination with the respective other HSP70 family member was detected in the eluate fractions.

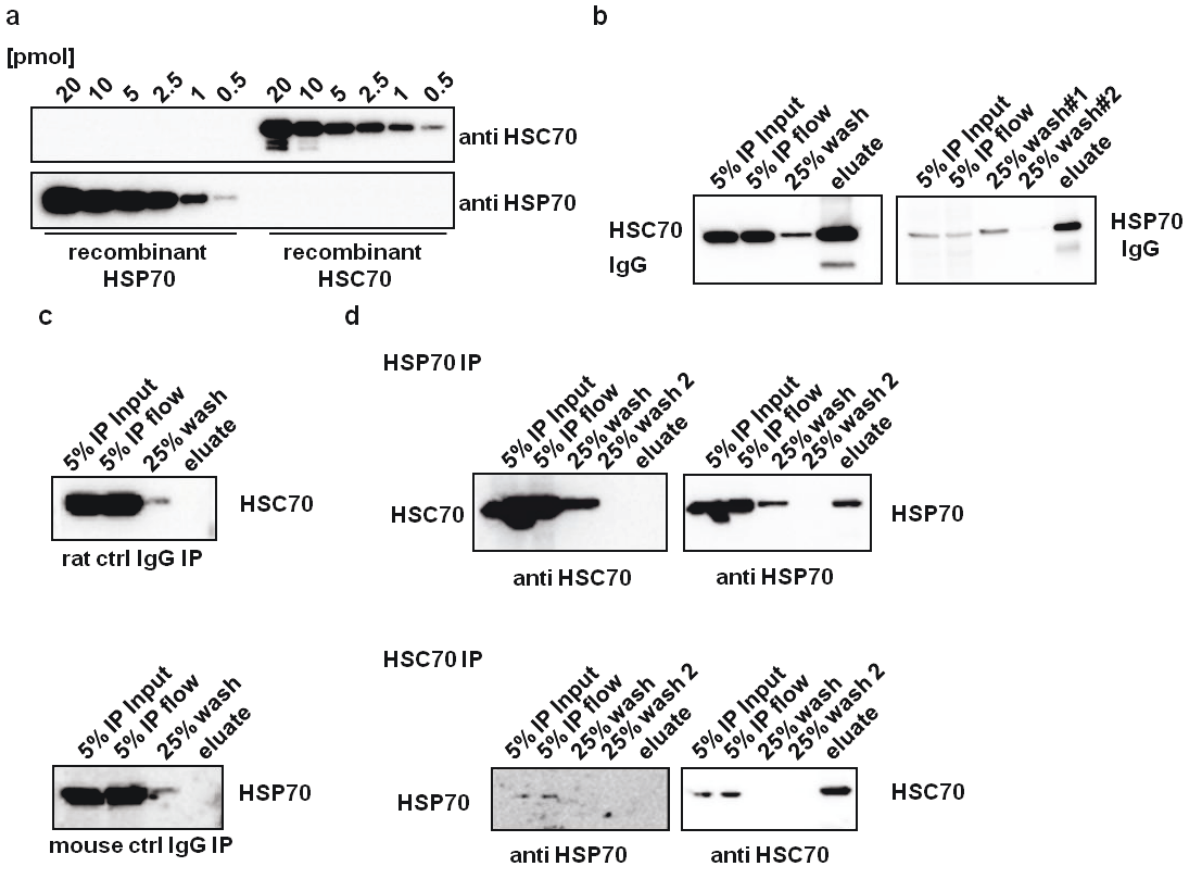

Figure 43: Optimization of immunoprecipitation protocols for separate enrichment of HSP70 and HSC70. (a) *Indicated amounts of recombinant HSP70 and HSC70 protein were separated via PAGE, blotted on a PVDF membrane and used for testing cross-reactivity of candidate HSP70 and HSC70 antibodies. Example shows identification of two non cross-reactive antibodies.* ***(b)*** *Western blot analysis of an exemplary HSC70 (left) and HSP70 (right) pulldown. Proteins were pulled down for 5h-6h at 4°C.* ***(c)*** *Non specific rat (top figure) and mouse (bottom figure) IgGs were used as control to exclude unspecific binding of HSP70 family members HSC70 and HSP70 to IgG antibodies.* ***(d)*** *Criss-Cross detection of HSC70 on HSP70 pulldown and vice versa in order to control pulldown specificity for either HSP family member. Membranes were afterwards re-probed with the respective correct HSP antibody.*

2.2.2 No HDAC10 specific deacetylation sites in HSP70 or HSC70 could be identified via tandem mass spectrometry

In order to identify HDAC10 specific deacetylation sites in HSP70 and HSC70, both proteins were separately enriched via immunoprecipitation (IP) from BE(2)-C lysates after 24h treatment with 7.5 µM tubastatin A (HDAC6/10 inhibitor) and 7.5 µM tubacin (HDAC6 inhibitor), as well as control treatment with solvent only. A pan HDAC inhibitor (500nM TSA) was added to all lysates prior to the IP in order to stop unspecific deacetylase activity after cell lysis. IP-enriched HSP70 and HSC70 proteins were separated on 1D-PAGE, excised at the target mass range, digested with trypsin and analyzed via LC-MS/MS (see section ***C2.8***). Peptides with putative acetylation sites on lysines directly N-terminal of tryptic cleavage were omitted as false positive.

In contrast to western blot analysis of HSP70 IPs (***Figure 43***), cross-contamination of HSC70 protein with HSP70 and *vice versa* were detected in all analyzed MS experiments (data not shown), probably due to the higher sensitivity of MS over western blot. In a first set of experiments, treatment with HDAC6/10 inhibitor tubastatin A but not with HDAC6 inhibitor tubacin increased acetylation of HSP70 but not HSC70 at lysine 159 (K159) (***Figure 44a***), a before reported target site of HDAC6, acetylation of which promoted autophagy (Yang et al. 2013). The contaminating HSP70 protein in the HSC70 pulldown showed a similar pattern of K159 acetylation, namely K159 acetylation only occurring after HDAC6/10 but not after HDAC6 inhibition (***Figure 44a***). None of the follow-up experiments, using either IP-enriched HSP70 (experiment 2) or a 70kDa target mass range slice from PAGE of postnuclear lysates (experiments 3 and 4) could however confirm that HSP70 was differentially acetylated at K159 HDAC6/10 or HDAC6 inhibition (***Figure 44c***). Common *de novo* acetylation patterns after either HDAC6/10 or HDAC6 inhibition were also not observed, pointing towards a poor HSP70 sequence coverage in some of the experiments (***Figure 44c***).

No conclusive pattern of additional acetylation sites was observed for HSC70 after treatment with HDAC6 or HDAC6/10 inhibitors (***Figure 44d***). Here, a high number of acetylated peptides could be identified when sequence coverage was good, but no *de novo* acetylation occurred after either HDAC6 or HDAC6/10 inhibitor treatment. Regardless, it cannot be ruled out that commonly acetylated sites like K128 become hyperacetylated in case of HDAC inhibitor treatment and a quantitative SILAC based approach might be more suitable to analyze stoichiometric changes in acetylation. In summary, the data do not provide conclusive evidence to confirm or rule out HSP70 or HSC70 as HDAC6 or HDAC10 targets and the approach used to answer this question should be refined.

a

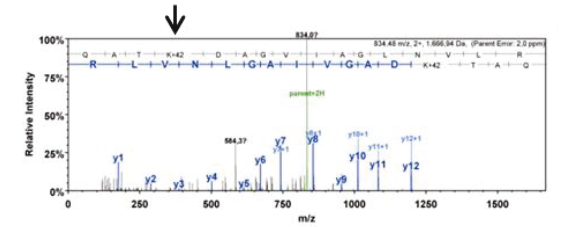

b

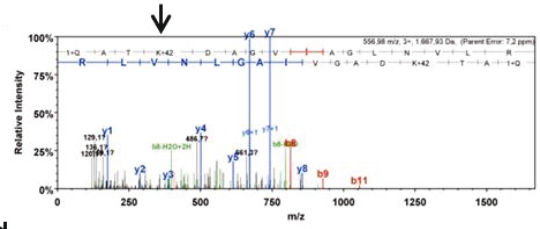

c

HSP70

K-Ac site	treatment	Exp.1	Exp.2	Exp. 3	Exp.4
K71	DMSO				
	tubastatin A		x		
	tubacin				
K128	DMSO	x			
	tubastatin A				
	tubacin				
K159	DMSO		x	x	x
	tubastatin A	x	x	x	
	tubacin		x	x	
K328	DMSO		x		
	tubastatin A		x		
	tubacin		x		
K507	DMSO				
	tubastatin A		x		
	tubacin				
K512	DMSO	x	x		
	tubastatin A		x		
	tubacin		x		
K526	DMSO		x		
	tubastatin A		x		
	tubacin		x		
% min. coverage		86	57	66	30

d

HSC70

K-Ac site	treatment	Exp.1	Exp.2	Exp. 3	Exp.4
K3	DMSO	x	n.i.		
	tubastatin A		n.i.		
	tubacin		n.i.		
K56	DMSO	x	n.i.		
	tubastatin A	x	n.i.		
	tubacin	x	n.i.		
K128	DMSO		n.i.	x	
	tubastatin A		n.i.		
	tubacin		n.i.	x	
K137	DMSO		n.i.	x	
	tubastatin A		n.i.	x	
	tubacin		n.i.		
K245	DMSO	x	n.i.		
	tubastatin A		n.i.		
	tubacin		n.i.		
K325	DMSO	x	n.i.		
	tubastatin A	x	n.i.		
	tubacin	x	n.i.		
K328	DMSO	x	n.i.	x	x
	tubastatin A	x	n.i.	x	x
	tubacin	x	n.i.	x	x
K357	DMSO		n.i.	x	
	tubastatin A		n.i.	x	
	tubacin		n.i.	x	
K423	DMSO		n.i.	x	
	tubastatin A		n.i.	x	
	tubacin		n.i.	x	
K512	DMSO	x	n.i.	x	
	tubastatin A	x	n.i.	x	
	tubacin	x	n.i.	x	
K526	DMSO		n.i.	x	
	tubastatin A		n.i.	x	
	tubacin		n.i.	x	
K589	DMSO		n.i.	x	
	tubastatin A		n.i.		
	tubacin		n.i.		
% min. coverage		90	n.i.	88	39

Figure 44: Analysis of HSP70 and HSC70 acetylation via LC-MS/MS. ***(a)*** *Fragmentation spectrum of HSP70 peptide after HSP70 IP showing lysine acetylation at K159 after 24h tubastatin A treatment.* ***(b)*** *Fragmentation spectrum of HSP70, which was detected as a contaminant in the HSC70 IP, also showing lysine acetylation at K159 after tubastatin A treatment.* ***(c, d)*** *Summary of HSP70 (left) and HSC70 (right) lysine acetylation of all four experiments. BE(2)-C cells were treated for 24h with HDAC6/10 inhibitor tubastatin A (7.5 µM), HDAC6 inhibitor tubacin (7.5 µM) or solvent. Experiment 1 (and 2 in case of HSP70) include IP-enrichment of HSP70 or HSC70. In experiments 3 and 4, 30 µg and 60 µg of postnuclear supernatants were separated via 1D PAGE, respectively, and gel slices were extracted at the target mass range (70 kDa).* ***Abbreviations:*** *n.i. - not investigated.*

2.3 LC-MS/MS on whole cell lysates reveal potential lysosomal and nuclear targets of HDAC10

In a parallel approach to the IP enrichment of HSP family members described in the previous section, whole cell lysates from BE(2)-C cells treated with HDAC6 inhibitor tubacin, HDAC6/10 inhibitor tubastatin A or solvent, were separated on 1D PAGE, followed by excision of small gel slices which were individually analyzed by LC-MS/MS (outlined in ***Figure 45a***). Although identification of HDAC10 specific acetylation sites in HSP70 were the primary aim of this screen, the mass range of gel slices was expanded to roughly 95 to 50 kDa, which allowed for screening for other potential HDAC10 downstream candidates (***Figure 45a***). As in the previous section, peptides with putative acetylation sites on lysines directly N-terminal of tryptic cleavage sites were omitted as false positives and excluded from further analysis. Moreover, true hits were sorted by peptide score (Mascot) by the DKFZ Proteomics Core Facility (Dr. Martina Schnölzer), omitting peptides with a score below 30. Both HDAC6 and HDAC6/10 inhibitor treated samples had a higher number of acetylated peptides than the DMSO group (***Figure 45b***). Duplicate peptides, i.e. peptides with identical sequence and posttranslational modification, were removed from each treatment group in order to yield lists where each specifically modified peptide was only represented once. Here, HDAC6 and HDAC6/10 inhibitor treated samples showed a similar number of acetylated peptides, which was only slightly increased compared to DMSO treated cells (***Figure 45b*** lower row). Analysis of overlapping peptides between treatment groups showed that 80 peptides overlapped between tubastatin A and tubacin treated samples, as well as 90 peptides that were identified in tubastatin A treated cells only (***Figure 45c***). More than half (44) of the 80 peptides shared between tubastatin A and tubacin treated samples also overlapped with DMSO control. Considering the fact that both tubastatin A and tubacin are excellent HDAC6 inhibitors (see ***Figure 12c***), the fraction of peptides specifically overlapping in these treatment groups (36) was comparably small (discussed in section ***F2***). Neither tubastatin A nor tubacin treated cells showed a strong increase in HSP70 or HSC70 peptides that were specifically acetylated under these conditions. In fact, only two HSP70 peptides were found differentially acetylated between treatment groups, namely K561 in DMSO treated cells and K77 in tubastatin A treated cells. This again suggested that these HSP70 family members were either no direct targets of HDAC6 or HDAC10, or that the approach was not suitable to properly detect acetylation on these proteins.

Treatment with tubastatin A causes lysosomal expansion and DNA double strand breaks (see sections ***E1.2*** and ***E1.10***). Thus, in a hypothesis driven approach, peptides that were specifically acetylated in the tubastatin A treated group were analyzed - in addition to HSP70 family - for candidate proteins that are involved in lysosomal homeostasis and the repair of DNA double strand breaks, respectively

(***Figure 45d***). Here, two peptides of subunit A of the vacuolar V-ATPase, which is responsible for acidification of lysosomes, were *de novo* acetylated after HDAC6/10 but not HDAC6 inhibitor treatment at two sites (K480, K506), and mutations introduced in this V-ATPase subunit in yeast have been associated with increased coupling efficiency of the V-ATPase complex (Shao et al. 2003; Owegi et al. 2006; Forgac 2007) (further discussed in section ***F1.1***). Moreover, tubastatin A treatment caused acetylation of Ku80 (XRCC5) at K443. Ku80 is a critical subunit of Ku70/Ku80 complex that initiates the repair of DSBS via NHEJ (Davis and Chen 2013). Lysine 443 lies within the central Ku core region that is important for DNA binding and Ku80 was reported to be differentially acetylated after application of pan HDAC inhibitors in a recent study (Robert et al. 2016). Although a specific site of lysine acetylation was not determined in the latter study, hyperacetylation of Ku protein was reported to impair DSB repair by NHEJ.

Although the above described data require validation in a biological replicate (see section ***F2***), it is conceivable that their function is critically regulated by HDACs. As acetylation at these sites occurred specifically after use of HDAC6/10 tubastatin A but not HDAC6 inhibitor tubacin, it is likely that deacetylation of these peptides was mediated by HDAC10 rather than HDAC6.

a

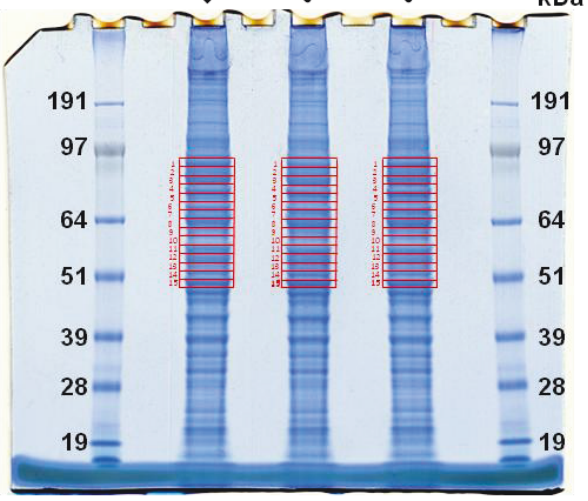

b

treatment	DMSO	tubastatin A	tubacin
number of acetylated peptides (score >30)	240	410	396
acetylated peptides without duplicates	119	179	185

c

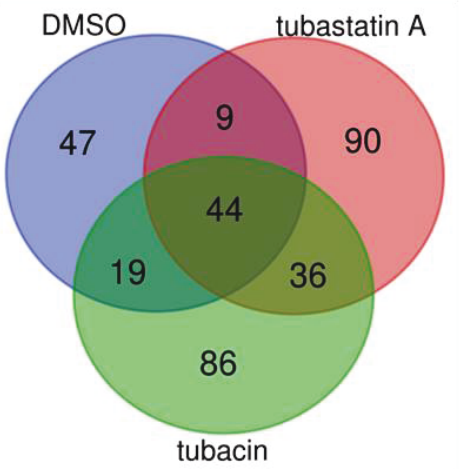

d

peptide sequence (acetylated lysine in red)	UniProt name	protein	acetylated site	peptide score
AKEILQEEEDLAEIVQLVGK	VATA/ATP6V1A1	V-ATPase subunit A	K480	88.04
ASLAETDKITLEVAK	VATA/ATP6V1A1	V-ATPase subunit A	K506	34.23
KYAPTEAQLNAVDALIDSMSLAK	XRCC5	X-ray repair cross-complementing protein 5 / Ku80	K443	84.22

Figure 45: LC-MS/MS on whole protein lysates from BE(2)-C cells after treatment with HDAC6 and HDAC6/10 inhibitors. ***(a)*** *Separation of whole cell lysates from BE(2)-C cells treated for 24h with HDAC6/10 inhibitor tubastatin A (7.5 µM), HDAC6 inhibitor tubacin (7.5 µM) and solvent (DMSO). Red boxes indicate target mass range and individually analyzed gel slices.* ***(b)*** *Number of acetylated peptides found after the respective treatment. Lower row gives number of acetylated peptides cleared of peptides with identical sequence and post translational modification.* ***(c)*** *Venn diagram depicting number of overlapping, acetylated, peptides between treatment groups.* ***(d)*** *A hypothesis driven approach looking for peptides only acetylated after treatment with HDAC6/10, which could be connected to enlargement of the lysosomal compartment (VATA) and impaired DNA damage repair (XRCC5), respectively.*

3 Generation of an HDAC10 antibody

Previous publications from our group have identified high HDAC10 expression as a risk factor in a sub-group high-risk neuroblastoma. The results collectively shown in previous sections (***E1***) further demonstrate that HDAC10 has a critical function in lysosomal homeostasis in a set of neuroblastoma cell lines and that interference with its function can sensitize chemoresistant neuroblastoma cells to chemotherapeutic agents such as doxorubicin (Oehme et al. 2013a). This makes HDAC10 an attractive target both for further mechanistic studies and clinical intervention, which require a high

quality antibody that allows for the analysis of subcellular localization, interaction partners and tissue expression, respectively. Such analyses are, however, drastically hampered by the poor quality of commercially available HDAC10 antibodies. This is highlighted by the fact that the most reliable of these antibodies (Sigma H3413) recognizes multiple bands on western blot (***Figure 46a***). Bands of higher molecular weight are unlikely to be HDAC10 isoforms, as the reported isoform2 has a slightly smaller molecular weight (69 kDa) than the predominantly expressed isoform 1 (roughly 71 kDa) due to the lack of an in-frame coding exons. Bands of smaller molecular weight most likely also did not represent isoform 2, as these bands did not fade upon HDAC10 knockdown even though HDAC10 siRNAs were designed to target both isoforms. Moreover, the commercial H3413 antibody is unspecific in immunofluorescence approaches (***Figure 46b***). Thus, a goal of this study was the generation of a highly specific, monoclonal HDAC10 antibody suitable for such purposes.

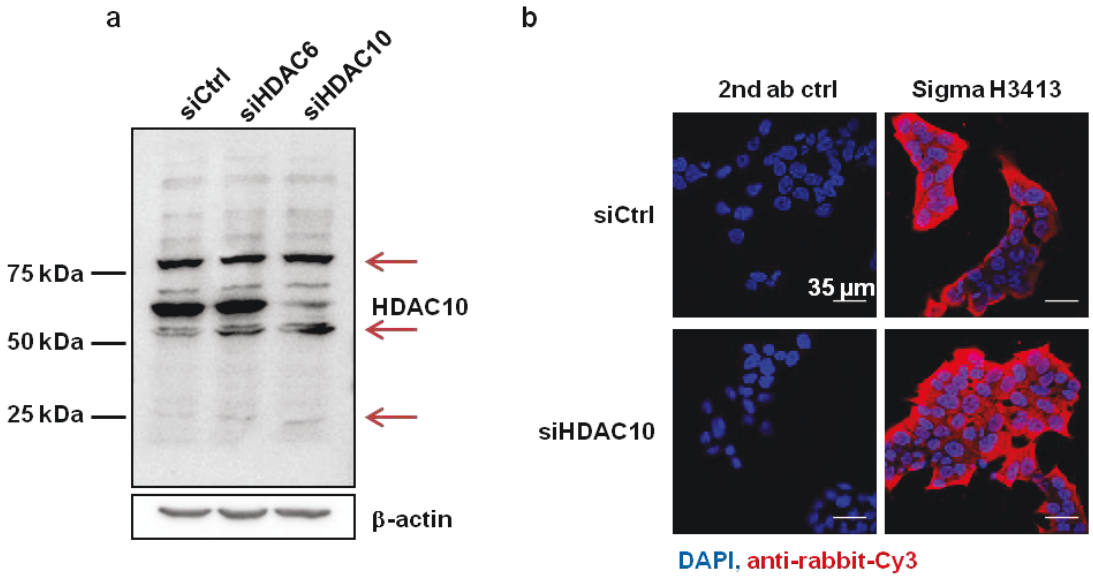

Figure 46: Characterization of the commercial Sigma H3413 polyclonal anti HDAC10 antibody. (a) *Specificity testing of the H3413 antibody via HDAC10 knockdown in BE(2)-C neuroblastoma cells 6d after siRNA transfection. Red arrows indicate off-target bands.* ***(b)*** *Immunofluorescence staining of BE(2)-C cells with the H3413 anti HDAC10 antibody 6d after transfection with siRNAs against HDAC10 and control siRNAs, respectively. Nuclei were counterstained with DAPI.*

3.1 Generation of a mouse monoclonal HDAC10 antibody

3.1.1 Selection of the HDAC10 immunization peptide and pipeline for testing of hybridoma supernatants

To generate HDAC10 reactive monoclonal antibodies, immunization of mice and hybridoma generation was performed as described in methods section ***C4.2*** by the monoclonal antibody facility (MAF) at the DKFZ, using a 6x histidine-tagged immunization peptide that included HDAC10 amino acids 501-617 (HDAC10T2, total length: 133 amino acids, see ***Table 51***) The respective fragment was

selected due to its comparably low amino acid sequence homology to other HDACs (***Figure 47a***). Unsurprisingly, the HDAC10T2 fragment was most homologous to the other class IIb HDAC member HDAC6, but alignment showed frequent amino acid mismatches, making a cross-reactivity of antibodies unlikely (***Figure 47b***). Cell culture supernatants from initial hybridoma clones which produced detectable amounts of IgG antibodies (ELISA performed by the MAF) were tested for HDAC10 reactivity on small western blot strips by transfer from preparative PAGE gels as outlined in ***Figure 47c***. IMR-32 cells stably transfected with HDAC10 or control plasmid were used as source for lysates, because IMR-32 do endogenously express low HDAC10 levels (***Figure 47d***). Initial western blot reactivity of hybridoma supernatants was tested on HDAC10 overexpressing IMR-32 cells only and reactive clones were counter-tested against empty vector transfected control cells in a second step.

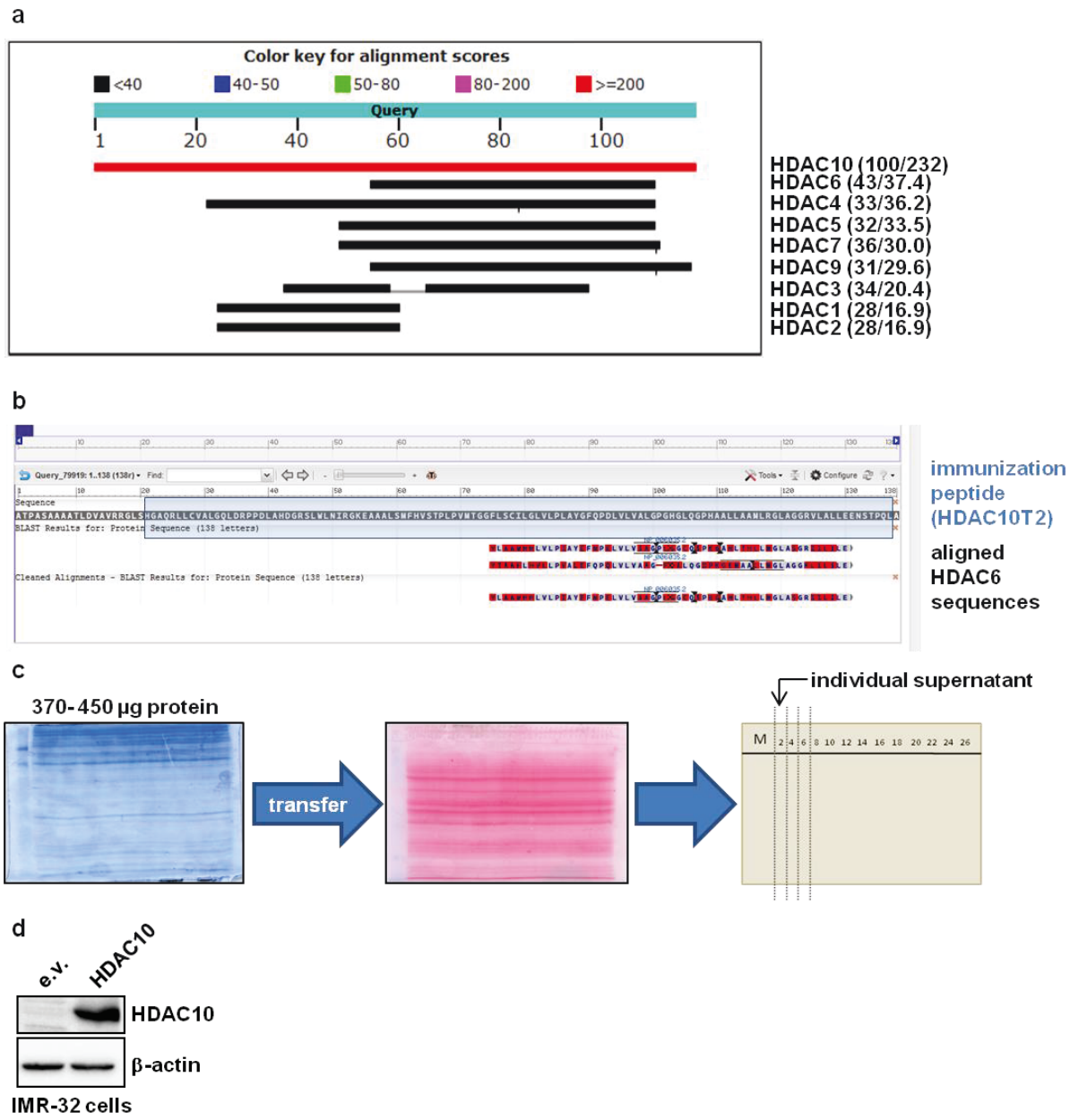

Figure 47: Selection of the HDAC10 immunization peptide and pipeline for western blot testing of hybridoma supernatants. (a) *A 133 amino acid peptide fragment including 117 amino acids of the c-terminal section of HDAC10 (amino acids 501-617) was selected for injection into mice due to its low homology to other HDACs (full sequence see* ***Table 51****). The peptide sequence was BLASTed search against other HDACs. Numbers in brackets indicate sequence identity (left) and maximum identity score (right) of the BLAST search.* ***(b)*** *BLAST alignment of HDAC6 sequences to the immunization peptide. Red color indicates mismatches.* ***(c)*** *Western blot pipeline for testing of hybridoma supernatants. 370 - 450 µg of protein lysate were added onto a preparative PAGE gel, transferred onto a pre-labeled PVDF membrane and cut into small membrane strips which were then incubated over night with undiluted hybridoma supernatants. Bound primary antibodies were detected with peroxidase-coupled anti mouse antibody.* ***(d)*** *Western blot showing expression of HDAC10 in IMR-32 cells stably transfected with HDAC10 expressing and control vector (e.v.), respectively.*

3.1.2 Identification of HDAC10 reactive mouse hybridoma clones via western blot

In total, 598 hybridoma parental cultures (numbered according their initial culture number regardless of ELISA reactivity) were identified as reactive against the HDAC10T2 peptide in initial ELISAs (performed by the MAF) and then tested via western blot using IMR-32 cells that stably expressed HDAC10. Of these 598 cultures, exactly 100 showed substantial reactivity against HDAC10 on western blot level, with a varying degree of reactivity and specificity. For example, the culture #477 displayed high reactivity against HDAC10 (***Figure 48a*** blue arrow), but also had significant activity against a protein of higher molecular weight (***Figure 48a*** red arrow). As this cross-reactivity also occurred in empty vector transfected, HDAC10 low-expressing IMR-32 cells, the second band was likely off-target activity or an HDAC10 isoform (example shown in ***Figure 52***). However, as known HDAC10 isoforms are smaller than the full-length protein, the latter was unlikely. Its strong reactivity made culture #477 interesting for subcloning and potentially antibody purification. Cultures #13, #17 (***Figure 48b***) and #50 (***Figure 48c***) also showed reactivity against HDAC10, which was lower compared to #477. However, in case of culture #13 and #17 off-target activity was completely absent. Thus, these two parental cultures were also selected for subcloning. The parental culture #1013 was of special interest as it showed very high HDAC10 reactivity and negligible off-target activity on western blot level, making it the most promising parental clone (***Figure 48d***). Unfortunately, this hybridoma ceased to produce IgGs even before initiation of subcloning, possibly due to overgrowth by non-producing hybridoma cells. Other cultures selected for subcloning and their fate over the course of the project are summarized in ***Figure 49a*** (section ***E3.1.3***).

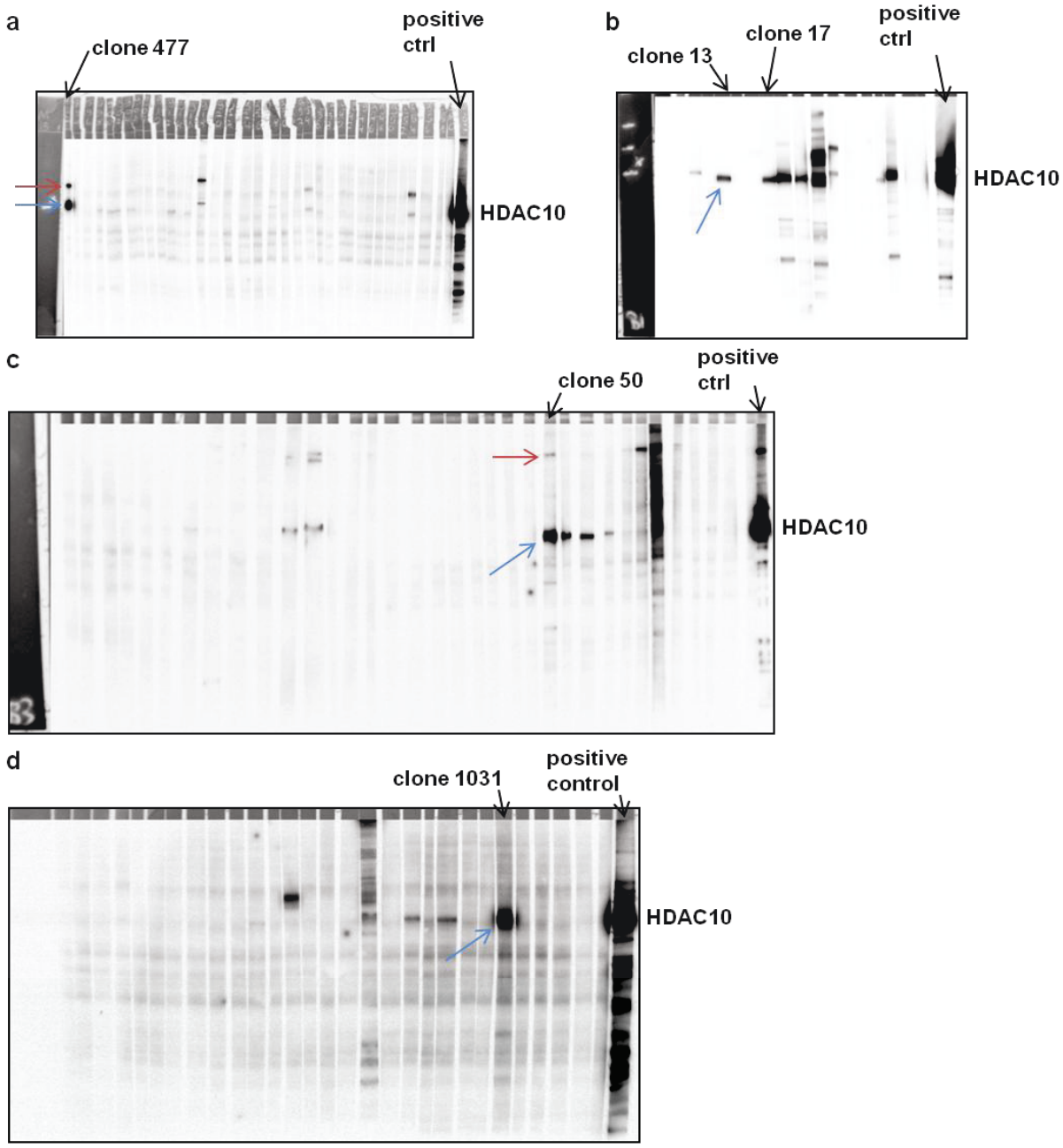

Figure 48: Testing of initial hybridoma cultures via Western Blot. *Undiluted hybridoma supernatants were tested on lysates from HDAC10 overexpressing IMR-32 cells. Examples of reactive parental clones 477* ***(a)****, 13 and 17* ***(b)****, 50* ***(c)*** *and 1013* ***(d)*** *are shown. Sigma H3413 polyclonal rabbit anti HDAC10 antibody (1 µg/ml) was used as positive control. Blue arrows indicate on-target activity, red arrows indicate off-target activity.*

3.1.3 Subcloning of hybridoma cultures and selection of hybridoma clones for clonal expansion

Initial hybridoma cultures consist of a mixed population of antibody producing and non-producing hybridoma cells, which carries the risk that non-producing cells overgrow the clones of interest, leading to an eventual loss of antibody production. Moreover, the initial cultures can contain more than one antibody-producing clone, potentially contaminating the antibody of interest and causing off-target activity. This problem can be overcome by seeding of individual hybridoma cells into 96-

well plates and clonal outgrowth (subcloning), which generates stable hybridoma cultures of identical cells that produce antibodies which bind to the same epitope (monoclonal antibodies).

Of the reactive hybridoma parental cultures described in section ***E3.1.2***, 27 were selected for at least one round of subcloning in order to shed non-producing cells or potential off-target activity in case that the off-target activity was not inherent to the HDAC10-recognizing antibody itself (summarized in ***Figure 49a***). In total, more than 400 supernatants from subclones and sub-subclones were tested. Of the 27 selected parental clones, 10 clones and their respective subclones had completely lost their reactivity against HDAC10 after subcloning, possibly by overgrowth of non-producing hybridoma cells (exemplary shown for clone 17 in ***Figure 49b***).

a

parental culture with reactive subclones	parental culture w/o reactive subclones
13	17
32	67
50	269
122	405
123	408
215	426
265	529
268	569
377	637
428	712
477	
492	
778	
795	
885	
889	
964	

b

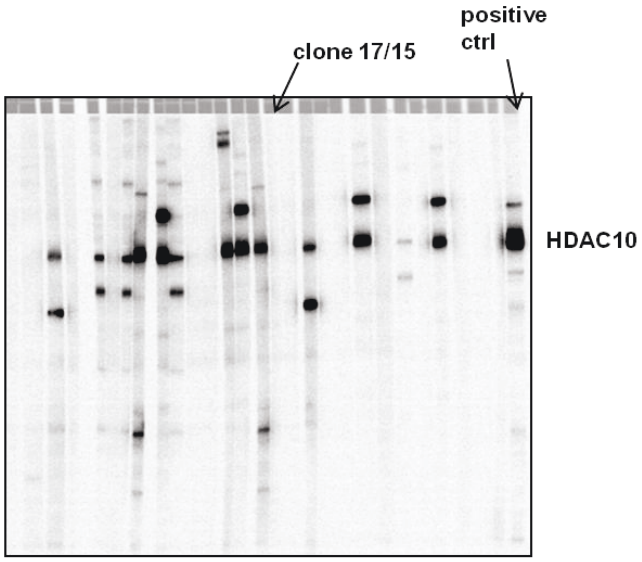

Figure 49: Subcloning of parental hybridoma cultures. (a) *Summary of western blot reactivity of subclones derived from parental hybridoma cultures. Undiluted hybridoma supernatants were tested on lysates from IMR-32 cells overexpressing HDAC10. At the stage of subcloning, several initially reactive clones and their subclones had lost reactivity.* ***(b)*** *Example of initially reactive clone 17, which lost HDAC10 reactivity at the stage of subcloning (17/15). Sigma H3413 polyclonal rabbit anti HDAC10 antibody (1 µg/ml) was used as positive control.*

Supernatants from the most promising subclones were tested on lysates from BE(2)-C neuroblastoma cells, which endogenously express HDAC10 at moderate levels, as well as on lysates from BE(2)-C cells that had been transfected with siRNAs against HDAC10. Here, many of the supernatants that reacted against overexpressed HDAC10 in IMR-32 cells failed to detect or only weakly detected endogenously expressed HDAC10 in BE(2)-C cells. These clones were not further considered for

clonal expansion or antibody purification. Supernatants of subclones from the #477 (***Figure 50a***) and #50 (***Figure 50b***) family commonly showed good reactivity against endogenously expressed HDAC10, although both of the above named clones had considerable reactivity against proteins of higher molecular weight, which did not fade in case of HDAC10 depletion. As reported HDAC10 isoforms have a smaller molecular weight than the full-length protein and because siRNAs were designed to target all HDAC10 isoforms, these bands were likely due to off-target activity (***Figure 50*** red arrows).

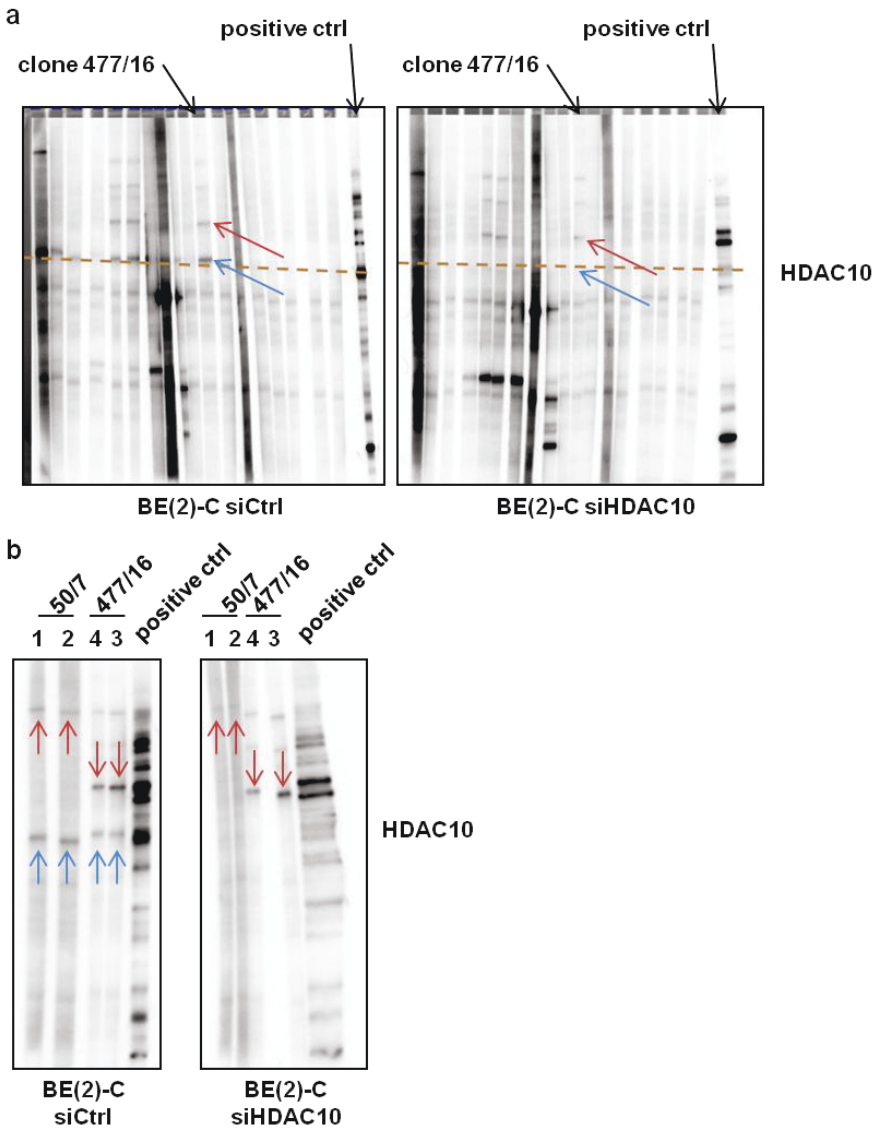

Figure 50: Testing of various subclones for reactivity against endogenously expressed HDAC10 in BE(2)-C cells. ***(a)*** *Undiluted hybridoma supernatant were tested on lysates from BE(2)-C cells transfected with HDAC10 and control siRNAs, respectively. Lysates were generated 6d after siRNA transfection. Subclones of the 477 clone (e.g. 477/16) showed good on-target activity (blue arrow) but also significant off-target activity at a higher molecular weight (red arrow). On target activity disappeared upon HDAC10 knockdown.* ***(b)*** *Testing of sub-subclones of the 50/7 and 477/16 family. Numbers below the subclone name indicate sub-subclone number. Blue and red arrows indicate on-target and off-target activity, respectively. Sigma H3413 polyclonal rabbit anti HDAC10 antibody (1 µg/ml) was used as positive control.*

3.1.4 Evaluation of the potential suitability of the 477/16/13 and 50/7/1 clones for immunofluorescence and immunohistochemistry

Of the #50 and #477 hybridoma family, subclones 50/7/1 and 477/16/3 were selected for hybridoma expansion and antibody purification, as they showed comparably good reactivity and signal-to-noise ratio in on endogenously expressed HDAC10 (see section ***E3.1.3***). During expansion, the 50/7/1 clone looked particularly promising and repeatedly displayed good reactivity against HDAC10 with limited off-target activity (***Figure 51a***). Undiluted supernatants from both clones were further able to specifically detect overexpressed HDAC10 in IMR-32 cells both in confocal immunofluorescence and in paraffin-embedded cells, showing their potential suitability for these approaches (***Figure 51b, c***). Immunofluorescence analysis on IMR-32 cells revealed that HDAC10 was not only localized in the cytoplasm but also in the nucleus, even though HDAC10 is thought to be a cytoplasmic HDAC due to the presence of nuclear export signals (NES) (Tong et al. 2002).

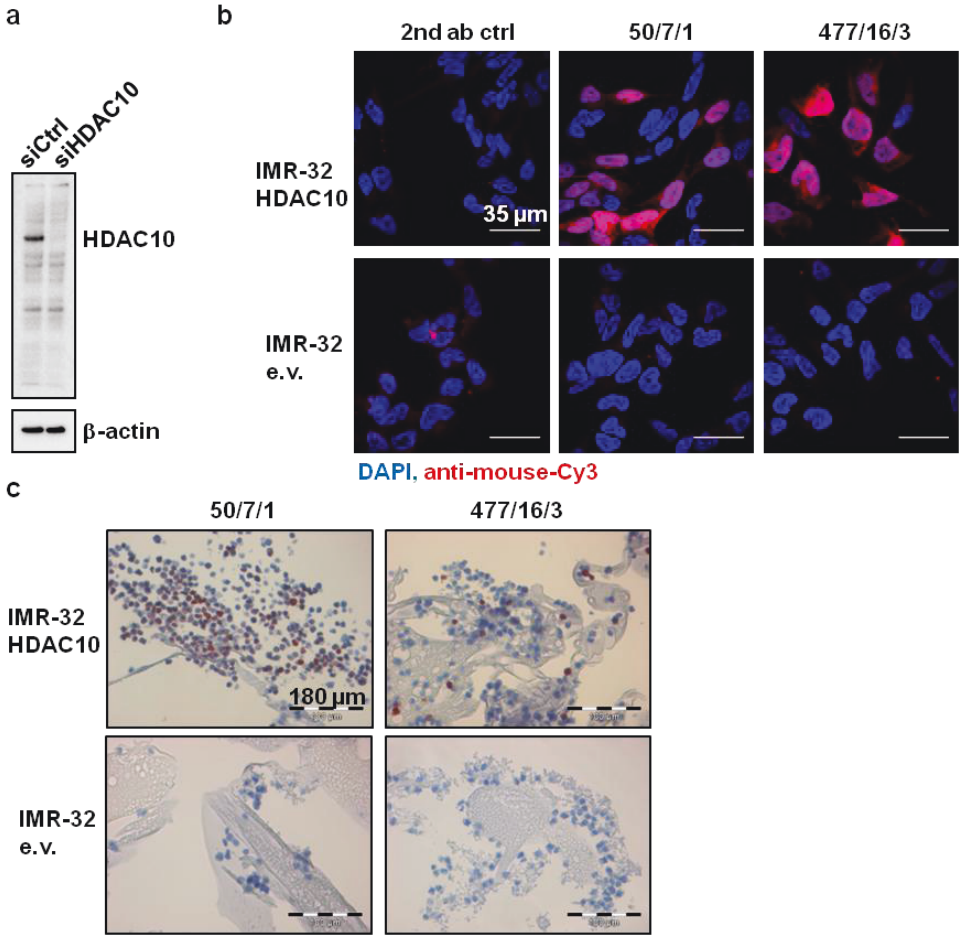

Figure 51: Testing of the 50/7/1 sub-subclone during clonal expansion. (a) *Testing of undiluted hybridoma supernatant via western blot on lysates from BE(2)-C cells transfected with HDAC10 siRNA and control siRNA, respectively. Lysates were generated 6d after siRNA transfection* ***(b)*** *Testing of undiluted 477/16/3 and 50/7/1 supernatants via confocal immunofluorescence microscopy using HDAC10 overexpressing IMR-32 cells and control cells.* ***(c)*** *HDAC10 expressing and control transfected IMR-32 cells were embedded into paraffin in order to test undiluted hybridoma supernatants in an immunohistochemistry setting. Embedding and staining of cells was performed by Dr. Marcus Renner (Heidelberg University Hospital).*

Protein G affinity based purification of antibodies from the 477/16/3 clone did not substantially alter off-target activity on western blot, suggesting that off-target activity was inherent to the HDAC10-reactive antibody itself (***Figure 52a***). Although previous immunofluorescence experiments with 477/16/3 hybridoma supernatant on HDAC10 overexpressing IMR-32 cells suggested potential suitability of this antibody for immunofluorescence approaches, this was not confirmed when purified 477/16/3 antibody was used for the staining of endogenous HDAC10 in BE(2)-C cells, as no differential staining was observed in siCtrl versus siHDAC10 transfected cells (***Figure 52b***).

In marked contrast to antibodies purified from 477/16/3 hybridoma cultures, purified antibodies of the 50/7/1 clone unexpectedly displayed strong off-target activity (***Figure 52c***) . Direct comparison of purified antibodies (50/7/1_03_15#1 and 50/7/1_03_15#2) with the respective source hybridoma supernatant revealed that off-target activity was strongly enriched in case of purified antibodies, suggesting potential enrichment of a secondary, off-target, antibody.

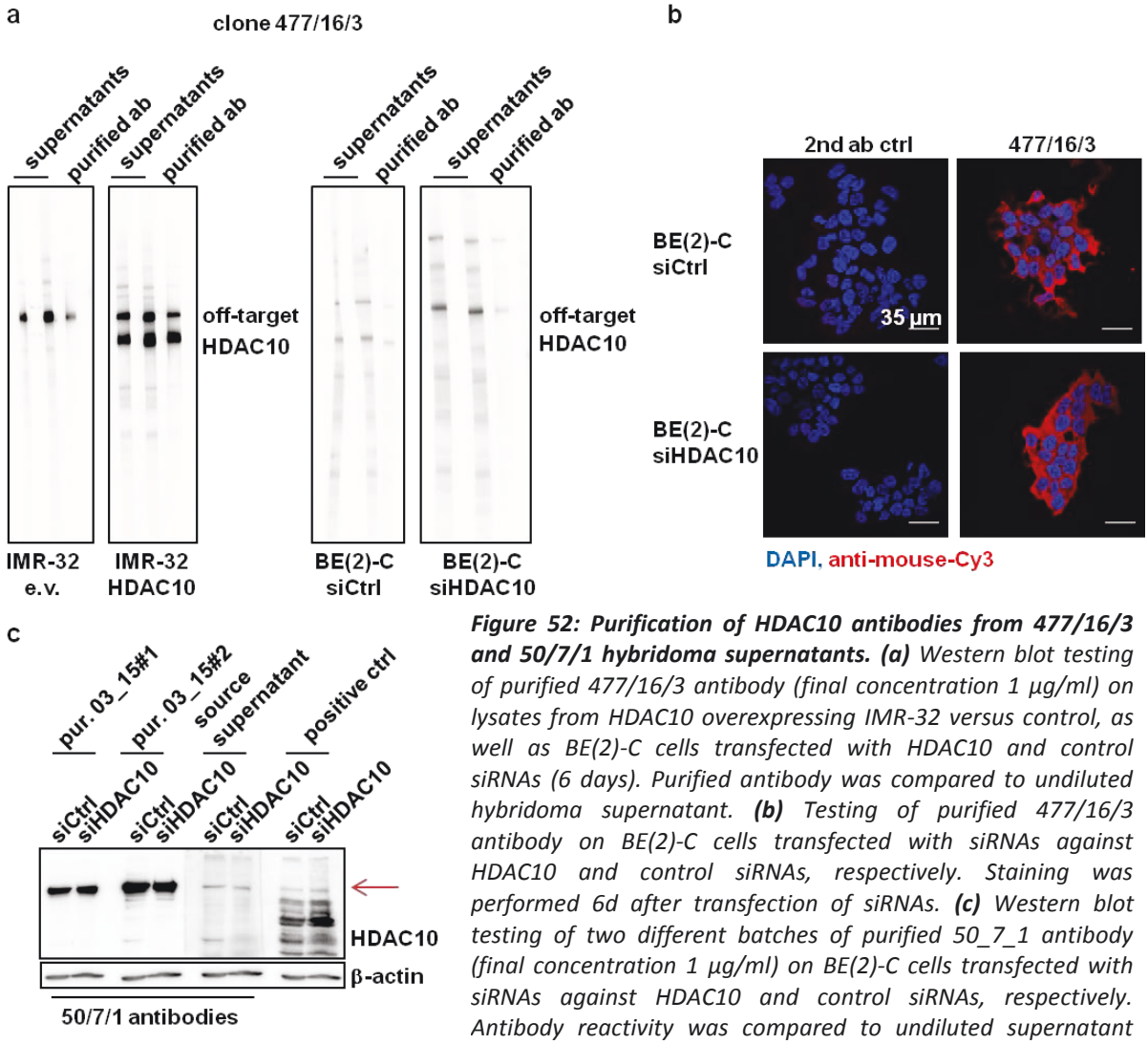

Figure 52: Purification of HDAC10 antibodies from 477/16/3 and 50/7/1 hybridoma supernatants. (a) *Western blot testing of purified 477/16/3 antibody (final concentration 1 µg/ml) on lysates from HDAC10 overexpressing IMR-32 versus control, as well as BE(2)-C cells transfected with HDAC10 and control siRNAs (6 days). Purified antibody was compared to undiluted hybridoma supernatant.* ***(b)*** *Testing of purified 477/16/3 antibody on BE(2)-C cells transfected with siRNAs against HDAC10 and control siRNAs, respectively. Staining was performed 6d after transfection of siRNAs.* ***(c)*** *Western blot testing of two different batches of purified 50_7_1 antibody (final concentration 1 µg/ml) on BE(2)-C cells transfected with siRNAs against HDAC10 and control siRNAs, respectively. Antibody reactivity was compared to undiluted supernatant used for purification (source supernatant). Sigma H3413 antibody was used as positive control. Red arrow indicates off-target activity, which was markedly increased after purification. Nuclei were counterstained with DAPI.*

3.1.5 Different batches of purified 50/7/1 antibody reveal that off-target activity of this clone depends on hybridoma batch but is likely not due to contamination with a secondary clone

After initial antibody purifications of the 50/7/1 clone had been unsatisfactory due to a strong increase in antibody off-target activity (see section ***E3.1.4***), various batches of 50/7/1 hybridoma cells were defrosted and taken into culture. Intriguingly, one of these batches completely lacked off-target activity and only detected the HDAC10 band on western blot (***Figure 53a***). When the respective blot was re-probed with previous batches of purified 50/7/1 antibody, the off-target band observed in section ***E3.1.4*** was readily detected, excluding that the absence of the off-target band was due to poor blotting or due to absence of the respective off-target protein in these lysates (***Figure 53a***). Purified 50/7/1 antibody that was immediately isolated from the above described hybridoma batch ("50/7/1_05/15") also completely lacked off-target activity, while the on-target HDAC10 band was comparable to previous 50/7/1 antibody batches (***Figure 53b***). Therefore, off-target activity of the 50/7/1 antibody was probably not inherent to the HDAC10-recognizing antibody itself but more likely caused by production of a second, unspecific, antibody, possibly due to contamination with a secondary hybridoma clone.

Purified antibody from the 50/7/1_05_15 batch allowed for the detection of endogenous HDAC10 in BE(2)-C via confocal microscopy (***Figure 53c***). Similar to the results obtained for overexpressed HDAC10 in IMR-32 cells, endogenous HDAC10 was preferably localized in the nucleus and cytoplasm of BE(2)-C cells. RNAi mediated knockdown confirmed that the detected signal was HDAC10, as it slightly but visibly decreased staining intensity. These results demonstrated the full potential of antibodies from the 50/7/1 hybridoma clone in case that off-target activity can be durably eliminated.

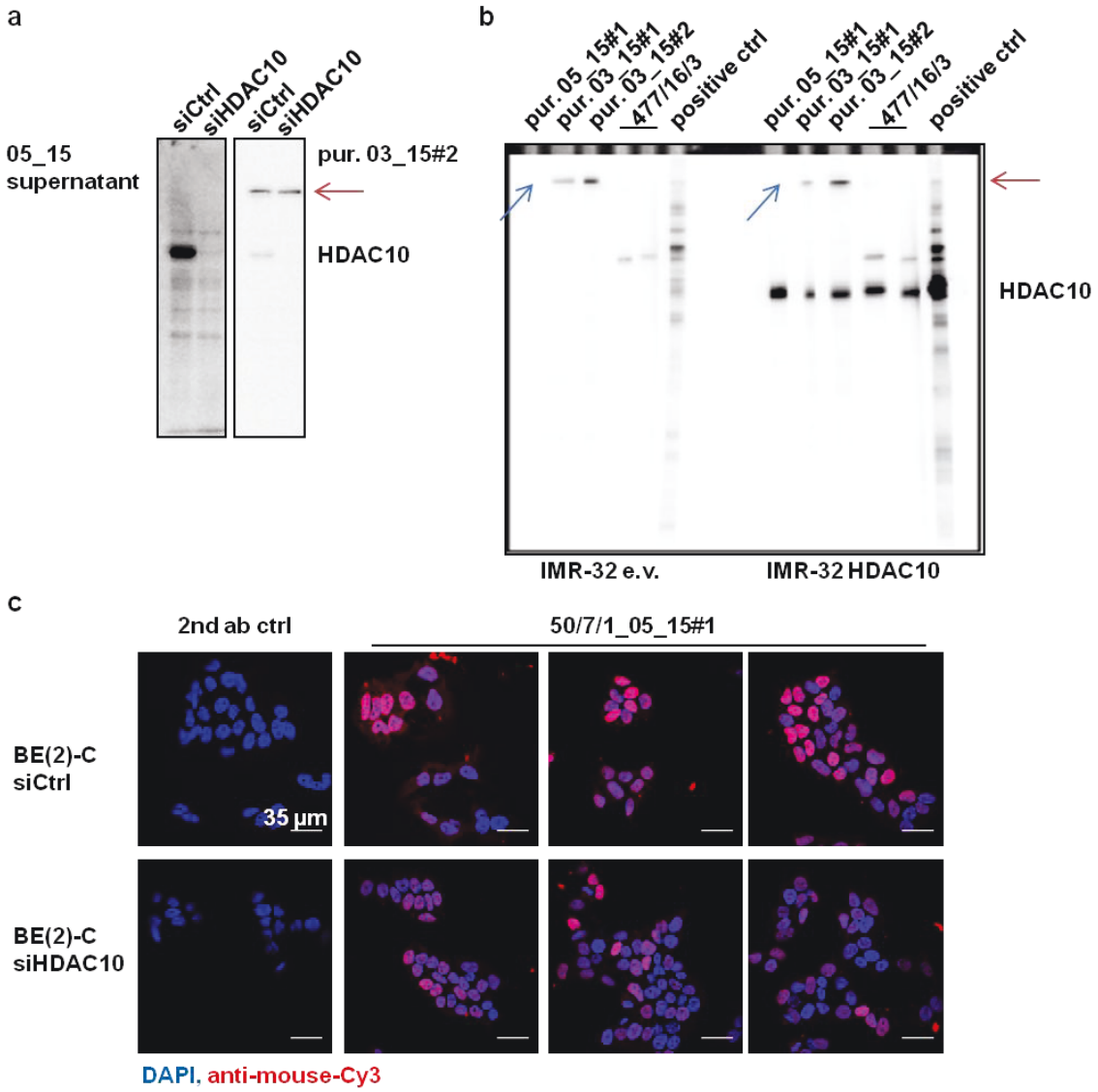

Figure 53: Comparison of various batches of purified 50/7/1 antibody. (a) *Supernatant from 50/7/1 cells that lacked secondary reactivity (05_15) was tested on BE(2)-C cells transfected with HDAC10 siRNA and control siRNA, respectively. The blot was re-incubated with 1µg/ml purified 50/7/1 antibody (03_15) which nearly exclusively displays off-target reactivity (right panel).* ***(b)*** *50/7/1 antibody purified from supernatants without secondary reactivity (05_15#1) was compared to previous 50/7/1 purifications (03_15#1 and 03_15#2) and antibodies from the 477/16/3 hybridoma HDAC10 overexpressing and control transfected IMR-32 cells. Sigma H3413 antibody was used as HDAC10 positive control. Antibodies were used at a concentration of 1 µg/ml.* ***(c)*** *186 µg/ml of 50/7/1 purified antibody 05_15#1 was used on PFA-fixed cells transfected with HDAC10 siRNA and control siRNA, respectively.*

In an attempt to exclude re-occurrence of off-target reactivity, the 50/7/1 culture lacking off-target activity was subjected to an extra round of subcloning. Paradoxically, subcloning caused the recurrence of off-target activity in all tested sub-subclones (***Figure 54a***). Consequently, antibodies purified from these supernatants (termed 50/7/1/7) also displayed off-target activity (***Figure 54b***).

In summary, multiple rounds of subcloning failed to isolate 50/7/1 clones with stable on-target and no off-target activity. It is unlikely that the 50/7/1 hybridoma clone is contaminated with a secondary hybridoma clone. At the same time, it is also unlikely that off-target activity is inherent to the

HDAC10-reactive antibody itself, as distinct antibody batches lacked off-target while retaining on-target activity (***Figure 54b***).

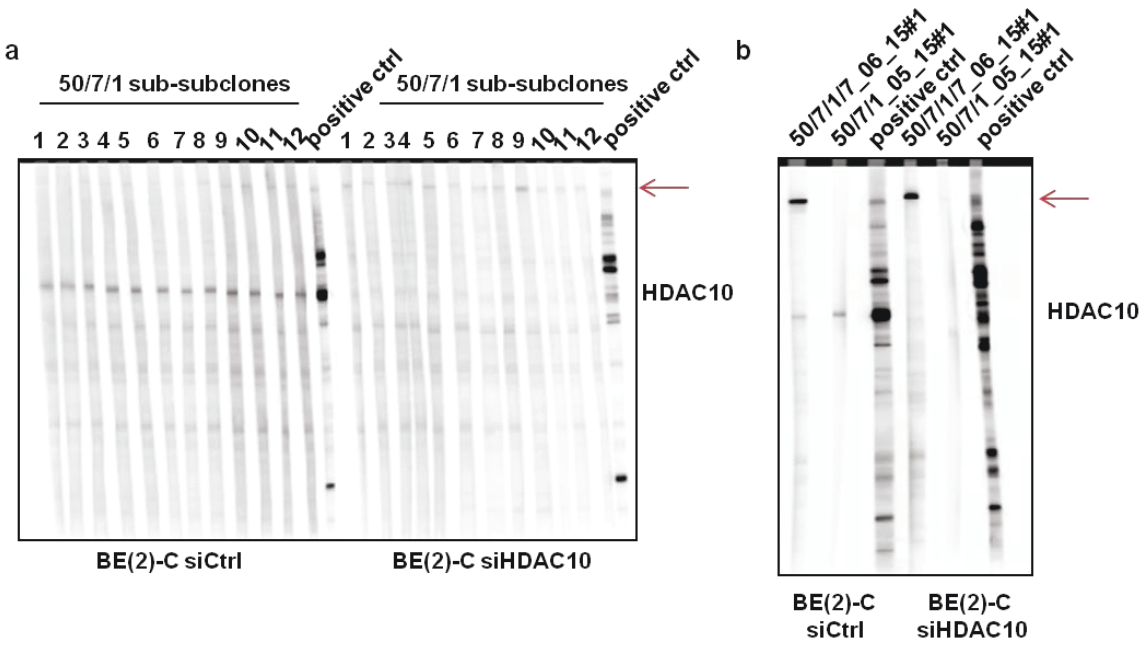

Figure 54: Sub-subcloning of 50/7/1 hybridoma batches that initially lacked off-target activity. (a) *Western blot testing of 12 sub-subclones of the 50/7/1 hybridoma batch that lacked off-target activity after defrosting. Sub-subcloning paradoxically caused recurrence of off-target activity in all tested sub-subclones.* ***(b)*** *Direct comparison of purified antibodies from sub-subcloned 50/7/1/7 cultures (50/7/1/7_06_15#1) with a purified 50/7/1 antibody batch that lacked off-target activity (50/7/1_05_15#1) on western blot. Antibodies were tested on lysates from BE(2)-C cells transfected with siRNAs against HDAC10 or control siRNAs. Both antibody batches were used at a final concentration of 1 µg/ml. Red arrow indicates off-target activity.*

3.1.6 The 50/7/1 hybridoma clone is potentially unstable

Continuous culturing of the 50/7/1 hybridoma clone caused the loss of off-target activity of the 50/7/1 hybridoma culture. However, clones lacking off-target activity were unstable and gradually also lost on-target reactivity (***Figure 55a***). Attempts to purify antibody from 50/7/1 cultures that had residual on-target reactivity and completely lacked off-target reactivity remained unsuccessful (***Figure 55b***). In this case, purified antibodies lacked reactivity even when used at the same or at higher concentrations than previously purified antibodies (2 µg/ml).

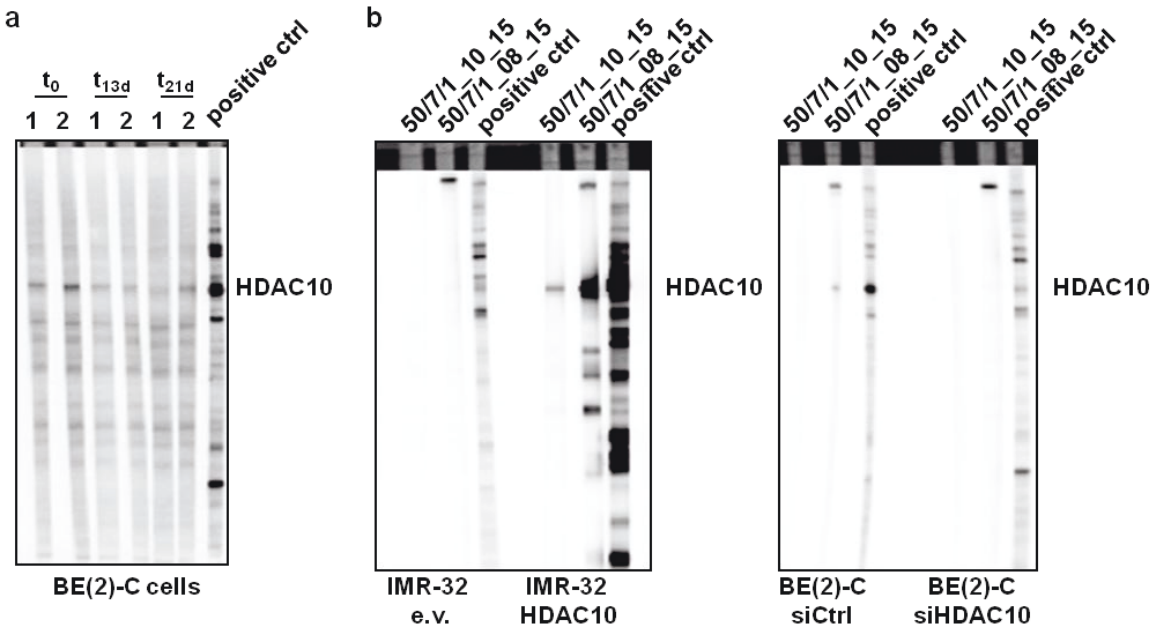

Figure 55: The 50/7/1 hybridoma clone can lose antibody productivity over longer periods of cultivation. (a) *Antibody productivity of 50/7/1 cells was assessed on western blot level using lysates of BE(2)-C cells. Supernatants from 50/7/1 hybridoma clones either cultivated at low* ***(1)*** *or high* ***(2)*** *confluency were collected at indicated timepoints after an arbitrarily set time point zero (t_0). Sigma H3413 HDAC10 antibody was used as positive control* ***(b)*** *Supernatants from around t_{21d} were collected, used for antibody purification (50/7/1_10_15) and tested on lysates from IMR-32 cells overexpressing HDAC10, as well as BE(2)-C cells with HDAC10 knockdown. HDAC10 reactivity was compared to earlier 50/7/1 purifications (in this case 50/7/1_08_15) as well as to the Sigma H3413 antibody (positive control). 50/7/1 antibodies were at used at a concentrations of 2 µg/ml.*

3.1.7 Purification of antibodies from alternative hybridoma clones and clones that should be considered for future re-testing

Due to the unsatisfactory quality and batch-to-batch variability of HDAC10 antibodies from the 50/7/1 hybridoma clone, a subset of alternative hybridoma clones was re-taken into culture and re-tested via western blot on lysates from cells overexpressing HDAC10, as well as on lysates from BE(2)-C cells with moderate HDAC10 expression. Empty vector transfected IMR-32 cells and BE(2)-C cells with RNAi-mediated HDAC10 knockdown were used as respective controls. In total, 10 clones were re-thawed, including parental hybridoma cultures (263, 428, 964, 17, 58, 885), as well as sub or sub-subclones (32/1, 13/1/6/1, 885/1/20) (***Figure 56***). With the exception of clone 17, which had been shown to be unstable before (***Figure 49b***), clones showed good reactivity and relatively good specificity on IMR-32 lysates with HDAC10 overexpression (***Figure 56*** left panel). However, most clones did show very limited reactivity against endogenously expressed HDAC10 in BE(2)-C cells, with the exception of clone 428, 13/1/6/1 and, to a limited extent, 885/1/20. As clone 428 showed high cross-reactivity to non-HDAC10 bands, it was excluded from antibody purification (***Figure 56*** right panel).

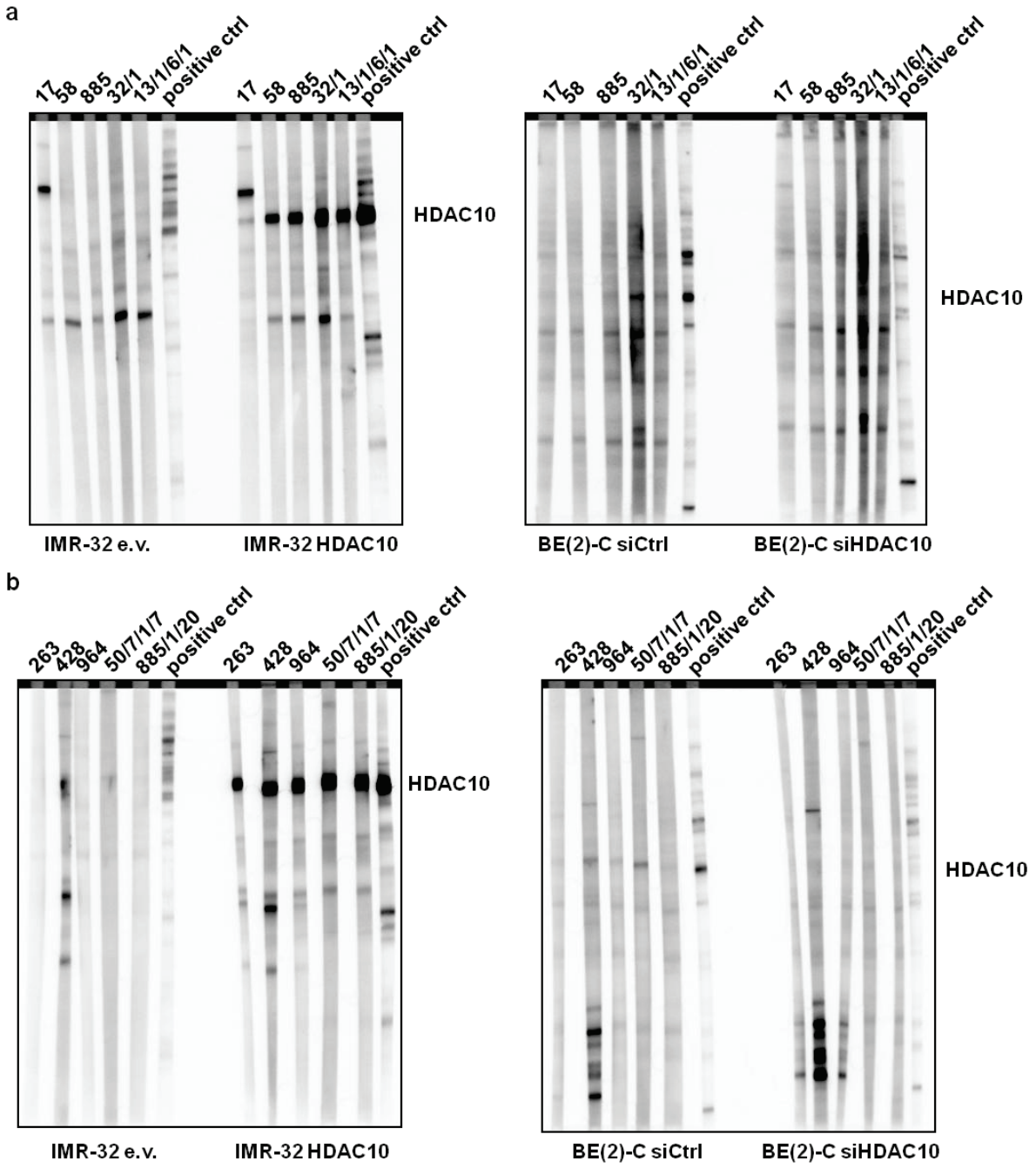

Figure 56: Testing of supernatants of defrosted alternative hybridoma clones. (a, b) *Suitability of various alternative hybridoma clones for antibody purification was assessed on western blot level using lysates from IMR-32 overexpressing HDAC10 (left panel) and BE(2)-C cells with HDAC10 knockdown (right panel). Sigma H3413 commercial HDAC10 antibody was used as positive control.*

When used at 1 µg/ml, purified 13/1/6/1 and 885/1/20 antibodies displayed little to no reactivity even towards overexpressed HDAC10, let alone towards endogenously expressed HDAC10 (***Figure 57a***). This suggested that either affinity of these antibodies towards HDAC10 was low or that antibody purifications were contaminated with undesired protein.

Alternative clones such as 22, 198, 256, 275 and 917 should be considered for re-testing. Here, especially clone 917 showed very high reactivity towards overexpressed HDAC10 (***Figure 57b***).

Although showing significant cross-reactivity towards proteins other than HDAC10, which likely makes it unusable for immunofluorescence or immunohistochemistry, this clone could still yield antibodies with high sensitivity on western blot level.

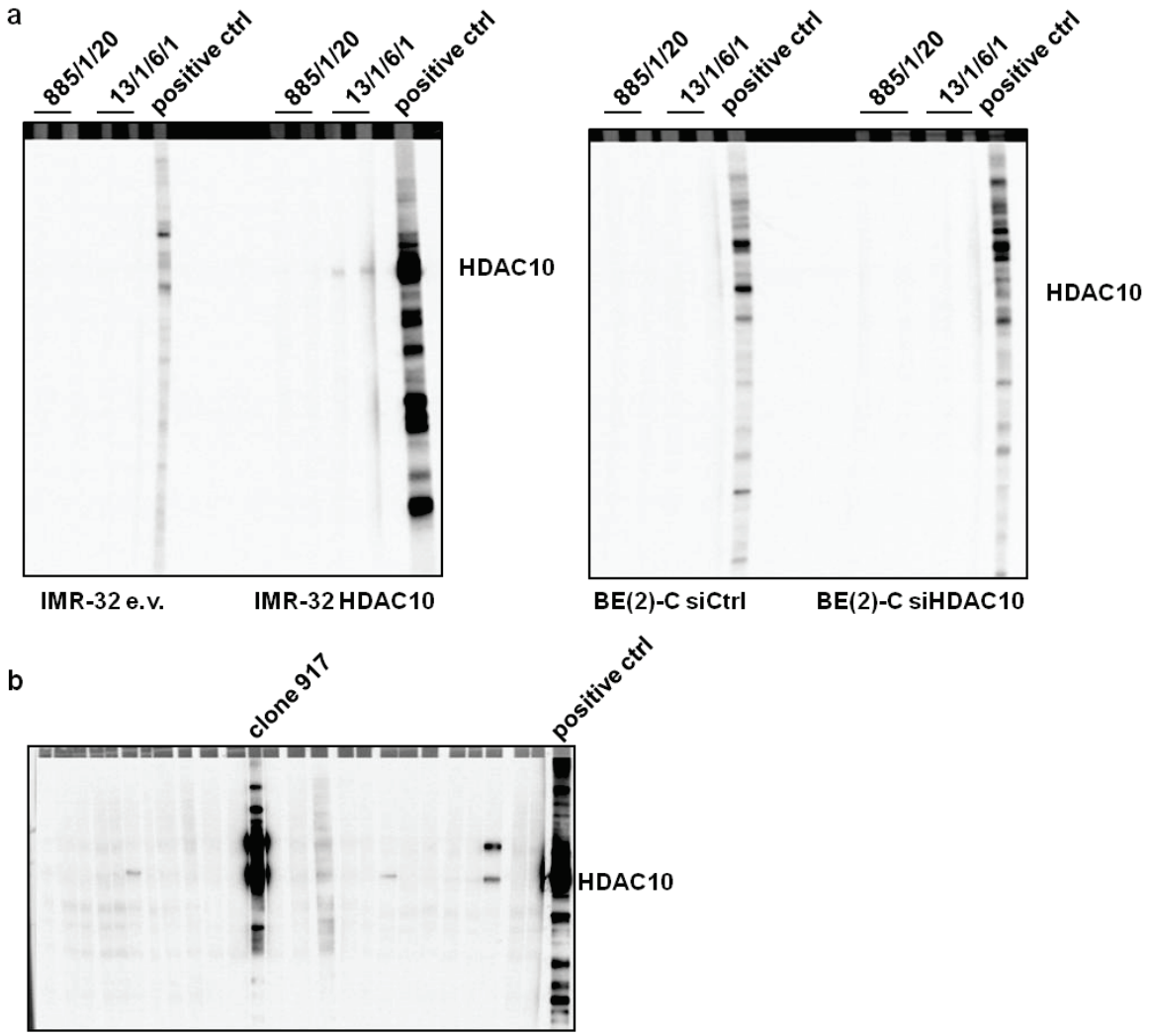

Figure 57: Purification of antibodies from 885/1/20 and 13/1/6/1 clones. (a) *885/1/20 and 13/1/6/1 antibodies purified from supernatants of the respective hybridoma clones were tested on western blot level using lysates from HDAC10 overexpressing IMR-32 cells and BE(2)-C cells with HDAC10 knockdown, respectively. Sigma H3413 commercial HDAC10 antibody was used as positive control.* ***(b)*** *Alternative clones (exemplary shown for clone 917) should be considered for future antibody purifications. Although hybridoma culture showed significant off-target activity, its strong reactivity could make it a useful source for a highly reactive western blot antibody. Sigma H3413 commercial HDAC10 antibody was used as positive control.*

3.2 Alternative approaches to generate an HDAC10 antibody

3.2.1 Generation of a commercial rabbit polyclonal HDAC10 antibody using short peptide epitopes

Since production of a monoclonal HDAC10 antibody could not be successfully completed, an attempt was made to generate a polyclonal HDAC10 antibody in rabbits with the help of the "speedy 28-day polyclonal protocol" provided by Eurogentec. Although polyclonal antibodies have clear

disadvantages like batch-to-batch variability or the presence of non-specific antibodies in sera of immunized animals, they can be produced quicker and cheaper than monoclonal antibodies, as production of the former bypasses cultivation of hybridoma cells and complex screening procedures. Moreover, unspecific antibodies can be in part circumvented by the injection of short peptide immunogens that recognize unique epitopes on the protein of interest and by purification of antibodies via immobilized injection peptide.

Of the eleven potential short injection peptide sequences provided by Eurogentec, two 15 amino acid peptides (P1610192 and P1610193) with the least amount of cross-reactivity to other human proteins in BLAST searches were selected. These were coupled to KLH as carrier protein (5 mg) and injected into two rabbits (SY7749 and SY7750). All peptide sequences provided by Eurogentec showed at least five sequential amino acids that were identical to other human peptides or proteins (***Figure 58a***). Eurogentec performed the coupling of the immunogens to KLH, animal immunization, ELISA-testing of animal sera against the immunogens, as well as purification of the antibodies against the respective peptides. Serum from one of the immunized animals (SY7749) that displayed higher antibody titers was used for purification. Two batches of purified antibodies were generated by affinity binding against either of the injection peptides (***Figure 58b***).

Purified antibodies, as well as sera from both immunized animals were tested on western blot using lysates from IMR-32 cells overexpressing HDAC10 and the respective empty vector control cells (***Figure 58b, c***). Here, all sera showed lacked reactivity against HDAC10 and showed cross-reactivity to other proteins. Only, in case of purified antibodies from rabbit SY7749, slight reactivity against HDAC10 was observed when antibodies were used at a concentration of 1 µg/ml (***Figure 58b***). At higher concentrations (5 µg/ml), both purified antibodies showed detectable but weak reactivity towards HDAC10, and, in case of antibody 1610192, also considerable cross-reactivity to other proteins (***Figure 58d***).

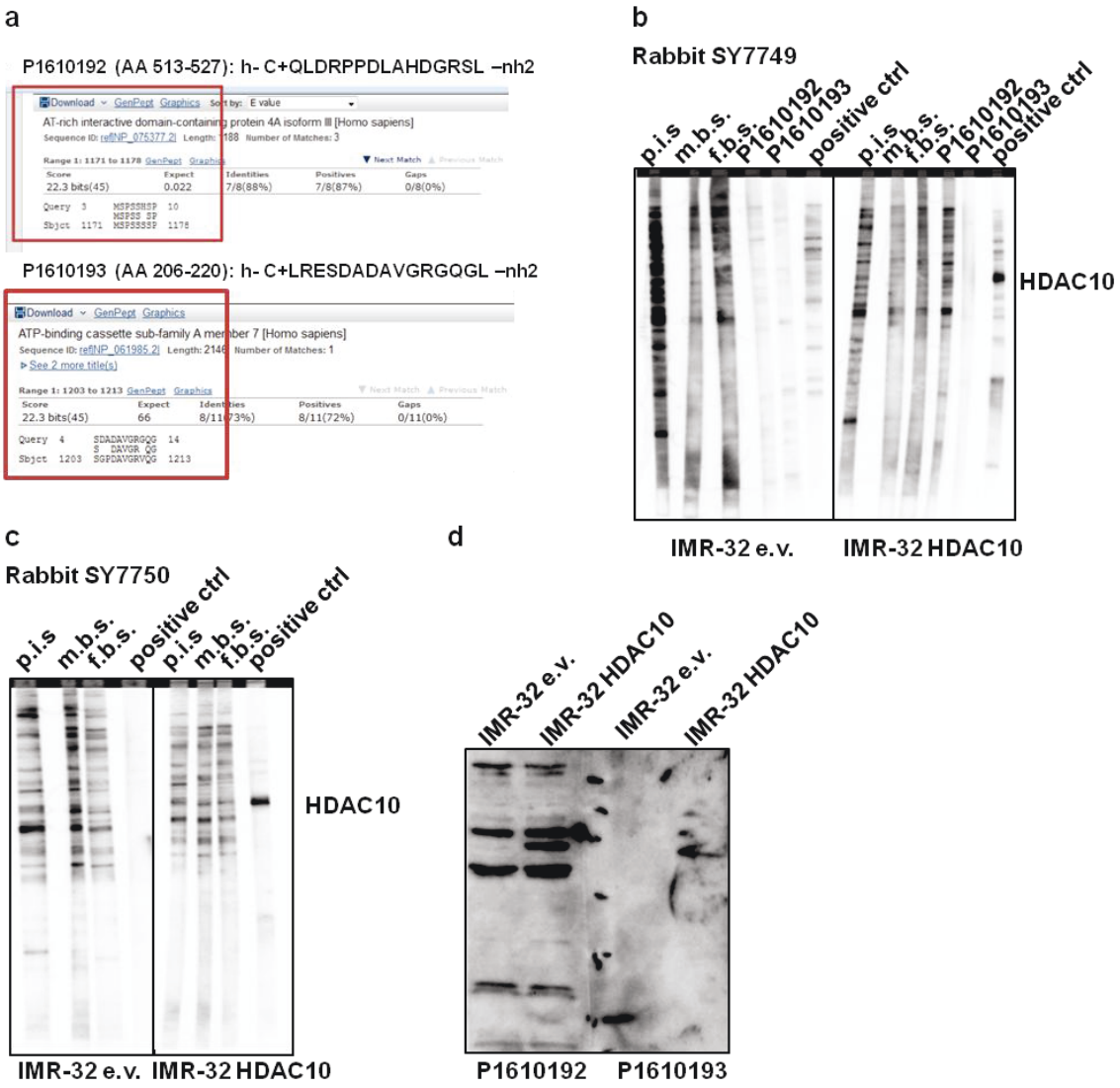

Figure 58: Testing of commercially generated HDAC10 antibodies, as well as immune sera from immunized animals. (a) *Selection of two 15 amino acid peptides for co-injection into two rabbits. Peptides that showed lowest cross-reactivity to other proteins on BLAST search were selected for coupling to KLH and injection into animals. Notably, no peptide of choice showed less than five sequential amino acids identical to other human proteins.* ***(b)*** *Western blot testing of sera and purified antibodies(P1610192, P1610193) from immunized rabbit SY7749 on lysates from IMR-32 cells overexpressing HDAC10 and empty vector transfected cells, respectively. Antibodies were purified separately against the immunization peptides P1610192 and P1610193 and used at a final concentration of 1 µg/ml. Sigma H3413 commercial HDAC10 antibody was used as positive control.* ***(c)*** *Western blot testing of sera from immunized rabbit SY7750. Sera from this rabbit did not undergo purification. Sigma H3413 commercial HDAC10 antibody was used as positive control* ***(d)*** *Western blot testing of purified antibodies from rabbit SY7749 at higher concentrations (5 µg/ml) on IMR-32 cells with HDAC10 overexpression or empty vector transfected control cells.* ***Abbreviations:*** *p.i.s. - pre-immune serum; m.b.s. - medium bleed serum; f.b.s. - final bleed serum.*

To test whether either purified antibody was useful for IF/IHC approaches, they were tested at various concentrations in immunofluorescence using paraformaldehyde-fixed HDAC10 transfected IMR-32 cells and empty vector transfected control cells. Here, both antibodies failed to differentially stain empty vector versus HDAC10 transfected IMR-32 cells and were thus considered as unspecific in an immunofluorescence setting (***Figure 59***). Moreover, the presence of highly-fluorescent artifacts

in the stainings hinted at the presence of impurities or aggregated antibodies. Therefore, the attempt to generate polyclonal rabbit antibodies against HDAC10 remained unsuccessful.

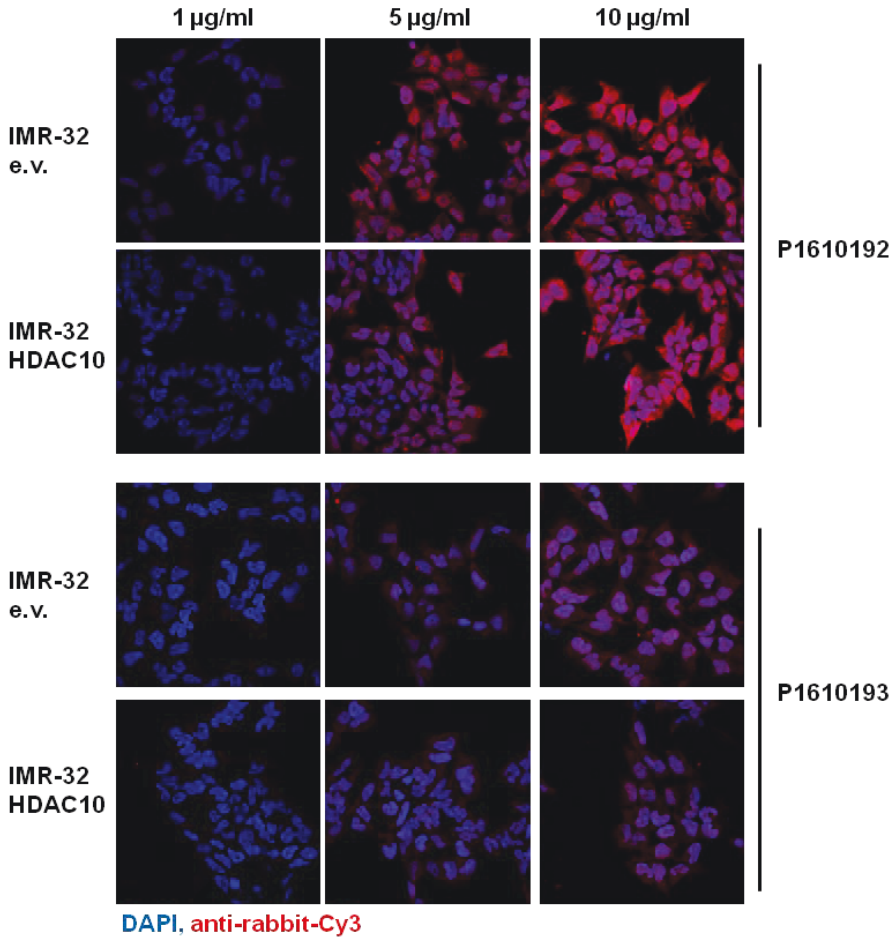

Figure 59: Assessing suitability of purified antibodies from immunized rabbit SY7749 for immunofluorescence analysis. *Various concentrations of antibodies purified from final bleed serum of rabbit SY7749 against the immunization peptides P1610192 and P1610193 were used to stain IMR-32 cells overexpressing HDAC10 and control transfected cells, respectively. Nuclei were counterstained with DAPI.*

3.2.2 Testing of potential HDAC10 antibodies generated by antibody phage display

Alternative to the classical way, which involves injection of an antigen into and isolation of B-cells from immunized animals, monoclonal antibodies can be generated without the use of animals via so called antibody phage display (see methods section ***C4.3***). Two linearized HDAC10 fragments (HDAC10T1 and HDAC10T2 in 8M Urea, see ***Table 51*** and methods section ***C4.1***), the latter of which was used to generate HDAC10-reactive mouse hybridoma clones (see section ***E3.1***), were used for testing against the human antibody phage libraries display libraries HAL9/10 (Kugler et al. 2015) in the lab of Dr. Michael Hust (TU Braunschweig). Panning revealed four clones reactive against the HDAC10T1 fragment, while no HDAC10T2 reactive clones were identified (data not shown). Titration ELISA assays of the four clones (performed by Saskia Helmsing, TU Braunschweig) showed binding of

these clones to HDAC10T1, but not to the negative control (BSA) or the HDAC10T2 fragment (***Figure 60a***). Here, especially clone C12 showed promisingly high affinity towards HDAC10T1. After recloning of the reactive VH and VL genes into the pCSE2.6-mIgG2a-Fc-XP plasmid, thus generating scFv-Fc fusion genes with a murine IgG2a Fc fragment (scFV-Fc antibody), antibody plasmids were ectopically expressed in Expi293F™ cells, followed by purification of scFV-Fc antibodies via protein A (performed by Saskia Helmsing, TU Braunschweig). Purified antibodies were then tested via western blot on lysates from HDAC10 overexpressing IMR-32 cells and the respective control cells (***Figure 60b-e***). Here, only antibodies from the H7 clone showed reactivity towards HDAC10 (***Figure 60c***), while antibodies from other clones were either unreactive (G2), or only recognized off-target proteins (A5 and C12). However, reactivity of the H7 antibody even against overexpressed HDAC10 in IMR-32 cells was low, as high concentrations of antibody and prolonged exposure were necessary. Thus, none of the clones was thus further developed.

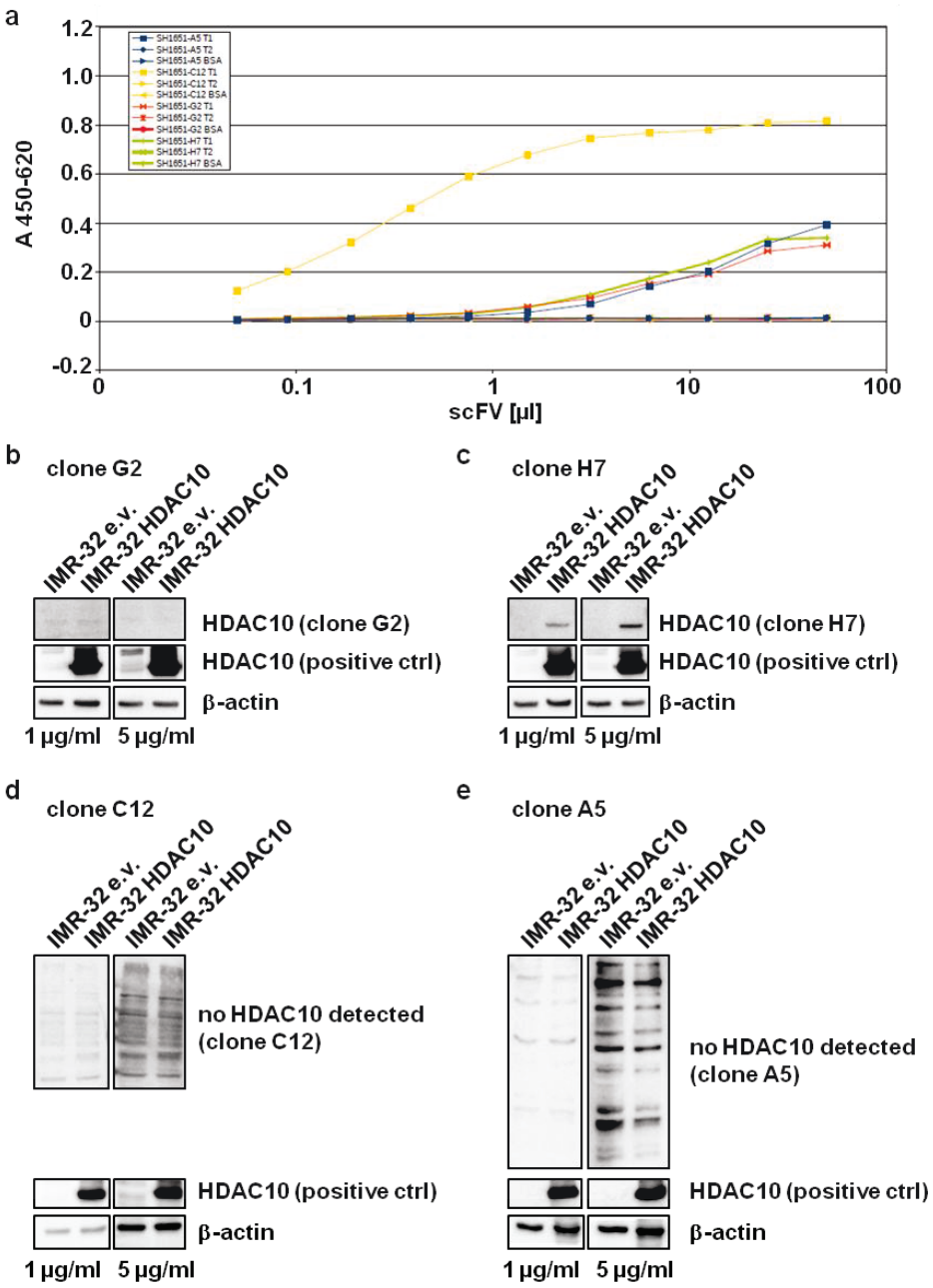

Figure 60: Testing of potentially HDAC10 reactive clones from antibody phage display. (a) *Titration ELISA of four scFv fragments that had been identified as reactive against the HDAC10T1 fragment in panning assays. ScFv fragments were also tested against BSA (negative control) and the HDAC10T2 antigen. Panning and ELISA assays were performed by Saskia Helmsing in the lab of Michael Hust (TU Braunschweig).* ***(b-e)*** *Testing of murine scFv-Fc fusion antibodies G2* ***(b)****, H7* ***(c)****, C12 (d) and A5* ***(e)*** *on western blot level. ScFv fragments, which had been cloned onto a mouse IgG2a Fc region and purified from HEK293 cells were used at two different concentrations (1 µg/ml and 5 µg/ml). Bound antibodies were detected using peroxidase-conjugated anti mouse antibodies.*

F DISCUSSION

Neuroblastomas have a fairly good outcome with a five year overall survival rate of almost 80 %. Nevertheless overall survival remains below 50 % in neuroblastomas categorized as high-risk tumors by the INRG classification system (see section ***A1.2***) (Cohn et al. 2009). Prognosis is even worse in patients with relapsed high-risk tumors, which occur in about 50 % of high-risk neuroblastoma cases and where five year overall survival is below 10 % in spite of intensification of treatment regimens (Basta et al. 2016). Resistance to a wide range of chemotherapeutics due to multidrug resistance (MDR) is one of the main factors limiting treatment success in high-risk and relapsed neuroblastoma patients, highlighting the need for novel, targeted therapy approaches capable of either circumventing or reversing MDR.

Aberrant HDAC activity is a common observation in cancer, and HDACs are critically involved in numerous cancer-relevant pathways (reviewed in (Ropero and Esteller 2007; Witt et al. 2009)). Together with their excellent druggability, this makes them an attractive target for cancer therapy. The efficacy of pan and broad-spectrum HDACi such as vorinostat (SAHA), romidepsin, belinostat and panobinostat has been proven in leukemias and lymphomas, leading to their approval for clinical application and further testing in numerous clinical trials in other cancer entities including neuroblastoma (Witt et al. 2012; Ceccacci and Minucci 2016)(clinical study: NCT01422499). The use of such broad-spectrum inhibitors is, however, hampered by dose limiting off-target toxicities including myelosuppression, fatigue and gastrointestinal symptoms like diarrhea, nausea and vomiting. It is postulated that such toxicities mainly arise from the inhibition of HDACs 1, 2 and 3, which epigenetically regulate the expression of a large number of genes in both neoplastic and non-neoplastic cells (Lane and Chabner 2009; Witt et al. 2009; Wilting et al. 2010). Thus, the key question remains, whether off-target toxicity can be reduced and on-target efficacy retained by a more specific inhibition of individual HDAC enzymes that are critical for the respective cancer entity or tumor subtype. Moreover, elucidating molecular mechanisms through which individual HDAC enzymes exert their tumor promoting function can help identify potential tumor escape mechanisms, as well as markers capable of monitoring or predicting the response of the tumor. The advantage of targeting individual HDACs in neuroblastoma has been demonstrated in a recent study, where specific inhibition of HDAC8 was as effective as vorinostat treatment with significantly lower dose-limiting side effects (Rettig et al. 2015).

One other HDAC suggested to be of particular importance in neuroblastoma biology is the class IIb member HDAC10, elevated expression of which correlates with poor prognosis specifically in INSS stage 4 neuroblastoma patients (Oehme et al. 2013a; Oehme et al. 2013b). Interference with

HDAC10 function sensitizes neuroblastoma cell lines to neuroblastoma-relevant chemotherapeutics such as doxorubicin and vincristine, suggesting that HDAC10 mediates chemoresistance. In contrast, high expression of HDAC6 does not correlate with poor prognosis in neuroblastoma (Oehme et al. 2009b; Oehme et al. 2013b), suggesting that despite their high homology (Fischer et al. 2002; Guardiola and Yao 2002; Kao et al. 2002), class IIb HDACs have partly non-redundant functions.

1 HDAC10 promotes lysosomal resistance mechanisms in neuroblastoma

1.1 Interference with HDAC10 function causes expansion of the lysosomal compartment via lysosomal accumulation

Both class IIb HDACs have been repeatedly linked to various modes of cellular stress response including DNA repair (Namdar et al. 2010; Kotian et al. 2011; Wang et al. 2012; Radhakrishnan et al. 2015), degradation of proteins and aggregates (Hook et al. 2002; Kawaguchi et al. 2003; Boyault et al. 2007; Pandey et al. 2007; Lee et al. 2010b; Ouyang et al. 2012), as well as lysosomal trafficking (Lee et al. 2010b; Oehme et al. 2013a). With regards to autophagy, HDAC6 appears to be particularly important for the induction of aggregate-induced autophagy (aggrephagy), as well as for autophagosome maturation during ubiquitin-mediated autophagy (Lee et al. 2010b). Conversely, HDAC10 is required for late stage autophagic flux, i.e. the delivery of autophagosomal material to lysosomes in a fusion process, in neuroblastoma, where lack of HDAC10 function further appears to interfere with lysosomal function (Oehme et al. 2013a). Given their high homology and partly overlapping functions, the role of HDAC6 and HDAC10 in lysosomal biology in neuroblastoma were dissected in this study using RNAi approaches, as well as HDAC6/10 (tubastatin A) and HDAC6 (tubacin) inhibitors with differential HDAC10 inhibitory capability (Butler et al. 2010; Bantscheff et al. 2011; Oehme et al. 2013a). Differential inhibitor specificities of tubacin (HDAC6) versus tubastatin A (HDAC6/10) were confirmed this study by NanoBRET tracer displacement assays (performed in the group of Dr. Aubry Miller, DKFZ Heidelberg), where tubastatin A but not tubacin showed high binding activity towards HDAC10 (Ridinger et al. 2018).

Several lines of evidence presented in this study demonstrate that HDAC10 but not HDAC6 is critical for lysosomal function in neuroblastoma. First, RNAi mediated depletion of HDAC10 but not HDAC6 increased the number of lysosomes as indicated by western blot analysis of lysosomal marker LAMP-2 and by fluorescence microscopic as well as flow cytometric analyses of stainings with acidotropic dyes such as LysoTracker DND-99 and acridine orange. Second, treatment with HDAC6/10 but not HDAC6 specific inhibitors phenocopied the above described expansion of the lysosomal

compartment. Third, HDAC6/10 inhibitors with abolished HDAC10- but intact HDAC6 binding capacity did not increase the number of lysosomes. Thus, and despite the absence of non HDAC6-crossreactive HDAC10 inhibitors, these data clearly point towards a distinct role of class IIb member HDAC10 in neuroblastoma lysosomal homeostasis.

The precise mechanism how HDAC10 affects lysosomal physiology in neuroblastoma cells was not conclusively identified in this study, and several distinct mechanisms might be contributing to the observed expansion of the lysosomal compartment. Transcriptional up-regulation of lysosomal genes by changes in histone acetylation seems unlikely, as HDAC10 has only rarely been reported to be a direct epigenetic regulator of gene expression (Li et al. 2015). Also, localization of the lysosomal master transcriptional regulator TFEB was unchanged after HDAC10 inhibitor treatment, speaking against induction of *de novo* lysosomal biogenesis via the CLEAR gene-regulatory network (Sardiello et al. 2009; Palmieri et al. 2011). Although the role of other autophagy-inducing transcription factors such as FoxO1 and FoxO3a was not further investigated, preliminary data from a follow-up project indicate that HDAC10 inhibition with tubastatin A does not promote induction of lysosomes via nuclear translocation of FoxO family transcription factors (Koerholz, unpublished). In line with this hypothesis, depletion of HDAC10 increased lysosomal numbers as well as protein levels of the lysosomal marker LAMP-2 without increasing *LAMP2* transcript levels, indicating that there is no global upregulation of lysosomal genes. Moreover, when lysosomal accumulation was induced with a lysosomal exocytosis inhibitor, no additional expansion of the lysosomal compartment was observed when HDAC10 inhibitors were added. This suggested that HDAC10 inhibition did not promote *de novo* biogenesis of lysosomes, as *de novo* production would have further increased lysosomal numbers.

Rather, interference with HDAC10 function likely caused an accumulation of dysfunctional lysosomes. Dysfunction of lysosomes, in turn, is known to promote lysosomal accumulation by various mechanisms. First, lack or malfunction of lysosomal enzymes, as observed in lysosomal storage diseases, leads to storage of "non-degraded" material in lysosomes, which in turn causes accumulation of lysosomes with impaired function (Sardiello et al. 2009; Durchfort et al. 2012; Appelqvist et al. 2013). Second, mutations in genes governing the autophagic lysosome reformation (ALR) pathway are known to cause accumulation of enlarged autophagolysosomes after longterm starvation probably due to defective degradation of cargo (Rong et al. 2011). ALR is required for the reformation of free lysosomes from autophagolysosomes, as the former are rapidly depleted by fusion with autophagosomes during periods of autophagy, and this reformation pathway is thus crucial for lysosomal homeostasis (Yu et al. 2010). Although ALR has been mainly characterized in Drosophila mutants, mouse models of human hereditary spastic paraplegia show defects in ALR, accompanied by depletion of free lysosomes and accumulation of autophagolysosomes that contain

undegraded material (Chang et al. 2014; Renvoise et al. 2014; Varga et al. 2015). Third, perturbance of the lysosome to cytoplasm pH gradient (de-acidification/alkalinization) can cause lysosomal accumulation. Although acidification of lysosomes is not absolutely required for fusion of lysosomes with cargo-carrying vesicles (Klionsky et al. 2008; Mauvezin et al. 2015; Mauvezin and Neufeld 2015), prolonged alkalinization e.g. by lysosomal inhibitors such as chloroquine or bafilomycin A promotes the accumulation of endo- and autophagosomal organelles, as well as de-acidified LAMP-positive lysosomes, by interfering with lysosomal fusion processes (Jahreiss et al. 2008; Yoon et al. 2010; Chen et al. 2011). Data reported in this study, namely the accumulation of acidotropic dyes in lysosomes after interference with HDAC10 function, preclude however, that interference with HDAC10 function caused de-acidification of lysosomes, as the number of acidic vesicles was clearly increased. Last, blocking of proteins or protein complexes required for lysosomal fusion events such as the HOPs complex triggers both autophagosome and lysosome accumulation (Jiang et al. 2014). In fact, data presented in a previous study show that interference with HDAC10 function causes accumulation of both acidic organelles and autophagosomes, as well as accumulation of the autophagosome cargo receptor SQSTM1/p62, suggestive of non-productive autophagy (Oehme et al. 2013a). Corroborating these findings, this study demonstrates that HDAC10 knockdown further blocks lysosomal exocytosis, i.e. the fusion of lysosomes with the plasma membrane (further discussed in section ***F1.2***). Taken together, the data presented in (Oehme et al. 2013a) and this study suggest that HDAC10 is crucial for lysosomal fusion events in neuroblastoma cells, although it remained unclear whether blocked fusion was cause or consequence of lysosomal dysfunction. Future studies could clarify for example if the degradative capacity of neuroblastoma cell lysosomes is impaired after interference with HDAC10 function by analyzing turnover of lysosomal substrates such as tagged EGF receptor (endocytic route) (Jiang et al. 2014) or overexpressed tagged polyglutamine (polyQ)-expanded huntingtin protein (Renna et al. 2011). Alternatively, lysosomal cathepsin activity could also be quantified using Magic Red™ dye (Johnson et al. 2016).

Although several lines of evidence suggest that interference with HDAC10 function caused the expansion of the lysosomal compartment in neuroblastoma cells by perturbing lysosomal function, it cannot be excluded that hyperacidification of lysosomes contributed to the above described phenotype. Indeed, increased V-ATPase function has been associated with lower lysosomal and enhanced acidification of post Golgi vesicles in cancer cells (Altan et al. 1998; Larsen et al. 2000; Gong et al. 2003; Hrabeta et al. 2015). The idea that HDAC10 could be involved in lysosomal acidification is supported by the identification of two acetylated lysine residues in subunit A of lysosomal V-ATPase complex (ATP6V1A) after HDAC6/10 but not after HDAC6 inhibition. This subunit of the cytosolic peripheral V_1 domain is critical for ATP hydrolysis and provides the energy required for pumping protons across the lysosomal membrane via the membrane-inserted V0 domain

(reviewed in (Forgac 2007)). Intriguingly, mutational analyses in subunit A of yeast V-ATPase have demonstrated that certain amino acid exchanges can increase coupling efficiency, i.e. the amount of protons pumped per ATP hydrolyzed, of the V-ATPase. Although the amino acid affected in the respective study was not a lysine residue, it is still conceivable that conformational changes induced by posttranslational modifications such as lysine acetylation alter ATP hydrolysis rates, V-ATPase assembly rates or coupling efficiency (Shao et al. 2003). Thus, HDAC10 potentially acts on the level of lysosome acidification by modulating V-ATPase function. Intriguingly, while lysosomal function critically depends on acidification of the lysosomal lumen due to the low pH optimum of lysosomal enzymes, some reports suggest that hyperacidification can also result in lysosomal dysfunction. Such hyperacidic lysosomes have been reported in cells from patients with the lysosomal storage disease mucolipidosis type IV (Soyombo et al. 2006). Here, mutations in the *MCOLN1/TRPML1* gene, which encodes for a lysosomal cation transporter, resulted in over-acidified lysosomes and impaired lysosomal lipid hydrolysis.

The lysosomal role of non class IIb HDACs in neuroblastoma lysosomal homeostasis

While the contribution of HDAC6 inhibition to the above described lysosomal phenotype in neuroblastoma cells was clearly omitted in this study, it remains to be clarified whether other HDACs apart from HDAC10 contribute to lysosomal function in the investigated cell lines. The data presented show that high concentrations of tubastatin A indeed cross-inhibit class I HDACs, depletion of which have been repeatedly associated with autophagy induction in various cancer models (Oh et al. 2008; Xie et al. 2012; Schipper et al. 2014; Koeneke et al. 2015). Regardless, results from RNAi mediated knockdown of individual HDACs do not support a marked role of class I HDACs in neuroblastoma lysosomal homeostasis, even though a small but not statistically significant expansion of the lysosomal compartment was observed in case of HDAC1 depletion. A similar phenotype to HDAC1 depletion was observed upon knockdown of the class IV member HDAC11, which was included in the analysis due to the high homology of its catalytic domain to both class I and class II HDACs (Gao et al. 2002; Seto and Yoshida 2014). Notably, class IIa HDACs 4, 5, 7 and 9 were not investigated in this study as they have been reported to have low intrinsic HDAC activity and to mostly exert they transcriptionally repressive activity via a SMRT/N-Cor corepressor complex that contains the class I member HDAC3 (Kao et al. 2000; Fischle et al. 2002; Jones et al. 2008; Gaur et al. 2016). While the knockdown data clearly dismissed a significant role for individual class I or class IV HDACs, it cannot be excluded that simultaneous inhibition of several HDACs cumulatively induces lysosomal dysfunction in neuroblastoma cells. Data obtained from two different designated class I HDAC inhibitors (valproic acid and entinostat/MS-275) showed conflicting results, as MS-275 induced lysosomal accumulation while VPA did not. A potential cross-reactivity of entinostat to HDAC10 was ruled out by NanoBRET assay. It remained unclear, whether lysosomal accumulation after entinostat

treatment was due to an off-target effect or whether it could be a result of simultaneous co-inhibition of class I HDACs and HDAC11. The HDAC11 binding capacity of entinostat, which was suggested in a recent study (Tian et al. 2017), and other HDAC inhibitors, as well as the effect of simultaneous inhibition of multiple individual HDACs on lysosomal homeostasis should thus be investigated more closely in consecutive studies.

1.2 HDAC10 promotes doxorubicin secretion via lysosomal exocytosis

An expansion of the lysosomal compartment often correlates with increased tumor chemoresistance e.g. via the sequestration of weakly basic drugs within lysosomes (Willingham et al. ; Zhitomirsky and Assaraf 2015; Guo et al. 2016). Therefore, a key question of this study was whether the expansion of the lysosomal compartment after interference with HDAC10 function triggered drug resistance by promoting lysosomal sequestration of chemotherapeutics. Indeed, lysosomal sequestration of chemotherapeutic drugs has been recently proposed as a resistance mechanism in neuroblastoma cells (Hrabeta et al. 2015). Doxorubicin, an anthracycline chemotherapeutic widely used for neuroblastoma therapy (Louis and Shohet 2015; Tran et al. 2015), has both weakly basic properties and - like its structural relative daunorubicin - a marked autofluorescence, which made it an ideal tool compound for the study of cellular drug uptake and subcellular drug distribution (Willingham et al. 1986). Despite elevated levels of doxorubicin-positive, perinuclear vesicles (likely doxorubicin loaded lysosomes) HDAC10 inhibition did not promote complete sequestration into lysosomal vesicles, as it also caused substantially elevated nuclear doxorubicin levels. In line with this, HDAC6/10 inhibitor tubastatin A increased sensitivity of neuroblastoma cells to doxorubicin rather than promoting doxorubicin resistance. Therefore, HDAC10 inhibition did not promote drug resistance via lysosomes. Rather, HDAC10 depletion or inhibition promoted globally increased intracellular doxorubicin levels in neuroblastoma cells, although this increase was not observed in every tested neuroblastoma cell line (further discussed in section ***F1.3***). However, it cannot be denied that a substantial fraction of doxorubicin was located in lysosomes, raising the question whether additional permeabilization of lysosomes could further increase treatment efficacy (vide infra).

Not all lysosomes were located perinuclearly under conditions of HDAC10 knockdown or inhibition. This, together with the previous finding that HDAC10 was required for lysosomal fusion with autophagosomes (Oehme et al. 2013a), prompted the idea that HDAC10 absence or inhibition blocks lysosomal fusion processes. In particular, lysosomes are known to fuse with the plasma membrane in a process called lysosomal exocytosis. Although the mechanistic details of this process are not fully understood, it is known that it involves two basic steps, namely the relocalization of lysosomes from the perinuclear cloud to the cell periphery (Jaiswal et al. 2002), which is followed by a Ca^{2+}

dependent fusion with the plasma membrane (Rodriguez et al. 1997; Reddy et al. 2001; Medina et al. 2011). Cell surface stainings for the lysosomal marker LAMP-1 indicate that both knockdown and inhibition of HDAC10 impaired lysosomal exocytosis in neuroblastoma cells. In contrast to a previous study, which suggested that HDAC6 was critical for IL-1β secretion via lysosomal exocytosis from human monocytes (Carta et al. 2006), HDAC6 was not required for lysosomal exocytosis in neuroblastoma cells. Coherently, HDAC10 but not HDAC6 inhibition reduced the rate of doxorubicin secretion in washout experiments. HDAC10 inhibition did not alter trafficking of P-glycoprotein, an ATP-driven drug efflux pump previously published to promote doxorubicin resistance in neuroblastoma (Michaelis et al. 2009), to the plasma membrane. Furthermore, the data presented indicate that HDAC10 inhibition promoted doxorubicin accumulation regardless of cellular P-glycoprotein levels.

The precise mechanism how HDAC10 promotes lysosomal exocytosis remains to be clarified, which is aggravated by the fact that lysosomal exocytosis itself is a poorly understood process (reviewed in (Samie and Xu 2014)). Interference with HDAC10 function neither caused clustering of lysosomal vesicles near the plasma membrane nor centripetal collapse of the lysosomal compartment near the MTOC, which has been observed in case of genetic ablation and overexpression of proteins required for binding of lysosomes to kinesin motor proteins, respectively (Pu et al. 2016; Wang et al. 2018). It is thus unlikely that HDAC10 is critically involved in antero- or retrograde trafficking of lysosomes along microtubules. The observed distribution of lysosomes throughout the cytoplasm after HDAC10 inhibition could be a consequence of lysosomal expansion, failed lysosomal exocytosis or both. Lysosomal exocytosis is regulated on many levels by vesicle tethering factors, SNARE proteins, cation channels and Ca^{2+}-sensing proteins (Rao et al. 2004; Verderio et al. 2012; Samie and Xu 2014). Future experiments could focus on the identification of HDAC10 binding partners that are involved in lysosomal exocytosis via immunoprecipitation and mass spectrometry approaches. However, pulldown experiments with endogenously expressed HDAC10 are currently hampered by the absence of HDAC10 antibodies of sufficient specificity (see section ***F3***). Intriguingly, dysfunction of the lysosomal cation channel MCOLN1 has not only been associated with lysosomal hyperacidification (Soyombo et al. 2006) but also with alterations in lysosomal fusion processes including lysosomal exocytosis (LaPlante et al. 2006; Dong et al. 2009). A more recent report indicates that MCOLN1 is required for the fusion of lysosomes with the plasma membrane by acting as a lysosomal Ca^{2+} efflux channel, providing locally elevated Ca^{2+} levels necessary for the fusion of lysosomes with the plasma membrane (Medina et al. 2011). Thus, the lysosomal expansion or possibly hyperacidification phenotype described in section ***F1.1***, and defects in lysosomal exocytosis after HDAC10 inhibition might be linked via MCOLN1. In this context, one study even suggests that activity of the MCOLN1 channel is negatively regulated by a decrease in lysosomal pH (Raychowdhury et al. 2004). It is thus

conceivable that HDAC10 is either a direct regulator of MCOLN1 function (e.g. via altering its acetylation) and thus lysosomal exocytosis, or that interference with HDAC10 function causes secondary dysfunction of MCOLN1 by increased lysosomal acidification.

Lysosomal exocytosis does not only favor tumor progression by promoting the sequestration and secretion of chemotherapeutic drugs, but also by the secretion of lysosomal hydrolases to the extracellular space which increases invasiveness of tumor cells by increased degradation of ECM components (Vasiljeva and Turk 2008; Liu et al. 2012b; Fonovic and Turk 2014; Machado et al. 2015). It is tempting to speculate that interfering with HDAC10 function *in vivo* could block tumor progression via two separate mechanisms, namely the reversal of tumor chemoresistance and the reduction of tumor cell invasion and metastasis formation. The data in this study further indicate that blockage of HDAC10 function does not sensitize proliferating human fibroblasts to doxorubicin, possibly because fibroblasts do not depend on lysosomes for the detoxification of doxorubicin. Although these findings suggests that interference with HDAC10 function can be used to specifically target tumor cells, this should be further investigated in other non-neoplastic cell models, such as cardiomyocytes which are especially sensitive to doxorubicin (Bristow et al. 1978; Doroshow et al. 1981; Arola et al. 2000).

Autophagic flux contributes to doxorubicin secretion under 3D conditions

Three main routes deliver membranes and cargo material to the lysosomal compartment: The biosynthetic route via the ER and Golgi, various modes of endocytosis, as well as (macro-)autophagy (Luzio et al. 2003). High autophagic flux requires adaptation of the lysosomal compartment. Not surprisingly, regulation of autophagy and lysosomal biogenesis under stress conditions are inherently linked by coordinated transcriptional programs via TFEB and FoxO family transcription factors (Zhao et al. 2007; Settembre et al. 2011). Basal autophagic flux occurs in normal cells, but especially cancer cells increase flux rates in order to cope with various stress conditions (reviewed in (White 2012)). This raised the question whether the flux of autophagosomes into the lysosomal compartment contributed to doxorubicin secretion in neuroblastoma cells. Under two-dimensional cell culture conditions, knockdown of ATG5, a central player in autophagosome formation, did not interfere with doxorubicin secretion, indicating that the disposal of doxorubicin via lysosomes did not require autophagic flux into the lysosomal compartment under these conditions. Also, remaining levels of ATG5 protein after knockdown could be sufficient to maintain the required basal autophagic flux under 2D conditions, as these conditions do not impose limits to nutrient and oxygen supply. Conversely, the limited levels of ATG5 after knockdown could become a restrictive factor for autophagic flux under the stress conditions imposed by three-dimensional culture. In line with this, autophagic flux contributed to doxorubicin secretion and reduction of ATG5 levels substantially increased intracellular doxorubicin accumulation. Neuroblastoma cells are known to increase

autophagic flux under 3D culture conditions, and this is mediated by the FoxO family transcription factor FoxO3a (Bingel et al. 2017). Under such conditions, autophagic flux becomes a major contributing factor to the lysosomal compartment by an increased formation of autophagolysosomes. This is supported by a substantially decreased number of autophago-lysosomal numbers under 3D conditions. Lastly, autophagosomes can also contribute to protein secretion by direct fusion with the plasma membrane in a process termed secretory autophagy (Kimura et al. 2017a; Kimura et al. 2017b). Although the presence of autophagosomal markers such as LC3-II at the plasma membrane under 2D- and 3D conditions was not analyzed in this study, the non-acidic pH of autophagosomes prior to their fusion with lysosomes makes it unlikely that doxorubicin substantially accumulates in autophagosomes, and thus that secretory autophagy was a major contributing factor to doxorubicin secretion.

Can addition of LMP provoking agents further increase the efficacy of doxorubicin and HDAC10 inhibitors in neuroblastoma cells?

HDAC6/10 inhibitor tubastatin A sensitized neuroblastoma cells to doxorubicin partly by increasing intracellular accumulation of doxorubicin. Although this, along with the fact that doxorubicin also significantly accumulated in nuclei after HDAC10 inhibition, suggests that interference with HDAC10 function does not actively promote lysosomal sequestration of weakly basic chemotherapeutic drugs, a substantial fraction of doxorubicin remained trapped in lysosomal vesicles and was thus biologically inactive. While cancer cells use lysosomes to acquire an increased capability to cope with various stress stimuli, increased lysosomal numbers make them also particularly vulnerable to lysosomal membrane permeabilization (LMP) (Bivik et al. 2006; Turk and Turk 2009; Enzenmuller et al. 2013). Induction of LMP would not only cause leakage of remaining drugs from lysosomes but also trigger the release of lysosomal cathepsins to the cytosol, where they induce apoptosis, thus further increasing the efficacy of treatment (Roberg and Ollinger 1998; Foghsgaard et al. 2001; Yuan et al. 2002; Bivik et al. 2006). Fluoremetric assays quantifying the cytosolic activity of lysosomal cathepsins performed in this study do not support that HDAC10 inhibitors themselves caused lysosomal permeabilization. However, the data presented are partly conflicting and have to be interpreted with great care due to several reasons. First, an increase cytoplasmic cathepsin activity after HDAC10 inhibition was occasionally observed in some of the experimental replicates. Second, even low doses of digitonin, which were used to selectively permeabilize the plasma membrane while leaving the lysosomal membrane intact, caused high basal cytosolic cathepsin activity in some instances, suggesting that the assay itself requires optimization, e.g. by lowering digitonin concentrations. Finally, the cathepsin release assay is not sensitive to permeabilization of individual lysosomes. While LysoTracker data suggest that most lysosomal membranes are indeed intact after HDAC10 inhibition, as the dye would otherwise leak to the cytosol, it cannot be excluded that a subset of dysfunctional

lysosomes becomes permeable, which in turn would explain the increased amount of nuclear doxorubicin after HDAC10 inhibition. More recent experimental tools, that use fluorescently labeled dextrans, are not only able to pick up lysosomal permeabilization more sensitively. Via the use of dextrans with different molecular weight, they can also be used to estimate the pore size upon lysosomal permeabilization (Aits et al. 2015). Small molecules like doxorubicin or other cytostatic drugs escape the lysosome at much smaller degrees of LMP than cathepsins, which have a considerably higher molecular weight.

One particularly interesting candidate for the induction of lysosomal permeabilization is the lysosomotropic agent chloroquine, prolonged exposure to which can cause lysosomal membrane destabilization (Boya et al. 2003; Enzenmuller et al. 2013). Currently ongoing studies demonstrate that addition of chloroquine can potentiate the treatment of various neuroblastoma cell lines with doxorubicin and HDAC inhibitors, underlining the importance of lysosomal membrane integrity for chemoresistance in the respective models (Koeneke, unpublished). Addition of chloroquine would also allow for the use of lower doxorubicin concentrations, which is critical for the reduction of doxorubicin-induced side effects such as cardiac dysfunction (Shan et al. 1996).

1.3 Lysosomal accumulation upon HDAC10 inhibition - a marker for dependency of tumor cells on lysosomal resistance mechanisms?

As briefly mentioned in section ***F1.1***, not all cell lines analyzed in this study accumulated higher levels of doxorubicin after HDAC10 inhibition. These include two neuroblastoma cell lines (NB-1, Kelly), as well as proliferating human foreskin fibroblasts. Differential doxorubicin accumulation in neuroblastoma cell lines did not correlate with HDAC10 protein expression, raising the question why HDAC10 inhibition promoted doxorubicin accumulation in some cell lines but not in others. Although the effect of HDAC10 inhibition on lysosomal exocytosis rates was not investigated for Kelly and NB-1 cells, HDAC10 inhibition did impair lysosomal exocytosis in fibroblasts and thus in a cell line that did not display increased doxorubicin accumulation. This suggested that fibroblasts either disposed of doxorubicin primarily by other mechanisms (e.g. ATP driven pumps) or that inhibition of lysosomal exocytosis was necessary but not sufficient for the intracellular accumulation of doxorubicin. Intriguingly, NB-1 and Kelly cells did not display expansion of the lysosomal compartment under HDAC10 inhibited conditions in this study, with Kelly cells being known to display increased lysosomal accumulation only at high HDAC10 inhibitor concentrations (Oehme et al. 2013a). The same study also indicates that HDAC10 inhibition does not induce lysosomal expansion in fibroblasts. Taken together, this suggests that HDAC10i-mediated doxorubicin accumulation requires an expansion of the lysosomal compartment. Lysosomal expansion causes a substantial fraction of

doxorubicin to be located in lysosomal vesicles, which can then be cleared from cells via lysosomal exocytosis.

The fact that some but not all cell lines react to HDAC10 inhibition with an expansion of the lysosomal compartment suggests that HDAC10 acts as a bottleneck for lysosomal homeostasis in some but not other cell lines (vide infra). Consequently, not all tumor cells or subtypes might be equally dependent on lysosomal resistance mechanisms. Such cells or tumor subtypes possibly rely on other resistance-promoting mechanisms including ATP-driven efflux pumps. In fact, tumor cells might decide on either lysosomal or pump-driven resistance mechanisms, or both, during initial treatment (Hu et al. 1995; Hurwitz et al. 1997; Maitra et al. 2001; Gotink et al. 2015; Zhitomirsky and Assaraf 2015). Future systematic viability screens, where clinically approved drugs will be combined with HDAC10- or other lysosomal inhibitors in the above described lysosomal responsive and non-responsive cell lines, could not only help identify drugs, resistance to which critically depends on lysosomal function. As all neuroblastoma model cell lines used in follow-up studies have been genetically fully characterized in the meantime via whole genome sequencing, gene expression profiling and 450k DNA methylation analysis, they could also help identify markers that are able predict if tumors depend on lysosomal function as a drug resistance mechanism and can thus be sensitized with lysosomal inhibitors. Identification of such response prediction markers are prerequisite to clinical testing of HDAC10- or pan HDAC inhibitors with high HDAC10 affinity, because they help exclude patients whose tumors do not rely on lysosomal resistance mechanisms and who will thus likely not benefit from treatment.

1.4 Additional mechanisms of cell sensitization after HDAC10 inhibition

In line with previous studies (Oehme et al. 2013a; Bingel et al. 2017), the data presented in section ***E1.9*** demonstrate that inhibition of HDAC6/10 sensitizes neuroblastoma cells to doxorubicin treatment. While increased doxorubicin accumulation likely contributes to sensitization, it cannot be the only contributing factor, as P-glycoprotein inhibition with verapamil did not sensitize neuroblastoma cells as effectively despite promoting stronger intracellular and nuclear accumulation of doxorubicin. It is thus likely that several other mechanisms contribute to increased cell death induction after chemotherapeutic treatment.

Inhibition of autophagy and lysosomal exocytosis contribute to cell death induction

Lysosomes are not only a central organelle of macromolecule degradation. They are also critical for various stress resistance mechanisms, and themselves act as sensor of cellular stress which is highlighted by their central role in amino acid sensing under starvation conditions (reviewed in

(Settembre et al. 2013)). This suggests that impaired lysosomal function itself was a contributing factor to sensitization of neuroblastoma cells to doxorubicin. As shown by (Oehme et al. 2013a), interference with HDAC10 function blocks autophagic flux at the stage of autophagosome lysosome fusion, causing the accumulation of autophagosomes and thus of aged macromolecules and damaged organelles like mitochondria that display elevated ROS production. In this context, several studies point at the importance of productive autophagic flux under cytotoxic treatment or other stress noxae, where blockage of flux can re-sensitize resistant cancer cells to the respective treatment (Carew et al. 2007; Wu et al. 2010). This is also highlighted under threedimensional culture conditions, where, due to starvation stress, neuroblastoma cells increase their autophagic flux and, as a consequence, become highly resistant to chemotherapeutic treatment. This resistance can be almost completely reverted by autophagic flux or HDAC10 inhibitors (Bingel et al. 2017).

The data presented in this study further demonstrate that lysosomal exocytosis itself can have a pro-survival function under cytotoxic treatment. Similar to HDAC10 inhibition, blockage of lysosomal exocytosis sensitized neuroblastoma cells to doxorubicin while having little effect as single treatment. This indicates that lysosomal exocytosis itself becomes important under such stress conditions. Increased rates of lysosomal exocytosis occur for example in case of plasma membrane disruption, where fusion of lysosomes with the plasma membrane promotes initial membrane resealing (Reddy et al. 2001). Moreover, lysosomal exocytosis rates are increased under oxidative stress, although excessive formation of ROS can also block lysosomal exocytosis (Liu et al. 2012a; Ravi et al. 2016). One of the side effects of doxorubicin is the induction of cumulative cardiomyopathy, and it is thought that doxorubicin promotes increased ROS generation, which contributes to both induction of cardiomyopathy, as well as to anti tumor effects. (Doroshow 1983; Minotti et al. 2004; Takemura and Fujiwara 2007). Increased ROS levels do not only cause the accumulation of DNA lesions and damaged organelles, but also promote peroxidation of membrane lipids (Barrera 2012), and doxorubicin itself has been shown to promote lipid peroxidation via ROS formation (Goodman and Hochstein 1977; Myers et al. 1977; Hrelia et al. 2002). Lipid peroxidation can in turn affect interfere with the integrity of cellular membranes or alter function of membrane-bound proteins (Stark 2005; Barrera 2012). Thus, plasma membrane repair is one possible mechanism how intact lysosomal exocytosis could promote cellular resistance to doxorubicin treatment.

HDAC6/10 inhibition induces DNA double strand breaks in neuroblastoma cells

Although class IIb HDACs are thought to be largely located in the cytoplasm (Guardiola and Yao 2002), several studies indicate that both HDAC6 and HDAC10 can be found the nucleus, where they have been suggested to be involved in DNA repair (Kao et al. 2002; Liu et al. 2012a; Wang et al. 2012; Radhakrishnan et al. 2015). As of yet, no mechanism has been proposed that explains how HDAC6 contributes to maintaining DNA integrity. In contrast, HDAC10 is involved in both DNA mismatch

repair, possibly by deacetylating MutS homolog 2 (MSH2) (Radhakrishnan et al. 2015), and in the repair of DNA double strand breaks by promoting homologous recombination (Kotian et al. 2011), although no downstream target was proposed in the latter study. These reports suggested that HDAC6/10 inhibition could promote increased sensitivity of neuroblastoma cells to genotoxic drugs by interfering with DNA repair processes. As doxorubicin induces DNA double strand breaks by topoisomerase II poisoning (Lyu et al. 2007; Nitiss 2009; Yang et al. 2014), a special focus in this study was laid on the effect of HDAC6/10 inhibition on DSB numbers. Here, HDAC6/10 inhibition did not only increase doxorubicin-induced DSBs to a substantially higher level than P-glycoprotein inhibitor verapamil, even though the latter promoted stronger nuclear doxorubicin accumulation. It also significantly increased DSBs in the absence of chemotherapeutic treatment, indicating that HDAC6 and/or HDAC10 are important for maintaining DNA integrity in neuroblastoma cells. Although these findings suggest that either or both class IIb HDACs are involved in DSB repair, no direct evidence for a decreased DNA repair capacity was provided in this study. Thus, it remains to be answered whether increased DSB formation was due to decreased DNA repair or due to other effects associated with impaired HDAC6/10 function such as increased ROS formation (Lee et al. 2010a; Oehme et al. 2013a; Bai et al. 2015) or changes in the expression of DNA repair genes. Moreover, it remained unclear whether increased DSB formation was mediated by inhibition of HDAC6 or HDAC10, as control experiments with an HDAC6 specific inhibitor (e.g. tubacin) were not performed. The immunofluorescence data provided in this study support the idea of a nuclear function of HDAC10, as they for the first time demonstrate nuclear localization of endogenously expressed HDAC10. Moreover, very preliminary data from mass spectrometry indicate that inhibition of HDAC6/10, but not of HDAC6 only, causes hyperacetylation of a lysine residue within the DNA binding region of Ku80, which together with its binding partner Ku70 is critical in the recognition of DSBs and the initiation of DSB repair via NHEJ, suggesting that HDAC10 could be critically involved in the regulation of the NHEJ repair pathway (reviewed in (Davis and Chen 2013) and also discussed in section ***F2***). Ku80 has been before reported to be acetylated after the use of pan HDAC inhibitors, which was associated with impaired DNA binding of Ku80, suggesting that classical HDACs are indeed involved in the regulation of NHEJ (Robert et al. 2016). Interestingly its binding partner Ku70 is deacetylated by the non-classical class III HDAC SIRT1, and deacetylation of Ku70 was associated with increased repair of DSBs (Jeong et al. 2007). Future experiments that directly assess the efficiency of homologous recombination or non-homologous end-joining (NHEJ) repair mechanisms could help clarify whether DNA repair is indeed compromised by HDAC6/10 inhibition and, if so, which repair pathway is affected (Mao et al. 2008; Seluanov et al. 2010; Kostyrko and Mermod 2016). Performing such assays in the absence of HDAC6 and HDAC10 protein, respectively, or in the presence of differential

HDAC6/10 inhibitors could show whether one or both class IIb HDACs promote DNA repair in neuroblastoma cells.

1.5 Future development of HDAC10 inhibitors

All recent studies demonstrating the potential of HDAC10 inhibition in neuroblastoma (Oehme et al. 2013a; Bingel et al. 2017; Kolbinger et al. 2018; Ridinger et al. 2018) have used HDAC10 inhibitors with significant cross-reactivity against HDAC6. Thus, one question that remains is, whether co-inhibition of HDAC6 contributes to the anti-tumor effects of HDAC6/10 inhibitors in neuroblastoma or whether the HDAC6 inhibitory activity should be abolished because it promotes resistance. In future studies, this issue can only be addressed by means of specific HDAC10 inhibitors. As such compounds have not yet been published, it is questionable whether the specific inhibition of HDAC10 is possible. The tubastatin A derivatives tested in this study (synthesized in the lab of Dr. Aubry Miller) demonstrate for the first time, that a basic amine group nitrogen atom in the cap structure of tubastatin A is required for efficient HDAC10 binding. Importantly, some of the tested tubastatin A derivatives (DKFZ-00546 and DKFZ-00574) demonstrated increased HDAC10 binding but unchanged HDAC6 affinity, indicating that modification of the cap group could at some point yield highly specific HDAC10 inhibitors. While these compounds have been generated by random modifications in the cap group, recently published crystal structures of zebrafish HDAC10 (zHDAC10) and both catalytic domains of human HDAC6 (Hai and Christianson 2016; Miyake et al. 2016; Hai et al. 2017) now allow for a targeted, structure-based development of novel HDAC6 and HDAC10 inhibitors, respectively. Such targeted approaches could finally enable the generation of HDAC6 non-cross-reactive HDAC10 inhibitors, which will serve as valuable tool compounds for deciphering anti-tumor effects of class IIb HDAC inhibitors. In this context, fitting of tubastatin A to HDAC6 and the human homology model derived from zHDAC10 recently demonstrated that the amine group of tubastatin A specifically mediates hydrogen bonding to Glu274 (Glu272 in human HDAC10), which is found in HDAC10 but not in HDAC6 (Hai et al. 2017). Conversely, the remaining cap group mediates binding to HDAC6 via hydrophobic interactions (Geraldy, unpublished).

Clinical testing and application of tubastatin A is limited by its unfavorable pharmacokinetic profile - a two hour plasmatic half-life was reported in a recent study in mice (Wang et al. 2016) -, and by the fact that it has not been optimized for oral application (Cosenza and Pozzi 2018). One way to circumvent this issue in the short-term would be the use of abexinostat, a pan HDAC inhibitor that has proven to be an excellent HDAC10 inhibitor in this study. In phase I/II clinical trials in adult patients with lymphoma and chronic lymphocytic leukemia, abexinostat had favorable pharmacokinetic properties and manageable toxicities, being readily taken up after oral administration with a plasma half-life of about 4h, and displaying promising clinical activity including

durable responses (Morschhauser et al. 2015) (Evens et al. 2016). Abexinostat was further tested in adult sarcoma patients in combination with doxorubicin, where partial responses were observed (Choy et al. 2015). It is currently also tested in renal cell carcinoma (NCT03592472), metastatic solid tumors (NCT01543763), relapsed and refractory follicular lymphoma (NCT03600441) and advanced cutaneous melanomas (NCT03590054), both as single treatment (NCT03600441) and in combination with the tyrosine kinase inhibitor pazopanib (NCT03592472, NCT01543763) or with the immune-checkpoint inhibitor pembrolizumab (NCT03590054). The highest reported peak plasma concentrations in lymphoma patients were 250 nM (Morschhauser et al. 2015) and >300 nM (Evens et al. 2016), respectively, at the recommended dose of 45 mg/m^2. These concentrations lie well within the concentration range where abexinostat treatment caused lysosomal accumulation in neuroblastoma cell lines, suggesting that it has the potential to become an HDAC10 inhibiting drug in neuroblastoma patients, although pharmacokinetics and maximum tolerated dose would have to be re-evaluated in children. As not all neuroblastoma cell lines equally displayed lysosomal expansion upon abexinostat treatment (see sections ***E1.4.3*** and ***F1.1***), it is more than likely that not all patients will equally benefit from combined treatment abexinostat and genotoxic drugs (e.g. doxorubicin). This underlines the need to systematically correlate the abexinostat-induced lysosomal expansion phenotype to cell viability after combination of abexinostat with a large number of clinically applied anti-cancer drugs. Correlating the hereby generated sensitivity profiles to gene expression data of fully characterized neuroblastoma models (including the cell lines in section ***E1.4.3***) can also help identify prospective biomarkers that are required for efficient selection of patients that are most likely to benefit from treatment.

Apart from HDAC10, inhibition of HDAC8 has shown promising effects in preclinical neuroblastoma models (Oehme et al. 2009a; Rettig et al. 2015), and co-inhibition of both enzymes might thus be desirable for the treatment of high-risk neuroblastoma. Co-inhibition would be greatly facilitated by a compound co-targeting both enzymes, as this would for example exclude differential metabolization of the drugs. However, attempts to create effective HDAC8/10 inhibitors by adding a second hydroxamic acid moiety to the cap group of tubastatin A derivatives, thus creating a chimeric compound reminiscent of both tubastatin A and the HDAC8 specific inhibitor PCI-34051, remained unsuccessful. Such compounds repeatedly displayed reduced inhibitory activity towards HDAC8 and HDAC10 in biochemical (HDAC-Glo for HDAC8) and cellular assays (SMC3 acetylation for HDAC8 and LysoTracker as well as NanoBRET assay for HDAC10). While it is true that addition of the second hydroxamic acid probably reduced affinity to HDAC8 and HDAC10 when compared to the respective analog containing only one hydroxamic acid residue, it is also obvious that the activity of the chimeric compound was more drastically reduced in BE(2)-C cells when compared to biochemical and NanoBRET data, the latter having been obtained in HeLa cells. In fact, HDAC8 (SMC3 acetylation) and

HDAC10 (lysosomal phenotype) inhibitory activity were completely abolished in BE(2)-C cells for the chimeric DKFZ-00580 analog. While the discrepancy between NanoBRET data in HeLa cells and functional assays in BE(2)-C cells, as well as the complete lack of HDAC8 inhibitory activity in BE(2)-C cells, cannot be fully explained, it has to be taken into account that addition of a second hydroxamic acid moiety increases polarity of the chimeric compounds. It is thus conceivable that reduced inhibitory capacity on HDAC8/10 in BE(2)-C cells was in fact related to decreased intracellular drug levels. Moreover, addition of a second hydroxamic acid could have also altered the affinity of the respective compounds to various drug efflux pumps. This raises the question, whether differential expression of such pumps in HeLa versus neuroblastoma cells, in turn, could explain why inhibitory activity was more drastically affected in one cell line than the other.

In a recent proof of concept study, the efficacy of combined HDAC8 and HDAC10 inhibition in neuroblastoma was demonstrated with the combined HDAC6/8/10 inhibitor TH34 (3-(N-benzylamino)-4-methylbenzhydroxamic acid), a non-tubastatin A based compound with strong HDAC6/8/10 binding capacity (Kolbinger et al. 2018). Single treatment with TH34 induced caspase-dependent cell death in a panel of high-risk neuroblastoma cell lines while being well tolerated in non-transformed cells.

2 Potential HDAC10 downstream targets

HDAC10 as a polyamine deacetylase

To date, no HDAC10 downstream target has been conclusively identified and it remains questionable whether HDAC10 serves as a lysine deacetylase. This debate was fueled by a recent study, in which both zebrafish and human HDAC10 demonstrated excellent polyamine deacetylase activity in biochemical assays, with high preference for N^8-acetylspermidine (PDAC activity) but poor activity on acetylated lysine substrates (Hai et al. 2017). Using the crystal structure of zebrafish HDAC10, the authors identified two major structural determinants that ensure PDAC activity specifically in HDAC10. A negatively charged Glutamine residue (Glu274, numbering according to its position in zHDAC10) establishes specificity for cationic substrates such as polyamines. This residue is conserved in human HDAC10 (Glu272), but is not found in the catalytic domains (CDs) of other HDACs, which, with the exception of a lysine residue in the HDAC6 CD1, display a conserved hydrophobic amino acid (leucine or methionine) at the respective site. Secondly, they identified a unique structural element in the L1 loop of the zHDAC10 CD (a 3_{10}-helix termed ηA2), that lengthens and constricts the active site tunnel, thus making acetylated lysine side chains too short to reach the enzyme's active site. While the report by (Hai et al. 2017) clearly demonstrates that HDAC10 is indeed an excellent deacetylase for N^8-acetylspermidine in biochemical assays, it is questionable whether this is its main

function in neuroblastoma cells. N^8-acetylated spermidine could neither be detected in BE(2)-C cells with full HDAC10 expression or function, nor in cells with HDAC10 knockdown or inhibition, making it unlikely that lysosomal expansion after interference with HDAC10 function was related to HDAC10's role as a N^8-acetylspermidine PDAC. While polyamines have been implicated in multiple cellular processes, including protein translation (Park et al. 2010; Mandal et al. 2013), DNA replication (Gallo et al. 1986), and also autophagy (Eisenberg et al. 2009), a clear link between polyamine levels and lysosomal function remains to be shown (Jonas et al. 1987), although it is conceivable that polyamines indirectly influence lysosomal function via the autophagy axis (Eisenberg et al. 2009).

In fact, literature evidence of N^8-acetylspermidine and its cellular function is sparse. Studies, mainly performed in HeLa cells or on homogenates from rat liver, suggest that N^8-acetylspermidine is generated in the nucleus by an enzyme with histone acetyltransferase (HAT) activity, and rapidly converted back to spermidine by a cytosolic PDAC without HDAC activity (Blankenship 1978; Libby 1978; Libby 1980; Marchant et al. 1986; Marchant et al. 1989). Moreover, the study by Marchant et al. found that N^8-acetylspermidine levels are hardly detectable with the HPLC gradient that is commonly used for detection of acetylated polyamines, suggesting that N^8-acetylspermidine levels are low in cultured cells (Marchant et al. 1989). It is not fully clear which HAT enzyme is responsible for N^8-acetylation, but a recent study proposed that P/CAF converts spermidine to N^8-acetylspermidine (Burgio et al. 2016). The cellular function of N^8-acetylspermidine is even more enigmatic and reports are conflicting, as it has been suggested to stimulate growth in a mouse lymphatic leukemia cell line (Wang et al. 1999), while promoting differentiation in rat pheochromocytoma cell line in another study (Mudumba et al. 2002). Although the data presented in this study, that suggest a subordinate role for N^8-acetylated polyamines in the lysosomal biology of BE(2)-C cells as they are not present at detectable levels, aberrant polyamine metabolism has been repeatedly associated with adverse outcome in neuroblastoma (Hogarty et al. 2008; Gamble et al. 2012). Therefore, future studies should focus on identifying neuroblastoma cell lines with detectable levels of N^8-acetylspermidine (currently ongoing). These could serve as valuable models for the identification of both physiological and tumor- or neuroblastoma-specific roles of N^8-acetylspermdine, and possibly other polyamines as well. Moreover, recent data from the Casero lab suggest that N^8-acetylspermidine is rapidly secreted from cells. Thus, cellular supernatants are likely more suitable to investigate the role of HDAC10 as PDAC.

Potential protein downstream targets of HDAC10

While the zHDAC10 model of (Hai et al. 2017) elegantly explains the preference of HDAC10 for polyamine substrates over acetylated lysines in biochemical assays, it also suggests that HDAC6/10 inhibitor tubastatin A does not fit into the catalytic domain due to the specific structure of the HDAC10 L1 loop, which restricts access of the inhibitor to the active site (Geraldy unpublished).

However, NanoBRET data generated by Aubry Miller and co-workers, as well as LysoTracker data (section ***E1.2.1***), demonstrate that tubastatin A and its derivatives are excellent HDAC10 binders and inhibitors in cells, suggesting that the L1 loop of human HDAC10 is flexible. Moreover, biochemical testing by Hai and colleagues does not take into accounts that protein conformation can be heavily modulated by protein-protein interactions. Therefore, lysine deacetylase activity might be restored by movement of the L1 loop in living cells. In this context, Hai and colleagues already demonstrated in their study that ablation of the ηA2 helix in HDAC10 (see previous section) generated a bifunctional HDAC-PDAC, while ablation of Glu274 generated a lysine deacetylase. Thus, it is reasonable to assume that HDAC10 can possess a lysine deacetylase function of HDAC10 in cells , e.g. via a conformational change in the L1 loop.

Two recent studies by (Lai et al. 2010) and (Oehme et al. 2013a) have proposed HSP70 family members HSC70 and HSP70 as HDAC10 interacting partners and potential downstream targets, and the latter study demonstrated that interaction of HDAC10 with HSP70/HSC70 is abolished in the presence of the broad-spectrum HDACi TSA. A further study by (Yang et al. 2013) suggested that HSP70 is deacetylated by HDAC6 at lysine 159 and that K159 acetylation of HSP70 was required for efficient autophagosome formation. Given the further involvement of HSP70 family members in lysosomal processes, such as chaperone-mediated autophagy (HSC70) (Cuervo and Dice 1996; Salvador et al. 2000) and stabilization of the lysosomal membrane (HSP70) (Daugaard et al. 2007a), a key question of this study was therefore, whether HDAC10 modulated lysosomal function via HSP70 family members. LC-MS/MS analyses, however, could not identify specific *de novo* acetylation sites neither after HDAC10 nor HDAC6 inhibition. While it is possible that these HSP70 family members are not targets of class IIb HDACs, the quality of data does not allow for a complete dismissal either. Since no SILAC based approach was used, quantitative comparison of HSP70 peptides that were commonly acetylated in control and treated conditions is difficult. Moreover, similar to other post-translational modifications such as phosphorylation, acetylation likely occurs at low frequency relative to the non-modified peptide, and might thus be missed in a complex mixture of proteins (Fila and Honys 2012). This suggests that the herein applied LC-MS/MS-based detection of acetylated peptides requires technical optimization, such as enrichment of acetylated proteins or peptides, which is routinely done for phosphorylated protein (Fila and Honys 2012). Recent acetylome studies have used acetyl-lysine specific antibodies after tryptic digestion to enrich for acetylated peptides (Choudhary et al. 2009; Scholz et al. 2015). However, in contrast to the mostly chemical or chromatography-based enrichment methods used in phosphoproteomic approaches, IP-based methods have several pitfalls. Firstly, acetyl-lysine antibodies tested in our lab have been mostly highly reactive towards acetylated histone and tubulin. Secondly, even though the IP-based enrichment of acetylated peptides after tryptic digestion allows for the enrichment of low abundance

peptides, protein identification via MS becomes more difficult when enrichment is performed with peptides rather than full-length protein. This is because protein identification after peptide enrichment is based only on a limited number of peptides that were successfully enriched - in some occasion potentially only one peptide -, while non-modified peptides are lost during the enrichment process. The former problem can be likely solved by separating the protein mixture via SDS-PAGE or HPLC prior to digestion and enrichment, as this would allow for the elimination of fractions where tubulin and histones are enriched. Still, the fact, that even in recent proteomic studies, a substantial number of acetylated peptides cannot be detected reproducibly in two independent runs, demonstrates that these IP-based methods require further optimization, possibly by improving quality of pan-acetyl reactive antibodies (Scholz et al. 2015).

More global analysis of lysine acetylation on whole cell lysates (mass range 95 to 50 kDa) revealed potential *de novo* acetylation sites after HDAC10 inhibition in subunit A of the V-ATPase complex (ATP6V1A K480 and K506) and in the DNA repair protein Ku80 (K443), respectively (also discussed in sections ***F1.1*** and ***F1.4***). While these hits are interesting from a mechanistic point of view as they could explain lysosomal expansion and increased DNA double strand breaks after HDAC10 inhibition, they have to be interpreted with care as long as they have not been confirmed in a second, independent approach. Moreover, the data from the initial run already suggest that a high number of identified peptides could be random hits. First, the total number of identified peptides did not substantially increase after treatment with HDAC6/10 or HDAC6 inhibitors. Second, the overlap of acetylated peptides between HDAC6/10 and HDAC6 inhibitor treated groups was small even though both inhibit one common enzyme. As discussed above, enrichment of acetylated peptides, possibly combined with quantitative MS approaches such as SILAC, could help to more robustly and quantitatively identify acetylated peptides. Intriguingly, both ATP6V1A and Ku80 were found to be hyperacetylated after treatment with bufexamac in the study of (Scholz et al. 2015). However, the identified peptides did not overlap with the ones found in this study. With the confirmation of ATP6V1A and Ku80 peptides still pending, binding of these proteins to HDAC6 and/or HDAC10 could be investigated in a yeast two-hybrid screen. If selective binding of either or both proteins to HDAC10 were observed, the lysine residues of interest could be replaced by arginine or glutamine residues to yield acetylation-dead or acetylation-mimicking mutants, respectively. However, it has to be considered that overexpression of such mutants would only work in case of an activating effect of acetylation (as suggested in case of ATP6V1A) or in case of a dominant negative effect (possibly the case for Ku80).

3 Development of an HDAC10 antibody - future perspectives

Three independent attempts to generate a highly specific HDAC10 antibody were made in this study. Generation of a polyclonal antibody in rabbit and affinity selection over a human antibody library via phage display remained largely unsuccessful due to low specificity and reactivity of the produced antibodies, respectively. In contrast, production of a monoclonal antibody from mice injected with a 118 amino acid peptide (termed HDAC10T2) corresponding to amino acids 501-618 of human HDAC10 yielded at least two highly specific hybridoma clones. Here, especially the clone termed 50/7/1 showed low off-target activity and, in contrast to the highly specific but weakly reactive 13/1/6/1 clone, decent reactivity towards endogenously expressed HDAC10 in both western blot and immunofluorescence approaches. Such an antibody could become a valuable tool in the future, as it allows for mechanistic studies with endogenously expressed HDAC10 (e.g. via immunofluorescence or IP-based approaches). Moreover, the 50/7/1 antibody showed promising results on paraffin-embedded neuroblastoma cells and is thus suitable for IHC approaches, which is crucial for evaluation of HDAC10 expression in human tumor tissues. However, high inter batch variability of 50/7/1 hybridoma cultures drastically hamper reliable antibody production at this point, as cultures of this clone repeatedly re-develop off-target activity which is enriched after antibody purification via solid phase binding against Protein G. Off-target activity was most likely not an inherent property of the HDAC10 binding antibody itself or due to cross-reactivity of the HDAC10-reactive antibody to a similar epitope (mimitope), as highly specific antibody could be purified from hybridoma culture batches without signs of cross-reactivity. Moreover, off-target activity randomly re-occurred in 50/7/1 hybridomas without prior off-target activity and could not be eliminated by repeated subcloning, making contamination with a second hybridoma clone unlikely. While this behavior seemed enigmatic at first sight, it is important to notice that, owing to the nature of hybridoma generation, hybridomas can co-express additional "background" antibody chains and that such chains can cause the production of additional combinatorial antibodies. In this context, a recent study analyzing sequence data from 185 random hybridomas (including commercial hybridomas), has found that additional heavy or light variable chains occur in up to 32 % of hybridomas deemed as monoclonal, thus making them non-mono-specific (Bradbury et al. 2018). In some instances, the authors reported that the most abundantly expressed chains were not even producing antibodies with the specificity of interest. The 50/7/1 clone has been derived from fusion of spleen cells with Sp2/0 myeloma cell line. In this myeloma line, background expression of the original productive antibody chains has been abolished (Shulman et al. 1978), but Sp2/0 cells are known to express an aberrant κ light chain transcript (Carroll et al. 1988; Duan and Pomerantz 1994). This transcript

normally does not contribute to antibody production due to a frameshift base pair deletion, resulting in non-functional rearrangement and a premature stop codon (Carroll et al. 1988). While this aberrant κ chain rarely causes the production of an additional κ chain, additional light and heavy chains can however, according to the study by Bradbury, originate via the following mechanisms: Fusion of myeloma cells with more than one B cell, additionally re-arranged light chain or heavy chain alleles prior to of post fusion with myeloma cells, or mutations acquired due to longterm cultivation of hybridomas (Bradbury et al. 2018). It is conceivable that the 50/7/1 hybridoma clone indeed produces more than one antibody due to one of the above named mechanism. This is supported by the finding that off-target binding antibody is enriched by Protein G-mediated antibody purification, which suggests that 50/7/1 cultures with off-target activity mainly produce off-target-reactive antibodies. Since this antibody has clearly shown a great deal of potential in western blot and immunofluorescence approaches, this problem should be remedied by sequencing and cloning of variable heavy and light chains, followed by overexpression of all possible chain combinations in HEK cells.

G REFERENCES

Abeloff, M. D., S. T. Rosen, G. D. Luk, S. B. Baylin, M. Zeltzman and A. Sjoerdsma (1986). "Phase II trials of alpha-difluoromethylornithine, an inhibitor of polyamine synthesis, in advanced small cell lung cancer and colon cancer." Cancer Treat Rep **70**(7): 843-845.

Abeloff, M. D., M. Slavik, G. D. Luk, C. A. Griffin, J. Hermann, O. Blanc, A. Sjoerdsma and S. B. Baylin (1984). "Phase I trial and pharmacokinetic studies of alpha-difluoromethylornithine--an inhibitor of polyamine biosynthesis." J Clin Oncol **2**(2): 124-130.

Agalioti, T., G. Chen and D. Thanos (2002). "Deciphering the transcriptional histone acetylation code for a human gene." Cell **111**(3): 381-392.

Aits, S. and M. Jaattela (2013). "Lysosomal cell death at a glance." J Cell Sci **126**(Pt 9): 1905-1912.

Aits, S., M. Jaattela and J. Nylandsted (2015). "Methods for the quantification of lysosomal membrane permeabilization: a hallmark of lysosomal cell death." Methods Cell Biol **126**: 261-285.

Ali, M. M., S. M. Roe, C. K. Vaughan, P. Meyer, B. Panaretou, P. W. Piper, C. Prodromou and L. H. Pearl (2006). "Crystal structure of an Hsp90-nucleotide-p23/Sba1 closed chaperone complex." Nature **440**(7087): 1013-1017.

Alland, L., G. David, H. Shen-Li, J. Potes, R. Muhle, H. C. Lee, H. Hou, Jr., K. Chen and R. A. DePinho (2002). "Identification of mammalian Sds3 as an integral component of the Sin3/histone deacetylase corepressor complex." Mol Cell Biol **22**(8): 2743-2750.

Altan, N., Y. Chen, M. Schindler and S. M. Simon (1998). "Defective acidification in human breast tumor cells and implications for chemotherapy." J Exp Med **187**(10): 1583-1598.

Anderson, D. J. (1993). "Molecular control of cell fate in the neural crest: the sympathoadrenal lineage." Annu Rev Neurosci **16**: 129-158.

Andrews, N. W. (2000). "Regulated secretion of conventional lysosomes." Trends Cell Biol **10**(8): 316-321.

Appelqvist, H., A. C. Johansson, E. Linderoth, U. Johansson, B. Antonsson, R. Steinfeld, K. Kagedal and K. Ollinger (2012). "Lysosome-mediated apoptosis is associated with cathepsin D-specific processing of bid at Phe24, Trp48, and Phe183." Ann Clin Lab Sci **42**(3): 231-242.

Appelqvist, H., P. Waster, K. Kagedal and K. Ollinger (2013). "The lysosome: from waste bag to potential therapeutic target." J Mol Cell Biol **5**(4): 214-226.

Aretz, S., T. U. Krohne, K. Kammerer, U. Warnken, A. Hotz-Wagenblatt, M. Bergmann, B. V. Stanzel, T. Kempf, F. G. Holz, M. Schnolzer and J. Kopitz (2013). "In-depth mass spectrometric mapping of the human vitreous proteome." Proteome Sci **11**(1): 22.

Arola, O. J., A. Saraste, K. Pulkki, M. Kallajoki, M. Parvinen and L. M. Voipio-Pulkki (2000). "Acute doxorubicin cardiotoxicity involves cardiomyocyte apoptosis." Cancer Res **60**(7): 1789-1792.

Arstila, A. U. and B. F. Trump (1968). "Studies on cellular autophagocytosis. The formation of autophagic vacuoles in the liver after glucagon administration." Am J Pathol **53**(5): 687-733.

Ashburner, M. and J. J. Bonner (1979). "The induction of gene activity in drosophilia by heat shock." Cell **17**(2): 241-254.

Attiyeh, E. F., W. B. London, Y. P. Mosse, Q. Wang, C. Winter, D. Khazi, P. W. McGrady, R. C. Seeger, A. T. Look, H. Shimada, G. M. Brodeur, S. L. Cohn, K. K. Matthay and J. M. Maris (2005). "Chromosome 1p and 11q deletions and outcome in neuroblastoma." N Engl J Med **353**(21): 2243-2253.

Ayer, D. E. (1999). "Histone deacetylases: transcriptional repression with SINers and NuRDs." Trends Cell Biol **9**(5): 193-198.

Babbar, N., N. A. Ignatenko, R. A. Casero, Jr. and E. W. Gerner (2003). "Cyclooxygenase-independent induction of apoptosis by sulindac sulfone is mediated by polyamines in colon cancer." J Biol Chem **278**(48): 47762-47775.

Bachetti, T., D. Di Paolo, S. Di Lascio, V. Mirisola, C. Brignole, M. Bellotti, I. Caffa, C. Ferraris, M. Fiore, D. Fornasari, R. Chiarle, S. Borghini, U. Pfeffer, M. Ponzoni, I. Ceccherini and P. Perri (2010). "PHOX2B-mediated regulation of ALK expression: in vitro identification of a functional relationship between two genes involved in neuroblastoma." PLoS One **5**(10).

Baekelandt, M. M., R. Holm, J. M. Nesland, C. G. Trope and G. B. Kristensen (2000). "P-glycoprotein expression is a marker for chemotherapy resistance and prognosis in advanced ovarian cancer." Anticancer Res **20**(2B): 1061-1067.

Bagchi, A., C. Papazoglu, Y. Wu, D. Capurso, M. Brodt, D. Francis, M. Bredel, H. Vogel and A. A. Mills (2007). "CHD5 is a tumor suppressor at human 1p36." Cell **128**(3): 459-475.

Bai, J., Y. Lei, G. L. An and L. He (2015). "Down-regulation of deacetylase HDAC6 inhibits the melanoma cell line A375.S2 growth through ROS-dependent mitochondrial pathway." PLoS One **10**(3): e0121247.

Baker, D. L., M. L. Schmidt, S. L. Cohn, J. M. Maris, W. B. London, A. Buxton, D. Stram, R. P. Castleberry, H. Shimada, A. Sandler, R. C. Shamberger, A. T. Look, C. P. Reynolds, R. C. Seeger and K. K. Matthay (2010). "Outcome after reduced chemotherapy for intermediate-risk neuroblastoma." N Engl J Med **363**(14): 1313-1323.

Bakthisaran, R., R. Tangirala and M. Rao Ch (2015). "Small heat shock proteins: Role in cellular functions and pathology." Biochim Biophys Acta **1854**(4): 291-319.

Balasubramanian, S., J. Ramos, W. Luo, M. Sirisawad, E. Verner and J. J. Buggy (2008). "A novel histone deacetylase 8 (HDAC8)-specific inhibitor PCI-34051 induces apoptosis in T-cell lymphomas." Leukemia **22**(5): 1026-1034.

Bali, P., M. Pranpat, J. Bradner, M. Balasis, W. Fiskus, F. Guo, K. Rocha, S. Kumaraswamy, S. Boyapalle, P. Atadja, E. Seto and K. Bhalla (2005). "Inhibition of histone deacetylase 6 acetylates and disrupts the chaperone function of heat shock protein 90: a novel basis for antileukemia activity of histone deacetylase inhibitors." J Biol Chem **280**(29): 26729-26734.

Bandyopadhyay, U., S. Kaushik, L. Varticovski and A. M. Cuervo (2008). "The chaperone-mediated autophagy receptor organizes in dynamic protein complexes at the lysosomal membrane." Mol Cell Biol **28**(18): 5747-5763.

Bantscheff, M., C. Hopf, M. M. Savitski, A. Dittmann, P. Grandi, A. M. Michon, J. Schlegl, Y. Abraham, I. Becher, G. Bergamini, M. Boesche, M. Delling, B. Dumpelfeld, D. Eberhard, C. Huthmacher, T. Mathieson, D. Poeckel, V. Reader, K. Strunk, G. Sweetman, U. Kruse, G. Neubauer, N. G. Ramsden and G. Drewes (2011). "Chemoproteomics profiling of HDAC inhibitors reveals selective targeting of HDAC complexes." Nat Biotechnol **29**(3): 255-265.

Baronas, V. A. and H. T. Kurata (2014). "Inward rectifiers and their regulation by endogenous polyamines." Front Physiol **5**: 325.

Barrera, G. (2012). "Oxidative stress and lipid peroxidation products in cancer progression and therapy." ISRN Oncol **2012**: 137289.

Basta, N. O., G. C. Halliday, G. Makin, J. Birch, R. Feltbower, N. Bown, M. Elliott, L. Moreno, G. Barone, A. D. Pearson, P. W. James, D. A. Tweddle and R. J. McNally (2016). "Factors associated with recurrence and survival length following relapse in patients with neuroblastoma." Br J Cancer **115**(9): 1048-1057.

Beckmann, R. P., L. E. Mizzen and W. J. Welch (1990). "Interaction of Hsp 70 with newly synthesized proteins: implications for protein folding and assembly." Science **248**(4957): 850-854.

Bellmeyer, A., J. Krase, J. Lindgren and C. LaBonne (2003). "The protooncogene c-myc is an essential regulator of neural crest formation in xenopus." Dev Cell **4**(6): 827-839.

Berthold, F. and B. Hero (2000). "Neuroblastoma: current drug therapy recommendations as part of the total treatment approach." Drugs **59**(6): 1261-1277.

Bertolotti, A., Y. Zhang, L. M. Hendershot, H. P. Harding and D. Ron (2000). "Dynamic interaction of BiP and ER stress transducers in the unfolded-protein response." Nat Cell Biol **2**(6): 326-332.

Bhattacharyya, T., A. N. Karnezis, S. P. Murphy, T. Hoang, B. C. Freeman, B. Phillips and R. I. Morimoto (1995). "Cloning and subcellular localization of human mitochondrial hsp70." J Biol Chem **270**(4): 1705-1710.

Bingel, C., E. Koeneke, J. Ridinger, A. Bittmann, M. Sill, H. Peterziel, J. K. Wrobel, I. Rettig, T. Milde, U. Fernekorn, F. Weise, A. Schober, O. Witt and I. Oehme (2017). "Three-dimensional tumor cell growth stimulates autophagic flux and recapitulates chemotherapy resistance." Cell Death Dis **8**(8): e3013.

Bivik, C. A., P. K. Larsson, K. M. Kagedal, I. K. Rosdahl and K. M. Ollinger (2006). "UVA/B-induced apoptosis in human melanocytes involves translocation of cathepsins and Bcl-2 family members." J Invest Dermatol **126**(5): 1119-1127.

Blackwood, E. M. and R. N. Eisenman (1991). "Max: a helix-loop-helix zipper protein that forms a sequence-specific DNA-binding complex with Myc." Science **251**(4998): 1211-1217.

Blankenship, J. (1978). "Deacetylation of N8-acetylspermidine by subcellular fractions of rat tissue." Arch Biochem Biophys **189**(1): 20-27.

Blott, E. J. and G. M. Griffiths (2002). "Secretory lysosomes." Nat Rev Mol Cell Biol **3**(2): 122-131.

Bluhm, E. C., J. Daniels, B. H. Pollock and A. F. Olshan (2006). "Maternal use of recreational drugs and neuroblastoma in offspring: a report from the Children's Oncology Group (United States)." Cancer Causes Control **17**(5): 663-669.

Bourhis, J., F. De Vathaire, G. D. Wilson, O. Hartmann, M. J. Terrier-Lacombe, L. Boccon-Gibod, N. J. McNally, J. Lemerle, G. Riou and J. Benard (1991). "Combined analysis of DNA ploidy index and N-myc genomic content in neuroblastoma." Cancer Res **51**(1): 33-36.

Bouwman, P. and J. Jonkers (2012). "The effects of deregulated DNA damage signalling on cancer chemotherapy response and resistance." Nat Rev Cancer **12**(9): 587-598.

Bown, N., S. Cotterill, M. Lastowska, S. O'Neill, A. D. Pearson, D. Plantaz, M. Meddeb, G. Danglot, C. Brinkschmidt, H. Christiansen, G. Laureys, F. Speleman, J. Nicholson, A. Bernheim, D. R. Betts, J. Vandesompele and N. Van Roy (1999). "Gain of chromosome arm 17q and adverse outcome in patients with neuroblastoma." N Engl J Med **340**(25): 1954-1961.

Boya, P., K. Andreau, D. Poncet, N. Zamzami, J. L. Perfettini, D. Metivier, D. M. Ojcius, M. Jaattela and G. Kroemer (2003). "Lysosomal membrane permeabilization induces cell death in a mitochondrion-dependent fashion." J Exp Med **197**(10): 1323-1334.

Boyault, C., Y. Zhang, S. Fritah, C. Caron, B. Gilquin, S. H. Kwon, C. Garrido, T. P. Yao, C. Vourc'h, P. Matthias and S. Khochbin (2007). "HDAC6 controls major cell response pathways to cytotoxic accumulation of protein aggregates." Genes Dev **21**(17): 2172-2181.

Boyer, L. A., R. R. Latek and C. L. Peterson (2004). "The SANT domain: a unique histone-tail-binding module?" Nat Rev Mol Cell Biol **5**(2): 158-163.

Bradbury, A. R. M., N. D. Trinklein, H. Thie, I. C. Wilkinson, A. K. Tandon, S. Anderson, C. L. Bladen, B. Jones, S. F. Aldred, M. Bestagno, O. Burrone, J. Maynard, F. Ferrara, J. S. Trimmer, J. Gornemann, J. Glanville, P. Wolf, A. Frenzel, J. Wong, X. Y. Koh, H. Y. Eng, D. Lane, M. P. Lefranc, M. Clark and S. Dubel (2018). "When monoclonal antibodies are not monospecific: Hybridomas frequently express additional functional variable regions." MAbs **10**(4): 539-546.

Bresler, S. C., D. A. Weiser, P. J. Huwe, J. H. Park, K. Krytska, H. Ryles, M. Laudenslager, E. F. Rappaport, A. C. Wood, P. W. McGrady, M. D. Hogarty, W. B. London, R. Radhakrishnan, M. A. Lemmon and Y. P. Mosse (2014). "ALK mutations confer differential oncogenic activation and sensitivity to ALK inhibition therapy in neuroblastoma." Cancer Cell **26**(5): 682-694.

Bright, N. A., L. J. Davis and J. P. Luzio (2016). "Endolysosomes Are the Principal Intracellular Sites of Acid Hydrolase Activity." Curr Biol **26**(17): 2233-2245.

Bright, N. A., M. J. Gratian and J. P. Luzio (2005). "Endocytic delivery to lysosomes mediated by concurrent fusion and kissing events in living cells." Curr Biol **15**(4): 360-365.

Bristow, M. R., P. D. Thompson, R. P. Martin, J. W. Mason, M. E. Billingham and D. C. Harrison (1978). "Early anthracycline cardiotoxicity." Am J Med **65**(5): 823-832.

Brodeur, G. M. (2003). "Neuroblastoma: biological insights into a clinical enigma." Nat Rev Cancer **3**(3): 203-216.

Brodeur, G. M., J. Pritchard, F. Berthold, N. L. Carlsen, V. Castel, R. P. Castelberry, B. De Bernardi, A. E. Evans, M. Favrot, F. Hedborg and et al. (1993). "Revisions of the international criteria for neuroblastoma diagnosis, staging, and response to treatment." J Clin Oncol **11**(8): 1466-1477.

Brodeur, G. M., R. C. Seeger, M. Schwab, H. E. Varmus and J. M. Bishop (1984). "Amplification of N-myc in untreated human neuroblastomas correlates with advanced disease stage." Science **224**(4653): 1121-1124.

Brunet, A., A. Bonni, M. J. Zigmond, M. Z. Lin, P. Juo, L. S. Hu, M. J. Anderson, K. C. Arden, J. Blenis and M. E. Greenberg (1999). "Akt promotes cell survival by phosphorylating and inhibiting a Forkhead transcription factor." Cell **96**(6): 857-868.

Brunet, A., L. B. Sweeney, J. F. Sturgill, K. F. Chua, P. L. Greer, Y. Lin, H. Tran, S. E. Ross, R. Mostoslavsky, H. Y. Cohen, L. S. Hu, H. L. Cheng, M. P. Jedrychowski, S. P. Gygi, D. A. Sinclair, F. W. Alt and M. E. Greenberg (2004). "Stress-dependent regulation of FOXO transcription factors by the SIRT1 deacetylase." Science **303**(5666): 2011-2015.

Buggy, J. J., M. L. Sideris, P. Mak, D. D. Lorimer, B. McIntosh and J. M. Clark (2000). "Cloning and characterization of a novel human histone deacetylase, HDAC8." Biochem J **350 Pt 1**: 199-205.

Buglio, D., N. M. Khaskhely, K. S. Voo, H. Martinez-Valdez, Y. J. Liu and A. Younes (2011). "HDAC11 plays an essential role in regulating OX40 ligand expression in Hodgkin lymphoma." Blood **117**(10): 2910-2917.

Burgio, G., D. F. Corona, C. M. Nicotra, G. Carruba and G. Taibi (2016). "P/CAF-mediated spermidine acetylation regulates histone acetyltransferase activity." J Enzyme Inhib Med Chem **31**(sup3): 75-82.

Butler, K. V., J. Kalin, C. Brochier, G. Vistoli, B. Langley and A. P. Kozikowski (2010). "Rational design and simple chemistry yield a superior, neuroprotective HDAC6 inhibitor, tubastatin A." J Am Chem Soc **132**(31): 10842-10846.

Buurman, R., E. Gurlevik, V. Schaffer, M. Eilers, M. Sandbothe, H. Kreipe, L. Wilkens, B. Schlegelberger, F. Kuhnel and B. Skawran (2012). "Histone deacetylases activate hepatocyte growth factor signaling by repressing microRNA-449 in hepatocellular carcinoma cells." Gastroenterology **143**(3): 811-820 e815.

Caren, H., H. Kryh, M. Nethander, R. M. Sjoberg, C. Trager, S. Nilsson, J. Abrahamsson, P. Kogner and T. Martinsson (2010). "High-risk neuroblastoma tumors with 11q-deletion display a poor prognostic, chromosome instability phenotype with later onset." Proc Natl Acad Sci U S A **107**(9): 4323-4328.

Carew, J. S., S. T. Nawrocki, C. N. Kahue, H. Zhang, C. Yang, L. Chung, J. A. Houghton, P. Huang, F. J. Giles and J. L. Cleveland (2007). "Targeting autophagy augments the anticancer activity of the histone deacetylase inhibitor SAHA to overcome Bcr-Abl-mediated drug resistance." Blood **110**(1): 313-322.

Caron, H., P. van Sluis, J. de Kraker, J. Bokkerink, M. Egeler, G. Laureys, R. Slater, A. Westerveld, P. A. Voute and R. Versteeg (1996). "Allelic loss of chromosome 1p as a predictor of unfavorable outcome in patients with neuroblastoma." N Engl J Med **334**(4): 225-230.

Carroll, W. L., E. Mendel and S. Levy (1988). "Hybridoma fusion cell lines contain an aberrant kappa transcript." Mol Immunol **25**(10): 991-995.

Carta, S., S. Tassi, C. Semino, G. Fossati, P. Mascagni, C. A. Dinarello and A. Rubartelli (2006). "Histone deacetylase inhibitors prevent exocytosis of interleukin-1beta-containing secretory lysosomes: role of microtubules." Blood **108**(5): 1618-1626.

Casero, R. A., Jr. and L. J. Marton (2007). "Targeting polyamine metabolism and function in cancer and other hyperproliferative diseases." Nat Rev Drug Discov **6**(5): 373-390.

Casero, R. A., Jr. and A. E. Pegg (1993). "Spermidine/spermine N1-acetyltransferase--the turning point in polyamine metabolism." FASEB J **7**(8): 653-661.

Ceccacci, E. and S. Minucci (2016). "Inhibition of histone deacetylases in cancer therapy: lessons from leukaemia." Br J Cancer **114**(6): 605-611.

Chakrabarti, A., I. Oehme, O. Witt, G. Oliveira, W. Sippl, C. Romier, R. J. Pierce and M. Jung (2015). "HDAC8: a multifaceted target for therapeutic interventions." Trends Pharmacol Sci **36**(7): 481-492.

Chakrabarti, S., K. S. Kobayashi, R. A. Flavell, C. B. Marks, K. Miyake, D. R. Liston, K. T. Fowler, F. S. Gorelick and N. W. Andrews (2003). "Impaired membrane resealing and autoimmune myositis in synaptotagmin VII-deficient mice." J Cell Biol **162**(4): 543-549.

Chan, L. L., D. Shen, A. R. Wilkinson, W. Patton, N. Lai, E. Chan, D. Kuksin, B. Lin and J. Qiu (2012). "A novel image-based cytometry method for autophagy detection in living cells." Autophagy **8**(9): 1371-1382.

Chang, J., S. Lee and C. Blackstone (2014). "Spastic paraplegia proteins spastizin and spatacsin mediate autophagic lysosome reformation." J Clin Invest **124**(12): 5249-5262.

Chappell, T. G., W. J. Welch, D. M. Schlossman, K. B. Palter, M. J. Schlesinger and J. E. Rothman (1986). "Uncoating ATPase is a member of the 70 kilodalton family of stress proteins." Cell **45**(1): 3-13.

Chapuy, B., R. Koch, U. Radunski, S. Corsham, N. Cheong, N. Inagaki, N. Ban, D. Wenzel, D. Reinhardt, A. Zapf, S. Schweyer, F. Kosari, W. Klapper, L. Truemper and G. G. Wulf (2008). "Intracellular ABC transporter A3 confers multidrug resistance in leukemia cells by lysosomal drug sequestration." Leukemia **22**(8): 1576-1586.

Charron, J., B. A. Malynn, P. Fisher, V. Stewart, L. Jeannotte, S. P. Goff, E. J. Robertson and F. W. Alt (1992). "Embryonic lethality in mice homozygous for a targeted disruption of the N-myc gene." Genes Dev **6**(12A): 2248-2257.

Chen, P. M., Z. J. Gombart and J. W. Chen (2011). "Chloroquine treatment of ARPE-19 cells leads to lysosome dilation and intracellular lipid accumulation: possible implications of lysosomal dysfunction in macular degeneration." Cell Biosci **1**(1): 10.

Chen, Y., J. Takita, Y. L. Choi, M. Kato, M. Ohira, M. Sanada, L. Wang, M. Soda, A. Kikuchi, T. Igarashi, A. Nakagawara, Y. Hayashi, H. Mano and S. Ogawa (2008). "Oncogenic mutations of ALK kinase in neuroblastoma." Nature **455**(7215): 971-974.

Cheng, T., L. Grasse, J. Shah and J. Chandra (2015). "Panobinostat, a pan-histone deacetylase inhibitor: rationale for and application to treatment of multiple myeloma." Drugs Today (Barc) **51**(8): 491-504.

Cheung, N. K. and M. A. Dyer (2013). "Neuroblastoma: developmental biology, cancer genomics and immunotherapy." Nat Rev Cancer **13**(6): 397-411.

Cheung, N. K., J. Zhang, C. Lu, M. Parker, A. Bahrami, S. K. Tickoo, A. Heguy, A. S. Pappo, S. Federico, J. Dalton, I. Y. Cheung, L. Ding, R. Fulton, J. Wang, X. Chen, J. Becksfort, J. Wu, C. A. Billups, D. Ellison, E. R. Mardis, R. K. Wilson, J. R. Downing and M. A. Dyer (2012). "Association of age at diagnosis and genetic mutations in patients with neuroblastoma." JAMA **307**(10): 1062-1071.

Choi, J. H., H. J. Kwon, B. I. Yoon, J. H. Kim, S. U. Han, H. J. Joo and D. Y. Kim (2001). "Expression profile of histone deacetylase 1 in gastric cancer tissues." Jpn J Cancer Res **92**(12): 1300-1304.

Choudhary, C., C. Kumar, F. Gnad, M. L. Nielsen, M. Rehman, T. C. Walther, J. V. Olsen and M. Mann (2009). "Lysine acetylation targets protein complexes and co-regulates major cellular functions." Science **325**(5942): 834-840.

Choudhary, C., B. T. Weinert, Y. Nishida, E. Verdin and M. Mann (2014). "The growing landscape of lysine acetylation links metabolism and cell signalling." Nat Rev Mol Cell Biol **15**(8): 536-550.

Choy, E., Y. Flamand, S. Balasubramanian, J. E. Butrynski, D. C. Harmon, S. George, G. M. Cote, A. J. Wagner, J. A. Morgan, M. Sirisawad, C. Mani, F. J. Hornicek, Z. Duan and G. D. Demetri (2015). "Phase 1 study of oral abexinostat, a histone deacetylase inhibitor, in combination with doxorubicin in patients with metastatic sarcoma." Cancer **121**(8): 1223-1230.

Ciocca, D. R. and S. K. Calderwood (2005). "Heat shock proteins in cancer: diagnostic, prognostic, predictive, and treatment implications." Cell Stress Chaperones **10**(2): 86-103.

Cloutier, P. and B. Coulombe (2013). "Regulation of molecular chaperones through post-translational modifications: decrypting the chaperone code." Biochim Biophys Acta **1829**(5): 443-454.

Cohn, S. L., A. D. Pearson, W. B. London, T. Monclair, P. F. Ambros, G. M. Brodeur, A. Faldum, B. Hero, T. Iehara, D. Machin, V. Mosseri, T. Simon, A. Garaventa, V. Castel and K. K. Matthay (2009). "The International Neuroblastoma Risk Group (INRG) classification system: an INRG Task Force report." J Clin Oncol **27**(2): 289-297.

Cosenza, M. and S. Pozzi (2018). "The Therapeutic Strategy of HDAC6 Inhibitors in Lymphoproliferative Disease." Int J Mol Sci **19**(8).

Cotterman, R. and P. S. Knoepfler (2009). "N-Myc regulates expression of pluripotency genes in neuroblastoma including lif, klf2, klf4, and lin28b." PLoS One **4**(6): e5799.

Crane, J. F. and P. A. Trainor (2006). "Neural crest stem and progenitor cells." Annu Rev Cell Dev Biol **22**: 267-286.

Cuervo, A. M. and J. F. Dice (1996). "A receptor for the selective uptake and degradation of proteins by lysosomes." Science **273**(5274): 501-503.

Cyr, D. M., X. Lu and M. G. Douglas (1992). "Regulation of Hsp70 function by a eukaryotic DnaJ homolog." J Biol Chem **267**(29): 20927-20931.

Czupalla, C., H. Mansukoski, T. Riedl, D. Thiel, E. Krause and B. Hoflack (2006). "Proteomic analysis of lysosomal acid hydrolases secreted by osteoclasts: implications for lytic enzyme transport and bone metabolism." Mol Cell Proteomics **5**(1): 134-143.

Daitoku, H., M. Hatta, H. Matsuzaki, S. Aratani, T. Ohshima, M. Miyagishi, T. Nakajima and A. Fukamizu (2004). "Silent information regulator 2 potentiates Foxo1-mediated transcription through its deacetylase activity." Proc Natl Acad Sci U S A **101**(27): 10042-10047.

Daitoku, H., J. Sakamaki and A. Fukamizu (2011). "Regulation of FoxO transcription factors by acetylation and protein-protein interactions." Biochim Biophys Acta **1813**(11): 1954-1960.

Dang, C. V. (2012). "MYC on the path to cancer." Cell **149**(1): 22-35.

Das, K. C. and H. P. Misra (2004). "Hydroxyl radical scavenging and singlet oxygen quenching properties of polyamines." Mol Cell Biochem **262**(1-2): 127-133.

Daugaard, M., T. Kirkegaard-Sorensen, M. S. Ostenfeld, M. Aaboe, M. Hoyer-Hansen, T. F. Orntoft, M. Rohde and M. Jaattela (2007a). "Lens epithelium-derived growth factor is an Hsp70-2 regulated guardian of lysosomal stability in human cancer." Cancer Res **67**(6): 2559-2567.

Daugaard, M., M. Rohde and M. Jaattela (2007b). "The heat shock protein 70 family: Highly homologous proteins with overlapping and distinct functions." FEBS Lett **581**(19): 3702-3710.

Davis, A. J. and D. J. Chen (2013). "DNA double strand break repair via non-homologous end-joining." Transl Cancer Res **2**(3): 130-143.

de Duve, C. (2005). "The lysosome turns fifty." Nat Cell Biol **7**(9): 847-849.

De Duve, C. and H. Beaufay (1959). "Tissue fractionation studies. 10. Influence of ischaemia on the state of some bound enzymes in rat liver." Biochem J **73**: 610-616.

De Duve, C., B. C. Pressman, R. Gianetto, R. Wattiaux and F. Appelmans (1955). "Tissue fractionation studies. 6. Intracellular distribution patterns of enzymes in rat-liver tissue." Biochem J **60**(4): 604-617.

De Preter, K., J. Vermeulen, B. Brors, O. Delattre, A. Eggert, M. Fischer, I. Janoueix-Lerosey, C. Lavarino, J. M. Maris, J. Mora, A. Nakagawara, A. Oberthuer, M. Ohira, G. Schleiermacher, A. Schramm, J. H. Schulte, Q. Wang, F. Westermann, F. Speleman and J. Vandesompele (2010). "Accurate outcome prediction in neuroblastoma across independent data sets using a multigene signature." Clin Cancer Res **16**(5): 1532-1541.

Deardorff, M. A., M. Bando, R. Nakato, E. Watrin, T. Itoh, M. Minamino, K. Saitoh, M. Komata, Y. Katou, D. Clark, K. E. Cole, E. De Baere, C. Decroos, N. Di Donato, S. Ernst, L. J. Francey, Y. Gyftodimou, K. Hirashima, M. Hullings, Y. Ishikawa, C. Jaulin, M. Kaur, T. Kiyono, P. M. Lombardi, L. Magnaghi-Jaulin, G. R. Mortier, N. Nozaki, M. B. Petersen, H. Seimiya, V. M. Siu, Y. Suzuki, K. Takagaki, J. J. Wilde, P. J. Willems, C. Prigent, G. Gillessen-Kaesbach, D. W. Christianson, F. J. Kaiser, L. G. Jackson, T. Hirota, I. D. Krantz and K. Shirahige (2012). "HDAC8 mutations in Cornelia de Lange syndrome affect the cohesin acetylation cycle." Nature **489**(7415): 313-317.

Debatin, K. M. and P. H. Krammer (2004). "Death receptors in chemotherapy and cancer." Oncogene **23**(16): 2950-2966.

Defferrari, R., K. Mazzocco, I. M. Ambros, P. F. Ambros, C. Bedwell, K. Beiske, J. Benard, A. P. Berbegall, N. Bown, V. Combaret, J. Couturier, G. Erminio, C. Gambini, A. Garaventa, N. Gross, R. Haupt, J. Kohler, M. Jeison, J. Lunec, B. Marques, T. Martinsson, R. Noguera, S. Parodi, G. Schleiermacher, D. A. Tweddle, A. Valent, N. Van Roy, A. Vicha, E. Villamon and G. P. Tonini (2015). "Influence of segmental chromosome abnormalities on survival in children over the age of 12 months with unresectable localised peripheral neuroblastic tumours without MYCN amplification." Br J Cancer **112**(2): 290-295.

Demetriades, C., N. Doumpas and A. A. Teleman (2014). "Regulation of TORC1 in response to amino acid starvation via lysosomal recruitment of TSC2." Cell **156**(4): 786-799.

Denslow, S. A. and P. A. Wade (2007). "The human Mi-2/NuRD complex and gene regulation." Oncogene **26**(37): 5433-5438.

Deubzer, H. E., M. C. Schier, I. Oehme, M. Lodrini, B. Haendler, A. Sommer and O. Witt (2013). "HDAC11 is a novel drug target in carcinomas." Int J Cancer **132**(9): 2200-2208.

Dhalluin, C., J. E. Carlson, L. Zeng, C. He, A. K. Aggarwal and M. M. Zhou (1999). "Structure and ligand of a histone acetyltransferase bromodomain." Nature **399**(6735): 491-496.

Diao, J., R. Liu, Y. Rong, M. Zhao, J. Zhang, Y. Lai, Q. Zhou, L. M. Wilz, J. Li, S. Vivona, R. A. Pfuetzner, A. T. Brunger and Q. Zhong (2015). "ATG14 promotes membrane tethering and fusion of autophagosomes to endolysosomes." Nature **520**(7548): 563-566.

Dikic, I. and Z. Elazar (2018). "Mechanism and medical implications of mammalian autophagy." Nat Rev Mol Cell Biol **19**(6): 349-364.

Dohse, M., C. Scharenberg, S. Shukla, R. W. Robey, T. Volkmann, J. F. Deeken, C. Brendel, S. V. Ambudkar, A. Neubauer and S. E. Bates (2010). "Comparison of ATP-binding cassette transporter interactions with the tyrosine kinase inhibitors imatinib, nilotinib, and dasatinib." Drug Metab Dispos **38**(8): 1371-1380.

Domanico, S. Z., D. C. DeNagel, J. N. Dahlseid, J. M. Green and S. K. Pierce (1993). "Cloning of the gene encoding peptide-binding protein 74 shows that it is a new member of the heat shock protein 70 family." Mol Cell Biol **13**(6): 3598-3610.

Dong, X. P., X. Wang, D. Shen, S. Chen, M. Liu, Y. Wang, E. Mills, X. Cheng, M. Delling and H. Xu (2009). "Activating mutations of the TRPML1 channel revealed by proline-scanning mutagenesis." J Biol Chem **284**(46): 32040-32052.

Dooley, H. C., M. Razi, H. E. Polson, S. E. Girardin, M. I. Wilson and S. A. Tooze (2014). "WIPI2 links LC3 conjugation with PI3P, autophagosome formation, and pathogen clearance by recruiting Atg12-5-16L1." Mol Cell **55**(2): 238-252.

Dorigo, B., T. Schalch, K. Bystricky and T. J. Richmond (2003). "Chromatin fiber folding: requirement for the histone H4 N-terminal tail." J Mol Biol **327**(1): 85-96.

Doroshow, J. H. (1983). "Effect of anthracycline antibiotics on oxygen radical formation in rat heart." Cancer Res **43**(2): 460-472.

Doroshow, J. H., G. Y. Locker, I. Ifrim and C. E. Myers (1981). "Prevention of doxorubicin cardiac toxicity in the mouse by N-acetylcysteine." J Clin Invest **68**(4): 1053-1064.

Drazic, A., L. M. Myklebust, R. Ree and T. Arnesen (2016). "The world of protein acetylation." Biochim Biophys Acta **1864**(10): 1372-1401.

Duan, L. and R. J. Pomerantz (1994). "Elimination of endogenous aberrant kappa chain transcripts from sp2/0-derived hybridoma cells by specific ribozyme cleavage: utility in genetic therapy of HIV-1 infections." Nucleic Acids Res **22**(24): 5433-5438.

Duband, J. L. (2010). "Diversity in the molecular and cellular strategies of epithelium-to-mesenchyme transitions: Insights from the neural crest." Cell Adh Migr **4**(3): 458-482.

Dubreuil, V., M. R. Hirsch, A. Pattyn, J. F. Brunet and C. Goridis (2000). "The Phox2b transcription factor coordinately regulates neuronal cell cycle exit and identity." Development **127**(23): 5191-5201.

Durchfort, N., S. Verhoef, M. B. Vaughn, R. Shrestha, D. Adam, J. Kaplan and D. M. Ward (2012). "The enlarged lysosomes in beige j cells result from decreased lysosome fission and not increased lysosome fusion." Traffic **13**(1): 108-119.

Dyballa, N. and S. Metzger (2009). "Fast and sensitive colloidal coomassie G-250 staining for proteins in polyacrylamide gels." J Vis Exp(30).

Ecker, J., I. Oehme, R. Mazitschek, A. Korshunov, M. Kool, T. Hielscher, J. Kiss, F. Selt, C. Konrad, M. Lodrini, H. E. Deubzer, A. von Deimling, A. E. Kulozik, S. M. Pfister, O. Witt and T. Milde (2015). "Targeting class I histone deacetylase 2 in MYC amplified group 3 medulloblastoma." Acta Neuropathol Commun **3**: 22.

Eckschlager, T., J. Plch, M. Stiborova and J. Hrabeta (2017). "Histone Deacetylase Inhibitors as Anticancer Drugs." Int J Mol Sci **18**(7).

Eisenberg, T., H. Knauer, A. Schauer, S. Buttner, C. Ruckenstuhl, D. Carmona-Gutierrez, J. Ring, S. Schroeder, C. Magnes, L. Antonacci, H. Fussi, L. Deszcz, R. Hartl, E. Schraml, A. Criollo, E. Megalou, D. Weiskopf, P. Laun, G. Heeren, M. Breitenbach, B. Grubeck-Loebenstein, E. Herker, B. Fahrenkrog, K. U. Frohlich, F. Sinner, N. Tavernarakis, N. Minois, G. Kroemer and F. Madeo (2009). "Induction of autophagy by spermidine promotes longevity." Nat Cell Biol **11**(11): 1305-1314.

Ellegaard, A. M., M. Jaattela and J. Nylandsted (2015). "Visualizing Lysosomal Membrane Permeabilization by Fluorescent Dextran Release." Cold Spring Harb Protoc **2015**(10): 900-903.

Ellis, J. (1987). "Proteins as molecular chaperones." Nature **328**(6129): 378-379.

Engelman, J. A., K. Zejnullahu, T. Mitsudomi, Y. Song, C. Hyland, J. O. Park, N. Lindeman, C. M. Gale, X. Zhao, J. Christensen, T. Kosaka, A. J. Holmes, A. M. Rogers, F. Cappuzzo, T. Mok, C. Lee, B. E. Johnson, L. C. Cantley and P. A. Janne (2007). "MET amplification leads to gefitinib resistance in lung cancer by activating ERBB3 signaling." Science **316**(5827): 1039-1043.

Enzenmuller, S., P. Gonzalez, G. Karpel-Massler, K. M. Debatin and S. Fulda (2013). "GDC-0941 enhances the lysosomal compartment via TFEB and primes glioblastoma cells to lysosomal membrane permeabilization and cell death." Cancer Lett **329**(1): 27-36.

Estable, C., W. Acosta-Ferreira and J. R. Sotelo (1957). "An electron microscope study of the regenerating nerve fibers." Z Zellforsch Mikrosk Anat **46**(4): 387-399.

Evageliou, N. F., M. Haber, A. Vu, T. W. Laetsch, J. Murray, L. D. Gamble, N. C. Cheng, K. Liu, M. Reese, K. A. Corrigan, D. S. Ziegler, H. Webber, C. S. Hayes, B. Pawel, G. M. Marshall, H. Zhao, S. K. Gilmour, M. D. Norris and M. D. Hogarty (2016). "Polyamine Antagonist Therapies Inhibit Neuroblastoma Initiation and Progression." Clin Cancer Res **22**(17): 4391-4404.

Evens, A. M., S. Balasubramanian, J. M. Vose, W. Harb, L. I. Gordon, R. Langdon, J. Sprague, M. Sirisawad, C. Mani, J. Yue, Y. Luan, S. Horton, T. Graef and N. L. Bartlett (2016). "A Phase I/II Multicenter, Open-Label Study of the Oral Histone Deacetylase Inhibitor Abexinostat in Relapsed/Refractory Lymphoma." Clin Cancer Res **22**(5): 1059-1066.

Ewald, B., D. Sampath and W. Plunkett (2007). "H2AX phosphorylation marks gemcitabine-induced stalled replication forks and their collapse upon S-phase checkpoint abrogation." Mol Cancer Ther **6**(4): 1239-1248.

Fan, J., B. Lou, W. Chen, J. Zhang, S. Lin, F. F. Lv and Y. Chen (2014). "Down-regulation of HDAC5 inhibits growth of human hepatocellular carcinoma by induction of apoptosis and cell cycle arrest." Tumour Biol **35**(11): 11523-11532.

Fedde, K. N. and W. S. Sly (1985). "Ricin-binding properties of acid hydrolases from isolated lysosomes implies prior processing by terminal transferases of the trans-Golgi apparatus." Biochem Biophys Res Commun **133**(2): 614-620.

Feeney, E. J., C. Spampanato, R. Puertollano, A. Ballabio, G. Parenti and N. Raben (2013). "What else is in store for autophagy? Exocytosis of autolysosomes as a mechanism of TFEB-mediated cellular clearance in Pompe disease." Autophagy **9**(7): 1117-1118.

Felder, S., K. Miller, G. Moehren, A. Ullrich, J. Schlessinger and C. R. Hopkins (1990). "Kinase activity controls the sorting of the epidermal growth factor receptor within the multivesicular body." Cell **61**(4): 623-634.

Feng, G. W., L. D. Dong, W. J. Shang, X. L. Pang, J. F. Li, L. Liu and Y. Wang (2014). "HDAC5 promotes cell proliferation in human hepatocellular carcinoma by up-regulating Six1 expression." Eur Rev Med Pharmacol Sci **18**(6): 811-816.

Fernandez, P. C., S. R. Frank, L. Wang, M. Schroeder, S. Liu, J. Greene, A. Cocito and B. Amati (2003). "Genomic targets of the human c-Myc protein." Genes Dev **17**(9): 1115-1129.

Ferrao, P., P. Sincock, S. Cole and L. Ashman (2001). "Intracellular P-gp contributes to functional drug efflux and resistance in acute myeloid leukaemia." Leuk Res **25**(5): 395-405.

Ferron, M., C. Settembre, J. Shimazu, J. Lacombe, S. Kato, D. J. Rawlings, A. Ballabio and G. Karsenty (2013). "A RANKL-PKCbeta-TFEB signaling cascade is necessary for lysosomal biogenesis in osteoclasts." Genes Dev **27**(8): 955-969.

Fila, J. and D. Honys (2012). "Enrichment techniques employed in phosphoproteomics." Amino Acids **43**(3): 1025-1047.

Filipits, M., R. Malayeri, R. W. Suchomel, G. Pohl, T. Stranzl, G. Dekan, A. Kaider, W. Stiglbauer, D. Depisch and R. Pirker (1999). "Expression of the multidrug resistance protein (MRP1) in breast cancer." Anticancer Res **19**(6B): 5043-5049.

Filippakopoulos, P. and S. Knapp (2014). "Targeting bromodomains: epigenetic readers of lysine acetylation." Nat Rev Drug Discov **13**(5): 337-356.

Finnin, M. S., J. R. Donigian, A. Cohen, V. M. Richon, R. A. Rifkind, P. A. Marks, R. Breslow and N. P. Pavletich (1999). "Structures of a histone deacetylase homologue bound to the TSA and SAHA inhibitors." Nature **401**(6749): 188-193.

Fischer, D. D., R. Cai, U. Bhatia, F. A. Asselbergs, C. Song, R. Terry, N. Trogani, R. Widmer, P. Atadja and D. Cohen (2002). "Isolation and characterization of a novel class II histone deacetylase, HDAC10." J Biol Chem **277**(8): 6656-6666.

Fischer, M., M. Skowron and F. Berthold (2005). "Reliable transcript quantification by real-time reverse transcriptase-polymerase chain reaction in primary neuroblastoma using normalization to averaged expression levels of the control genes HPRT1 and SDHA." J Mol Diagn **7**(1): 89-96.

Fischle, W., F. Dequiedt, M. J. Hendzel, M. G. Guenther, M. A. Lazar, W. Voelter and E. Verdin (2002). "Enzymatic activity associated with class II HDACs is dependent on a multiprotein complex containing HDAC3 and SMRT/N-CoR." Mol Cell **9**(1): 45-57.

Flaherty, K. M., C. DeLuca-Flaherty and D. B. McKay (1990). "Three-dimensional structure of the ATPase fragment of a 70K heat-shock cognate protein." Nature **346**(6285): 623-628.

Flynn, G. C., T. G. Chappell and J. E. Rothman (1989). "Peptide binding and release by proteins implicated as catalysts of protein assembly." Science **245**(4916): 385-390.

Flynn, G. C., J. Pohl, M. T. Flocco and J. E. Rothman (1991). "Peptide-binding specificity of the molecular chaperone BiP." Nature **353**(6346): 726-730.

Foghsgaard, L., D. Wissing, D. Mauch, U. Lademann, L. Bastholm, M. Boes, F. Elling, M. Leist and M. Jaattela (2001). "Cathepsin B acts as a dominant execution protease in tumor cell apoptosis induced by tumor necrosis factor." J Cell Biol **153**(5): 999-1010.

Fonovic, M. and B. Turk (2014). "Cysteine cathepsins and extracellular matrix degradation." Biochim Biophys Acta **1840**(8): 2560-2570.

Forgac, M. (1999). "Structure and properties of the vacuolar (H+)-ATPases." J Biol Chem **274**(19): 12951-12954.

Forgac, M. (2007). "Vacuolar ATPases: rotary proton pumps in physiology and pathophysiology." Nat Rev Mol Cell Biol **8**(11): 917-929.

Fraga, M. F., E. Ballestar, A. Villar-Garea, M. Boix-Chornet, J. Espada, G. Schotta, T. Bonaldi, C. Haydon, S. Ropero, K. Petrie, N. G. Iyer, A. Perez-Rosado, E. Calvo, J. A. Lopez, A. Cano, M. J. Calasanz, D. Colomer, M. A. Piris, N. Ahn, A. Imhof, C. Caldas, T. Jenuwein and M. Esteller (2005). "Loss of acetylation at Lys16 and trimethylation at Lys20 of histone H4 is a common hallmark of human cancer." Nat Genet **37**(4): 391-400.

Frenzel, A., J. Kugler, S. Helmsing, D. Meier, T. Schirrmann, M. Hust and S. Dubel (2017). "Designing Human Antibodies by Phage Display." Transfus Med Hemother **44**(5): 312-318.

Friedler, A., D. B. Veprintsev, S. M. Freund, K. I. von Glos and A. R. Fersht (2005). "Modulation of binding of DNA to the C-terminal domain of p53 by acetylation." Structure **13**(4): 629-636.

Frydman, J., E. Nimmesgern, K. Ohtsuka and F. U. Hartl (1994). "Folding of nascent polypeptide chains in a high molecular mass assembly with molecular chaperones." Nature **370**(6485): 111-117.

Fujita, N., T. Itoh, H. Omori, M. Fukuda, T. Noda and T. Yoshimori (2008). "The Atg16L complex specifies the site of LC3 lipidation for membrane biogenesis in autophagy." Mol Biol Cell **19**(5): 2092-2100.

Fullgrabe, J., E. Kavanagh and B. Joseph (2011). "Histone onco-modifications." Oncogene **30**(31): 3391-3403.

Gallo, C. J., R. A. Koza and E. J. Herbst (1986). "Polyamines and HeLa-cell DNA replication." Biochem J **238**(1): 37-42.

Gamble, L. D., M. D. Hogarty, X. Liu, D. S. Ziegler, G. Marshall, M. D. Norris and M. Haber (2012). "Polyamine pathway inhibition as a novel therapeutic approach to treating neuroblastoma." Front Oncol **2**: 162.

Gan, Z., S. Ram, C. Vaccaro, R. J. Ober and E. S. Ward (2009). "Analyses of the recycling receptor, FcRn, in live cells reveal novel pathways for lysosomal delivery." Traffic **10**(5): 600-614.

Gao, L., M. A. Cueto, F. Asselbergs and P. Atadja (2002). "Cloning and functional characterization of HDAC11, a novel member of the human histone deacetylase family." J Biol Chem **277**(28): 25748-25755.

Gao, Y. S., C. C. Hubbert and T. P. Yao (2010). "The microtubule-associated histone deacetylase 6 (HDAC6) regulates epidermal growth factor receptor (EGFR) endocytic trafficking and degradation." J Biol Chem **285**(15): 11219-11226.

Gardner, J. G., F. J. Grundy, T. M. Henkin and J. C. Escalante-Semerena (2006). "Control of acetyl-coenzyme A synthetase (AcsA) activity by acetylation/deacetylation without NAD(+) involvement in Bacillus subtilis." J Bacteriol **188**(15): 5460-5468.

Gaur, V., T. Connor, A. Sanigorski, S. D. Martin, C. R. Bruce, D. C. Henstridge, S. T. Bond, K. A. McEwen, L. Kerr-Bayles, T. D. Ashton, C. Fleming, M. Wu, L. S. Pike Winer, D. Chen, G. M. Hudson, J. W. R. Schwabe, K. Baar, M. A. Febbraio, P. Gregorevic, F. M. Pfeffer, K. R. Walder, M. Hargreaves and S. L. McGee (2016). "Disruption of the Class IIa HDAC Corepressor Complex Increases Energy Expenditure and Lipid Oxidation." Cell Rep **16**(11): 2802-2810.

George, R. E., T. Sanda, M. Hanna, S. Frohling, W. Luther, 2nd, J. Zhang, Y. Ahn, W. Zhou, W. B. London, P. McGrady, L. Xue, S. Zozulya, V. E. Gregor, T. R. Webb, N. S. Gray, D. G. Gilliland, L. Diller, H. Greulich, S. W. Morris, M. Meyerson and A. T. Look (2008). "Activating mutations in ALK provide a therapeutic target in neuroblastoma." Nature **455**(7215): 975-978.

Gocheva, V., W. Zeng, D. Ke, D. Klimstra, T. Reinheckel, C. Peters, D. Hanahan and J. A. Joyce (2006). "Distinct roles for cysteine cathepsin genes in multistage tumorigenesis." Genes Dev **20**(5): 543-556.

Gogolin, S., V. Ehemann, G. Becker, L. M. Brueckner, D. Dreidax, S. Bannert, I. Nolte, L. Savelyeva, E. Bell and F. Westermann (2013). "CDK4 inhibition restores G(1)-S arrest in MYCN-amplified neuroblastoma cells in the context of doxorubicin-induced DNA damage." Cell Cycle **12**(7): 1091-1104.

Gong, Y., M. Duvvuri and J. P. Krise (2003). "Separate roles for the Golgi apparatus and lysosomes in the sequestration of drugs in the multidrug-resistant human leukemic cell line HL-60." J Biol Chem **278**(50): 50234-50239.

Goodman, J. and P. Hochstein (1977). "Generation of free radicals and lipid peroxidation by redox cycling of adriamycin and daunomycin." Biochem Biophys Res Commun **77**(2): 797-803.

Gorden, P., J. L. Carpentier, S. Cohen and L. Orci (1978). "Epidermal growth factor: morphological demonstration of binding, internalization, and lysosomal association in human fibroblasts." Proc Natl Acad Sci U S A **75**(10): 5025-5029.

Goridis, C. and H. Rohrer (2002). "Specification of catecholaminergic and serotonergic neurons." Nat Rev Neurosci **3**(7): 531-541.

Gotink, K. J., M. Rovithi, R. R. de Haas, R. J. Honeywell, H. Dekker, D. Poel, K. Azijli, G. J. Peters, H. J. Broxterman and H. M. Verheul (2015). "Cross-resistance to clinically used tyrosine kinase inhibitors sunitinib, sorafenib and pazopanib." Cell Oncol (Dordr) **38**(2): 119-129.

Gottesman, M. M., T. Fojo and S. E. Bates (2002). "Multidrug resistance in cancer: role of ATP-dependent transporters." Nat Rev Cancer **2**(1): 48-58.

Greene, W. C. and L. F. Chen (2004). "Regulation of NF-kappaB action by reversible acetylation." Novartis Found Symp **259**: 208-217; discussion 218-225.

Gregoretti, I. V., Y. M. Lee and H. V. Goodson (2004). "Molecular evolution of the histone deacetylase family: functional implications of phylogenetic analysis." J Mol Biol **338**(1): 17-31.

Greve, B., T. Bolling, S. Amler, U. Rossler, M. Gomolka, C. Mayer, O. Popanda, K. Dreffke, A. Rickinger, E. Fritz, F. Eckardt-Schupp, C. Sauerland, H. Braselmann, W. Sauter, T. Illig, D. Riesenbeck, S. Konemann, N. Willich, S. Mortl, H. T. Eich and P. Schmezer (2012). "Evaluation of different biomarkers to predict individual radiosensitivity in an inter-laboratory comparison--lessons for future studies." PLoS One **7**(10): e47185.

Griffiths, G., B. Hoflack, K. Simons, I. Mellman and S. Kornfeld (1988). "The mannose 6-phosphate receptor and the biogenesis of lysosomes." Cell **52**(3): 329-341.

Groenewoud, M. J. and F. J. Zwartkruis (2013). "Rheb and Rags come together at the lysosome to activate mTORC1." Biochem Soc Trans **41**(4): 951-955.

Gros, P., Y. B. Ben Neriah, J. M. Croop and D. E. Housman (1986). "Isolation and expression of a complementary DNA that confers multidrug resistance." Nature **323**(6090): 728-731.

Groth-Pedersen, L., M. S. Ostenfeld, M. Hoyer-Hansen, J. Nylandsted and M. Jaattela (2007). "Vincristine induces dramatic lysosomal changes and sensitizes cancer cells to lysosome-destabilizing siramesine." Cancer Res **67**(5): 2217-2225.

Gruenberg, J. and H. Stenmark (2004). "The biogenesis of multivesicular endosomes." Nat Rev Mol Cell Biol **5**(4): 317-323.

Guardiola, A. R. and T. P. Yao (2002). "Molecular cloning and characterization of a novel histone deacetylase HDAC10." J Biol Chem **277**(5): 3350-3356.

Guo, B., A. Tam, S. A. Santi and A. M. Parissenti (2016). "Role of autophagy and lysosomal drug sequestration in acquired resistance to doxorubicin in MCF-7 cells." BMC Cancer **16**(1): 762.

Guo, J. Y., B. Xia and E. White (2013). "Autophagy-mediated tumor promotion." Cell **155**(6): 1216-1219.

Gupta, M., J. J. Han, M. Stenson, L. Wellik and T. E. Witzig (2012). "Regulation of STAT3 by histone deacetylase-3 in diffuse large B-cell lymphoma: implications for therapy." Leukemia **26**(6): 1356-1364.

Ha, J. H. and D. B. McKay (1995). "Kinetics of nucleotide-induced changes in the tryptophan fluorescence of the molecular chaperone Hsc70 and its subfragments suggest the ATP-induced conformational change follows initial ATP binding." Biochemistry **34**(36): 11635-11644.

Haas, I. G. and M. Wabl (1983). "Immunoglobulin heavy chain binding protein." Nature **306**(5941): 387-389.

Haber, M., J. Smith, S. B. Bordow, C. Flemming, S. L. Cohn, W. B. London, G. M. Marshall and M. D. Norris (2006). "Association of high-level MRP1 expression with poor clinical outcome in a large prospective study of primary neuroblastoma." J Clin Oncol **24**(10): 1546-1553.

Haberland, M., M. H. Mokalled, R. L. Montgomery and E. N. Olson (2009). "Epigenetic control of skull morphogenesis by histone deacetylase 8." Genes Dev **23**(14): 1625-1630.

Hageman, J., M. A. Rujano, M. A. van Waarde, V. Kakkar, R. P. Dirks, N. Govorukhina, H. M. Oosterveld-Hut, N. H. Lubsen and H. H. Kampinga (2010). "A DNAJB chaperone subfamily with HDAC-dependent activities suppresses toxic protein aggregation." Mol Cell **37**(3): 355-369.

Haggarty, S. J., K. M. Koeller, J. C. Wong, C. M. Grozinger and S. L. Schreiber (2003). "Domain-selective small-molecule inhibitor of histone deacetylase 6 (HDAC6)-mediated tubulin deacetylation." Proc Natl Acad Sci U S A **100**(8): 4389-4394.

Hai, Y. and D. W. Christianson (2016). "Histone deacetylase 6 structure and molecular basis of catalysis and inhibition." Nat Chem Biol **12**(9): 741-747.

Hai, Y., S. A. Shinsky, N. J. Porter and D. W. Christianson (2017). "Histone deacetylase 10 structure and molecular function as a polyamine deacetylase." Nat Commun **8**: 15368.

Hakimi, M. A., D. A. Bochar, J. Chenoweth, W. S. Lane, G. Mandel and R. Shiekhattar (2002). "A core-BRAF35 complex containing histone deacetylase mediates repression of neuronal-specific genes." Proc Natl Acad Sci U S A **99**(11): 7420-7425.

Halkidou, K., L. Gaughan, S. Cook, H. Y. Leung, D. E. Neal and C. N. Robson (2004). "Upregulation and nuclear recruitment of HDAC1 in hormone refractory prostate cancer." Prostate **59**(2): 177-189.

Hamman, B. D., L. M. Hendershot and A. E. Johnson (1998). "BiP maintains the permeability barrier of the ER membrane by sealing the lumenal end of the translocon pore before and early in translocation." Cell **92**(6): 747-758.

Hanahan, D. and R. A. Weinberg (2011). "Hallmarks of cancer: the next generation." Cell **144**(5): 646-674.

Harding, H. P., M. Calfon, F. Urano, I. Novoa and D. Ron (2002). "Transcriptional and translational control in the Mammalian unfolded protein response." Annu Rev Cell Dev Biol **18**: 575-599.

Hartl, F. U., A. Bracher and M. Hayer-Hartl (2011). "Molecular chaperones in protein folding and proteostasis." Nature **475**(7356): 324-332.

Hashizume, R. (2017). "Epigenetic Targeted Therapy for Diffuse Intrinsic Pontine Glioma." Neurol Med Chir (Tokyo) **57**(7): 331-342.

Hatton, B. A., P. S. Knoepfler, A. M. Kenney, D. H. Rowitch, I. M. de Alboran, J. M. Olson and R. N. Eisenman (2006). "N-myc is an essential downstream effector of Shh signaling during both normal and neoplastic cerebellar growth." Cancer Res **66**(17): 8655-8661.

Heideman, M. R., R. H. Wilting, E. Yanover, A. Velds, J. de Jong, R. M. Kerkhoven, H. Jacobs, L. F. Wessels and J. H. Dannenberg (2013). "Dosage-dependent tumor suppression by histone deacetylases 1 and 2 through regulation of c-Myc collaborating genes and p53 function." Blood **121**(11): 2038-2050.

Hemelaar, J., V. S. Lelyveld, B. M. Kessler and H. L. Ploegh (2003). "A single protease, Apg4B, is specific for the autophagy-related ubiquitin-like proteins GATE-16, MAP1-LC3, GABARAP, and Apg8L." J Biol Chem **278**(51): 51841-51850.

Henrich, K. O., T. Bauer, J. Schulte, V. Ehemann, H. Deubzer, S. Gogolin, D. Muth, M. Fischer, A. Benner, R. Konig, M. Schwab and F. Westermann (2011). "CAMTA1, a 1p36 tumor suppressor candidate, inhibits growth and activates differentiation programs in neuroblastoma cells." Cancer Res **71**(8): 3142-3151.

Henrich, K. O., S. Bender, M. Saadati, D. Dreidax, M. Gartlgruber, C. Shao, C. Herrmann, M. Wiesenfarth, M. Parzonka, L. Wehrmann, M. Fischer, D. J. Duffy, E. Bell, A. Torkov, P. Schmezer, C. Plass, T. Hofer, A. Benner, S. M. Pfister and F. Westermann (2016). "Integrative Genome-Scale Analysis Identifies Epigenetic Mechanisms of Transcriptional Deregulation in Unfavorable Neuroblastomas." Cancer Res **76**(18): 5523-5537.

Henrich, K. O., M. Schwab and F. Westermann (2012). "1p36 tumor suppression--a matter of dosage?" Cancer Res **72**(23): 6079-6088.

Herlevsen, M., G. Oxford, C. R. Owens, M. Conaway and D. Theodorescu (2007). "Depletion of major vault protein increases doxorubicin sensitivity and nuclear accumulation and disrupts its sequestration in lysosomes." Mol Cancer Ther **6**(6): 1804-1813.

Hero, B., T. Simon, R. Spitz, K. Ernestus, A. K. Gnekow, H. G. Scheel-Walter, D. Schwabe, F. H. Schilling, G. Benz-Bohm and F. Berthold (2008). "Localized infant neuroblastomas often show spontaneous regression: results of the prospective trials NB95-S and NB97." J Clin Oncol **26**(9): 1504-1510.

Hogarty, M. D., M. D. Norris, K. Davis, X. Liu, N. F. Evageliou, C. S. Hayes, B. Pawel, R. Guo, H. Zhao, E. Sekyere, J. Keating, W. Thomas, N. C. Cheng, J. Murray, J. Smith, R. Sutton, N. Venn, W. B. London, A. Buxton, S. K. Gilmour, G. M. Marshall and M. Haber (2008). "ODC1 is a critical determinant of MYCN oncogenesis and a therapeutic target in neuroblastoma." Cancer Res **68**(23): 9735-9745.

Holohan, C., S. Van Schaeybroeck, D. B. Longley and P. G. Johnston (2013). "Cancer drug resistance: an evolving paradigm." Nat Rev Cancer **13**(10): 714-726.

Hook, S. S., A. Orian, S. M. Cowley and R. N. Eisenman (2002). "Histone deacetylase 6 binds polyubiquitin through its zinc finger (PAZ domain) and copurifies with deubiquitinating enzymes." Proc Natl Acad Sci U S A **99**(21): 13425-13430.

Housman, G., S. Byler, S. Heerboth, K. Lapinska, M. Longacre, N. Snyder and S. Sarkar (2014). "Drug resistance in cancer: an overview." Cancers (Basel) **6**(3): 1769-1792.

Hrabeta, J., T. Groh, M. A. Khalil, J. Poljakova, V. Adam, R. Kizek, J. Uhlik, H. Doktorova, T. Cerna, E. Frei, M. Stiborova and T. Eckschlager (2015). "Vacuolar-ATPase-mediated intracellular sequestration of ellipticine contributes to drug resistance in neuroblastoma cells." Int J Oncol **47**(3): 971-980.

Hrelia, S., D. Fiorentini, T. Maraldi, C. Angeloni, A. Bordoni, P. L. Biagi and G. Hakim (2002). "Doxorubicin induces early lipid peroxidation associated with changes in glucose transport in cultured cardiomyocytes." Biochim Biophys Acta **1567**(1-2): 150-156.

Hu, X. F., A. Slater, D. M. Wall, P. Kantharidis, J. D. Parkin, A. Cowman and J. R. Zalcberg (1995). "Rapid up-regulation of mdr1 expression by anthracyclines in a classical multidrug-resistant cell line." Br J Cancer **71**(5): 931-936.

Huang, M. and W. A. Weiss (2013). "Neuroblastoma and MYCN." Cold Spring Harb Perspect Med **3**(10): a014415.

Hubbert, C., A. Guardiola, R. Shao, Y. Kawaguchi, A. Ito, A. Nixon, M. Yoshida, X. F. Wang and T. P. Yao (2002). "HDAC6 is a microtubule-associated deacetylase." Nature **417**(6887): 455-458.

Hunt, C. and R. I. Morimoto (1985). "Conserved features of eukaryotic hsp70 genes revealed by comparison with the nucleotide sequence of human hsp70." Proc Natl Acad Sci U S A **82**(19): 6455-6459.

Huotari, J. and A. Helenius (2011). "Endosome maturation." EMBO J **30**(17): 3481-3500.

Hurwitz, S. J., M. Terashima, N. Mizunuma and C. A. Slapak (1997). "Vesicular anthracycline accumulation in doxorubicin-selected U-937 cells: participation of lysosomes." Blood **89**(10): 3745-3754.

Huynh, K. K., E. L. Eskelinen, C. C. Scott, A. Malevanets, P. Saftig and S. Grinstein (2007). "LAMP proteins are required for fusion of lysosomes with phagosomes." EMBO J **26**(2): 313-324.

Ichimura, Y., T. Kirisako, T. Takao, Y. Satomi, Y. Shimonishi, N. Ishihara, N. Mizushima, I. Tanida, E. Kominami, M. Ohsumi, T. Noda and Y. Ohsumi (2000). "A ubiquitin-like system mediates protein lipidation." Nature **408**(6811): 488-492.

Iehara, T., M. Hamazaki, T. Tajiri, Y. Kawano, M. Kaneko, H. Ikeda, H. Hosoi, T. Sugimoto and T. Sawada (2013). "Successful treatment of infants with localized neuroblastoma based on their MYCN status." Int J Clin Oncol **18**(3): 389-395.

Ingolia, T. D. and E. A. Craig (1982). "Drosophila gene related to the major heat shock-induced gene is transcribed at normal temperatures and not induced by heat shock." Proc Natl Acad Sci U S A **79**(2): 525-529.

Ingolia, T. D., M. R. Slater and E. A. Craig (1982). "Saccharomyces cerevisiae contains a complex multigene family related to the major heat shock-inducible gene of Drosophila." Mol Cell Biol **2**(11): 1388-1398.

Islam, M. M., T. Banerjee, C. Z. Packard, S. Kotian, K. Selvendiran, D. E. Cohn and J. D. Parvin (2017). "HDAC10 as a potential therapeutic target in ovarian cancer." Gynecol Oncol **144**(3): 613-620.

Itakura, E., C. Kishi-Itakura and N. Mizushima (2012). "The hairpin-type tail-anchored SNARE syntaxin 17 targets to autophagosomes for fusion with endosomes/lysosomes." Cell **151**(6): 1256-1269.

Izumi, H. and Y. Kaneko (2012). "Evidence of asymmetric cell division and centrosome inheritance in human neuroblastoma cells." Proc Natl Acad Sci U S A **109**(44): 18048-18053.

Jager, V., K. Bussow, A. Wagner, S. Weber, M. Hust, A. Frenzel and T. Schirrmann (2013). "High level transient production of recombinant antibodies and antibody fusion proteins in HEK293 cells." BMC Biotechnol **13**: 52.

Jahreiss, L., F. M. Menzies and D. C. Rubinsztein (2008). "The itinerary of autophagosomes: from peripheral formation to kiss-and-run fusion with lysosomes." Traffic **9**(4): 574-587.

Jaiswal, J. K., N. W. Andrews and S. M. Simon (2002). "Membrane proximal lysosomes are the major vesicles responsible for calcium-dependent exocytosis in nonsecretory cells." J Cell Biol **159**(4): 625-635.

Janoueix-Lerosey, I., D. Lequin, L. Brugieres, A. Ribeiro, L. de Pontual, V. Combaret, V. Raynal, A. Puisieux, G. Schleiermacher, G. Pierron, D. Valteau-Couanet, T. Frebourg, J. Michon, S. Lyonnet, J. Amiel and O. Delattre (2008). "Somatic and germline activating mutations of the ALK kinase receptor in neuroblastoma." Nature **455**(7215): 967-970.

Jenuwein, T. and C. D. Allis (2001). "Translating the histone code." Science **293**(5532): 1074-1080.

Jeong, J., K. Juhn, H. Lee, S. H. Kim, B. H. Min, K. M. Lee, M. H. Cho, G. H. Park and K. H. Lee (2007). "SIRT1 promotes DNA repair activity and deacetylation of Ku70." Exp Mol Med **39**(1): 8-13.

Jiang, M., J. Stanke and J. M. Lahti (2011). "The connections between neural crest development and neuroblastoma." Curr Top Dev Biol **94**: 77-127.

Jiang, P., T. Nishimura, Y. Sakamaki, E. Itakura, T. Hatta, T. Natsume and N. Mizushima (2014). "The HOPS complex mediates autophagosome-lysosome fusion through interaction with syntaxin 17." Mol Biol Cell **25**(8): 1327-1337.

Jin, Z., W. Jiang, F. Jiao, Z. Guo, H. Hu and L. Wang (2014). "Decreased expression of histone deacetylase 10 predicts poor prognosis of gastric cancer patients." Int J Clin Exp Pathol **7**(9): 5872-5879.

Johnson, D. E., P. Ostrowski, V. Jaumouille and S. Grinstein (2016). "The position of lysosomes within the cell determines their luminal pH." J Cell Biol **212**(6): 677-692.

Jonas, A. J., L. J. Symons and R. J. Speller (1987). "Polyamines stimulate lysosomal cystine transport." J Biol Chem **262**(34): 16391-16393.

Jones, P., S. Altamura, R. De Francesco, P. Gallinari, A. Lahm, P. Neddermann, M. Rowley, S. Serafini and C. Steinkuhler (2008). "Probing the elusive catalytic activity of vertebrate class IIa histone deacetylases." Bioorg Med Chem Lett **18**(6): 1814-1819.

Jovic, M., M. Sharma, J. Rahajeng and S. Caplan (2010). "The early endosome: a busy sorting station for proteins at the crossroads." Histol Histopathol **25**(1): 99-112.

Jung, K. H., J. H. Noh, J. K. Kim, J. W. Eun, H. J. Bae, H. J. Xie, Y. G. Chang, M. G. Kim, H. Park, J. Y. Lee and S. W. Nam (2012). "HDAC2 overexpression confers oncogenic potential to human lung cancer cells by deregulating expression of apoptosis and cell cycle proteins." J Cell Biochem **113**(6): 2167-2177.

Kaatsch, P., D. Grabow and C. Spix (2018). "German Childhood Cancer Registry - Annual Report 2017 (1980-2016)." Institute of Medical Biostatistics, Epidemiology and Informatics (IMBEI) at the University Medical Center of the Johannes Gutenberg University Mainz.

Kabeya, Y., N. Mizushima, T. Ueno, A. Yamamoto, T. Kirisako, T. Noda, E. Kominami, Y. Ohsumi and T. Yoshimori (2000). "LC3, a mammalian homologue of yeast Apg8p, is localized in autophagosome membranes after processing." EMBO J **19**(21): 5720-5728.

Kallunki, T., O. D. Olsen and M. Jaattela (2013). "Cancer-associated lysosomal changes: friends or foes?" Oncogene **32**(16): 1995-2004.

Kang, J., P. G. Rychahou, T. A. Ishola, J. M. Mourot, B. M. Evers and D. H. Chung (2008). "N-myc is a novel regulator of PI3K-mediated VEGF expression in neuroblastoma." Oncogene **27**(28): 3999-4007.

Kao, H. Y., M. Downes, P. Ordentlich and R. M. Evans (2000). "Isolation of a novel histone deacetylase reveals that class I and class II deacetylases promote SMRT-mediated repression." Genes Dev **14**(1): 55-66.

Kao, H. Y., C. H. Lee, A. Komarov, C. C. Han and R. M. Evans (2002). "Isolation and characterization of mammalian HDAC10, a novel histone deacetylase." J Biol Chem **277**(1): 187-193.

Kaplan, A., D. T. Achord and W. S. Sly (1977). "Phosphohexosyl components of a lysosomal enzyme are recognized by pinocytosis receptors on human fibroblasts." Proc Natl Acad Sci U S A **74**(5): 2026-2030.

Karantza-Wadsworth, V., S. Patel, O. Kravchuk, G. Chen, R. Mathew, S. Jin and E. White (2007). "Autophagy mitigates metabolic stress and genome damage in mammary tumorigenesis." Genes Dev **21**(13): 1621-1635.

Karolczak-Bayatti, M., M. Sweeney, J. Cheng, L. Edey, S. C. Robson, S. M. Ulrich, A. Treumann, M. J. Taggart and G. N. Europe-Finner (2011). "Acetylation of heat shock protein 20 (Hsp20) regulates human myometrial activity." J Biol Chem **286**(39): 34346-34355.

Katayama, M., T. Kawaguchi, M. S. Berger and R. O. Pieper (2007). "DNA damaging agent-induced autophagy produces a cytoprotective adenosine triphosphate surge in malignant glioma cells." Cell Death Differ **14**(3): 548-558.

Katzmann, D. J., M. Babst and S. D. Emr (2001). "Ubiquitin-dependent sorting into the multivesicular body pathway requires the function of a conserved endosomal protein sorting complex, ESCRT-I." Cell **106**(2): 145-155.

Kaushik, S. and A. M. Cuervo (2018). "The coming of age of chaperone-mediated autophagy." Nat Rev Mol Cell Biol **19**(6): 365-381.

Kawaguchi, Y., J. J. Kovacs, A. McLaurin, J. M. Vance, A. Ito and T. P. Yao (2003). "The deacetylase HDAC6 regulates aggresome formation and cell viability in response to misfolded protein stress." Cell **115**(6): 727-738.

Kekatpure, V. D., A. J. Dannenberg and K. Subbaramaiah (2009). "HDAC6 modulates Hsp90 chaperone activity and regulates activation of aryl hydrocarbon receptor signaling." J Biol Chem **284**(12): 7436-7445.

Keller, A., A. I. Nesvizhskii, E. Kolker and R. Aebersold (2002). "Empirical statistical model to estimate the accuracy of peptide identifications made by MS/MS and database search." Anal Chem **74**(20): 5383-5392.

Kenney, A. M., M. D. Cole and D. H. Rowitch (2003). "Nmyc upregulation by sonic hedgehog signaling promotes proliferation in developing cerebellar granule neuron precursors." Development **130**(1): 15-28.

Keshelava, N., J. J. Zuo, N. S. Waidyaratne, T. J. Triche and C. P. Reynolds (2000). "p53 mutations and loss of p53 function confer multidrug resistance in neuroblastoma." Med Pediatr Oncol **35**(6): 563-568.

Khalil, M. A., J. Hrabeta, S. Cipro, M. Stiborova, A. Vicha and T. Eckschlager (2012). "Neuroblastoma stem cells - mechanisms of chemoresistance and histone deacetylase inhibitors." Neoplasma **59**(6): 737-746.

Khan, N., M. Jeffers, S. Kumar, C. Hackett, F. Boldog, N. Khramtsov, X. Qian, E. Mills, S. C. Berghs, N. Carey, P. W. Finn, L. S. Collins, A. Tumber, J. W. Ritchie, P. B. Jensen, H. S. Lichenstein and M. Sehested (2008). "Determination of the class and isoform selectivity of small-molecule histone deacetylase inhibitors." Biochem J **409**(2): 581-589.

Kim, J., M. Kundu, B. Viollet and K. L. Guan (2011). "AMPK and mTOR regulate autophagy through direct phosphorylation of Ulk1." Nat Cell Biol **13**(2): 132-141.

Kimura, T., J. Jia, A. Claude-Taupin, S. Kumar, S. W. Choi, Y. Gu, M. Mudd, N. Dupont, S. Jiang, R. Peters, F. Farzam, A. Jain, K. A. Lidke, C. M. Adams, T. Johansen and V. Deretic (2017a). "Cellular and molecular mechanism for secretory autophagy." Autophagy **13**(6): 1084-1085.

Kimura, T., J. Jia, S. Kumar, S. W. Choi, Y. Gu, M. Mudd, N. Dupont, S. Jiang, R. Peters, F. Farzam, A. Jain, K. A. Lidke, C. M. Adams, T. Johansen and V. Deretic (2017b). "Dedicated SNAREs and specialized TRIM cargo receptors mediate secretory autophagy." EMBO J **36**(1): 42-60.

Kirkegaard, T. and M. Jaattela (2009). "Lysosomal involvement in cell death and cancer." Biochim Biophys Acta **1793**(4): 746-754.

Kleff, S., E. D. Andrulis, C. W. Anderson and R. Sternglanz (1995). "Identification of a gene encoding a yeast histone H4 acetyltransferase." J Biol Chem **270**(42): 24674-24677.

Klionsky, D. J., Z. Elazar, P. O. Seglen and D. C. Rubinsztein (2008). "Does bafilomycin A1 block the fusion of autophagosomes with lysosomes?" Autophagy **4**(7): 849-850.

Klumperman, J. and G. Raposo (2014). "The complex ultrastructure of the endolysosomal system." Cold Spring Harb Perspect Biol **6**(10): a016857.

Kobayashi, S., T. J. Boggon, T. Dayaram, P. A. Janne, O. Kocher, M. Meyerson, B. E. Johnson, M. J. Eck, D. G. Tenen and B. Halmos (2005). "EGFR mutation and resistance of non-small-cell lung cancer to gefitinib." N Engl J Med **352**(8): 786-792.

Koeneke, E., O. Witt and I. Oehme (2015). "HDAC Family Members Intertwined in the Regulation of Autophagy: A Druggable Vulnerability in Aggressive Tumor Entities." Cells **4**(2): 135-168.

Kohl, N. E., C. E. Gee and F. W. Alt (1984). "Activated expression of the N-myc gene in human neuroblastomas and related tumors." Science **226**(4680): 1335-1337.

Köhler, G. and C. Milstein (1975). "Continuous cultures of fused cells secreting antibody of predefined specificity." Nature **256**(5517): 495-497.

Kohler, J. A., H. Rubie, V. Castel, K. Beiske, K. Holmes, C. Gambini, F. Casale, C. Munzer, G. Erminio, S. Parodi, S. Navarro, C. Marquez, M. Peuchmaur, C. Cullinane, P. Brock, D. Valteau-Couanet, A. Garaventa and R. Haupt (2013). "Treatment of children over the age of one year with unresectable localised neuroblastoma without MYCN amplification: results of the SIOPEN study." Eur J Cancer **49**(17): 3671-3679.

Kolbinger, F. R., E. Koeneke, J. Ridinger, T. Heimburg, M. Muller, T. Bayer, W. Sippl, M. Jung, N. Gunkel, A. K. Miller, F. Westermann, O. Witt and I. Oehme (2018). "The HDAC6/8/10 inhibitor TH34 induces DNA damage-mediated cell death in human high-grade neuroblastoma cell lines." Arch Toxicol **92**(8): 2649-2664.

Korhonen, V. P., M. Halmekyto, L. Kauppinen, S. Myohanen, J. Wahlfors, T. Keinanen, T. Hyvonen, L. Alhonen, T. Eloranta and J. Janne (1995). "Molecular cloning of a cDNA encoding human spermine synthase." DNA Cell Biol **14**(10): 841-847.

Kornberg, R. D. (1974). "Chromatin structure: a repeating unit of histones and DNA." Science **184**(4139): 868-871.

Kornfeld, S. and I. Mellman (1989). "The biogenesis of lysosomes." Annu Rev Cell Biol **5**: 483-525.

Korolchuk, V. I., S. Saiki, M. Lichtenberg, F. H. Siddiqi, E. A. Roberts, S. Imarisio, L. Jahreiss, S. Sarkar, M. Futter, F. M. Menzies, C. J. O'Kane, V. Deretic and D. C. Rubinsztein (2011). "Lysosomal positioning coordinates cellular nutrient responses." Nat Cell Biol **13**(4): 453-460.

Kostyrko, K. and N. Mermod (2016). "Assays for DNA double-strand break repair by microhomology-based end-joining repair mechanisms." Nucleic Acids Res **44**(6): e56.

Kotian, S., S. Liyanarachchi, A. Zelent and J. D. Parvin (2011). "Histone deacetylases 9 and 10 are required for homologous recombination." J Biol Chem **286**(10): 7722-7726.

Kouzarides, T. (2007). "Chromatin modifications and their function." Cell **128**(4): 693-705.

Kovacs, J. J., P. J. Murphy, S. Gaillard, X. Zhao, J. T. Wu, C. V. Nicchitta, M. Yoshida, D. O. Toft, W. B. Pratt and T. P. Yao (2005). "HDAC6 regulates Hsp90 acetylation and chaperone-dependent activation of glucocorticoid receptor." Mol Cell **18**(5): 601-607.

Krispin, S., E. Nitzan, Y. Kassem and C. Kalcheim (2010). "Evidence for a dynamic spatiotemporal fate map and early fate restrictions of premigratory avian neural crest." Development **137**(4): 585-595.

Krusche, C. A., P. Wulfing, C. Kersting, A. Vloet, W. Bocker, L. Kiesel, H. M. Beier and J. Alfer (2005). "Histone deacetylase-1 and -3 protein expression in human breast cancer: a tissue microarray analysis." Breast Cancer Res Treat **90**(1): 15-23.

Kugler, J., S. Wilke, D. Meier, F. Tomszak, A. Frenzel, T. Schirrmann, S. Dubel, H. Garritsen, B. Hock, L. Toleikis, M. Schutte and M. Hust (2015). "Generation and analysis of the improved human HAL9/10 antibody phage display libraries." BMC Biotechnol **15**: 10.

Kuo, L. J. and L. X. Yang (2008). "Gamma-H2AX - a novel biomarker for DNA double-strand breaks." In Vivo **22**(3): 305-309.

Lahm, A., C. Paolini, M. Pallaoro, M. C. Nardi, P. Jones, P. Neddermann, S. Sambucini, M. J. Bottomley, P. Lo Surdo, A. Carfi, U. Koch, R. De Francesco, C. Steinkuhler and P. Gallinari (2007). "Unraveling the hidden catalytic activity of vertebrate class IIa histone deacetylases." Proc Natl Acad Sci U S A **104**(44): 17335-17340.

Lai, I. L., T. P. Lin, Y. L. Yao, C. Y. Lin, M. J. Hsieh and W. M. Yang (2010). "Histone deacetylase 10 relieves repression on the melanogenic program by maintaining the deacetylation status of repressors." J Biol Chem **285**(10): 7187-7196.

Lane, A. A. and B. A. Chabner (2009). "Histone deacetylase inhibitors in cancer therapy." J Clin Oncol **27**(32): 5459-5468.

Langer, T., C. Lu, H. Echols, J. Flanagan, M. K. Hayer and F. U. Hartl (1992). "Successive action of DnaK, DnaJ and GroEL along the pathway of chaperone-mediated protein folding." Nature **356**(6371): 683-689.

Lapierre, M., A. Linares, M. Dalvai, C. Duraffourd, S. Bonnet, A. Boulahtouf, C. Rodriguez, S. Jalaguier, S. Assou, B. Orsetti, P. Balaguer, T. Maudelonde, P. Blache, K. Bystricky, N. Boulle and V. Cavailles (2016). "Histone deacetylase 9 regulates breast cancer cell proliferation and the response to histone deacetylase inhibitors." Oncotarget **7**(15): 19693-19708.

LaPlante, J. M., M. Sun, J. Falardeau, D. Dai, E. M. Brown, S. A. Slaugenhaupt and P. M. Vassilev (2006). "Lysosomal exocytosis is impaired in mucolipidosis type IV." Mol Genet Metab **89**(4): 339-348.

Laplante, M. and D. M. Sabatini (2012). "mTOR signaling in growth control and disease." Cell **149**(2): 274-293.

Larsen, A. K., A. E. Escargueil and A. Skladanowski (2000). "Resistance mechanisms associated with altered intracellular distribution of anticancer agents." Pharmacol Ther **85**(3): 217-229.

Lasorella, A., R. Boldrini, C. Dominici, A. Donfrancesco, Y. Yokota, A. Inserra and A. Iavarone (2002). "Id2 is critical for cellular proliferation and is the oncogenic effector of N-myc in human neuroblastoma." Cancer Res **62**(1): 301-306.

Lasorella, A., A. Iavarone and M. A. Israel (1996). "Id2 specifically alters regulation of the cell cycle by tumor suppressor proteins." Mol Cell Biol **16**(6): 2570-2578.

Laubach, J. P., P. Moreau, J. F. San-Miguel and P. G. Richardson (2015). "Panobinostat for the Treatment of Multiple Myeloma." Clin Cancer Res **21**(21): 4767-4773.

Laulagnier, K., N. L. Schieber, T. Maritzen, V. Haucke, R. G. Parton and J. Gruenberg (2011). "Role of AP1 and Gadkin in the traffic of secretory endo-lysosomes." Mol Biol Cell **22**(12): 2068-2082.

Laurenti, E., B. Varnum-Finney, A. Wilson, I. Ferrero, W. E. Blanco-Bose, A. Ehninger, P. S. Knoepfler, P. F. Cheng, H. R. MacDonald, R. N. Eisenman, I. D. Bernstein and A. Trumpp (2008). "Hematopoietic stem cell function and survival depend on c-Myc and N-Myc activity." Cell Stem Cell **3**(6): 611-624.

Lee, H., N. Rezai-Zadeh and E. Seto (2004). "Negative regulation of histone deacetylase 8 activity by cyclic AMP-dependent protein kinase A." Mol Cell Biol **24**(2): 765-773.

Lee, J. H., E. G. Jeong, M. C. Choi, S. H. Kim, J. H. Park, S. H. Song, J. Park, Y. J. Bang and T. Y. Kim (2010a). "Inhibition of histone deacetylase 10 induces thioredoxin-interacting protein and causes accumulation of reactive oxygen species in SNU-620 human gastric cancer cells." Mol Cells **30**(2): 107-112.

Lee, J. Y., H. Koga, Y. Kawaguchi, W. Tang, E. Wong, Y. S. Gao, U. B. Pandey, S. Kaushik, E. Tresse, J. Lu, J. P. Taylor, A. M. Cuervo and T. P. Yao (2010b). "HDAC6 controls autophagosome maturation essential for ubiquitin-selective quality-control autophagy." EMBO J **29**(5): 969-980.

Levinger, I., Y. Ventura and R. Vago (2014). "Life is three dimensional-as in vitro cancer cultures should be." Adv Cancer Res **121**: 383-414.

Li, M., J. Luo, C. L. Brooks and W. Gu (2002). "Acetylation of p53 inhibits its ubiquitination by Mdm2." J Biol Chem **277**(52): 50607-50611.

Li, W. W., J. Li and J. K. Bao (2012). "Microautophagy: lesser-known self-eating." Cell Mol Life Sci **69**(7): 1125-1136.

Li, Y., L. Peng and E. Seto (2015). "Histone Deacetylase 10 Regulates the Cell Cycle G2/M Phase Transition via a Novel Let-7-HMGA2-Cyclin A2 Pathway." Mol Cell Biol **35**(20): 3547-3565.

Li, Y. and E. Seto (2016). "HDACs and HDAC Inhibitors in Cancer Development and Therapy." Cold Spring Harb Perspect Med **6**(10).

Li, Z. and P. Srivastava (2004). "Heat-shock proteins." Curr Protoc Immunol **Appendix 1**: Appendix 1T.

Libby, P. R. (1978). "Properties of an acetylspermidine deacetylase from rat liver." Arch Biochem Biophys **188**(2): 360-363.

Libby, P. R. (1980). "Rat liver nuclear N-acetyltransferases: separation of two enzymes with both histone and spermidine acetyltransferase activity." Arch Biochem Biophys **203**(1): 384-389.

Lindberg, I., J. Shorter, R. L. Wiseman, F. Chiti, C. A. Dickey and P. J. McLean (2015). "Chaperones in Neurodegeneration." J Neurosci **35**(41): 13853-13859.

Lindquist, S. (1986). "The heat-shock response." Annu Rev Biochem **55**: 1151-1191.

Lindquist, S. and E. A. Craig (1988). "The heat-shock proteins." Annu Rev Genet **22**: 631-677.

Liu, Y., L. Peng, E. Seto, S. Huang and Y. Qiu (2012a). "Modulation of histone deacetylase 6 (HDAC6) nuclear import and tubulin deacetylase activity through acetylation." J Biol Chem **287**(34): 29168-29174.

Liu, Y., Y. Zhou and K. Zhu (2012b). "Inhibition of glioma cell lysosome exocytosis inhibits glioma invasion." PLoS One **7**(9): e45910.

Liu, Z., X. Yang, Z. Li, C. McMahon, C. Sizer, L. Barenboim-Stapleton, V. Bliskovsky, B. Mock, T. Ried, W. B. London, J. Maris, J. Khan and C. J. Thiele (2011). "CASZ1, a candidate tumor-suppressor gene, suppresses neuroblastoma tumor growth through reprogramming gene expression." Cell Death Differ **18**(7): 1174-1183.

Livak, K. J. and T. D. Schmittgen (2001). "Analysis of relative gene expression data using real-time quantitative PCR and the 2(-Delta Delta C(T)) Method." Methods **25**(4): 402-408.

Lodrini, M., I. Oehme, C. Schroeder, T. Milde, M. C. Schier, A. Kopp-Schneider, J. H. Schulte, M. Fischer, K. De Preter, F. Pattyn, M. Castoldi, M. U. Muckenthaler, A. E. Kulozik, F. Westermann, O. Witt and H. E. Deubzer (2013). "MYCN and HDAC2 cooperate to repress miR-183 signaling in neuroblastoma." Nucleic Acids Res **41**(12): 6018-6033.

London, W. B., V. Castel, T. Monclair, P. F. Ambros, A. D. Pearson, S. L. Cohn, F. Berthold, A. Nakagawara, R. L. Ladenstein, T. Iehara and K. K. Matthay (2011). "Clinical and biologic features predictive of survival

after relapse of neuroblastoma: a report from the International Neuroblastoma Risk Group project." J Clin Oncol **29**(24): 3286-3292.

Longley, D. B. and P. G. Johnston (2005). "Molecular mechanisms of drug resistance." J Pathol **205**(2): 275-292.

Louis, C. U. and J. M. Shohet (2015). "Neuroblastoma: molecular pathogenesis and therapy." Annu Rev Med **66**: 49-63.

Loven, J., N. Zinin, T. Wahlstrom, I. Muller, P. Brodin, E. Fredlund, U. Ribacke, A. Pivarcsi, S. Pahlman and M. Henriksson (2010). "MYCN-regulated microRNAs repress estrogen receptor-alpha (ESR1) expression and neuronal differentiation in human neuroblastoma." Proc Natl Acad Sci U S A **107**(4): 1553-1558.

Lu, Z., Y. Chen, A. M. Aponte, V. Battaglia, M. Gucek and M. N. Sack (2015). "Prolonged fasting identifies heat shock protein 10 as a Sirtuin 3 substrate: elucidating a new mechanism linking mitochondrial protein acetylation to fatty acid oxidation enzyme folding and function." J Biol Chem **290**(4): 2466-2476.

Luo, J., F. Su, D. Chen, A. Shiloh and W. Gu (2000). "Deacetylation of p53 modulates its effect on cell growth and apoptosis." Nature **408**(6810): 377-381.

Luzio, J. P., Y. Hackmann, N. M. Dieckmann and G. M. Griffiths (2014). "The biogenesis of lysosomes and lysosome-related organelles." Cold Spring Harb Perspect Biol **6**(9): a016840.

Luzio, J. P., V. Poupon, M. R. Lindsay, B. M. Mullock, R. C. Piper and P. R. Pryor (2003). "Membrane dynamics and the biogenesis of lysosomes." Mol Membr Biol **20**(2): 141-154.

Luzio, J. P., P. R. Pryor and N. A. Bright (2007). "Lysosomes: fusion and function." Nat Rev Mol Cell Biol **8**(8): 622-632.

Lyu, Y. L., J. E. Kerrigan, C. P. Lin, A. M. Azarova, Y. C. Tsai, Y. Ban and L. F. Liu (2007). "Topoisomerase IIbeta mediated DNA double-strand breaks: implications in doxorubicin cardiotoxicity and prevention by dexrazoxane." Cancer Res **67**(18): 8839-8846.

Machado, E., S. White-Gilbertson, D. van de Vlekkert, L. Janke, S. Moshiach, Y. Campos, D. Finkelstein, E. Gomero, R. Mosca, X. Qiu, C. L. Morton, I. Annunziata and A. d'Azzo (2015). "Regulated lysosomal exocytosis mediates cancer progression." Sci Adv **1**(11): e1500603.

Maitra, R., P. A. Halpin, K. H. Karlson, R. L. Page, D. Y. Paik, M. O. Leavitt, B. D. Moyer, B. A. Stanton and J. W. Hamilton (2001). "Differential effects of mitomycin C and doxorubicin on P-glycoprotein expression." Biochem J **355**(Pt 3): 617-624.

Malynn, B. A., I. M. de Alboran, R. C. O'Hagan, R. Bronson, L. Davidson, R. A. DePinho and F. W. Alt (2000). "N-myc can functionally replace c-myc in murine development, cellular growth, and differentiation." Genes Dev **14**(11): 1390-1399.

Mandal, S., A. Mandal, H. E. Johansson, A. V. Orjalo and M. H. Park (2013). "Depletion of cellular polyamines, spermidine and spermine, causes a total arrest in translation and growth in mammalian cells." Proc Natl Acad Sci U S A **110**(6): 2169-2174.

Mann, B. S., J. R. Johnson, M. H. Cohen, R. Justice and R. Pazdur (2007). "FDA approval summary: vorinostat for treatment of advanced primary cutaneous T-cell lymphoma." Oncologist **12**(10): 1247-1252.

Mao, Z., M. Bozzella, A. Seluanov and V. Gorbunova (2008). "Comparison of nonhomologous end joining and homologous recombination in human cells." DNA Repair (Amst) **7**(10): 1765-1771.

Marchant, P., S. Dredar, V. Manneh, O. Alshabanah, H. Matthews, D. Fries and J. Blankenship (1989). "A selective inhibitor of N8-acetylspermidine deacetylation in mice and HeLa cells without effects on histone deacetylation." Arch Biochem Biophys **273**(1): 128-136.

Marchant, P., V. A. Manneh and J. Blankenship (1986). "N1-acetylspermidine is not a substrate for N-acetylspermidine deacetylase." Biochim Biophys Acta **881**(2): 297-299.

Maris, J. M., C. Guo, D. Blake, P. S. White, M. D. Hogarty, P. M. Thompson, V. Rajalingam, R. Gerbing, D. O. Stram, K. K. Matthay, R. C. Seeger and G. M. Brodeur (2001). "Comprehensive analysis of chromosome 1p deletions in neuroblastoma." Med Pediatr Oncol **36**(1): 32-36.

Marks, B. D., S. A. Fakhoury, W. J. Frazee, H. C. Eliason and S. M. Riddle (2011). "A substrate-independent TR-FRET histone deacetylase inhibitor assay." J Biomol Screen **16**(10): 1247-1253.

Marks, M. S., H. F. Heijnen and G. Raposo (2013). "Lysosome-related organelles: unusual compartments become mainstream." Curr Opin Cell Biol **25**(4): 495-505.

Martens, S., S. Nakamura and T. Yoshimori (2016). "Phospholipids in Autophagosome Formation and Fusion." J Mol Biol.

Martina, J. A., Y. Chen, M. Gucek and R. Puertollano (2012). "MTORC1 functions as a transcriptional regulator of autophagy by preventing nuclear transport of TFEB." Autophagy **8**(6): 903-914.

Martina, J. A. and R. Puertollano (2013). "Rag GTPases mediate amino acid-dependent recruitment of TFEB and MITF to lysosomes." J Cell Biol **200**(4): 475-491.

Mathew, R., S. Kongara, B. Beaudoin, C. M. Karp, K. Bray, K. Degenhardt, G. Chen, S. Jin and E. White (2007). "Autophagy suppresses tumor progression by limiting chromosomal instability." Genes Dev **21**(11): 1367-1381.

Matteoni, R. and T. E. Kreis (1987). "Translocation and clustering of endosomes and lysosomes depends on microtubules." J Cell Biol **105**(3): 1253-1265.

Matthay, K. K., J. M. Maris, G. Schleiermacher, A. Nakagawara, C. L. Mackall, L. Diller and W. A. Weiss (2016). "Neuroblastoma." Nat Rev Dis Primers **2**: 16078.

Matthay, K. K., C. Perez, R. C. Seeger, G. M. Brodeur, H. Shimada, J. B. Atkinson, C. T. Black, R. Gerbing, G. M. Haase, D. O. Stram, P. Swift and J. N. Lukens (1998). "Successful treatment of stage III neuroblastoma based on prospective biologic staging: a Children's Cancer Group study." J Clin Oncol **16**(4): 1256-1264.

Mauvezin, C., P. Nagy, G. Juhasz and T. P. Neufeld (2015). "Autophagosome-lysosome fusion is independent of V-ATPase-mediated acidification." Nat Commun **6**: 7007.

Mauvezin, C. and T. P. Neufeld (2015). "Bafilomycin A1 disrupts autophagic flux by inhibiting both V-ATPase-dependent acidification and Ca-P60A/SERCA-dependent autophagosome-lysosome fusion." Autophagy **11**(8): 1437-1438.

Mayer, C., O. Popanda, O. Zelezny, M. C. von Brevern, A. Bach, H. Bartsch and P. Schmezer (2002). "DNA repair capacity after gamma-irradiation and expression profiles of DNA repair genes in resting and proliferating human peripheral blood lymphocytes." DNA Repair (Amst) **1**(3): 237-250.

Mayer, M. P. (2010). "Gymnastics of molecular chaperones." Mol Cell **39**(3): 321-331.

Mayer, M. P. (2013). "Hsp70 chaperone dynamics and molecular mechanism." Trends Biochem Sci **38**(10): 507-514.

Mayor, R. and E. Theveneau (2013). "The neural crest." Development **140**(11): 2247-2251.

Mayor, S., J. F. Presley and F. R. Maxfield (1993). "Sorting of membrane components from endosomes and subsequent recycling to the cell surface occurs by a bulk flow process." J Cell Biol **121**(6): 1257-1269.

McCall, E. E., A. F. Olshan and J. L. Daniels (2005). "Maternal hair dye use and risk of neuroblastoma in offspring." Cancer Causes Control **16**(6): 743-748.

McCarty, J. S., A. Buchberger, J. Reinstein and B. Bukau (1995). "The role of ATP in the functional cycle of the DnaK chaperone system." J Mol Biol **249**(1): 126-137.

McGinty, R. K. and S. Tan (2015). "Nucleosome structure and function." Chem Rev **115**(6): 2255-2273.

Medina, D. L., S. Di Paola, I. Peluso, A. Armani, D. De Stefani, R. Venditti, S. Montefusco, A. Scotto-Rosato, C. Prezioso, A. Forrester, C. Settembre, W. Wang, Q. Gao, H. Xu, M. Sandri, R. Rizzuto, M. A. De Matteis and A. Ballabio (2015). "Lysosomal calcium signalling regulates autophagy through calcineurin and TFEB." Nat Cell Biol **17**(3): 288-299.

Medina, D. L., A. Fraldi, V. Bouche, F. Annunziata, G. Mansueto, C. Spampanato, C. Puri, A. Pignata, J. A. Martina, M. Sardiello, M. Palmieri, R. Polishchuk, R. Puertollano and A. Ballabio (2011). "Transcriptional activation of lysosomal exocytosis promotes cellular clearance." Dev Cell **21**(3): 421-430.

Meyer, A. S., J. R. Gillespie, D. Walther, I. S. Millet, S. Doniach and J. Frydman (2003a). "Closing the folding chamber of the eukaryotic chaperonin requires the transition state of ATP hydrolysis." Cell **113**(3): 369-381.

Meyer, P., C. Prodromou, B. Hu, C. Vaughan, S. M. Roe, B. Panaretou, P. W. Piper and L. H. Pearl (2003b). "Structural and functional analysis of the middle segment of hsp90: implications for ATP hydrolysis and client protein and cochaperone interactions." Mol Cell **11**(3): 647-658.

Meyskens, F. L., E. M. Kingsley, T. Glattke, L. Loescher and A. Booth (1986). "A phase II study of alpha-difluoromethylornithine (DFMO) for the treatment of metastatic melanoma." Invest New Drugs **4**(3): 257-262.

Michaelis, M., F. Rothweiler, D. Klassert, A. von Deimling, K. Weber, B. Fehse, B. Kammerer, H. W. Doerr and J. Cinatl, Jr. (2009). "Reversal of P-glycoprotein-mediated multidrug resistance by the murine double minute 2 antagonist nutlin-3." Cancer Res **69**(2): 416-421.

Michalak, M., U. Warnken, S. Andre, M. Schnolzer, H. J. Gabius and J. Kopitz (2016). "Detection of Proteome Changes in Human Colon Cancer Induced by Cell Surface Binding of Growth-Inhibitory Human Galectin-4 Using Quantitative SILAC-Based Proteomics." J Proteome Res **15**(12): 4412-4422.

Milde, T., I. Oehme, A. Korshunov, A. Kopp-Schneider, M. Remke, P. Northcott, H. E. Deubzer, M. Lodrini, M. D. Taylor, A. von Deimling, S. Pfister and O. Witt (2010). "HDAC5 and HDAC9 in medulloblastoma: novel markers for risk stratification and role in tumor cell growth." Clin Cancer Res **16**(12): 3240-3252.

Minami, Y., Y. Kimura, H. Kawasaki, K. Suzuki and I. Yahara (1994). "The carboxy-terminal region of mammalian HSP90 is required for its dimerization and function in vivo." Mol Cell Biol **14**(2): 1459-1464.

Mindell, J. A. (2012). "Lysosomal acidification mechanisms." Annu Rev Physiol **74**: 69-86.

Minotti, G., P. Menna, E. Salvatorelli, G. Cairo and L. Gianni (2004). "Anthracyclines: molecular advances and pharmacologic developments in antitumor activity and cardiotoxicity." Pharmacol Rev **56**(2): 185-229.

Miyake, Y., J. J. Keusch, L. Wang, M. Saito, D. Hess, X. Wang, B. J. Melancon, P. Helquist, H. Gut and P. Matthias (2016). "Structural insights into HDAC6 tubulin deacetylation and its selective inhibition." Nat Chem Biol **12**(9): 748-754.

Miyashita, T. and J. C. Reed (1992). "bcl-2 gene transfer increases relative resistance of S49.1 and WEHI7.2 lymphoid cells to cell death and DNA fragmentation induced by glucocorticoids and multiple chemotherapeutic drugs." Cancer Res **52**(19): 5407-5411.

Mizushima, N., H. Sugita, T. Yoshimori and Y. Ohsumi (1998). "A new protein conjugation system in human. The counterpart of the yeast Apg12p conjugation system essential for autophagy." J Biol Chem **273**(51): 33889-33892.

Mizushima, N., T. Yoshimori and B. Levine (2010). "Methods in mammalian autophagy research." Cell **140**(3): 313-326.

Mlakar, V., S. Jurkovic Mlakar, G. Lopez, J. M. Maris, M. Ansari and F. Gumy-Pause (2017). "11q deletion in neuroblastoma: a review of biological and clinical implications." Mol Cancer **16**(1): 114.

Molinari, A., A. Calcabrini, S. Meschini, A. Stringaro, P. Crateri, L. Toccacieli, M. Marra, M. Colone, M. Cianfriglia and G. Arancia (2002). "Subcellular detection and localization of the drug transporter P-glycoprotein in cultured tumor cells." Curr Protein Pept Sci **3**(6): 653-670.

Monclair, T., G. M. Brodeur, P. F. Ambros, H. J. Brisse, G. Cecchetto, K. Holmes, M. Kaneko, W. B. London, K. K. Matthay, J. G. Nuchtern, D. von Schweinitz, T. Simon, S. L. Cohn and A. D. Pearson (2009). "The International Neuroblastoma Risk Group (INRG) staging system: an INRG Task Force report." J Clin Oncol **27**(2): 298-303.

Moriyama, Y., T. Takano and S. Ohkuma (1982). "Acridine orange as a fluorescent probe for lysosomal proton pump." J Biochem **92**(4): 1333-1336.

Morschhauser, F., L. Terriou, B. Coiffier, E. Bachy, A. Varga, I. Kloos, H. Lelievre, A. L. Sarry, S. Depil and V. Ribrag (2015). "Phase 1 study of the oral histone deacetylase inhibitor abexinostat in patients with Hodgkin lymphoma, non-Hodgkin lymphoma, or chronic lymphocytic leukaemia." Invest New Drugs **33**(2): 423-431.

Mosse, Y. P., M. Laudenslager, D. Khazi, A. J. Carlisle, C. L. Winter, E. Rappaport and J. M. Maris (2004). "Germline PHOX2B mutation in hereditary neuroblastoma." Am J Hum Genet **75**(4): 727-730.

Mosse, Y. P., M. Laudenslager, L. Longo, K. A. Cole, A. Wood, E. F. Attiyeh, M. J. Laquaglia, R. Sennett, J. E. Lynch, P. Perri, G. Laureys, F. Speleman, C. Kim, C. Hou, H. Hakonarson, A. Torkamani, N. J. Schork, G. M. Brodeur, G. P. Tonini, E. Rappaport, M. Devoto and J. M. Maris (2008). "Identification of ALK as a major familial neuroblastoma predisposition gene." Nature **455**(7215): 930-935.

Mottamal, M., S. Zheng, T. L. Huang and G. Wang (2015). "Histone deacetylase inhibitors in clinical studies as templates for new anticancer agents." Molecules **20**(3): 3898-3941.

Mottet, D., A. Bellahcene, S. Pirotte, D. Waltregny, C. Deroanne, V. Lamour, R. Lidereau and V. Castronovo (2007). "Histone deacetylase 7 silencing alters endothelial cell migration, a key step in angiogenesis." Circ Res **101**(12): 1237-1246.

Mrakovic, A., J. G. Kay, W. Furuya, J. H. Brumell and R. J. Botelho (2012). "Rab7 and Arl8 GTPases are necessary for lysosome tubulation in macrophages." Traffic **13**(12): 1667-1679.

Mudumba, S., A. Menezes, D. Fries and J. Blankenship (2002). "Differentiation of PC12 cells induced by N8-acetylspermidine and by N8-acetylspermidine deacetylase inhibition." Biochem Pharmacol **63**(11): 2011-2018.

Mueller, S. and K. K. Matthay (2009). "Neuroblastoma: biology and staging." Curr Oncol Rep **11**(6): 431-438.

Mujtaba, S., Y. He, L. Zeng, S. Yan, O. Plotnikova, Sachchidanand, R. Sanchez, N. J. Zeleznik-Le, Z. Ronai and M. M. Zhou (2004). "Structural mechanism of the bromodomain of the coactivator CBP in p53 transcriptional activation." Mol Cell **13**(2): 251-263.

Mullins, C. and J. S. Bonifacino (2001). "The molecular machinery for lysosome biogenesis." Bioessays **23**(4): 333-343.

Mullock, B. M., N. A. Bright, C. W. Fearon, S. R. Gray and J. P. Luzio (1998). "Fusion of lysosomes with late endosomes produces a hybrid organelle of intermediate density and is NSF dependent." J Cell Biol **140**(3): 591-601.

Munirajan, A. K., K. Ando, A. Mukai, M. Takahashi, Y. Suenaga, M. Ohira, T. Koda, T. Hirota, T. Ozaki and A. Nakagawara (2008). "KIF1Bbeta functions as a haploinsufficient tumor suppressor gene mapped to chromosome 1p36.2 by inducing apoptotic cell death." J Biol Chem **283**(36): 24426-24434.

Munro, S. and H. R. Pelham (1986). "An Hsp70-like protein in the ER: identity with the 78 kd glucose-regulated protein and immunoglobulin heavy chain binding protein." Cell **46**(2): 291-300.

Murakami-Tonami, Y., H. Ikeda, R. Yamagishi, M. Inayoshi, S. Inagaki, S. Kishida, Y. Komata, K. Jan, I. Takeuchi, Y. Kondo, T. Maeda, Y. Sekido, H. Murakami and K. Kadomatsu (2016). "SGO1 is involved in the DNA damage response in MYCN-amplified neuroblastoma cells." Sci Rep **6**: 31615.

Murphy, M. E. (2013). "The HSP70 family and cancer." Carcinogenesis **34**(6): 1181-1188.

Murphy, P. J., Y. Morishima, J. J. Kovacs, T. P. Yao and W. B. Pratt (2005). "Regulation of the dynamics of hsp90 action on the glucocorticoid receptor by acetylation/deacetylation of the chaperone." J Biol Chem **280**(40): 33792-33799.

Myers, C. E., W. P. McGuire, R. H. Liss, I. Ifrim, K. Grotzinger and R. C. Young (1977). "Adriamycin: the role of lipid peroxidation in cardiac toxicity and tumor response." Science **197**(4299): 165-167.

Nagy, L., H. Y. Kao, D. Chakravarti, R. J. Lin, C. A. Hassig, D. E. Ayer, S. L. Schreiber and R. M. Evans (1997). "Nuclear receptor repression mediated by a complex containing SMRT, mSin3A, and histone deacetylase." Cell **89**(3): 373-380.

Nakatogawa, H., K. Suzuki, Y. Kamada and Y. Ohsumi (2009). "Dynamics and diversity in autophagy mechanisms: lessons from yeast." Nat Rev Mol Cell Biol **10**(7): 458-467.

Namdar, M., G. Perez, L. Ngo and P. A. Marks (2010). "Selective inhibition of histone deacetylase 6 (HDAC6) induces DNA damage and sensitizes transformed cells to anticancer agents." Proc Natl Acad Sci U S A **107**(46): 20003-20008.

Napier, C. E., L. I. Huschtscha, A. Harvey, K. Bower, J. R. Noble, E. A. Hendrickson and R. R. Reddel (2015). "ATRX represses alternative lengthening of telomeres." Oncotarget **6**(18): 16543-16558.

Neckers, L. and P. Workman (2012). "Hsp90 molecular chaperone inhibitors: are we there yet?" Clin Cancer Res **18**(1): 64-76.

Nesvizhskii, A. I., A. Keller, E. Kolker and R. Aebersold (2003). "A statistical model for identifying proteins by tandem mass spectrometry." Anal Chem **75**(17): 4646-4658.

Ni Chonghaile, T., K. A. Sarosiek, T. T. Vo, J. A. Ryan, A. Tammareddi, G. Moore Vdel, J. Deng, K. C. Anderson, P. Richardson, Y. T. Tai, C. S. Mitsiades, U. A. Matulonis, R. Drapkin, R. Stone, D. J. Deangelo, D. J. McConkey, S. E. Sallan, L. Silverman, M. S. Hirsch, D. R. Carrasco and A. Letai (2011). "Pretreatment

mitochondrial priming correlates with clinical response to cytotoxic chemotherapy." Science **334**(6059): 1129-1133.

Nicolai, S., M. Pieraccioli, A. Peschiaroli, G. Melino and G. Raschella (2015). "Neuroblastoma: oncogenic mechanisms and therapeutic exploitation of necroptosis." Cell Death Dis **6**: e2010.

Nishimura, Y., K. Itoh, K. Yoshioka, K. Tokuda and M. Himeno (2003). "Overexpression of ROCK in human breast cancer cells: evidence that ROCK activity mediates intracellular membrane traffic of lysosomes." Pathol Oncol Res **9**(2): 83-95.

Nishioka, C., T. Ikezoe, J. Yang, S. Takeuchi, H. P. Koeffler and A. Yokoyama (2008). "MS-275, a novel histone deacetylase inhibitor with selectivity against HDAC1, induces degradation of FLT3 via inhibition of chaperone function of heat shock protein 90 in AML cells." Leuk Res **32**(9): 1382-1392.

Nishiyama, T., R. Ladurner, J. Schmitz, E. Kreidl, A. Schleiffer, V. Bhaskara, M. Bando, K. Shirahige, A. A. Hyman, K. Mechtler and J. M. Peters (2010). "Sororin mediates sister chromatid cohesion by antagonizing Wapl." Cell **143**(5): 737-749.

Nitiss, J. L. (2009). "Targeting DNA topoisomerase II in cancer chemotherapy." Nat Rev Cancer **9**(5): 338-350.

Nitzan, E. and C. Kalcheim (2013). "Neural crest and somitic mesoderm as paradigms to investigate cell fate decisions during development." Dev Growth Differ **55**(1): 60-78.

Nuchtern, J. G., W. B. London, C. E. Barnewolt, A. Naranjo, P. W. McGrady, J. D. Geiger, L. Diller, M. L. Schmidt, J. M. Maris, S. L. Cohn and R. C. Shamberger (2012). "A prospective study of expectant observation as primary therapy for neuroblastoma in young infants: a Children's Oncology Group study." Ann Surg **256**(4): 573-580.

Oakhill, J. S., R. Steel, Z. P. Chen, J. W. Scott, N. Ling, S. Tam and B. E. Kemp (2011). "AMPK is a direct adenylate charge-regulated protein kinase." Science **332**(6036): 1433-1435.

Oberthuer, A., B. Hero, F. Berthold, D. Juraeva, A. Faldum, Y. Kahlert, S. Asgharzadeh, R. Seeger, P. Scaruffi, G. P. Tonini, I. Janoueix-Lerosey, O. Delattre, G. Schleiermacher, J. Vandesompele, J. Vermeulen, F. Speleman, R. Noguera, M. Piqueras, J. Benard, A. Valent, S. Avigad, I. Yaniv, A. Weber, H. Christiansen, R. G. Grundy, K. Schardt, M. Schwab, R. Eils, P. Warnat, L. Kaderali, T. Simon, B. Decarolis, J. Theissen, F. Westermann, B. Brors and M. Fischer (2010). "Prognostic impact of gene expression-based classification for neuroblastoma." J Clin Oncol **28**(21): 3506-3515.

Oehme, I., H. E. Deubzer, M. Lodrini, T. Milde and O. Witt (2009a). "Targeting of HDAC8 and investigational inhibitors in neuroblastoma." Expert Opin Investig Drugs **18**(11): 1605-1617.

Oehme, I., H. E. Deubzer, D. Wegener, D. Pickert, J. P. Linke, B. Hero, A. Kopp-Schneider, F. Westermann, S. M. Ulrich, A. von Deimling, M. Fischer and O. Witt (2009b). "Histone deacetylase 8 in neuroblastoma tumorigenesis." Clin Cancer Res **15**(1): 91-99.

Oehme, I., J. P. Linke, B. C. Bock, T. Milde, M. Lodrini, B. Hartenstein, I. Wiegand, C. Eckert, W. Roth, M. Kool, S. Kaden, H. J. Grone, J. H. Schulte, S. Lindner, A. Hamacher-Brady, N. R. Brady, H. E. Deubzer and O. Witt (2013a). "Histone deacetylase 10 promotes autophagy-mediated cell survival." Proc Natl Acad Sci U S A **110**(28): E2592-2601.

Oehme, I., M. Lodrini, N. R. Brady and O. Witt (2013b). "Histone deacetylase 10-promoted autophagy as a druggable point of interference to improve the treatment response of advanced neuroblastomas." Autophagy **9**(12): 2163-2165.

Ogawa, S., J. Takita, M. Sanada and Y. Hayashi (2011). "Oncogenic mutations of ALK in neuroblastoma." Cancer Sci **102**(2): 302-308.

Oh, M., I. K. Choi and H. J. Kwon (2008). "Inhibition of histone deacetylase1 induces autophagy." Biochem Biophys Res Commun **369**(4): 1179-1183.

Ohkuma, S., Y. Moriyama and T. Takano (1982). "Identification and characterization of a proton pump on lysosomes by fluorescein-isothiocyanate-dextran fluorescence." Proc Natl Acad Sci U S A **79**(9): 2758-2762.

Ohsumi, Y. (2014). "Historical landmarks of autophagy research." Cell Res **24**(1): 9-23.

Okamoto, K. (2014). "Organellophagy: eliminating cellular building blocks via selective autophagy." J Cell Biol **205**(4): 435-445.

Olsen, R. R., J. H. Otero, J. Garcia-Lopez, K. Wallace, D. Finkelstein, J. E. Rehg, Z. Yin, Y. D. Wang and K. W. Freeman (2017). "MYCN induces neuroblastoma in primary neural crest cells." Oncogene **36**(35): 5075-5082.

Olson, D. E., N. D. Udeshi, N. A. Wolfson, C. A. Pitcairn, E. D. Sullivan, J. D. Jaffe, T. Svinkina, T. Natoli, X. Lu, J. Paulk, P. McCarren, F. F. Wagner, D. Barker, E. Howe, F. Lazzaro, J. P. Gale, Y. L. Zhang, A. Subramanian, C. A. Fierke, S. A. Carr and E. B. Holson (2014). "An unbiased approach to identify endogenous substrates of "histone" deacetylase 8." ACS Chem Biol **9**(10): 2210-2216.

Olsvik, H. L., T. Lamark, K. Takagi, K. B. Larsen, G. Evjen, A. Overvatn, T. Mizushima and T. Johansen (2015). "FYCO1 Contains a C-terminally Extended, LC3A/B-preferring LC3-interacting Region (LIR) Motif Required for Efficient Maturation of Autophagosomes during Basal Autophagy." J Biol Chem **290**(49): 29361-29374.

Ouyang, H., Y. O. Ali, M. Ravichandran, A. Dong, W. Qiu, F. MacKenzie, S. Dhe-Paganon, C. H. Arrowsmith and R. G. Zhai (2012). "Protein aggregates are recruited to aggresome by histone deacetylase 6 via unanchored ubiquitin C termini." J Biol Chem **287**(4): 2317-2327.

Owegi, M. A., D. L. Pappas, M. W. Finch, Jr., S. A. Bilbo, C. A. Resendiz, L. J. Jacquemin, A. Warrier, J. D. Trombley, K. M. McCulloch, K. L. Margalef, M. J. Mertz, J. M. Storms, C. A. Damin and K. J. Parra (2006). "Identification of a domain in the V0 subunit d that is critical for coupling of the yeast vacuolar proton-translocating ATPase." J Biol Chem **281**(40): 30001-30014.

Page, L. J., A. J. Darmon, R. Uellner and G. M. Griffiths (1998). "L is for lytic granules: lysosomes that kill." Biochim Biophys Acta **1401**(2): 146-156.

Palmer, A. J. and H. M. Wallace (2010). "The polyamine transport system as a target for anticancer drug development." Amino Acids **38**(2): 415-422.

Palmieri, M., S. Impey, H. Kang, A. di Ronza, C. Pelz, M. Sardiello and A. Ballabio (2011). "Characterization of the CLEAR network reveals an integrated control of cellular clearance pathways." Hum Mol Genet **20**(19): 3852-3866.

Pandey, U. B., Y. Batlevi, E. H. Baehrecke and J. P. Taylor (2007). "HDAC6 at the intersection of autophagy, the ubiquitin-proteasome system and neurodegeneration." Autophagy **3**(6): 643-645.

Park, M. H., K. Nishimura, C. F. Zanelli and S. R. Valentini (2010). "Functional significance of eIF5A and its hypusine modification in eukaryotes." Amino Acids **38**(2): 491-500.

Parra, M. and E. Verdin (2010). "Regulatory signal transduction pathways for class IIa histone deacetylases." Curr Opin Pharmacol **10**(4): 454-460.

Pasini, A., C. M. Caldarera and E. Giordano (2014). "Chromatin remodeling by polyamines and polyamine analogs." Amino Acids **46**(3): 595-603.

Pattyn, A., X. Morin, H. Cremer, C. Goridis and J. F. Brunet (1999). "The homeobox gene Phox2b is essential for the development of autonomic neural crest derivatives." Nature **399**(6734): 366-370.

Pegg, A. E. (2006). "Regulation of ornithine decarboxylase." J Biol Chem **281**(21): 14529-14532.

Pei, D., W. Luther, W. Wang, B. H. Paw, R. A. Stewart and R. E. George (2013). "Distinct neuroblastoma-associated alterations of PHOX2B impair sympathetic neuronal differentiation in zebrafish models." PLoS Genet **9**(6): e1003533.

Peifer, M., F. Hertwig, F. Roels, D. Dreidax, M. Gartlgruber, R. Menon, A. Kramer, J. L. Roncaioli, F. Sand, J. M. Heuckmann, F. Ikram, R. Schmidt, S. Ackermann, A. Engesser, Y. Kahlert, W. Vogel, J. Altmuller, P. Nurnberg, J. Thierry-Mieg, D. Thierry-Mieg, A. Mariappan, S. Heynck, E. Mariotti, K. O. Henrich, C. Gloeckner, G. Bosco, I. Leuschner, M. R. Schweiger, L. Savelyeva, S. C. Watkins, C. Shao, E. Bell, T. Hofer, V. Achter, U. Lang, J. Theissen, R. Volland, M. Saadati, A. Eggert, B. de Wilde, F. Berthold, Z. Peng, C. Zhao, L. Shi, M. Ortmann, R. Buttner, S. Perner, B. Hero, A. Schramm, J. H. Schulte, C. Herrmann, R. J. O'Sullivan, F. Westermann, R. K. Thomas and M. Fischer (2015). "Telomerase activation by genomic rearrangements in high-risk neuroblastoma." Nature **526**(7575): 700-704.

Pena-Llopis, S., S. Vega-Rubin-de-Celis, J. C. Schwartz, N. C. Wolff, T. A. Tran, L. Zou, X. J. Xie, D. R. Corey and J. Brugarolas (2011). "Regulation of TFEB and V-ATPases by mTORC1." EMBO J **30**(16): 3242-3258.

Perera, R. M. and R. Zoncu (2016). "The Lysosome as a Regulatory Hub." Annu Rev Cell Dev Biol **32**: 223-253.

Peters, C. and K. von Figura (1994). "Biogenesis of lysosomal membranes." FEBS Lett **346**(1): 108-114.

Peukert, K., P. Staller, A. Schneider, G. Carmichael, F. Hanel and M. Eilers (1997). "An alternative pathway for gene regulation by Myc." EMBO J **16**(18): 5672-5686.

Pflum, M. K., J. K. Tong, W. S. Lane and S. L. Schreiber (2001). "Histone deacetylase 1 phosphorylation promotes enzymatic activity and complex formation." J Biol Chem **276**(50): 47733-47741.

Piao, S. and R. K. Amaravadi (2016). "Targeting the lysosome in cancer." Ann N Y Acad Sci **1371**(1): 45-54.

Piekarz, R. L., R. Frye, M. Turner, J. J. Wright, S. L. Allen, M. H. Kirschbaum, J. Zain, H. M. Prince, J. P. Leonard, L. J. Geskin, C. Reeder, D. Joske, W. D. Figg, E. R. Gardner, S. M. Steinberg, E. S. Jaffe, M. Stetler-Stevenson, S. Lade, A. T. Fojo and S. E. Bates (2009). "Phase II multi-institutional trial of the histone deacetylase inhibitor romidepsin as monotherapy for patients with cutaneous T-cell lymphoma." J Clin Oncol **27**(32): 5410-5417.

Pierzynska-Mach, A., P. A. Janowski and J. W. Dobrucki (2014). "Evaluation of acridine orange, LysoTracker Red, and quinacrine as fluorescent probes for long-term tracking of acidic vesicles." Cytometry A **85**(8): 729-737.

Pinto, N. R., M. A. Applebaum, S. L. Volchenboum, K. K. Matthay, W. B. London, P. F. Ambros, A. Nakagawara, F. Berthold, G. Schleiermacher, J. R. Park, D. Valteau-Couanet, A. D. Pearson and S. L. Cohn (2015). "Advances in Risk Classification and Treatment Strategies for Neuroblastoma." J Clin Oncol **33**(27): 3008-3017.

Platt, F. M., B. Boland and A. C. van der Spoel (2012). "The cell biology of disease: lysosomal storage disorders: the cellular impact of lysosomal dysfunction." J Cell Biol **199**(5): 723-734.

Poole, R. M. (2014). "Belinostat: first global approval." Drugs **74**(13): 1543-1554.

Prasad, M. S., T. Sauka-Spengler and C. LaBonne (2012). "Induction of the neural crest state: control of stem cell attributes by gene regulatory, post-transcriptional and epigenetic interactions." Dev Biol **366**(1): 10-21.

Prodromou, C., B. Panaretou, S. Chohan, G. Siligardi, R. O'Brien, J. E. Ladbury, S. M. Roe, P. W. Piper and L. H. Pearl (2000). "The ATPase cycle of Hsp90 drives a molecular 'clamp' via transient dimerization of the N-terminal domains." EMBO J **19**(16): 4383-4392.

Prodromou, C., S. M. Roe, R. O'Brien, J. E. Ladbury, P. W. Piper and L. H. Pearl (1997). "Identification and structural characterization of the ATP/ADP-binding site in the Hsp90 molecular chaperone." Cell **90**(1): 65-75.

Pryor, P. R., B. M. Mullock, N. A. Bright, S. R. Gray and J. P. Luzio (2000). "The role of intraorganellar Ca(2+) in late endosome-lysosome heterotypic fusion and in the reformation of lysosomes from hybrid organelles." J Cell Biol **149**(5): 1053-1062.

Pryor, P. R., B. M. Mullock, N. A. Bright, M. R. Lindsay, S. R. Gray, S. C. Richardson, A. Stewart, D. E. James, R. C. Piper and J. P. Luzio (2004). "Combinatorial SNARE complexes with VAMP7 or VAMP8 define different late endocytic fusion events." EMBO Rep **5**(6): 590-595.

Pryor, P. R. and S. A. Raines (2010). "Manipulation of the host by pathogens to survive the lysosome." Biochem Soc Trans **38**(6): 1417-1419.

Pu, J., C. M. Guardia, T. Keren-Kaplan and J. S. Bonifacino (2016). "Mechanisms and functions of lysosome positioning." J Cell Sci **129**(23): 4329-4339.

Pugh, T. J., O. Morozova, E. F. Attiyeh, S. Asgharzadeh, J. S. Wei, D. Auclair, S. L. Carter, K. Cibulskis, M. Hanna, A. Kiezun, J. Kim, M. S. Lawrence, L. Lichenstein, A. McKenna, C. S. Pedamallu, A. H. Ramos, E. Shefler, A. Sivachenko, C. Sougnez, C. Stewart, A. Ally, I. Birol, R. Chiu, R. D. Corbett, M. Hirst, S. D. Jackman, B. Kamoh, A. H. Khodabakshi, M. Krzywinski, A. Lo, R. A. Moore, K. L. Mungall, J. Qian, A. Tam, N. Thiessen, Y. Zhao, K. A. Cole, M. Diamond, S. J. Diskin, Y. P. Mosse, A. C. Wood, L. Ji, R. Sposto, T. Badgett, W. B. London, Y. Moyer, J. M. Gastier-Foster, M. A. Smith, J. M. Guidry Auvil, D. S. Gerhard, M. D. Hogarty, S. J. Jones, E. S. Lander, S. B. Gabriel, G. Getz, R. C. Seeger, J. Khan, M. A. Marra, M. Meyerson and J. M. Maris (2013). "The genetic landscape of high-risk neuroblastoma." Nat Genet **45**(3): 279-284.

Raabe, E. H., M. Laudenslager, C. Winter, N. Wasserman, K. Cole, M. LaQuaglia, D. J. Maris, Y. P. Mosse and J. M. Maris (2008). "Prevalence and functional consequence of PHOX2B mutations in neuroblastoma." Oncogene **27**(4): 469-476.

Radhakrishnan, R., Y. Li, S. Xiang, F. Yuan, Z. Yuan, E. Telles, J. Fang, D. Coppola, D. Shibata, W. S. Lane, Y. Zhang, X. Zhang and E. Seto (2015). "Histone deacetylase 10 regulates DNA mismatch repair and may involve the deacetylation of MutS homolog 2." J Biol Chem **290**(37): 22795-22804.

Rajagopal, A. and S. M. Simon (2003). "Subcellular localization and activity of multidrug resistance proteins." Mol Biol Cell **14**(8): 3389-3399.

Ramessur, K. T., P. Greenwell, R. Nash and M. V. Dwek (2010). "Breast cancer invasion is mediated by beta-N-acetylglucosaminidase (beta-NAG) and associated with a dysregulation in the secretory pathway of cancer cells." Br J Biomed Sci **67**(4): 189-196.

Rao, R., W. Fiskus, Y. Yang, P. Lee, R. Joshi, P. Fernandez, A. Mandawat, P. Atadja, J. E. Bradner and K. Bhalla (2008). "HDAC6 inhibition enhances 17-AAG--mediated abrogation of hsp90 chaperone function in human leukemia cells." Blood **112**(5): 1886-1893.

Rao, R., S. Nalluri, R. Kolhe, Y. Yang, W. Fiskus, J. Chen, K. Ha, K. M. Buckley, R. Balusu, V. Coothankandaswamy, A. Joshi, P. Atadja and K. N. Bhalla (2010). "Treatment with panobinostat induces glucose-regulated protein 78 acetylation and endoplasmic reticulum stress in breast cancer cells." Mol Cancer Ther **9**(4): 942-952.

Rao, S. K., C. Huynh, V. Proux-Gillardeaux, T. Galli and N. W. Andrews (2004). "Identification of SNAREs involved in synaptotagmin VII-regulated lysosomal exocytosis." J Biol Chem **279**(19): 20471-20479.

Rappa, F., F. Farina, G. Zummo, S. David, C. Campanella, F. Carini, G. Tomasello, P. Damiani, F. Cappello, D. E. M. EC and A. J. Macario (2012). "HSP-molecular chaperones in cancer biogenesis and tumor therapy: an overview." Anticancer Res **32**(12): 5139-5150.

Ravi, S., K. A. Pena, C. T. Chu and K. Kiselyov (2016). "Biphasic regulation of lysosomal exocytosis by oxidative stress." Cell Calcium **60**(5): 356-362.

Raychowdhury, M. K., S. Gonzalez-Perrett, N. Montalbetti, G. A. Timpanaro, B. Chasan, W. H. Goldmann, S. Stahl, A. Cooney, E. Goldin and H. F. Cantiello (2004). "Molecular pathophysiology of mucolipidosis type IV: pH dysregulation of the mucolipin-1 cation channel." Hum Mol Genet **13**(6): 617-627.

Reddy, A., E. V. Caler and N. W. Andrews (2001). "Plasma membrane repair is mediated by Ca(2+)-regulated exocytosis of lysosomes." Cell **106**(2): 157-169.

Reiff, T., L. Huber, M. Kramer, O. Delattre, I. Janoueix-Lerosey and H. Rohrer (2011). "Midkine and Alk signaling in sympathetic neuron proliferation and neuroblastoma predisposition." Development **138**(21): 4699-4708.

Renna, M., C. Schaffner, A. R. Winslow, F. M. Menzies, A. A. Peden, R. A. Floto and D. C. Rubinsztein (2011). "Autophagic substrate clearance requires activity of the syntaxin-5 SNARE complex." J Cell Sci **124**(Pt 3): 469-482.

Renvoise, B., J. Chang, R. Singh, S. Yonekawa, E. J. FitzGibbon, A. Mankodi, A. Vanderver, A. Schindler, C. Toro, W. A. Gahl, D. J. Mahuran, C. Blackstone and T. M. Pierson (2014). "Lysosomal abnormalities in hereditary spastic paraplegia types SPG15 and SPG11." Ann Clin Transl Neurol **1**(6): 379-389.

Repnik, U., M. Borg Distefano, M. T. Speth, M. Y. W. Ng, C. Progida, B. Hoflack, J. Gruenberg and G. Griffiths (2017). "L-leucyl-L-leucine methyl ester does not release cysteine cathepsins to the cytosol but inactivates them in transiently permeabilized lysosomes." J Cell Sci **130**(18): 3124-3140.

Repnik, U., V. Stoka, V. Turk and B. Turk (2012). "Lysosomes and lysosomal cathepsins in cell death." Biochim Biophys Acta **1824**(1): 22-33.

Rettig, I., E. Koeneke, F. Trippel, W. C. Mueller, J. Burhenne, A. Kopp-Schneider, J. Fabian, A. Schober, U. Fernekorn, A. von Deimling, H. E. Deubzer, T. Milde, O. Witt and I. Oehme (2015). "Selective inhibition of HDAC8 decreases neuroblastoma growth in vitro and in vivo and enhances retinoic acid-mediated differentiation." Cell Death Dis **6**: e1657.

Ribatti, D., L. Raffaghello, F. Pastorino, B. Nico, C. Brignole, A. Vacca and M. Ponzoni (2002). "In vivo angiogenic activity of neuroblastoma correlates with MYCN oncogene overexpression." Int J Cancer **102**(4): 351-354.

Ridinger, J., E. Koeneke, F. R. Kolbinger, K. Koerholz, S. Mahboobi, L. Hellweg, N. Gunkel, A. K. Miller, H. Peterziel, P. Schmezer, A. Hamacher-Brady, O. Witt and I. Oehme (2018). "Dual role of HDAC10 in lysosomal exocytosis and DNA repair promotes neuroblastoma chemoresistance." Sci Rep **8**(1): 10039.

Ritossa, F. (1996). "Discovery of the heat shock response." Cell Stress Chaperones **1**(2): 97-98.

Roberg, K. and K. Ollinger (1998). "Oxidative stress causes relocation of the lysosomal enzyme cathepsin D with ensuing apoptosis in neonatal rat cardiomyocytes." Am J Pathol **152**(5): 1151-1156.

Robers, M. B., M. L. Dart, C. C. Woodroofe, C. A. Zimprich, T. A. Kirkland, T. Machleidt, K. R. Kupcho, S. Levin, J. R. Hartnett, K. Zimmerman, A. L. Niles, R. F. Ohana, D. L. Daniels, M. Slater, M. G. Wood, M. Cong, Y. Q. Cheng and K. V. Wood (2015). "Target engagement and drug residence time can be observed in living cells with BRET." Nat Commun **6**: 10091.

Robert, C., P. K. Nagaria, N. Pawar, A. Adewuyi, I. Gojo, D. J. Meyers, P. A. Cole and F. V. Rassool (2016). "Histone deacetylase inhibitors decrease NHEJ both by acetylation of repair factors and trapping of PARP1 at DNA double-strand breaks in chromatin." Leuk Res **45**: 14-23.

Robey, R. W., K. M. Pluchino, M. D. Hall, A. T. Fojo, S. E. Bates and M. M. Gottesman (2018). "Revisiting the role of ABC transporters in multidrug-resistant cancer." Nat Rev Cancer **18**(7): 452-464.

Roczniak-Ferguson, A., C. S. Petit, F. Froehlich, S. Qian, J. Ky, B. Angarola, T. C. Walther and S. M. Ferguson (2012). "The transcription factor TFEB links mTORC1 signaling to transcriptional control of lysosome homeostasis." Sci Signal **5**(228): ra42.

Rodriguez, A., P. Webster, J. Ortego and N. W. Andrews (1997). "Lysosomes behave as Ca2+-regulated exocytic vesicles in fibroblasts and epithelial cells." J Cell Biol **137**(1): 93-104.

Rogakou, E. P., D. R. Pilch, A. H. Orr, V. S. Ivanova and W. M. Bonner (1998). "DNA double-stranded breaks induce histone H2AX phosphorylation on serine 139." J Biol Chem **273**(10): 5858-5868.

Rong, Y., C. K. McPhee, S. Deng, L. Huang, L. Chen, M. Liu, K. Tracy, E. H. Baehrecke, L. Yu and M. J. Lenardo (2011). "Spinster is required for autophagic lysosome reformation and mTOR reactivation following starvation." Proc Natl Acad Sci U S A **108**(19): 7826-7831.

Ropero, S. and M. Esteller (2007). "The role of histone deacetylases (HDACs) in human cancer." Mol Oncol **1**(1): 19-25.

Ropero, S., M. F. Fraga, E. Ballestar, R. Hamelin, H. Yamamoto, M. Boix-Chornet, R. Caballero, M. Alaminos, F. Setien, M. F. Paz, M. Herranz, J. Palacios, D. Arango, T. F. Orntoft, L. A. Aaltonen, S. Schwartz, Jr. and M. Esteller (2006). "A truncating mutation of HDAC2 in human cancers confers resistance to histone deacetylase inhibition." Nat Genet **38**(5): 566-569.

Rudiger, S., L. Germeroth, J. Schneider-Mergener and B. Bukau (1997). "Substrate specificity of the DnaK chaperone determined by screening cellulose-bound peptide libraries." EMBO J **16**(7): 1501-1507.

Russell, R. C., Y. Tian, H. Yuan, H. W. Park, Y. Y. Chang, J. Kim, H. Kim, T. P. Neufeld, A. Dillin and K. L. Guan (2013). "ULK1 induces autophagy by phosphorylating Beclin-1 and activating VPS34 lipid kinase." Nat Cell Biol **15**(7): 741-750.

Russo, G., D. Meier, S. Helmsing, E. Wenzel, F. Oberle, A. Frenzel and M. Hust (2018). "Parallelized Antibody Selection in Microtiter Plates." Methods Mol Biol **1701**: 273-284.

Saftig, P. and J. Klumperman (2009). "Lysosome biogenesis and lysosomal membrane proteins: trafficking meets function." Nat Rev Mol Cell Biol **10**(9): 623-635.

Sakuma, T., K. Uzawa, T. Onda, M. Shiiba, H. Yokoe, T. Shibahara and H. Tanzawa (2006). "Aberrant expression of histone deacetylase 6 in oral squamous cell carcinoma." Int J Oncol **29**(1): 117-124.

Salvador, N., C. Aguado, M. Horst and E. Knecht (2000). "Import of a cytosolic protein into lysosomes by chaperone-mediated autophagy depends on its folding state." J Biol Chem **275**(35): 27447-27456.

Samal, K., P. Zhao, A. Kendzicky, L. P. Yco, H. McClung, E. Gerner, M. Burns, A. S. Bachmann and G. Sholler (2013). "AMXT-1501, a novel polyamine transport inhibitor, synergizes with DFMO in inhibiting neuroblastoma cell proliferation by targeting both ornithine decarboxylase and polyamine transport." Int J Cancer **133**(6): 1323-1333.

Samie, M. A. and H. Xu (2014). "Lysosomal exocytosis and lipid storage disorders." J Lipid Res **55**(6): 995-1009.

Sancak, Y., L. Bar-Peled, R. Zoncu, A. L. Markhard, S. Nada and D. M. Sabatini (2010). "Ragulator-Rag complex targets mTORC1 to the lysosomal surface and is necessary for its activation by amino acids." Cell **141**(2): 290-303.

Sancak, Y., T. R. Peterson, Y. D. Shaul, R. A. Lindquist, C. C. Thoreen, L. Bar-Peled and D. M. Sabatini (2008). "The Rag GTPases bind raptor and mediate amino acid signaling to mTORC1." Science **320**(5882): 1496-1501.

Santo, L., T. Hideshima, A. L. Kung, J. C. Tseng, D. Tamang, M. Yang, M. Jarpe, J. H. van Duzer, R. Mazitschek, W. C. Ogier, D. Cirstea, S. Rodig, H. Eda, T. Scullen, M. Canavese, J. Bradner, K. C. Anderson, S. S. Jones and N. Raje (2012). "Preclinical activity, pharmacodynamic, and pharmacokinetic properties of a selective HDAC6 inhibitor, ACY-1215, in combination with bortezomib in multiple myeloma." Blood **119**(11): 2579-2589.

Santoro, F., O. A. Botrugno, R. Dal Zuffo, I. Pallavicini, G. M. Matthews, L. Cluse, I. Barozzi, S. Senese, L. Fornasari, S. Moretti, L. Altucci, P. G. Pelicci, S. Chiocca, R. W. Johnstone and S. Minucci (2013). "A dual role for Hdac1: oncosuppressor in tumorigenesis, oncogene in tumor maintenance." Blood **121**(17): 3459-3468.

Santoro, M. G. (2000). "Heat shock factors and the control of the stress response." Biochem Pharmacol **59**(1): 55-63.

Sardiello, M., M. Palmieri, A. di Ronza, D. L. Medina, M. Valenza, V. A. Gennarino, C. Di Malta, F. Donaudy, V. Embrione, R. S. Polishchuk, S. Banfi, G. Parenti, E. Cattaneo and A. Ballabio (2009). "A gene network regulating lysosomal biogenesis and function." Science **325**(5939): 473-477.

Sauka-Spengler, T. and M. Bronner-Fraser (2008). "A gene regulatory network orchestrates neural crest formation." Nat Rev Mol Cell Biol **9**(7): 557-568.

Saulnier Sholler, G. L., E. W. Gerner, G. Bergendahl, R. B. MacArthur, A. VanderWerff, T. Ashikaga, J. P. Bond, W. Ferguson, W. Roberts, R. K. Wada, D. Eslin, J. M. Kraveka, J. Kaplan, D. Mitchell, N. S. Parikh, K. Neville, L. Sender, T. Higgins, M. Kawakita, K. Hiramatsu, S. S. Moriya and A. S. Bachmann (2015). "A Phase I Trial of DFMO Targeting Polyamine Addiction in Patients with Relapsed/Refractory Neuroblastoma." PLoS One **10**(5): e0127246.

Sauna, Z. E. and S. V. Ambudkar (2001). "Characterization of the catalytic cycle of ATP hydrolysis by human P-glycoprotein. The two ATP hydrolysis events in a single catalytic cycle are kinetically similar but affect different functional outcomes." J Biol Chem **276**(15): 11653-11661.

Sautin, Y. Y., M. Lu, A. Gaugler, L. Zhang and S. L. Gluck (2005). "Phosphatidylinositol 3-kinase-mediated effects of glucose on vacuolar H+-ATPase assembly, translocation, and acidification of intracellular compartments in renal epithelial cells." Mol Cell Biol **25**(2): 575-589.

Sawai, S., A. Shimono, Y. Wakamatsu, C. Palmes, K. Hanaoka and H. Kondoh (1993). "Defects of embryonic organogenesis resulting from targeted disruption of the N-myc gene in the mouse." Development **117**(4): 1445-1455.

Schilling, F. H., C. Spix, F. Berthold, R. Erttmann, N. Fehse, B. Hero, G. Klein, J. Sander, K. Schwarz, J. Treuner, U. Zorn and J. Michaelis (2002). "Neuroblastoma screening at one year of age." N Engl J Med **346**(14): 1047-1053.

Schindler, M., S. Grabski, E. Hoff and S. M. Simon (1996). "Defective pH regulation of acidic compartments in human breast cancer cells (MCF-7) is normalized in adriamycin-resistant cells (MCF-7adr)." Biochemistry **35**(9): 2811-2817.

Schipper, H., V. Alla, C. Meier, D. M. Nettelbeck, O. Herchenroder and B. M. Putzer (2014). "Eradication of metastatic melanoma through cooperative expression of RNA-based HDAC1 inhibitor and p73 by oncolytic adenovirus." Oncotarget **5**(15): 5893-5907.

Schleiermacher, G., V. Mosseri, W. B. London, J. M. Maris, G. M. Brodeur, E. Attiyeh, M. Haber, J. Khan, A. Nakagawara, F. Speleman, R. Noguera, G. P. Tonini, M. Fischer, I. Ambros, T. Monclair, K. K. Matthay, P. Ambros, S. L. Cohn and A. D. Pearson (2012). "Segmental chromosomal alterations have prognostic impact in neuroblastoma: a report from the INRG project." Br J Cancer **107**(8): 1418-1422.

Schleiermacher, G., V. Raynal, I. Janoueix-Lerosey, V. Combaret, A. Aurias and O. Delattre (2004). "Variety and complexity of chromosome 17 translocations in neuroblastoma." Genes Chromosomes Cancer **39**(2): 143-150.

Schlesinger, M. J. (1990). "Heat shock proteins." J Biol Chem **265**(21): 12111-12114.

Scholz, C., B. T. Weinert, S. A. Wagner, P. Beli, Y. Miyake, J. Qi, L. J. Jensen, W. Streicher, A. R. McCarthy, N. J. Westwood, S. Lain, J. Cox, P. Matthias, M. Mann, J. E. Bradner and C. Choudhary (2015). "Acetylation site specificities of lysine deacetylase inhibitors in human cells." Nat Biotechnol **33**(4): 415-423.

Schroder, B. A., C. Wrocklage, A. Hasilik and P. Saftig (2010). "The proteome of lysosomes." Proteomics **10**(22): 4053-4076.

Schulte, J. H., H. S. Bachmann, B. Brockmeyer, K. Depreter, A. Oberthur, S. Ackermann, Y. Kahlert, K. Pajtler, J. Theissen, F. Westermann, J. Vandesompele, F. Speleman, F. Berthold, A. Eggert, B. Brors, B. Hero, A. Schramm and M. Fischer (2011). "High ALK receptor tyrosine kinase expression supersedes ALK mutation as a determining factor of an unfavorable phenotype in primary neuroblastoma." Clin Cancer Res **17**(15): 5082-5092.

Schulte, J. H., S. Lindner, A. Bohrer, J. Maurer, K. De Preter, S. Lefever, L. Heukamp, S. Schulte, J. Molenaar, R. Versteeg, T. Thor, A. Kunkele, J. Vandesompele, F. Speleman, H. Schorle, A. Eggert and A. Schramm (2013). "MYCN and ALKF1174L are sufficient to drive neuroblastoma development from neural crest progenitor cells." Oncogene **32**(8): 1059-1065.

Schunck, C., T. Johannes, D. Varga, T. Lorch and A. Plesch (2004). "New developments in automated cytogenetic imaging: unattended scoring of dicentric chromosomes, micronuclei, single cell gel electrophoresis, and fluorescence signals." Cytogenet Genome Res **104**(1-4): 383-389.

Schwab, M., K. Alitalo, K. H. Klempnauer, H. E. Varmus, J. M. Bishop, F. Gilbert, G. Brodeur, M. Goldstein and J. Trent (1983). "Amplified DNA with limited homology to myc cellular oncogene is shared by human neuroblastoma cell lines and a neuroblastoma tumour." Nature **305**(5931): 245-248.

Schwake, M., B. Schroder and P. Saftig (2013). "Lysosomal membrane proteins and their central role in physiology." Traffic **14**(7): 739-748.

Scroggins, B. T. and L. Neckers (2007). "Post-translational modification of heat-shock protein 90: impact on chaperone function." Expert Opin Drug Discov **2**(10): 1403-1414.

Scroggins, B. T., K. Robzyk, D. Wang, M. G. Marcu, S. Tsutsumi, K. Beebe, R. J. Cotter, S. Felts, D. Toft, L. Karnitz, N. Rosen and L. Neckers (2007). "An acetylation site in the middle domain of Hsp90 regulates chaperone function." Mol Cell **25**(1): 151-159.

Seidel, C., M. Schnekenburger, M. Dicato and M. Diederich (2015). "Histone deacetylase 6 in health and disease." Epigenomics **7**(1): 103-118.

Sellmer, A., H. Stangl, M. Beyer, E. Grunstein, M. Leonhardt, H. Pongratz, E. Eichhorn, S. Elz, B. Striegl, Z. Jenei-Lanzl, S. Dove, R. H. Straub, O. H. Kramer and S. Mahboobi (2018). "Marbostat-100 Defines a New Class of Potent and Selective Antiinflammatory and Antirheumatic Histone Deacetylase 6 Inhibitors." J Med Chem **61**(8): 3454-3477.

Seluanov, A., Z. Mao and V. Gorbunova (2010). "Analysis of DNA double-strand break (DSB) repair in mammalian cells." J Vis Exp(43).

Senese, S., K. Zaragoza, S. Minardi, I. Muradore, S. Ronzoni, A. Passafaro, L. Bernard, G. F. Draetta, M. Alcalay, C. Seiser and S. Chiocca (2007). "Role for histone deacetylase 1 in human tumor cell proliferation." Mol Cell Biol **27**(13): 4784-4795.

Seo, J. H., J. H. Park, E. J. Lee, T. T. Vo, H. Choi, J. Y. Kim, J. K. Jang, H. J. Wee, H. S. Lee, S. H. Jang, Z. Y. Park, J. Jeong, K. J. Lee, S. H. Seok, J. Y. Park, B. J. Lee, M. N. Lee, G. T. Oh and K. W. Kim (2016). "ARD1-mediated Hsp70 acetylation balances stress-induced protein refolding and degradation." Nat Commun **7**: 12882.

Sergina, N. V., M. Rausch, D. Wang, J. Blair, B. Hann, K. M. Shokat and M. M. Moasser (2007). "Escape from HER-family tyrosine kinase inhibitor therapy by the kinase-inactive HER3." Nature **445**(7126): 437-441.

Seto, E. and M. Yoshida (2014). "Erasers of histone acetylation: the histone deacetylase enzymes." Cold Spring Harb Perspect Biol **6**(4): a018713.

Settembre, C., C. Di Malta, V. A. Polito, M. Garcia Arencibia, F. Vetrini, S. Erdin, S. U. Erdin, T. Huynh, D. Medina, P. Colella, M. Sardiello, D. C. Rubinsztein and A. Ballabio (2011). "TFEB links autophagy to lysosomal biogenesis." Science **332**(6036): 1429-1433.

Settembre, C., A. Fraldi, D. L. Medina and A. Ballabio (2013). "Signals from the lysosome: a control centre for cellular clearance and energy metabolism." Nat Rev Mol Cell Biol **14**(5): 283-296.

Settembre, C., R. Zoncu, D. L. Medina, F. Vetrini, S. Erdin, T. Huynh, M. Ferron, G. Karsenty, M. C. Vellard, V. Facchinetti, D. M. Sabatini and A. Ballabio (2012). "A lysosome-to-nucleus signalling mechanism senses and regulates the lysosome via mTOR and TFEB." EMBO J **31**(5): 1095-1108.

Shan, B., T. P. Yao, H. T. Nguyen, Y. Zhuo, D. R. Levy, R. C. Klingsberg, H. Tao, M. L. Palmer, K. N. Holder and J. A. Lasky (2008). "Requirement of HDAC6 for transforming growth factor-beta1-induced epithelial-mesenchymal transition." J Biol Chem **283**(30): 21065-21073.

Shan, K., A. M. Lincoff and J. B. Young (1996). "Anthracycline-induced cardiotoxicity." Ann Intern Med **125**(1): 47-58.

Shao, E., T. Nishi, S. Kawasaki-Nishi and M. Forgac (2003). "Mutational analysis of the non-homologous region of subunit A of the yeast V-ATPase." J Biol Chem **278**(15): 12985-12991.

Sharma, S., T. K. Kelly and P. A. Jones (2010). "Epigenetics in cancer." Carcinogenesis **31**(1): 27-36.

Shevchenko, A., H. Tomas, J. Havlis, J. V. Olsen and M. Mann (2006). "In-gel digestion for mass spectrometric characterization of proteins and proteomes." Nat Protoc **1**(6): 2856-2860.

Shi, Y., M. Dong, X. Hong, W. Zhang, J. Feng, J. Zhu, L. Yu, X. Ke, H. Huang, Z. Shen, Y. Fan, W. Li, X. Zhao, J. Qi, D. Zhou, Z. Ning and X. Lu (2015). "Results from a multicenter, open-label, pivotal phase II study of chidamide in relapsed or refractory peripheral T-cell lymphoma." Ann Oncol **26**(8): 1766-1771.

Shimada, H., I. M. Ambros, L. P. Dehner, J. Hata, V. V. Joshi, B. Roald, D. O. Stram, R. B. Gerbing, J. N. Lukens, K. K. Matthay and R. P. Castleberry (1999). "The International Neuroblastoma Pathology Classification (the Shimada system)." Cancer **86**(2): 364-372.

Shimada, H., J. Chatten, W. A. Newton, Jr., N. Sachs, A. B. Hamoudi, T. Chiba, H. B. Marsden and K. Misugi (1984). "Histopathologic prognostic factors in neuroblastic tumors: definition of subtypes of ganglioneuroblastoma and an age-linked classification of neuroblastomas." J Natl Cancer Inst **73**(2): 405-416.

Shogren-Knaak, M., H. Ishii, J. M. Sun, M. J. Pazin, J. R. Davie and C. L. Peterson (2006). "Histone H4-K16 acetylation controls chromatin structure and protein interactions." Science **311**(5762): 844-847.

Shulman, M., C. D. Wilde and G. Kohler (1978). "A better cell line for making hybridomas secreting specific antibodies." Nature **276**(5685): 269-270.

Singh, A. and J. Settleman (2010). "EMT, cancer stem cells and drug resistance: an emerging axis of evil in the war on cancer." Oncogene **29**(34): 4741-4751.

Singh, R., S. Kaushik, Y. Wang, Y. Xiang, I. Novak, M. Komatsu, K. Tanaka, A. M. Cuervo and M. J. Czaja (2009). "Autophagy regulates lipid metabolism." Nature **458**(7242): 1131-1135.

Singh, R., S. Pervin, A. Karimi, S. Cederbaum and G. Chaudhuri (2000). "Arginase activity in human breast cancer cell lines: N(omega)-hydroxy-L-arginine selectively inhibits cell proliferation and induces apoptosis in MDA-MB-468 cells." Cancer Res **60**(12): 3305-3312.

Sleat, D. E., P. Sun, J. A. Wiseman, L. Huang, M. El-Banna, H. Zheng, D. F. Moore and P. Lobel (2013). "Extending the mannose 6-phosphate glycoproteome by high resolution/accuracy mass spectrometry analysis of control and acid phosphatase 5-deficient mice." Mol Cell Proteomics **12**(7): 1806-1817.

Smith, P. K., R. I. Krohn, G. T. Hermanson, A. K. Mallia, F. H. Gartner, M. D. Provenzano, E. K. Fujimoto, N. M. Goeke, B. J. Olson and D. C. Klenk (1985). "Measurement of protein using bicinchoninic acid." Anal Biochem **150**(1): 76-85.

Sorkin, A. and M. von Zastrow (2009). "Endocytosis and signalling: intertwining molecular networks." Nat Rev Mol Cell Biol **10**(9): 609-622.

Soyombo, A. A., S. Tjon-Kon-Sang, Y. Rbaibi, E. Bashllari, J. Bisceglia, S. Muallem and K. Kiselyov (2006). "TRP-ML1 regulates lysosomal pH and acidic lysosomal lipid hydrolytic activity." J Biol Chem **281**(11): 7294-7301.

Stanley, B. A., A. E. Pegg and I. Holm (1989). "Site of pyruvate formation and processing of mammalian S-adenosylmethionine decarboxylase proenzyme." J Biol Chem **264**(35): 21073-21079.

Starai, V. J., I. Celic, R. N. Cole, J. D. Boeke and J. C. Escalante-Semerena (2002). "Sir2-dependent activation of acetyl-CoA synthetase by deacetylation of active lysine." Science **298**(5602): 2390-2392.

Stark, G. (2005). "Functional consequences of oxidative membrane damage." J Membr Biol **205**(1): 1-16.

Steinbach, D., W. Sell, A. Voigt, J. Hermann, F. Zintl and A. Sauerbrey (2002). "BCRP gene expression is associated with a poor response to remission induction therapy in childhood acute myeloid leukemia." Leukemia **16**(8): 1443-1447.

Sternson, S. M., J. C. Wong, C. M. Grozinger and S. L. Schreiber (2001). "Synthesis of 7200 small molecules based on a substructural analysis of the histone deacetylase inhibitors trichostatin and trapoxin." Org Lett **3**(26): 4239-4242.

Stinchcombe, J. C., E. Majorovits, G. Bossi, S. Fuller and G. M. Griffiths (2006). "Centrosome polarization delivers secretory granules to the immunological synapse." Nature **443**(7110): 462-465.

Storrie, B. and M. Desjardins (1996). "The biogenesis of lysosomes: is it a kiss and run, continuous fusion and fission process?" Bioessays **18**(11): 895-903.

Stoscheck, C. M. and G. Carpenter (1984). "Down regulation of epidermal growth factor receptors: direct demonstration of receptor degradation in human fibroblasts." J Cell Biol **98**(3): 1048-1053.

Strahl, B. D. and C. D. Allis (2000). "The language of covalent histone modifications." Nature **403**(6765): 41-45.

Strohecker, A. M., J. Y. Guo, G. Karsli-Uzunbas, S. M. Price, G. J. Chen, R. Mathew, M. McMahon and E. White (2013). "Autophagy sustains mitochondrial glutamine metabolism and growth of BrafV600E-driven lung tumors." Cancer Discov **3**(11): 1272-1285.

Strother, D. R., W. B. London, M. L. Schmidt, G. M. Brodeur, H. Shimada, P. Thorner, M. H. Collins, E. Tagge, S. Adkins, C. P. Reynolds, K. Murray, R. S. Lavey, K. K. Matthay, R. Castleberry, J. M. Maris and S. L. Cohn (2012). "Outcome after surgery alone or with restricted use of chemotherapy for patients with low-risk neuroblastoma: results of Children's Oncology Group study P9641." J Clin Oncol **30**(15): 1842-1848.

Sturm, D., S. Bender, D. T. Jones, P. Lichter, J. Grill, O. Becher, C. Hawkins, J. Majewski, C. Jones, J. F. Costello, A. Iavarone, K. Aldape, C. W. Brennan, N. Jabado and S. M. Pfister (2014). "Paediatric and adult glioblastoma: multiform (epi)genomic culprits emerge." Nat Rev Cancer **14**(2): 92-107.

Suzuki, K., Y. Kubota, T. Sekito and Y. Ohsumi (2007). "Hierarchy of Atg proteins in pre-autophagosomal structure organization." Genes Cells **12**(2): 209-218.

Szakacs, G., J. K. Paterson, J. A. Ludwig, C. Booth-Genthe and M. M. Gottesman (2006). "Targeting multidrug resistance in cancer." Nat Rev Drug Discov **5**(3): 219-234.

Tabor, C. W. and H. Tabor (1984). "Polyamines." Annu Rev Biochem **53**: 749-790.

Taipale, M., D. F. Jarosz and S. Lindquist (2010). "HSP90 at the hub of protein homeostasis: emerging mechanistic insights." Nat Rev Mol Cell Biol **11**(7): 515-528.

Takahashi, H., J. R. Mayers, L. Wang, J. M. Edwardson and A. Audhya (2015). "Hrs and STAM function synergistically to bind ubiquitin-modified cargoes in vitro." Biophys J **108**(1): 76-84.

Takemura, G. and H. Fujiwara (2007). "Doxorubicin-induced cardiomyopathy from the cardiotoxic mechanisms to management." Prog Cardiovasc Dis **49**(5): 330-352.

Takigawa, M., M. Enomoto, Y. Nishida, H. O. Pan, A. Kinoshita and F. Suzuki (1990). "Tumor angiogenesis and polyamines: alpha-difluoromethylornithine, an irreversible inhibitor of ornithine decarboxylase, inhibits B16 melanoma-induced angiogenesis in ovo and the proliferation of vascular endothelial cells in vitro." Cancer Res **50**(13): 4131-4138.

Tanida, I., T. Ueno and E. Kominami (2004). "Human light chain 3/MAP1LC3B is cleaved at its carboxyl-terminal Met121 to expose Gly120 for lipidation and targeting to autophagosomal membranes." J Biol Chem **279**(46): 47704-47710.

Tao, X., Y. Yan, L. Lu and B. Chen (2017). "HDAC10 expression is associated with DNA mismatch repair gene and is a predictor of good prognosis in colon carcinoma." Oncol Lett **14**(4): 4923-4929.

Taunton, J., C. A. Hassig and S. L. Schreiber (1996). "A mammalian histone deacetylase related to the yeast transcriptional regulator Rpd3p." Science **272**(5260): 408-411.

Tavaria, M., T. Gabriele, I. Kola and R. L. Anderson (1996). "A hitchhiker's guide to the human Hsp70 family." Cell Stress Chaperones **1**(1): 23-28.

Tessarz, P. and T. Kouzarides (2014). "Histone core modifications regulating nucleosome structure and dynamics." Nat Rev Mol Cell Biol **15**(11): 703-708.

Theyssen, H., H. P. Schuster, L. Packschies, B. Bukau and J. Reinstein (1996). "The second step of ATP binding to DnaK induces peptide release." J Mol Biol **263**(5): 657-670.

Thole, T. M., M. Lodrini, J. Fabian, J. Wuenschel, S. Pfeil, T. Hielscher, A. Kopp-Schneider, U. Heinicke, S. Fulda, O. Witt, A. Eggert, M. Fischer and H. E. Deubzer (2017). "Neuroblastoma cells depend on HDAC11 for mitotic cell cycle progression and survival." Cell Death Dis **8**(3): e2635.

Thome, M. P., E. C. Filippi-Chiela, E. S. Villodre, C. B. Migliavaca, G. R. Onzi, K. B. Felipe and G. Lenz (2016). "Ratiometric analysis of Acridine Orange staining in the study of acidic organelles and autophagy." J Cell Sci **129**(24): 4622-4632.

Tian, Y., W. Lv, X. Li, C. Wang, D. Wang, P. G. Wang, J. Jin and J. Shen (2017). "Stabilizing HDAC11 with SAHA to assay slow-binding benzamide inhibitors." Bioorg Med Chem Lett **27**(13): 2943-2945.

Ting, J. and A. S. Lee (1988). "Human gene encoding the 78,000-dalton glucose-regulated protein and its pseudogene: structure, conservation, and regulation." DNA **7**(4): 275-286.

Tong, J. J., J. Liu, N. R. Bertos and X. J. Yang (2002). "Identification of HDAC10, a novel class II human histone deacetylase containing a leucine-rich domain." Nucleic Acids Res **30**(5): 1114-1123.

Tran, A. D., T. P. Marmo, A. A. Salam, S. Che, E. Finkelstein, R. Kabarriti, H. S. Xenias, R. Mazitschek, C. Hubbert, Y. Kawaguchi, M. P. Sheetz, T. P. Yao and J. C. Bulinski (2007). "HDAC6 deacetylation of tubulin modulates dynamics of cellular adhesions." J Cell Sci **120**(Pt 8): 1469-1479.

Tran, H. C., A. Marachelian, R. Venkatramani, R. F. Jubran and L. Mascarenhas (2015). "Oxaliplatin and Doxorubicin for relapsed or refractory high-risk neuroblastoma." Pediatr Hematol Oncol **32**(1): 26-31.

Trochet, D., F. Bourdeaut, I. Janoueix-Lerosey, A. Deville, L. de Pontual, G. Schleiermacher, C. Coze, N. Philip, T. Frebourg, A. Munnich, S. Lyonnet, O. Delattre and J. Amiel (2004). "Germline mutations of the paired-like homeobox 2B (PHOX2B) gene in neuroblastoma." Am J Hum Genet **74**(4): 761-764.

Trochet, D., S. J. Hong, J. K. Lim, J. F. Brunet, A. Munnich, K. S. Kim, S. Lyonnet, C. Goridis and J. Amiel (2005). "Molecular consequences of PHOX2B missense, frameshift and alanine expansion mutations leading to autonomic dysfunction." Hum Mol Genet **14**(23): 3697-3708.

Tsai, S. C. and E. Seto (2002). "Regulation of histone deacetylase 2 by protein kinase CK2." J Biol Chem **277**(35): 31826-31833.

Tsukada, M. and Y. Ohsumi (1993). "Isolation and characterization of autophagy-defective mutants of Saccharomyces cerevisiae." FEBS Lett **333**(1-2): 169-174.

Tucker, W. C., T. Weber and E. R. Chapman (2004). "Reconstitution of Ca2+-regulated membrane fusion by synaptotagmin and SNAREs." Science **304**(5669): 435-438.

Turk, B. and V. Turk (2009). "Lysosomes as "suicide bags" in cell death: myth or reality?" J Biol Chem **284**(33): 21783-21787.

Turk, V., V. Stoka, O. Vasiljeva, M. Renko, T. Sun, B. Turk and D. Turk (2012). "Cysteine cathepsins: from structure, function and regulation to new frontiers." Biochim Biophys Acta **1824**(1): 68-88.

Turtoi, A., D. Mottet, N. Matheus, B. Dumont, P. Peixoto, V. Hennequiere, C. Deroanne, A. Colige, E. De Pauw, A. Bellahcene and V. Castronovo (2012). "The angiogenesis suppressor gene AKAP12 is under the epigenetic control of HDAC7 in endothelial cells." Angiogenesis **15**(4): 543-554.

Tweddle, D. A., A. J. Malcolm, M. Cole, A. D. Pearson and J. Lunec (2001). "p53 cellular localization and function in neuroblastoma: evidence for defective G(1) arrest despite WAF1 induction in MYCN-amplified cells." Am J Pathol **158**(6): 2067-2077.

Udugama, M., M. C. FT, F. L. Chan, M. C. Tang, H. A. Pickett, R. M. JD, L. Mayne, P. Collas, J. R. Mann and L. H. Wong (2015). "Histone variant H3.3 provides the heterochromatic H3 lysine 9 tri-methylation mark at telomeres." Nucleic Acids Res **43**(21): 10227-10237.

Ueda, K., C. Cardarelli, M. M. Gottesman and I. Pastan (1987). "Expression of a full-length cDNA for the human "MDR1" gene confers resistance to colchicine, doxorubicin, and vinblastine." Proc Natl Acad Sci U S A **84**(9): 3004-3008.

Uemura, T. and E. W. Gerner (2011). "Polyamine transport systems in mammalian cells and tissues." Methods Mol Biol **720**: 339-348.

Uemura, T., H. F. Yerushalmi, G. Tsaprailis, D. E. Stringer, K. E. Pastorian, L. Hawel, 3rd, C. V. Byus and E. W. Gerner (2008). "Identification and characterization of a diamine exporter in colon epithelial cells." J Biol Chem **283**(39): 26428-26435.

Ullrich, K., G. Mersmann, E. Weber and K. Von Figura (1978). "Evidence for lysosomal enzyme recognition by human fibroblasts via a phosphorylated carbohydrate moiety." Biochem J **170**(3): 643-650.

Valentijn, L. J., J. Koster, D. A. Zwijnenburg, N. E. Hasselt, P. van Sluis, R. Volckmann, M. M. van Noesel, R. E. George, G. A. Tytgat, J. J. Molenaar and R. Versteeg (2015). "TERT rearrangements are frequent in neuroblastoma and identify aggressive tumors." Nat Genet **47**(12): 1411-1414.

van der Vos, K. E., P. Eliasson, T. Proikas-Cezanne, S. J. Vervoort, R. van Boxtel, M. Putker, I. J. van Zutphen, M. Mauthe, S. Zellmer, C. Pals, L. P. Verhagen, M. J. Groot Koerkamp, A. K. Braat, T. B. Dansen, F. C. Holstege, R. Gebhardt, B. M. Burgering and P. J. Coffer (2012). "Modulation of glutamine metabolism by the PI(3)K-PKB-FOXO network regulates autophagy." Nat Cell Biol **14**(8): 829-837.

van Golen, C. M., M. E. Soules, A. R. Grauman and E. L. Feldman (2003). "N-Myc overexpression leads to decreased beta1 integrin expression and increased apoptosis in human neuroblastoma cells." Oncogene **22**(17): 2664-2673.

van Groningen, T., J. Koster, L. J. Valentijn, D. A. Zwijnenburg, N. Akogul, N. E. Hasselt, M. Broekmans, F. Haneveld, N. E. Nowakowska, J. Bras, C. J. M. van Noesel, A. Jongejan, A. H. van Kampen, L. Koster, F. Baas, L. van Dijk-Kerkhoven, M. Huizer-Smit, M. C. Lecca, A. Chan, A. Lakeman, P. Molenaar, R. Volckmann, E. M. Westerhout, M. Hamdi, P. G. van Sluis, M. E. Ebus, J. J. Molenaar, G. A. Tytgat, B. A. Westerman, J. van Nes and R. Versteeg (2017). "Neuroblastoma is composed of two super-enhancer-associated differentiation states." Nat Genet **49**(8): 1261-1266.

Varga, R. E., M. Khundadze, M. Damme, S. Nietzsche, B. Hoffmann, T. Stauber, N. Koch, J. C. Hennings, P. Franzka, A. K. Huebner, M. M. Kessels, C. Biskup, T. J. Jentsch, B. Qualmann, T. Braulke, I. Kurth, C. Beetz and C. A. Hubner (2015). "In Vivo Evidence for Lysosome Depletion and Impaired Autophagic Clearance in Hereditary Spastic Paraplegia Type SPG11." PLoS Genet **11**(8): e1005454.

Vasiliou, V., K. Vasiliou and D. W. Nebert (2009). "Human ATP-binding cassette (ABC) transporter family." Hum Genomics **3**(3): 281-290.

Vasiljeva, O. and B. Turk (2008). "Dual contrasting roles of cysteine cathepsins in cancer progression: apoptosis versus tumour invasion." Biochimie **90**(2): 380-386.

Vaziri, H., S. K. Dessain, E. Ng Eaton, S. I. Imai, R. A. Frye, T. K. Pandita, L. Guarente and R. A. Weinberg (2001). "hSIR2(SIRT1) functions as an NAD-dependent p53 deacetylase." Cell **107**(2): 149-159.

Verderio, C., C. Cagnoli, M. Bergami, M. Francolini, U. Schenk, A. Colombo, L. Riganti, C. Frassoni, E. Zuccaro, L. Danglot, C. Wilhelm, T. Galli, M. Canossa and M. Matteoli (2012). "TI-VAMP/VAMP7 is the SNARE of secretory lysosomes contributing to ATP secretion from astrocytes." Biol Cell **104**(4): 213-228.

Villagra, A., F. Cheng, H. W. Wang, I. Suarez, M. Glozak, M. Maurin, D. Nguyen, K. L. Wright, P. W. Atadja, K. Bhalla, J. Pinilla-Ibarz, E. Seto and E. M. Sotomayor (2009). "The histone deacetylase HDAC11 regulates the expression of interleukin 10 and immune tolerance." Nat Immunol **10**(1): 92-100.

Vogl, D. T., N. Raje, S. Jagannath, P. Richardson, P. Hari, R. Orlowski, J. G. Supko, D. Tamang, M. Yang, S. S. Jones, C. Wheeler, R. J. Markelewicz and S. Lonial (2017). "Ricolinostat, the First Selective Histone Deacetylase 6 Inhibitor, in Combination with Bortezomib and Dexamethasone for Relapsed or Refractory Multiple Myeloma." Clin Cancer Res **23**(13): 3307-3315.

Vujcic, S., P. Diegelman, C. J. Bacchi, D. L. Kramer and C. W. Porter (2002). "Identification and characterization of a novel flavin-containing spermine oxidase of mammalian cell origin." Biochem J **367**(Pt 3): 665-675.

Vujcic, S., P. Liang, P. Diegelman, D. L. Kramer and C. W. Porter (2003). "Genomic identification and biochemical characterization of the mammalian polyamine oxidase involved in polyamine back-conversion." Biochem J **370**(Pt 1): 19-28.

Wagner, F. F., U. M. Wesmall yi, M. C. Lewis and E. B. Holson (2013). "Small molecule inhibitors of zinc-dependent histone deacetylases." Neurotherapeutics **10**(4): 589-604.

Wahlfors, J., L. Alhonen, L. Kauppinen, T. Hyvonen, J. Janne and T. O. Eloranta (1990). "Human spermidine synthase: cloning and primary structure." DNA Cell Biol **9**(2): 103-110.

Wakamatsu, Y., Y. Watanabe, H. Nakamura and H. Kondoh (1997). "Regulation of the neural crest cell fate by N-myc: promotion of ventral migration and neuronal differentiation." Development **124**(10): 1953-1962.

Walczak, M. and S. Martens (2013). "Dissecting the role of the Atg12-Atg5-Atg16 complex during autophagosome formation." Autophagy **9**(3): 424-425.

Wang, G., S. Nola, S. Bovio, P. Bun, M. Coppey-Moisan, F. Lafont and T. Galli (2018). "Biomechanical Control of Lysosomal Secretion Via the VAMP7 Hub: A Tug-of-War between VARP and LRRK1." iScience **4**: 127-143.

Wang, L., S. Xiang, K. A. Williams, H. Dong, W. Bai, S. V. Nicosia, S. Khochbin, G. Bepler and X. Zhang (2012). "Depletion of HDAC6 enhances cisplatin-induced DNA damage and apoptosis in non-small cell lung cancer cells." PLoS One **7**(9): e44265.

Wang, W., Q. Zhong, L. Teng, N. Bhatnagar, B. Sharma, X. Zhang, W. Luther, 2nd, L. P. Haynes, R. D. Burgoyne, M. Vidal, S. Volchenboum, D. E. Hill and R. E. George (2014). "Mutations that disrupt PHOXB interaction with the neuronal calcium sensor HPCAL1 impede cellular differentiation in neuroblastoma." Oncogene **33**(25): 3316-3324.

Wang, Y., T. Murray-Stewart, W. Devereux, A. Hacker, B. Frydman, P. M. Woster and R. A. Casero, Jr. (2003). "Properties of purified recombinant human polyamine oxidase, PAOh1/SMO." Biochem Biophys Res Commun **304**(4): 605-611.

Wang, Z., D. Fries and J. Blankenship (1999). "Effect of N8-acetylspermidine deacetylase inhibition on the growth of L1210 cells." Biochem Pharmacol **57**(10): 1095-1103.

Wang, Z., Y. Leng, J. Wang, H. M. Liao, J. Bergman, P. Leeds, A. Kozikowski and D. M. Chuang (2016). "Tubastatin A, an HDAC6 inhibitor, alleviates stroke-induced brain infarction and functional deficits: potential roles of alpha-tubulin acetylation and FGF-21 up-regulation." Sci Rep **6**: 19626.

Ward, E., C. DeSantis, A. Robbins, B. Kohler and A. Jemal (2014). "Childhood and adolescent cancer statistics, 2014." CA Cancer J Clin **64**(2): 83-103.

Wei, B. L., P. W. Denton, E. O'Neill, T. Luo, J. L. Foster and J. V. Garcia (2005). "Inhibition of lysosome and proteasome function enhances human immunodeficiency virus type 1 infection." J Virol **79**(9): 5705-5712.

Wei, J. S., Y. K. Song, S. Durinck, Q. R. Chen, A. T. Cheuk, P. Tsang, Q. Zhang, C. J. Thiele, A. Slack, J. Shohet and J. Khan (2008). "The MYCN oncogene is a direct target of miR-34a." Oncogene **27**(39): 5204-5213.

Weichert, W., A. Roske, V. Gekeler, T. Beckers, M. P. Ebert, M. Pross, M. Dietel, C. Denkert and C. Rocken (2008a). "Association of patterns of class I histone deacetylase expression with patient prognosis in gastric cancer: a retrospective analysis." Lancet Oncol **9**(2): 139-148.

Weichert, W., A. Roske, S. Niesporek, A. Noske, A. C. Buckendahl, M. Dietel, V. Gekeler, M. Boehm, T. Beckers and C. Denkert (2008b). "Class I histone deacetylase expression has independent prognostic impact in human colorectal cancer: specific role of class I histone deacetylases in vitro and in vivo." Clin Cancer Res **14**(6): 1669-1677.

Weise, F., U. Fernekorn, J. Hampl, M. Klett and A. Schober (2013). "Analysis and comparison of oxygen consumption of HepG2 cells in a monolayer and three-dimensional high density cell culture by use of a matrigrid(R)." Biotechnol Bioeng **110**(9): 2504-2512.

Weiss, W. A., K. Aldape, G. Mohapatra, B. G. Feuerstein and J. M. Bishop (1997). "Targeted expression of MYCN causes neuroblastoma in transgenic mice." EMBO J **16**(11): 2985-2995.

Welch, C., Y. Chen and R. L. Stallings (2007). "MicroRNA-34a functions as a potential tumor suppressor by inducing apoptosis in neuroblastoma cells." Oncogene **26**(34): 5017-5022.

Wellstein, A. (2012). "ALK receptor activation, ligands and therapeutic targeting in glioblastoma and in other cancers." Front Oncol **2**: 192.

Wen, Y. D., V. Perissi, L. M. Staszewski, W. M. Yang, A. Krones, C. K. Glass, M. G. Rosenfeld and E. Seto (2000). "The histone deacetylase-3 complex contains nuclear receptor corepressors." Proc Natl Acad Sci U S A **97**(13): 7202-7207.

Westerheide, S. D., J. Anckar, S. M. Stevens, Jr., L. Sistonen and R. I. Morimoto (2009). "Stress-inducible regulation of heat shock factor 1 by the deacetylase SIRT1." Science **323**(5917): 1063-1066.

White, E. (2012). "Deconvoluting the context-dependent role for autophagy in cancer." Nat Rev Cancer **12**(6): 401-410.

White, E. and R. S. DiPaola (2009). "The double-edged sword of autophagy modulation in cancer." Clin Cancer Res **15**(17): 5308-5316.

Whittaker, S. J., M. F. Demierre, E. J. Kim, A. H. Rook, A. Lerner, M. Duvic, J. Scarisbrick, S. Reddy, T. Robak, J. C. Becker, A. Samtsov, W. McCulloch and Y. H. Kim (2010). "Final results from a multicenter, international, pivotal study of romidepsin in refractory cutaneous T-cell lymphoma." J Clin Oncol **28**(29): 4485-4491.

Willett, R., J. A. Martina, J. P. Zewe, R. Wills, G. R. V. Hammond and R. Puertollano (2017). "TFEB regulates lysosomal positioning by modulating TMEM55B expression and JIP4 recruitment to lysosomes." Nat Commun **8**(1): 1580.

Williams, K. (1997). "Interactions of polyamines with ion channels." Biochem J **325 (Pt 2)**: 289-297.

Willingham, M. C., M. M. Cornwell, C. O. Cardarelli, M. M. Gottesman and I. Pastan (1986). "Single cell analysis of daunomycin uptake and efflux in multidrug-resistant and -sensitive KB cells: effects of verapamil and other drugs." Cancer Res **46**(11): 5941-5946.

Wilson, A. J., D. S. Byun, N. Popova, L. B. Murray, K. L'Italien, Y. Sowa, D. Arango, A. Velcich, L. H. Augenlicht and J. M. Mariadason (2006). "Histone deacetylase 3 (HDAC3) and other class I HDACs regulate colon cell maturation and p21 expression and are deregulated in human colon cancer." J Biol Chem **281**(19): 13548-13558.

Wilson, B. J., A. M. Tremblay, G. Deblois, G. Sylvain-Drolet and V. Giguere (2010). "An acetylation switch modulates the transcriptional activity of estrogen-related receptor alpha." Mol Endocrinol **24**(7): 1349-1358.

Wilson, T. R., P. G. Johnston and D. B. Longley (2009). "Anti-apoptotic mechanisms of drug resistance in cancer." Curr Cancer Drug Targets **9**(3): 307-319.

Wilting, R. H., E. Yanover, M. R. Heideman, H. Jacobs, J. Horner, J. van der Torre, R. A. DePinho and J. H. Dannenberg (2010). "Overlapping functions of Hdac1 and Hdac2 in cell cycle regulation and haematopoiesis." EMBO J **29**(15): 2586-2597.

Winer, J., C. K. Jung, I. Shackel and P. M. Williams (1999). "Development and validation of real-time quantitative reverse transcriptase-polymerase chain reaction for monitoring gene expression in cardiac myocytes in vitro." Anal Biochem **270**(1): 41-49.

Witt, A. E., C. W. Lee, T. I. Lee, D. J. Azzam, B. Wang, C. Caslini, F. Petrocca, J. Grosso, M. Jones, E. B. Cohick, A. B. Gropper, C. Wahlestedt, A. L. Richardson, R. Shiekhattar, R. A. Young and T. A. Ince (2017). "Identification of a cancer stem cell-specific function for the histone deacetylases, HDAC1 and HDAC7, in breast and ovarian cancer." Oncogene **36**(12): 1707-1720.

Witt, O., H. E. Deubzer, T. Milde and I. Oehme (2009). "HDAC family: What are the cancer relevant targets?" Cancer Lett **277**(1): 8-21.

Witt, O., T. Milde, H. E. Deubzer, I. Oehme, R. Witt, A. Kulozik, A. Eisenmenger, U. Abel and I. Karapanagiotou-Schenkel (2012). "Phase I/II intra-patient dose escalation study of vorinostat in children with relapsed solid tumor, lymphoma or leukemia." Klin Padiatr **224**(6): 398-403.

Wolfson, N. A., C. A. Pitcairn and C. A. Fierke (2013). "HDAC8 substrates: Histones and beyond." Biopolymers **99**(2): 112-126.

Wong, L. H., J. D. McGhie, M. Sim, M. A. Anderson, S. Ahn, R. D. Hannan, A. J. George, K. A. Morgan, J. R. Mann and K. H. Choo (2010). "ATRX interacts with H3.3 in maintaining telomere structural integrity in pluripotent embryonic stem cells." Genome Res **20**(3): 351-360.

Woods, W. G., M. Tuchman, L. L. Robison, M. Bernstein, J. M. Leclerc, L. C. Brisson, J. Brossard, G. Hill, J. Shuster, R. Luepker, T. Byrne, S. Weitzman, G. Bunin and B. Lemieux (1996). "A population-based study of the usefulness of screening for neuroblastoma." Lancet **348**(9043): 1682-1687.

Wu, B., C. Hunt and R. Morimoto (1985). "Structure and expression of the human gene encoding major heat shock protein HSP70." Mol Cell Biol **5**(2): 330-341.

Wu, Z., P. C. Chang, J. C. Yang, C. Y. Chu, L. Y. Wang, N. T. Chen, A. H. Ma, S. J. Desai, S. H. Lo, C. P. Evans, K. S. Lam and H. J. Kung (2010). "Autophagy Blockade Sensitizes Prostate Cancer Cells towards Src Family Kinase Inhibitors." Genes Cancer **1**(1): 40-49.

Xie, H. J., J. H. Noh, J. K. Kim, K. H. Jung, J. W. Eun, H. J. Bae, M. G. Kim, Y. G. Chang, J. Y. Lee, H. Park and S. W. Nam (2012). "HDAC1 inactivation induces mitotic defect and caspase-independent autophagic cell death in liver cancer." PLoS One **7**(4): e34265.

Yamagishi, T., S. Sahni, D. M. Sharp, A. Arvind, P. J. Jansson and D. R. Richardson (2013). "P-glycoprotein mediates drug resistance via a novel mechanism involving lysosomal sequestration." J Biol Chem **288**(44): 31761-31771.

Yanes, R. E., D. Tarn, A. A. Hwang, D. P. Ferris, S. P. Sherman, C. R. Thomas, J. Lu, A. D. Pyle, J. I. Zink and F. Tamanoi (2013). "Involvement of lysosomal exocytosis in the excretion of mesoporous silica nanoparticles and enhancement of the drug delivery effect by exocytosis inhibition." Small **9**(5): 697-704.

Yang, C., E. Choy, F. J. Hornicek, K. B. Wood, J. H. Schwab, X. Liu, H. Mankin and Z. Duan (2011). "Histone deacetylase inhibitor (HDACI) PCI-24781 potentiates cytotoxic effects of doxorubicin in bone sarcoma cells." Cancer Chemother Pharmacol **67**(2): 439-446.

Yang, C. J., Y. P. Liu, H. Y. Dai, Y. L. Shiue, C. J. Tsai, M. S. Huang and Y. T. Yeh (2015). "Nuclear HDAC6 inhibits invasion by suppressing NF-kappaB/MMP2 and is inversely correlated with metastasis of non-small cell lung cancer." Oncotarget **6**(30): 30263-30276.

Yang, D. Q., S. Feng, W. Chen, H. Zhao, C. Paulson and Y. P. Li (2012). "V-ATPase subunit ATP6AP1 (Ac45) regulates osteoclast differentiation, extracellular acidification, lysosomal trafficking, and protease exocytosis in osteoclast-mediated bone resorption." J Bone Miner Res **27**(8): 1695-1707.

Yang, F., S. S. Teves, C. J. Kemp and S. Henikoff (2014). "Doxorubicin, DNA torsion, and chromatin dynamics." Biochim Biophys Acta **1845**(1): 84-89.

Yang, X. J. and S. Gregoire (2005). "Class II histone deacetylases: from sequence to function, regulation, and clinical implication." Mol Cell Biol **25**(8): 2873-2884.

Yang, X. J. and E. Seto (2008a). "Lysine acetylation: codified crosstalk with other posttranslational modifications." Mol Cell **31**(4): 449-461.

Yang, X. J. and E. Seto (2008b). "The Rpd3/Hda1 family of lysine deacetylases: from bacteria and yeast to mice and men." Nat Rev Mol Cell Biol **9**(3): 206-218.

Yang, Y., W. Fiskus, B. Yong, P. Atadja, Y. Takahashi, T. K. Pandita, H. G. Wang and K. N. Bhalla (2013). "Acetylated hsp70 and KAP1-mediated Vps34 SUMOylation is required for autophagosome creation in autophagy." Proc Natl Acad Sci U S A **110**(17): 6841-6846.

Yang, Y., R. Rao, J. Shen, Y. Tang, W. Fiskus, J. Nechtman, P. Atadja and K. Bhalla (2008). "Role of acetylation and extracellular location of heat shock protein 90alpha in tumor cell invasion." Cancer Res **68**(12): 4833-4842.

Yao, S., M. Cheng, Q. Zhang, M. Wasik, R. Kelsh and C. Winkler (2013). "Anaplastic lymphoma kinase is required for neurogenesis in the developing central nervous system of zebrafish." PLoS One **8**(5): e63757.

Yasui, W., N. Oue, S. Ono, Y. Mitani, R. Ito and H. Nakayama (2003). "Histone acetylation and gastrointestinal carcinogenesis." Ann N Y Acad Sci **983**: 220-231.

Ye, J., X. Ai, E. E. Eugeni, L. Zhang, L. R. Carpenter, M. A. Jelinek, M. A. Freitas and M. R. Parthun (2005). "Histone H4 lysine 91 acetylation a core domain modification associated with chromatin assembly." Mol Cell **18**(1): 123-130.

Yee, A. J., W. I. Bensinger, J. G. Supko, P. M. Voorhees, J. G. Berdeja, P. G. Richardson, E. N. Libby, E. E. Wallace, N. E. Birrer, J. N. Burke, D. L. Tamang, M. Yang, S. S. Jones, C. A. Wheeler, R. J. Markelewicz and N. S. Raje (2016). "Ricolinostat plus lenalidomide, and dexamethasone in relapsed or refractory multiple myeloma: a multicentre phase 1b trial." Lancet Oncol **17**(11): 1569-1578.

Yonehara, R., S. Nada, T. Nakai, M. Nakai, A. Kitamura, A. Ogawa, H. Nakatsumi, K. I. Nakayama, S. Li, D. M. Standley, E. Yamashita, A. Nakagawa and M. Okada (2017). "Structural basis for the assembly of the Ragulator-Rag GTPase complex." Nat Commun **8**(1): 1625.

Yoon, Y. H., K. S. Cho, J. J. Hwang, S. J. Lee, J. A. Choi and J. Y. Koh (2010). "Induction of lysosomal dilatation, arrested autophagy, and cell death by chloroquine in cultured ARPE-19 cells." Invest Ophthalmol Vis Sci **51**(11): 6030-6037.

Yoshida, M. and T. Beppu (1988). "Reversible arrest of proliferation of rat 3Y1 fibroblasts in both the G1 and G2 phases by trichostatin A." Exp Cell Res **177**(1): 122-131.

Yoshida, M., M. Kijima, M. Akita and T. Beppu (1990). "Potent and specific inhibition of mammalian histone deacetylase both in vivo and in vitro by trichostatin A." J Biol Chem **265**(28): 17174-17179.

Yu, D. H., R. A. Waterland, P. Zhang, D. Schady, M. H. Chen, Y. Guan, M. Gadkari and L. Shen (2014). "Targeted p16(Ink4a) epimutation causes tumorigenesis and reduces survival in mice." J Clin Invest **124**(9): 3708-3712.

Yu, L., C. K. McPhee, L. Zheng, G. A. Mardones, Y. Rong, J. Peng, N. Mi, Y. Zhao, Z. Liu, F. Wan, D. W. Hailey, V. Oorschot, J. Klumperman, E. H. Baehrecke and M. J. Lenardo (2010). "Termination of autophagy and reformation of lysosomes regulated by mTOR." Nature **465**(7300): 942-946.

Yuan, X. M., W. Li, H. Dalen, J. Lotem, R. Kama, L. Sachs and U. T. Brunk (2002). "Lysosomal destabilization in p53-induced apoptosis." Proc Natl Acad Sci U S A **99**(9): 6286-6291.

Zhang, J., R. Sprung, J. Pei, X. Tan, S. Kim, H. Zhu, C. F. Liu, N. V. Grishin and Y. Zhao (2009a). "Lysine acetylation is a highly abundant and evolutionarily conserved modification in Escherichia coli." Mol Cell Proteomics **8**(2): 215-225.

Zhang, R., J. Erler and J. Langowski (2017a). "Histone Acetylation Regulates Chromatin Accessibility: Role of H4K16 in Inter-nucleosome Interaction." Biophys J **112**(3): 450-459.

Zhang, Y., M. Zhang, H. Dong, S. Yong, X. Li, N. Olashaw, P. A. Kruk, J. Q. Cheng, W. Bai, J. Chen, S. V. Nicosia and X. Zhang (2009b). "Deacetylation of cortactin by SIRT1 promotes cell migration." Oncogene **28**(3): 445-460.

Zhang, Z., Y. Cao, W. Zhao, L. Guo and W. Liu (2017b). "HDAC6 serves as a biomarker for the prognosis of patients with renal cell carcinoma." Cancer Biomark **19**(2): 169-175.

Zhang, Z., H. Yamashita, T. Toyama, H. Sugiura, Y. Ando, K. Mita, M. Hamaguchi, Y. Hara, S. Kobayashi and H. Iwase (2005). "Quantitation of HDAC1 mRNA expression in invasive carcinoma of the breast*." Breast Cancer Res Treat **94**(1): 11-16.

Zhang, Z., H. Yamashita, T. Toyama, H. Sugiura, Y. Omoto, Y. Ando, K. Mita, M. Hamaguchi, S. Hayashi and H. Iwase (2004). "HDAC6 expression is correlated with better survival in breast cancer." Clin Cancer Res **10**(20): 6962-6968.

Zhao, H., Y. Ito, J. Chappel, N. W. Andrews, S. L. Teitelbaum and F. P. Ross (2008). "Synaptotagmin VII regulates bone remodeling by modulating osteoclast and osteoblast secretion." Dev Cell **14**(6): 914-925.

Zhao, J., J. J. Brault, A. Schild, P. Cao, M. Sandri, S. Schiaffino, S. H. Lecker and A. L. Goldberg (2007). "FoxO3 coordinately activates protein degradation by the autophagic/lysosomal and proteasomal pathways in atrophying muscle cells." Cell Metab **6**(6): 472-483.

Zhao, Y., J. Yang, W. Liao, X. Liu, H. Zhang, S. Wang, D. Wang, J. Feng, L. Yu and W. G. Zhu (2010). "Cytosolic FoxO1 is essential for the induction of autophagy and tumour suppressor activity." Nat Cell Biol **12**(7): 665-675.

Zhao, Y. M., X. Chen, H. Sun, Z. G. Yuan, G. L. Ren, X. X. Li, J. Lu and B. Q. Huang (2006). "Effects of histone deacetylase inhibitors on transcriptional regulation of the hsp70 gene in Drosophila." Cell Res **16**(6): 566-576.

Zheng, G. and Y. C. Yang (2005). "Sumoylation and acetylation play opposite roles in the transactivation of PLAG1 and PLAGL2." J Biol Chem **280**(49): 40773-40781.

Zhitomirsky, B. and Y. G. Assaraf (2015). "Lysosomal sequestration of hydrophobic weak base chemotherapeutics triggers lysosomal biogenesis and lysosome-dependent cancer multidrug resistance." Oncotarget **6**(2): 1143-1156.

Zhitomirsky, B. and Y. G. Assaraf (2016). "Lysosomes as mediators of drug resistance in cancer." Drug Resist Updat **24**: 23-33.

Zhitomirsky, B. and Y. G. Assaraf (2017). "Lysosomal accumulation of anticancer drugs triggers lysosomal exocytosis." Oncotarget **8**(28): 45117-45132.

Zhou, Q., A. T. Agoston, P. Atadja, W. G. Nelson and N. E. Davidson (2008). "Inhibition of histone deacetylases promotes ubiquitin-dependent proteasomal degradation of DNA methyltransferase 1 in human breast cancer cells." Mol Cancer Res **6**(5): 873-883.

Zhu, X., X. Zhao, W. F. Burkholder, A. Gragerov, C. M. Ogata, M. E. Gottesman and W. A. Hendrickson (1996). "Structural analysis of substrate binding by the molecular chaperone DnaK." Science **272**(5268): 1606-1614.

Zimmerman, K. A., G. D. Yancopoulos, R. G. Collum, R. K. Smith, N. E. Kohl, K. A. Denis, M. M. Nau, O. N. Witte, D. Toran-Allerand, C. E. Gee and et al. (1986). "Differential expression of myc family genes during murine development." Nature **319**(6056): 780-783.

Zoncu, R., L. Bar-Peled, A. Efeyan, S. Wang, Y. Sancak and D. M. Sabatini (2011). "mTORC1 senses lysosomal amino acids through an inside-out mechanism that requires the vacuolar H(+)-ATPase." Science **334**(6056): 678-683.